DESIGN, SYNTHESIS AND MOLECULAR MODELLING STUDIES OF ARYL SUBSTITUTED 2-(4-(SULFONYL) STYRYL)QUINAZOLIN-4(*3H*)-ONES AS POTENTIAL ANTICANCER AGENTS

by

KHOMOTSO JAMIE MOKGANYA

Presented in compliance with the specifications for the attainment of the Master of science degree in

CHEMISTRY

FACULTY OF SCIENCE AND AGRICULTURE

School of Physical and Mineral Sciences

at the

UNIVERSITY OF LIMPOPO

SUPERVISOR: Prof RM MAMPA

Co-SUPERVISOR: Dr MM MALULEKA

2024

DESIGN, SYNTHESIS AND MOLECULAR MODELLING STUDIES OF ARYL SUBSTITUTED 2-(4-(SULFONYL) STYRYL)QUINAZOLIN-4(*3H*)-ONES AS POTENTIAL ANTICANCER AGENTS

I affirm that the thesis is a product of my independent efforts, and I take full responsibility for its creation. Throughout the document, I have diligently acknowledged and provided comprehensive references for all the sources I have utilized or quoted. By doing so, I have ensured that proper credit is given to the original authors and that the integrity of their work remains intact. This declaration serves as a testament to the meticulousness with which I have approached my research, upholding the principles of academic honesty and intellectual integrity.

08/07/2024

…… ……..

SIGNATURE DATE

DEDICATION

I would like to dedicate this thesis to two extraordinary individuals in my life, my mother and younger sister, Motshekgene and Raesetja. Their unwavering support, pure hearts, and genuine enthusiasm have been invaluable throughout my academic journey.

ACKNOWLEGDEMENTS

I extend my heartfelt gratitude to the individuals who made my MSc journey an absolute joy. This includes my beloved family, supervisors, supportive lab mates, dedicated lecturers, instrumental personnel, and the guiding force of my faith. Their contributions, encouragement, and guidance have been instrumental in my success, and I am immensely thankful for their presence in my academic pursuit.

- I am profoundly grateful to my family and friends, their steadfast belief in me, constant encouragement, and uplifting prayers have been a source of strength and motivation during both challenging times and moments of triumph. (Mommy, Raesetja, Lethabo, Malose)

- Immensely grateful to the department of chemistry and university of Limpopo for providing me with the opportunity to pursue and successfully complete my MSc degree.

- NRF bursary for investing in my education, their generous funding and provision of efficient resources that were contributory in helping me complete my qualification.

- My deepest appreciation to my supervisors Prof R.M. Mampa, Dr M.M. Maluleka for their invaluable wisdom throughout my journey. Their guidance, expertise, and dedication have been influential in shaping my research, refining my skills, and ultimately achieving this milestone.

- My sincere gratitude to Professor Mbazima from the biochemistry department for their invaluable assistance and expertise in guiding the biological studies conducted as part of my dissertation.

- My lab mates T.P. Mokoena and J.K. Nkoana, much appreciation for creating a harmonious, enjoyable, and uplifting workplace environment.

- Ms L.A. Raphoko (MS personnel) and T.G. Ramakadi (NMR personnel) for acquisition of data on the mass spectrometry (MS) and nuclear magnetic resonance (NMR) instruments.

TABLE OF CONTENTS

SCIENTIFIC CONTRIBUTIONS

Oral presentations at 16th Frank Warren conference 2023, Protea Hotel Ranch Resort, 3 - 7 December 2023

Title: Design, synthesis, and molecular modelling of aryl substituted 2-(4-(sulfonyl) styryl) quinazolin-4(3*H*)-ones as potential anticancer agents

P35: Design, synthesis, and molecular modelling of aryl substituted 2-(4-(sulfonyl) styryl)quinazolin-4(3*H*)-ones as potential anticancer agents.

Jamie Mokganya[1], Marole Maluleka[2], Richard Mampa[1]

[1]University of Limpopo, Department of Chemistry, Private Bag X1106, Sovenga, 0727
[2]University of Johannesburg, Department of Chemistry, P.O Box 524 Auckland Park, 2006
e-mail address: khomotsomokganya18@gmail.com

Keywords: Quinazolinone, 2-(4-(sulfonyl)styryl)quinazolin-4(3*H*)-one

Cancer encompasses a wide range of diseases characterized by irregular cellular proliferation that can infiltrate various areas of the body, breaking down and disrupting normal tissue and organ functioning[i]. The current available drugs are compromised by numerous side effects and development of resistance[ii]. In this study, we aim to synthesize styryl-dihydroquinazolinone[iii] derivatives for biological evaluation against cancer.

The target compounds were achieved through reaction of iodination of 2-aminobenzamide to yield 5-iodo-2-aminobenzamide, followed by a nucleophilic substitution acetylation reaction, resulting in 2-aceto-5-iodobenzamide. The resulting product underwent cyclization under reflux conditions forming 2-methylquinazolin-(3*H*)-one. Salicylaldehydes were sulphonated to afford four intermediate derivatives, that were subsequently reacted with 2-methylquinazolin-4(3*H*)-one to afford sulfonyl styrylquinazolin-4(3*H*)-ones through condensation reaction under reflux conditions. Application of Suzuki coupling reaction using six different boronic acids under inert conditions afforded novel 6-aryl (2-(4-(sulfonyl)styryl)quinazolin-4(3*H*)-one derivatives. Synthesized compounds were characterized using a nuclear magnetic resonance (^{1}H and ^{13}C-NMR), infrared spectroscopy (IR), and mass spectrometry (MS) techniques, computational and biological studies.

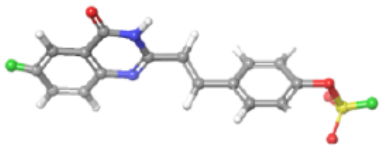

Hassanpour, S. H., & Dehghani, M. Cancer Res. Pract. (2017), 4(4), 127-129.
Alfarouk, K. O., Stock, C. M., Taylor, S., Walsh, M., Muddathir, A. K., Verduzco, D., Bashir, A. H., Mohammed, O. Y., Elhassan, G. O., Harguindey, S., Reshkin, S. J., Ibrahim, M. E., & Rauch, C. Cancer Cell Int, (2015)15, 71.
Sridhar, R., Takei, H., Syed, R., Kobayashi, I. S., Hui, L. B., Kamal, A., Tenen, D. G., & Kobayashi, S. S. (2018). Molecules, (2018). 23(8), 1938.

LIST OF FIGURES

CHAPTER 1: Rationale

CHAPTER 2: literature review

CHAPTER 3: Results and discussion

LIST OF SCHEMES

CHAPTER 2: literature review

CHAPTER 3: Results and discussion

LIST OF TABLES

CHAPTER 3: Results and discussion

ABSTRACT

In this study, we aimed to synthesize styryl-dihydroquinazolinone derivatives for biological evaluation against cancer. The target compounds were achieved through Iodination of 2-aminobenzamide to yield 5-iodo-2-aminobenzamide **75**, followed by a nucleophilic acetyl substitution reaction, to result in 2-aceto-5-iodobenzamide **76**. This was then followed by base mediated cyclization reaction of **77** under reflux conditions forming 6-iodo-2-methylquinazolin-(3*H*)-one **78**. A series of substituted-2-hydroxybenzaldehyde derivatives were sulphonated using alkyl and aryl sulfonylchloride derivatives to afford derivatives **79a-r**. Amongst them compound **79a, 79b, 79j, 79k** were used as substrates for the base mediated Aldol condensation reaction with 6-iodo-2-methylquinazolin-4(3*H*)-one **78**, resulting in the formation of the (*E*)-4-(2-(6-iodo-4-oxo-3,4-dihydroquinazolin-2-yl)vinyl)-2-sulfonates **80a-d**. Application of compounds **80a-d** to Suzuki coupling reaction using arylboronic acids under inert conditions afforded novel (*E*)-4-(2-(6-aryl-4-oxo-3,4-dihydroquinazolin-2-yl)vinyl)-2-sulfonates **81a-e**. The synthesized compounds were characterized by a combination of techniques that included nuclear magnetic resonance spectroscopy (^{1}H and ^{13}C NMR), infrared spectroscopy (IR) and mass spectrometry (MS). X-ray analyses were carried out for three sulfonated benzaldehydes **79a, 79b, and 79k.** Compound **79a** crystalized in a monoclinic crystal system and **79b** and **79k** in a triclinic crystal system, respectively with space groups P-1 and P21/n respectively. The intermolecular interactions of crystal structures **79a** and **79b** were further analysed using the Hirshfeld surface analysis. The surface volume and area for **79a** (244.26 Å³ and 236.92 Å², respectively) is lower than **79b** (322.51 Å³ and 303.35 Å², respectively). A comparison of compound **79a** (globularity value of 0.798) relative to **79b** (globularity value of 0.750) shows it is higher, meaning it is less spherical. Furthermore, the synthesized compounds were tested for anti-proliferative activity against the

breast cancer cells (MCF-7), cervical cancer (HeLa), lung (A549) and human embryonic kidney cells (HEK293-T) using curcumin and camptothecin as a positive control in a MTT cell viability analysis. Compounds **79 a-r** were also tested for antioxidative activity using DPPH assay with ascorbic acid as a reference standard. From the preliminary tests, the most active compound, **80c** showed 30% cell viability when compared with curcumin 90% cell viability at 100 μM against MCF-7. Compound **80b** and **80c** and **81e** had the most activity against the HeLa cells with a percentage viability of 50%, 51%, and 55% respectively, compared to curcumin at 90%. Compound **80b** and **81e** resulted in similar %viability of 40% against the HEK293-T cells at 100 μM but the **80b** would be most preferred since adhering to ADMET properties. Compounds **79a-79i** were also tested for %viability but with camptothecin as a control. Compound **79i** was found to be most active with the IC_{50} value of 0.042 100 μM compared to camptothecin of an IC_{50} value of 6.32 100 μM. Thereafter compounds **79a-79i** were tested for antioxidant activity using the DPPH assay, compounds **79d, 79e, 79f, 79h** and **79i** have been found to have more scavenging activity (IC_{50} = 0.29 μM, 0.67 μM, 0.0273 μM and 0.0617 μM) than ascorbic acid (IC_{50} = 5.87 ± 0.88 μM) and showed strong peroxidase interactions (-7.219 Kcal/mol., -7.087 Kcal/mol., -7.648 Kcal/mol., -7.330 Kcal/mol., and -7.671 Kcal/mol). Perioxidase docking was conducted to elucidate their efficiency of compound **79a-79i**, they demonstrated significantly higher binding affinities (ΔG = -5.4 to -8.1 kcal/mol) compared to benzimidazole (ΔG = -5.3 kcal/mol), underscoring their promising potencies. Among these, molecules **79d, 79e, 79h**, and **79i** displayed particularly strong attachments within the protein binding pockets, interacting with hydrophobic residues such as VAL 916, LEU 889, and VAL 899, akin to the binding pattern observed with benzimidazole. The most active inhibitors of peroxidase were found to be compounds **79h** and **79i**. Compound **79h** formed strong O---H interactions with both hydrophilic

(ARG 48, PRO 145, HIS 175, LYS 179, THR 234, TYR 187) and hydrophobic (PHE 147) residues, while compound **79i** interacted with hydrophilic residues (ARG 48, PRO 145, LYS 179) and one π-π interaction with hydrophobic residue (PHE 191). Compounds **79d** and **79e** showed the same inhibitory activity, but also differed in their binding energies of -7.087 Kcal/mol. and -7.219 Kcal/mol.

CHAPTER 1: RATIONALE

Cancer ranks among the leading causes of death worldwide and it encompasses a wide range of diseases characterized by irregular cellular proliferation that can potentially metastasize or infiltrate various parts of the body[1]. These diseases often lead to a breakdown and disruption in normal tissue and organ functioning by producing enzymes that degrade healthy cells and tissues[2]. Cancer's origins can be traced back to ancient times, with its earliest documentation found in Egypt around 1500 BC. Doctors started to comprehend the connection between cells and cancer in the late 1800s, after which chemotherapy and radiation treatments were implemented in the early 1900s. The first authorized chemotherapeutic agents were applied in the 1950s[3].

Targeted therapy, radiation therapy, surgery, hormone therapy, and chemotherapy immunotherapy are just a few of the many methods used to treat cancer today. Unexplained weight loss, lumps, change in bowel habits, a tenacious cough and uncommon bleeding, are all persistent signs and symptoms of cancer. While these cancer symptoms may be evident, other medical conditions could also be responsible. Humans are susceptible to over 100 different malignancies[4].

Chemotherapy remains the widely used treatment approach for cancer where pharmaceuticals are used to eradicate cancerous cells. The success of chemotherapy depends on the understanding of the underlying chemistry of the drugs[5]. Knowledge of more potent drugs with less side effects leads to improved treatment. Therefore, understanding the chemistry of

chemotherapy medications is critical, more especially with the newly developed drugs and improving existing ones. Knowledge of more potent drugs with less side effects leads to improved treatment. Chemotherapeutic medications inhibit the growth and proliferation of cancerous cells, but they can also have negative effects on healthy cells in the body[6]. Chemotherapy has been a mainstay in cancer treatment, but it is not without drawbacks. Chemotherapy treatments can lead to the occurrence of side effects such as vomiting, fatigue, nausea, hair loss and an increased susceptibility to infections. Another concern is the development of resistance to the chemotherapy drugs, where cancer cells become less responsive to their effects overtime. Furthermore, chemotherapeutic drugs suffer from limited effectives and can harm healthy cells in the body due to lack specificity, potentially leading to long-term adverse effects such as infertility and an increased risk of secondary malignancies[7, 8]. Chemotherapy treatments can be highly pricey, and not every patient has access to therapies that are within their financial means.

The significance of 2-styryl substituted quinazolinone derivatives has been increasingly recognized due to the broad range of biological activities they exhibit. These activities encompass tubulin polymerization inhibition[9], cytotoxicity[10], Hsp90 inhibition[11], anticonvulsant properties[12], sedative-hypnotic effects[13], anti-proliferative effects[14], as well as antibacterial and antifungal activities[15].Observation by Radhakrishnan *et al* suggests that 5-nitrofuran-2-ylstyrylquinazolinones **1** hold great promise for promoting leukemic cell differentiation[16]. They synthesized and assessed novel series of compounds including ethynylstyrylquinazolinones, styrylquinazolinones, thienopyrimidinones and styryl quinolinones. Following RNA-seq analysis, it was observed that fluorinated styryl quinazolinones **2** triggers the activation of molecular

pathways related to apoptosis and cellular differentiation, while concurrently inhibiting pathways associated with cellular growth and development within CAL-27 cancer cells. In light of this, the study by Dinesh *et al* presents the discovery of a potential therapeutic candidate for oral cancer treatment in the form of fluorinated 2-styrylquinazolin-4(3*H*)-ones **2**[17]. These methods present several intriguing characteristics of synthesis of derivatives of styrylquinazolinones, including mild, shortened reaction conditions and improved selectivity. Considering these observations, the idea of utilizing microwave irradiation to incorporate the thiazole moiety at the third position in the synthesis of a fresh series of 2-styrylquinazolin-4(3*H*)-one derivatives seemed valuable, this concept is illustrated in **Figure 1.1**.

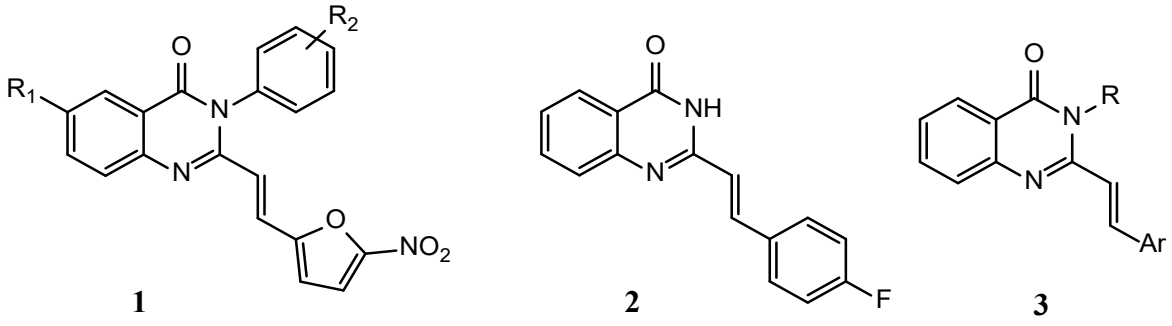

Figure 1. 1: 2-styryl substituted quinazolinone derivatives with biological activities.

A new series of 3-[5-substituted phenyl-1,3,4-thiadiazole-2-yl]-2-styrylquinazoline-4(3*H*)-ones **3** was synthesized and assessed for their anticonvulsant, sedative-hypnotic, and central nervous system (CNS) depression effects as seen in **Figure 1.1**[18].These compounds were administered via intraperitoneal injection to mice and rats at different doses per body weight, and their performance was evaluated in seizure models induced by maximal electroshock (MES) and subcutaneous pentylenetetrazole (scPTZ). Neurotoxicity was determined using the Rotorod

method. The study findings suggest that the synthesized styryl quinazolinone compounds exhibited more pronounced sedative-hypnotic and CNS depressant activities compared to their anticonvulsant effects[19]. A selection of 3-aryl-2-styryl substituted-4(3*H*)-quinazolinones was successfully synthesized, and their potential as antimalarial and antileishmanial agents was explored through in vivo and in vitro assays in a study by Girma *et al*[20].

In the case of antimalarial activity, some of the tested compounds as seen in **Figure 1.2,** demonstrated approximately 70.01% suppression of Plasmodium berghi ANKA infection. Notably, the compound (*E*)-2-(4-nitrostyryl)-3-phenylquinazolin-4(3*H*)-one **5** exhibited particularly promising antileishmanial activity with an IC_{50} value of 0.0212 µg/mL, surpassing the efficacy of standard drugs amphotericin B deoxycholate (IC_{50} = 0.0460 µg/mL) and miltefosine (IC_{50} = 3.1911 µg/mL)[21] by factors of 2 and 150, respectively. Furthermore, molecular docking studies targeting Lm-PTR1's active site supported the superior in vitro antileishmanial activity of the compound **4**. Overall, the synthesized 3-aryl-2-styryl substituted-4(3*H*)-quinazolinones exhibit promising potential as scaffolds for the development of diverse antileishmanial and antimalarial agents[22].

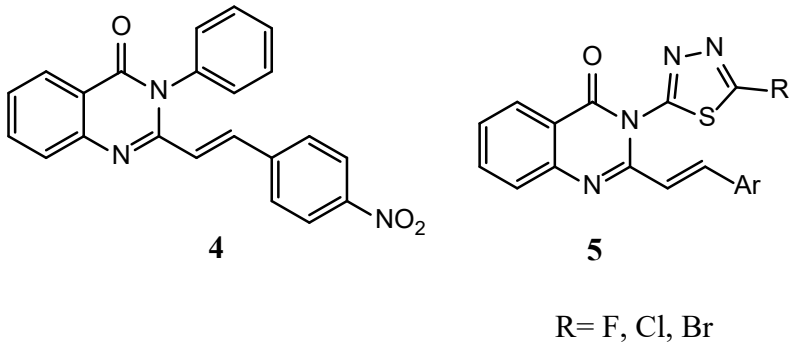

Figure 1. 2 : Styryl substituted quinazolinone derivatives accessed for central nervous system depression effects.

The incorporation of sulfonyl moiety on quinazolinone molecules was found to increase their overall biological activity.[23] Inspired by this we became interested in infusing a sulfonyl framework on the styryl quinazolinones to afford new therapeutic compounds **6** with enhanced selectivity and potency as seen in **Figure 1.3**[24]. However, literature has revealed that the sulphonated appended styryl quinazolinone derivatives have not been extensively investigated. Synthesizing these novel compounds and characterizing them will add to the body of knowledge and bridge the gap in their synthesis, characterization and application thus providing a steppingstone for further investigations for potential anti-cancer activity. To achieve our goal, we conducted a thorough literature search on medicinally relevant quinazolinones derivatives and quinoline analogues. In the following sections, we will look at the discovery and characterization of quinazolinones and quinazoline derivatives possessing significant biological relevance.

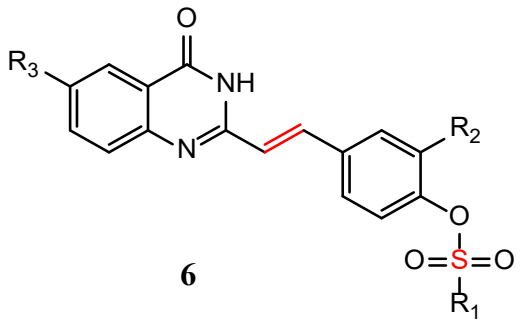

6

R_1= OMe, OCH
R_2= OMe
R_3= Cl, F, Br

Figure 1. 3: Integration of a sulfonyl functional group on to a quinazolinone.[25]

CHAPTER 2: LITERATURE REVIEW

2.1 Discovery and structure of quinazoline and quinazolinone derivatives with biological importance

Heterocycles are commonly found in both active pharmaceutical ingredients and additives. They are isosterically or bioisosterically substituted carbons in aliphatic structures. Nitrogen-containing heterocycles or combinations of nitrogen, sulphur, and oxygen in five- or six-membered rings are frequently encountered[26]. Over 85% of biologically active compounds contain a heterocycle, highlighting their pivotal role in modern drug design. Among the most important heterocycles are compounds called quinazolines and quinazolinones[27].

Quinazoline is a bicyclic aromatic heterocyclic compound composed of a benzene ring fused with a pyrimidine ring. It has the molecular formula $C_8H_6N_2$. Naturally occurring quinazolines exist in the plant families and microorganisms, the scaffold for the structure accounts for over 200 alkaloids that have been isolated[28]. Quinazoline and its derivatives have attracted considerable attention due to their diverse biological activities and pharmaceutical potential[29]. They are known to exhibit anticancer, antiviral, antibacterial, and anti-inflammatory properties. In 1903, Ranawat *et al* achieved the pioneering synthesis of a quinazoline nucleus within a laboratory setting.[30] Later, Asif *et al* proposed the name "quinazoline" for this nucleus based on its resemblance to the isomeric structure of the quinoxaline ring[31, 32]. The synthesis of various compounds containing the quinazoline core largely depends on the specific substitution patterns on the 1,3-diazine moiety of the system[33]. Researchers have extensively explored the synthesis of diverse compounds featuring the quinazoline core by considering the substitution patterns on the 1,3-diazine component. These findings have significantly contributed to the understanding

and utilization of quinazoline derivatives in various scientific fields[34, 35]. There are several isomers of quinazolines[36], which differ in the position of the two nitrogen atoms in the heterocyclic ring as shown in **Figure 2.1**.

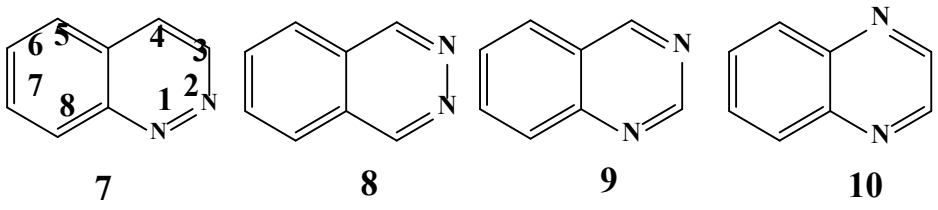

Figure 2. 1: Quinazoline isomers.

Quinazolinone is a heterocyclic compound belonging to the quinazoline family, it is a type of oxidized quinazoline featuring a carbonyl group within its C_4N_2 ring[37]. It exists in two isomeric forms: 2-quinazolinone and 4-quinazolinone, with the latter being the more prevalent. Quinazolinones can be classified into four groups, including quinazoline-4(1*H*,3*H*)-one **11**, quinazoline-2(1*H*,3*H*)-one **12**, and quinazoline-2(1*H*)-one **13** and quinazoline-4(3*H*)-one **14** derivatives[38] and the degree of unsaturation of the ring as depicted by **Figure 2.2**

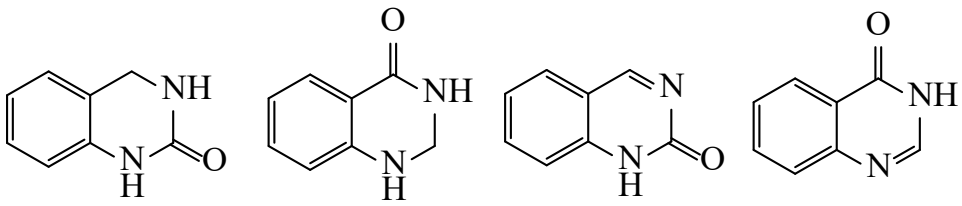

11 **12** **13** **14**

Figure 2. 2: Illustrative types of quinazolinones structures.

Quinazolinones are heterocyclic compounds that continue to receive considerable attention from researchers due to their wide spectrum biological properties such as antifungal, anti-cancer and anti-HIV activities [39,40,41]. The first example of a quinazolinone was synthesized in the laboratory by Griess in 1869 who reacted anthranilic acid with cyanide in ethanol to afford a 2-ethoxy-4(3*H*)-quinazolinone[42]. However, the first example of a naturally occurring quinazolinone was extracted from a Chinese plant, *Dichroa Febrifunga*, only in 1950[43] .

Styryl quinazolinones are a class of organic compounds that are characterized by the presence of a quinazolinone core structure attached to a styryl group[44,45]. Some of these compounds can be seen in **Figure 2.3**, where the inhibitory effects of compound **15** on various enzymes and receptors have been extensively investigated, such as protein kinases and G-protein-coupled receptors[46]. Compound **16** has shown promising results as kinase inhibitor, particularly as receptor tyrosine kinase inhibitors, including vascular endothelial growth factor receptor 2 (VEGFR-2) inhibitors, which are important targets in angiogenesis[47] inhibition and cancer treatments. Moreover, the synthesis and structural modifications of styrylquinazolinones have

been explored to enhance their potency and selectivity against specific targets. These modifications involve varying the substitution pattern on both the quinazolinone and styryl moieties, exploring different substituents, and introducing various functional groups to optimize their pharmacological properties[48].

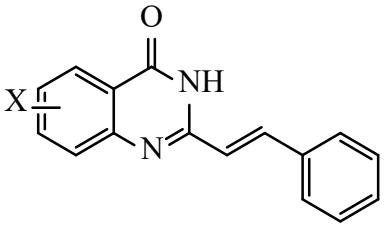

15

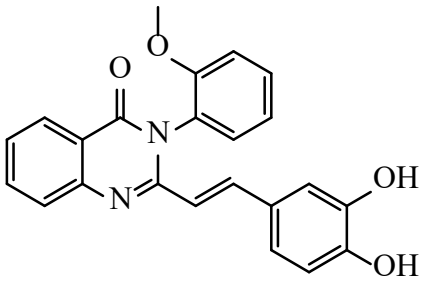

16

Figure 2. 3: Styryl quinazolinones explored for biological activity.

2.1.1 Application of quinazolinones and quinazoline derivatives

Various derivatives of quinazolinones have shown significant effects on hypertension, cancer, depression, and psychosis in patients, examples are shown in **Figure 2.4**.[49] Furthermore, certain quinazolinones possess properties that make them useful as sedatives[50], antibacterial[51], and anti-inflammatory agents[52]. There are many quinazoline compounds with biological importance that have been approved by FDA over the years[53]. Lapatinib (Tykreb®) **17** for example was approved by FDA in 2012 for treatment against breast cancer[54]. The drug effectively hinders the function of both the human epidermal growth factor receptor-2 (HER2/neu) and the epidermal growth factor receptor (EGFR) pathways. Vandetanib (Caprelsa®) **19**, on the other hand, was endorsed by the FDA in 2011, was prescribed for the management of metastatic medullary thyroid cancer[55]. It functions as a kinase inhibitor targeting

various cell receptors, primarily the vascular endothelial growth factor receptor (VEGFR), EGFR, and the rearranged transfection (RET)-tyrosine kinase (TK)[56]. Afatinib (Gilotrif®) **18**, permitted by the FDA in 2013 for treatment of non-small cell lung cancer, worked as an irreversible covalent inhibitor of receptor tyrosine kinases (RTK) associated with EGFR and erbB-2 (HER2)[57].

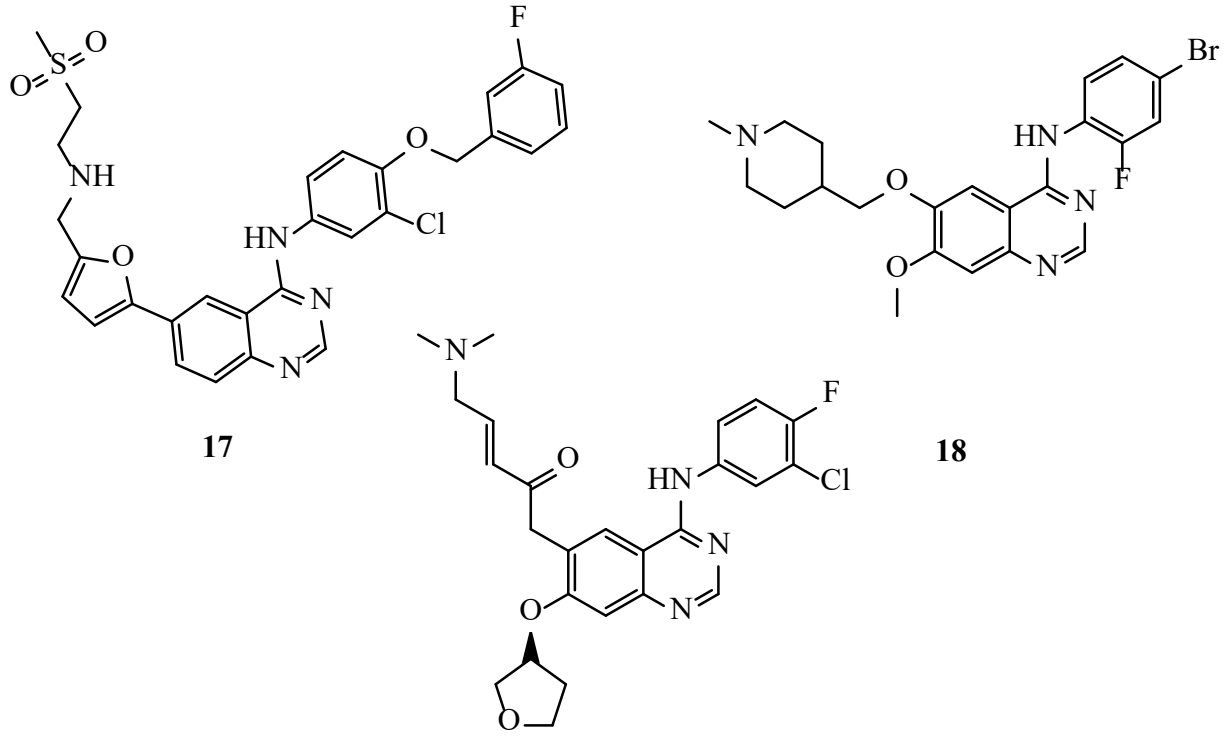

Figure 2. 4: FDA history of quinazolinones**.**

Mecloqualone[58] **20**, a widely recognized hypnotic and anti-convulsive medication, possesses a chiral axis consisting of a carbon-nitrogen bond. The rotation around this axis was impeded due to steric hindrance at normal body temperature. Afloqualone[59] (**21**), an analog of mecloqualone, exhibited sedative and muscle-relaxant properties. It was commonly administered as racemates, containing equal amounts of its two enantiomers. Halofuginone[59], a derivative of febrifugine[60],

garnered attention for its potential as an antimalarial agent and exhibited various intriguing biological effects in animal studies. One notable characteristic of halofuginone **22** is its ability to inhibit the synthesis of collagen type 1[61]. The *in vivo* investigations have demonstrated its significant efficacy in treating fibrosis[62].

Balaglitazone[63], is a quinazolinone derivative that was at phase (III) clinical trials, and it is specifically formulated for the management of type 2 diabetes mellitus **23**. It acts as a peroxisome proliferator-activated receptor-gamma agonist[64].

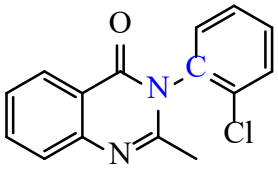

Mecloqualone

20

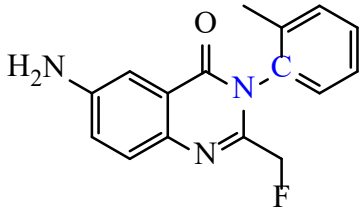

Afloqualone

21

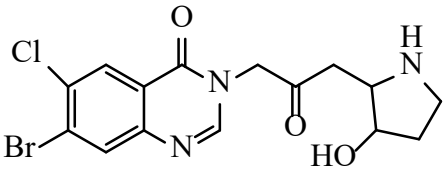

Halofuginone

22

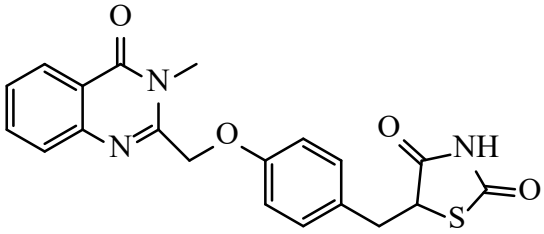

Balaglitazone

23

Figure 2. 5:Recently FDA approved and phase (III) clinical trials drugs with the quinazolinone scaffold.

In a study of quinazolinones conducted in 2015, the focus was on the synthesis and evaluation of fluorinated quinazolinone-sulphonamide hybrids **24** for their potential anticancer properties[65]. The quinazolinone-sulphonamides were synthesized and subjected to *in vitro* cytotoxicity activity against breast cancer cells while maintaining a safe profile on non-cancerous cells. Furthermore, a series of 2,3,6-trisubstitutedquinazolin-4(3*H*)-ones such as compound **25** in **Figure 2.6** were synthesized and assessed *in vitro* for their anticancer activity against breast cancer, hepatocellular carcinoma, cervical cancer, and promyelocytic leukemia cell lines[66]. In this case, structure–activity relationship (SAR) investigations have highlighted the crucial importance of positions 2, 6, and 8 within the ring system. Abuelizz *et al*. investigated the synthesis and anticancer activity of 2-thioxoquinazolin-4-ones **26,** and the synthesized compounds demonstrated significant anticancer activity against MDA-MB-231 and Hela cell lines, when compared to the positive standard gefitinib[67].

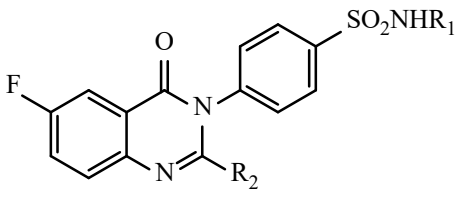

24

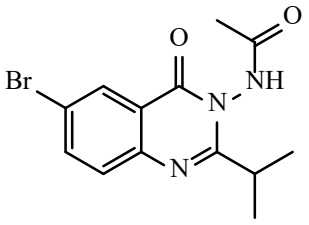

25

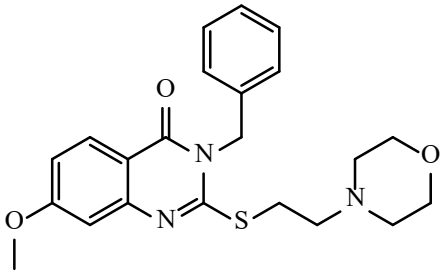

26

-

Figure 2. 6: Activity at different substitutions on scaffold of quinazolinone.

Maddali and coworkers synthesized a series of quinazolin-4(3*H*)-ones linked to 1,2,3-triazole hybrids **27** in 2019 and was found to have potential anti-tuberculosis properties[68] **Figure 2.7**. The study encompassed the design, synthesis, and docking studies of these proposed agents. The findings indicated that the inclusion of the triazole component improved the effectiveness of the quinazolinone derivatives, while the incorporation of aromatic groups increased the binding interactions[69].

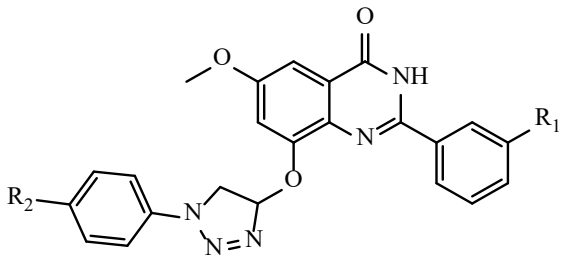

27

Figure 2. 7: Anti-tuberculosis activity on quinazoline moiety.

In the next section, we will explore the various approaches and techniques used in the synthesis of quinazolinones. These methods have played a crucial role in enabling the discovery of quinazolinones as a versatile class of compounds with diverse biological activities. By understanding the different synthetic pathways and strategies, researchers have been able to access a wide range of quinazolinone derivatives, each potentially holding unique pharmacological properties.

2.2. Methods for the synthesis of quinazolin-4-one derivatives

2.2.1 Synthesis of dihydroquinazoline-4(1*H*)-ones

2.2.1.1 Synthesis of dihydroquinazolin-4(1*H*)-one through the reductive cyclization method

Reductive cyclization method involves the condensation of anthranilamide or its derivatives with an aldehyde or a ketone followed by ring closure to yield a dihydroquinazolinone derivative[70]. Reagents such as fumaric acid[71], ammonium chloride[72] or sodium bisulfate[73] have been employed as catalysts for the cyclocondensation of anthranilamide with carbonyl compounds to afford quinazolinones. Amberlyst-15 and Silica-perchloric acid ($HClO_4$) have also been employed as efficient and re-usable catalysts to promote the reductive cyclization of anthranilamide **28** and ketones **29** to afford the corresponding 2,3-dihydroquinazolin-4(*1H*)-one derivatives **30** (**Scheme 2.1**)[74]. The reaction was found to be rapid, and it involves relatively mild conditions.

A low cost and environmentally friendly method for the synthesis of 2,3-dihydroquinazolin-4(1*H*)-one was unexpectedly discovered by Zong *et al*. The method involves the reaction of anthranilamide and 4-methylbenzaldehyde with water as a reaction medium to afford 83% yield of 2,3-dihydroquinazolin-4(1*H*)-one derivative[75]. Another method was reported for the synthesis of 2,3-dihydroquinazolin-4(1*H*)-ones by Gashang *et al*. using silica-supported ferric chloride as a catalyst under solvent-free conditions. The authors demonstrated the cyclocondensation of anthranilamide and aldehydes[76].

Meanwhile, Wang *et al*. proposed a green chemistry approach for the synthesis of the same compounds. They utilized the grinding method with anthranilamide, ketones or aldehydes,

cerium (IV) ammonium nitrate (CAN), and water at room temperature. This approach resulted in improved product yield by increasing the surface area[77].

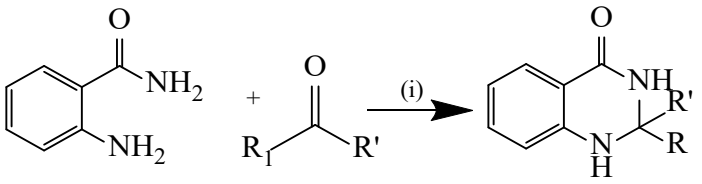

28 **29** **30**

Methodology 1: (i) Amberlyst-15, r.t.,1-2 h

Methodology 2: (i) Cerium (IV) ammonium nitrate

Scheme 2. 1: Cyclization of anthranilamide **28** with aldehydes or ketones.

2.2.1.2 Synthesis of dihydroquinazolin-4(1*H*)-one through metal-mediated reaction

2.2.1.2.1 Synthesis of dihydroquinazolin-4(1*H*)-one through titanium-mediated cyclocondensation

Transition metal-based reagents have been employed as catalysts in the cyclocondensation of anthranilamide derivatives with carbonyl compounds. For instance, $Sc(OTf)_3$, SmI_2 , or $CuCl_2$ have been utilized in previous studies[78]. Daqing *et al*. conducted a reaction between *ortho*-nitrobenzamides **31** and aldehydes or ketones **32**, using a $TiCl_4$/Zn mixture as a catalyst under reflux conditions. The reaction took place under anhydrous and inert conditions, resulting in the formation of 2,3-dihydroquinazolin-4(1*H*)-ones derivatives **33** (**Scheme 2.2**)[79]. In this reaction, zinc plays a role in reducing *ortho*-nitrobenzamide to *ortho*-aminobenzamide, while titanium

tetrachloride acts as a Lewis acid catalyst to activate the carbonyl group and facilitate the cyclocondensation step.

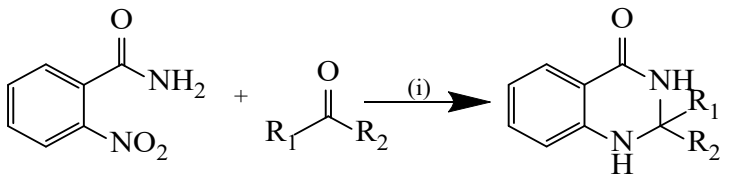

31 **32** **33**

Methodology: (i) $TiCl_4$/Zn, THF

Scheme 2. 2: Titanium -mediated cyclocondensation of **31** and **32**.

2.2.1.3 Synthesis of dihydroquinazolin-4(1*H*)-one through microwave conditions

Wang *et al.* developed a high yielding and efficient method for the synthesis of the 2,3-dihydroquinazolin-4(1*H*)-one derivatives under microwave conditions[80]. The reaction involves reacting anthranilamide **28** with ketones **34** in acetic acid in the presence of *p*-toluenesulfonic acid as a catalyst at 300 W to afford the 2,3-dihydroquinazolin-4(1*H*)-one derivatives **35** **(Scheme 2.3**). The reaction was completed within five minutes. and microwave conditions were also found to eliminate impurities in the product.

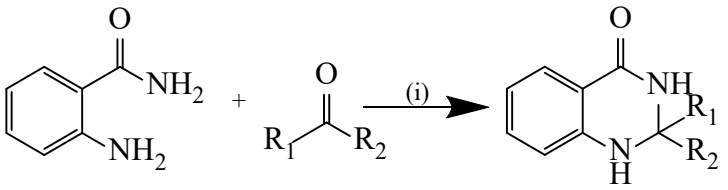

28 **34** **35**

Methodology: (i) TsOH, MW

Scheme 2. 3: Microwave-assisted synthesis of 2,3-dihydroquinazolin-4(1*H*)-ones.

New methods continue to appear in the literature for the synthesis of dihydroquinazolinones, which involve the change of catalysts. The heterocyclic ring of the 2,3-dihydroquinazolin-4(1*H)*-ones has been found to undergo dehydrogenation or aromatization[81] to afford the potentially tautomeric quinazolin-4*(*3*H)*-ones or their quinazoline derivatives, respectively. The methods for the synthesis of quinazolin-4(3*H*)-ones are described sequentially in the next sections.

2.2.2 Synthesis of quinazolin-4(3*H*)-ones

2.2.2.1 Synthesis of quinazolin-4(3*H*)-ones via dehydrogenation of dihydroquinazolin-4(1*H*)-ones

The N-1 and C-2 bonds of the dihydroquinazolin-4(1*H*)-ones can be dehydrogenated using oxidizing agents to afford the potentially tautomeric quinazolin-4(3*H*)-ones. Wang *et al.*, for example, dehydrogenated the 2,3-dihydroquinazolin-4(1*H*)-ones **36** using iron (III) chloride hexahydrate ($FeCl_3.6H_2O$) in water under reflux to afford quinazolin-4(3*H*)-one derivatives[82] **37** (**Scheme 2.4)**.

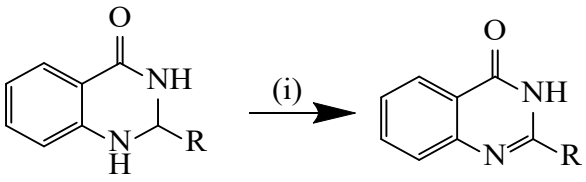

36 **37**

Methodology: (i) $FeCl_3.6H_2O$, H_2O, reflux

Scheme 2. 4: Dehydrogenation of the 2,3-dihydroquinazolin-4(1*H*)-ones into quinazolin-4(3*H*)-ones.

The primary drawback of using stoichiometric or excessive amounts of oxidizing reagents is their high cost and the challenges associated with handling and disposing of these corrosive substances, which can pose environmental risks. To mitigate these limitations, researchers have developed direct synthesis methods for quinazolin-4(3*H*)-ones. These approaches predominantly involve the use of anthranilic acid derivatives and carbonyl compounds as substrates, allowing to produce the desired quinazolin-4(3*H*)-ones in a single-pot process. The subsequent section delves into a discussion of these methods and their variations.

2.2.2.2 Direct methods for the synthesis of quinazolin-4(3*H*)-ones

2.2.2.2.1 Niementowski Synthesis

The direct synthesis of quinazolin-4(3*H*)-one includes a condensation reaction named Niementowski Synthesis. This method involves the synthesis of quinazolin-4(3*H*)-one from anthranilic acid and a ketone or an aldehyde[83]. Anthranilic acid **31**, for example, was condensed with formamide to afford quinazolin-4(3*H*)-one **39** (**Scheme 2.5**).

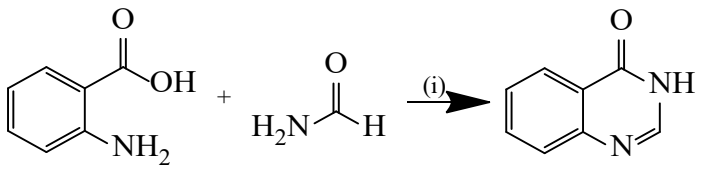

31 **38** **39**

Methodology: (i) 128° C, 4 h

Scheme 2. 5: Synthesis of quinazolin-4(3*H*)-ones **39** through Niementowski Synthesis

2.2.2.2.2 Metal catalyzed synthesis 4(3*H*)-quinazolinone

Cobalt and copper[84] have also been used as catalyst for the synthesis of 4(3*H*)-quinazolinone derivatives. The 2-substituted quinazolin-4(*3H*)-ones **40** (R′ = H) or their 3-substituted quinazolin-4(*3H)*-one derivatives (R′ = H) were prepared in high yield by reacting aliphatic, aromatic or hetero-aromatic aldehydes **41** with anthranilamide **28** in the presence of Cobalt (II) chloride or Copper (ii) chloride as catalysts in acetonitrile and ethanol at 70 °C (**Scheme 2.6**).

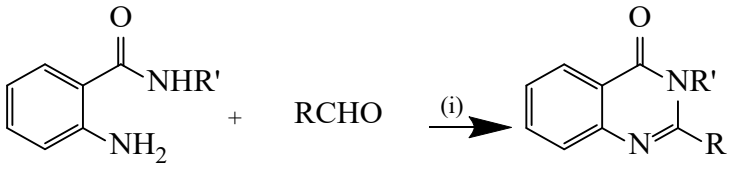

28 **40** **41**

R = Alkyl, aryl, heteroaryl

Methodology 1: (i) $CoCl_2$, CH_3CN, 70 °C

Methodology 2: (i) RCHO, EtOH, 70 °C, 3 h

(ii) 3 e.q. $CuCl_2$, EtOH, 70 °C, 3 h

Scheme 2. 6: Cobalt (II) chloride and Copper (II) chloride catalyzed synthesis of quinazolin-4(3H)-ones derivatives.

2.2.2.2.3 Synthesis of quinazolin-4(3*H*)-ones by Aza-Wittig reaction

The Aza-Wittig reaction typically encompasses a mild, multi-component synthesis of N-heterocycles[85]. In this case, iminophosphorane **42**, obtained separately by esterifying anthranilic acid with ethanol in the presence of HCl, was subjected to a reaction with an aromatic isocyanate, resulting in the formation of carbodiimide[86] **43** (**Scheme 2.7**). Subsequently, carbodiimide was reacted with ethanol to produce compound **44**, which, upon cyclization, led to the formation of the desired quinazolinones **45**.

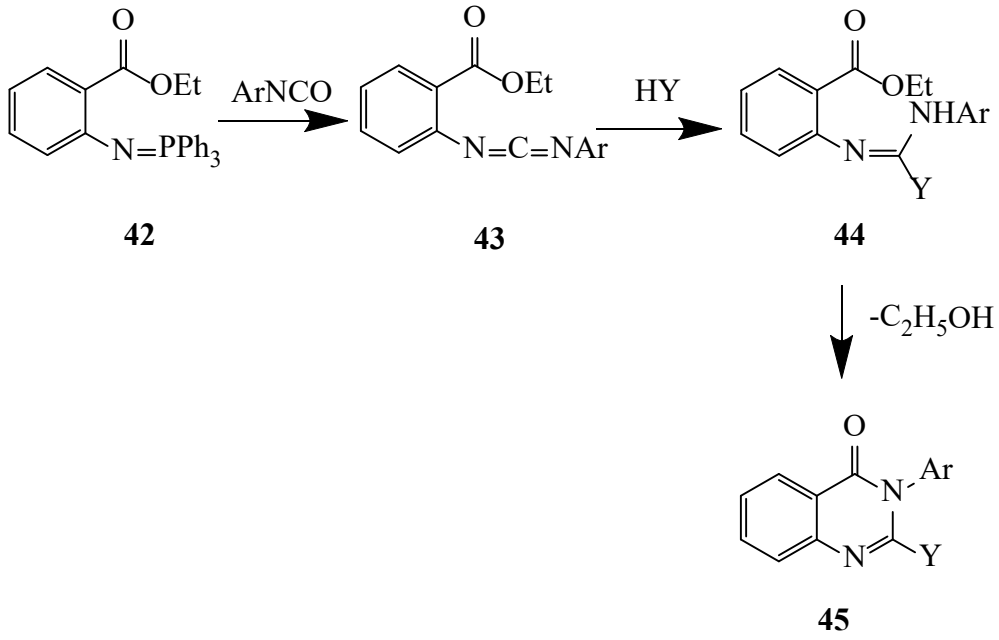

Scheme 2. 7: Aza-Wittig synthesis of quinazolin-4(3*H*)-ones.

The intriguing biological properties observed in quinazolinones are substituted with halogen atoms on the fused benzo ring (where X, X_1 = Br, I, Cl, F) (Figure 9). The incorporation of a halogen atom is through a substitution reaction on compounds like anthranilamide, aminobenzoic acid and anthranilic acid. The outcome of halogenation can yield either a monohalogenated, dihalogenated or both products, depending on the choice of halogenating

agent or the stoichiometry employed in the reaction[87]. The addition of a halogen introduces changes in the molecular properties of the compound, leading to advantageous effects such as increased fat solubility, resulting in altered absorption and transport rates, modified electronic effects, enhanced stability, and comparable steric dimensions[88]

2.2.2.2.4 Synthesis of halogenated quinazolinones

Anthranilic acid **31** was reacted with bromine (2.2 eq) in acetic acid to afford a mixture of a mono- **46** (minor) and a dibrominated anthranilic acid derivative **47** as the major product[89] **Scheme 2.8**. These compounds were further subjected to cyclocondensation with acetic anhydride or an acyl chloride to produce isatoic anhydride derivatives **48**, which were in turn reacted with primary amines to yield the corresponding halogenated quinazolinone derivatives **49**.

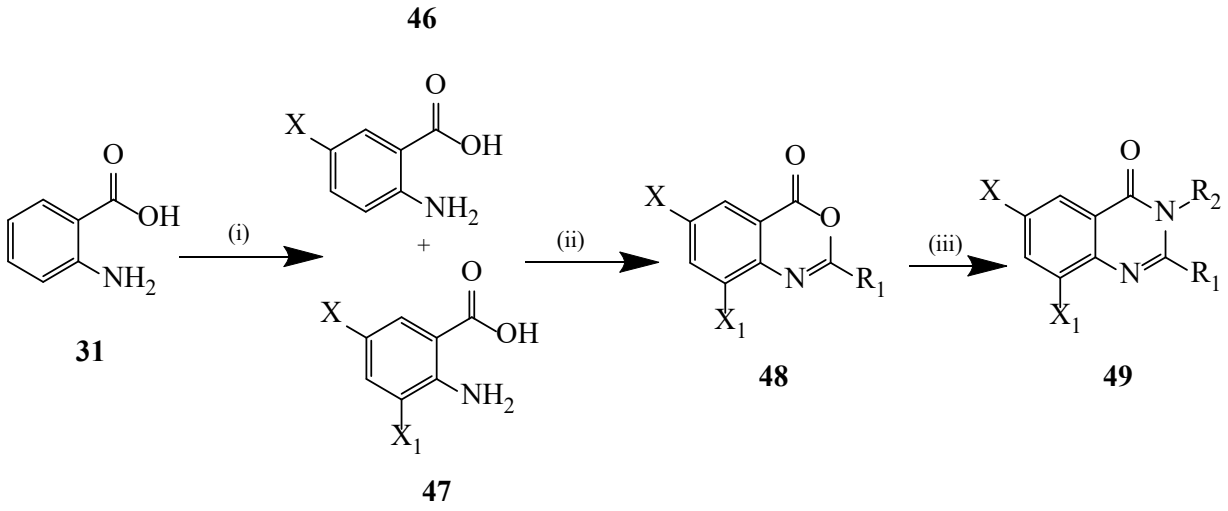

Methodology (i) Br_2/AcOH, 12 h

(ii) R_1COCl

(iii) R_2NH_2, Pyridine, reflux

Scheme 2. 8: Halogenation reaction of anthranilic acid **31** to afford quinazolinones.

Due to the hazardous nature and difficulties in handling liquid bromine, alternative brominating agents have been utilized in recent studies to achieve mono- or dibromination of anthranilamide **29**. For instance, a mixture of *N*-bromosuccinimide (NBS) in chloroform-carbon tetrachloride at room temperature[90], or pyridinium tribromide in acetic acid at room temperature[91], have been employed. These agents enable the formation of 2-amino-5-bromobenzamide or 2-amino-3,5-dibromobenzamide **50**. Subsequently, the obtained 2-amino-3,5-dibromobenzamide was subjected to a cyclocondensation reaction with benzaldehyde derivatives under solvent-free conditions, utilizing boric acid as a catalyst. This reaction yielded the corresponding quinazolin-4(3H)-ones **51** (**Scheme 2.9**).

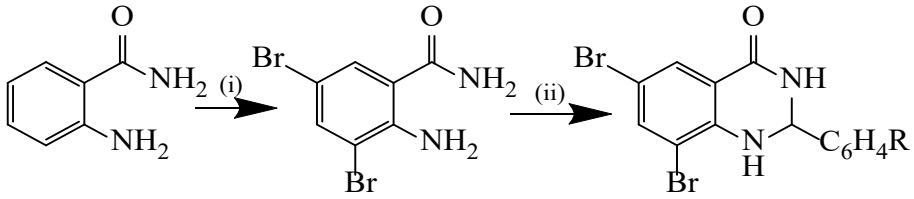

28 **50** **51**

Methodology (i) NBS, $CHCl_3$-CCl_4, rt, 3 h

(ii) ArCHO, boric acid, 120 ºC

Scheme 2. 9: Dibromination of **28** and subsequent cyclocondensation of **51** with benzaldehydes.

Mudassar *et al.* used iodine monochloride as a source of iodine to effect direct iodination of quinazolinone **52** to afford the 6-iodo-3-amino-2-methylquinazolin-4(*3H*)-ones[92] **54** (**Scheme 2.10**). Compound **53** was prepared from cyclocondensation of anthranilic acid **31** with acetic

anhydride followed by reaction of the incipient isatoic anhydride derivative **53** with hydrazine monohydrate. Nucleophilic attack of an aldehyde to compound **54** afforded compound **55.**

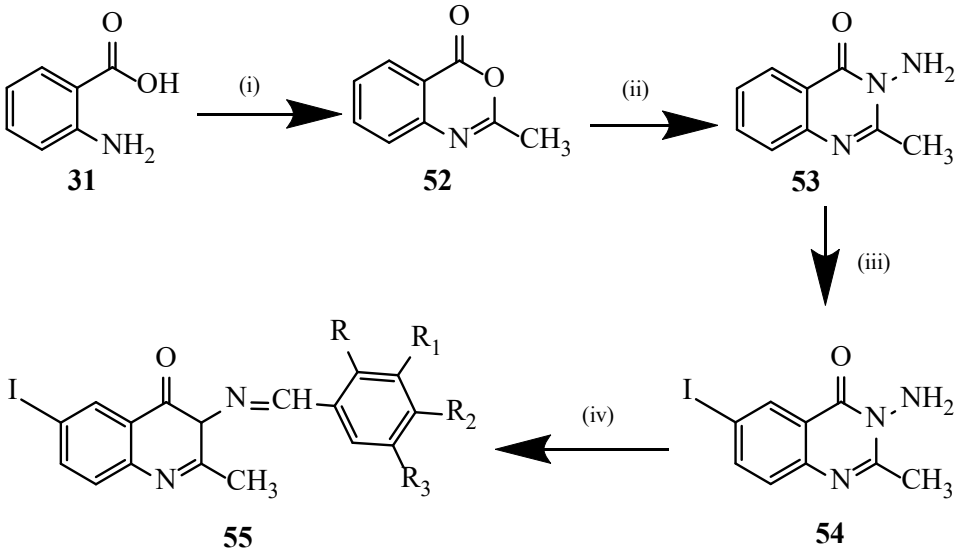

Methodology: (i) Ac_2O, 3h

(ii) $NH_2NH_2.H_2O$, MeOH

(iii) ICl in AcOH, rt, overnight

(iv) hydroxysubstituted benzaldehyde, MeOH, AcOH, rt, 3 h

Scheme 2. 10: Preparation of derivatives of iodinated quinazolinone **54**.

2.2.2.2.5 Methods for the synthesis of quinazolin-4(3*H*)-one derivatives using transition metals.

Methods for the synthesis of quinazolin-4(3*H*)-one derivatives that make use of transition metals as catalysts in this transformation have also been developed and some of these are described in detail below.

2.2.3 Application of transition metals in the synthesis of quinazolin-4(3*H*)-ones

Several methods for the synthesis of quinazolin-4(*3H*)-ones that make use of transition metals as catalysts in the synthesis of quinazolinones have been described in the literature. Xia *et al*, for example, reacted a mixture of halogenated anthranilamide **56**, aryl halides **57** and *tert*-butyl isocyanide **58** in the presence of palladium dichloride–1,3-bis(diphenylphosphino)propane (DPPP) catalyst complex and calcium chloride in toluene at 145 °C to afford the corresponding halogenated quinazolin-4(3*H*)-ones **59** in moderate to high yields[93] **Scheme 2.11**. The analogous 6,8-dibromo-2-methylquinazolin-4(1*H*)-one and 6-iodo-2-methylquinazolin-4(1*H*)-one were found to exhibit some antihyperlipidemic activity through the inhibition of dietary cholesterol absorption[94]. 6,8-Dibromo-3-phenyl-2-styrylquinazolin-4(3*H*) one, on the other hand, has been found to exhibit antihypertensive activity comparable to prazosin's[95].

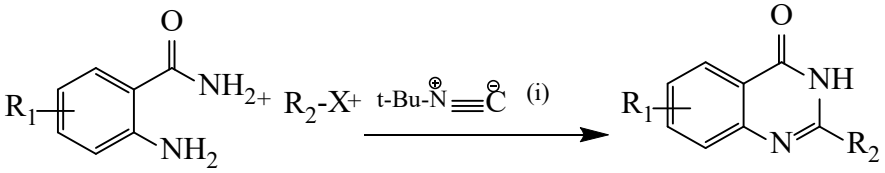

56 **57** **58** **59**

Methodology: (i) $PdCl_2$, DPPP, $CaCl_2$, toluene, 145 °C

Scheme 2. 11: Palladium catalyzed one pot synthesis of quinazolin-4(3*H*)-one's derivatives.

Jianguang *et al.*[96] reported a one pot synthesis of quinazolinone derivatives **63** involving the reaction of anthranilamide derivatives **60** with primary alcohol **61** in the presence pentamethylcyclopentadienyl iridium dichloride $[CpIrCl_2]_2$ as catalyst under hydrogen transfer conditions (**Scheme 2.12**).

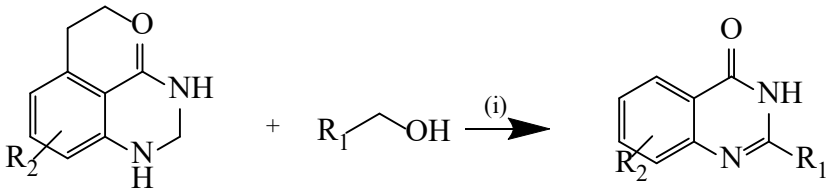

60 **61** **62**

Methodology: (i) $[CpIrCl_2]_2$, xylene, reflux with or without styrene

Scheme 2. 12: $[CpIrCl_2]_2$ catalyzed synthesis of quinzaolin-4(3*H*)-ones derivatives.

The next sections describe the transition metal catalyzed cross-coupling of halogenated quinazolinones to afford polysubstituted derivatives. Halogenated quinazolinones serve as adaptable building blocks in various metal-catalyzed reactions that involve the formation of carbon-carbon bonds, including the Stille, Kumada, Negishi, Suzuki-Miyaura, Sonogashira, Heck and Buchwald-Hartwig cross-coupling reactions.

2.2.4 Application of transition metal catalyzed cross-coupling reaction in the synthesis of polysubstituted quinazolinones from halogenated precursors.

2.2.4.1 Application of Suzuki-Miyaura cross coupling reaction

Suzuki-Miyaura cross coupling reaction involves the reaction of organoboron compound with organic halides or related electrophile in the presence of a palladium as a catalyst for carbon-carbon bond formation. To introduce novel substituted quinazolinones, modifications were made to **63** at the C-6 position using the Suzuki-Miyaura cross-coupling reaction[97]. Two distinct

palladium-based pre-catalyst systems, namely [$PdCl_2$(dcpf)] and $Pd(PPh_3)_4$, were selected for screening. The Na_2CO_3 was used as a base in a mixture of 1,4-dioxane and water (3:1) at reflux temperature[98].

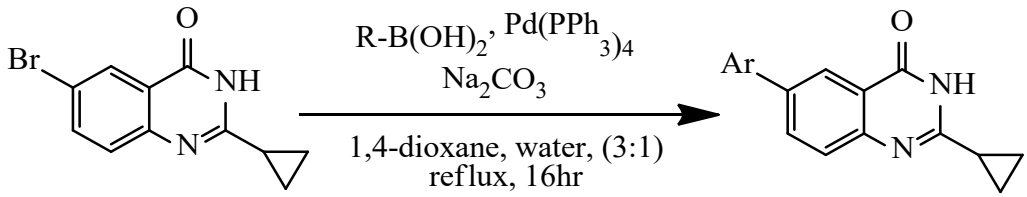

63 **64**

Scheme 2. 13: Suzuki -Miyaura application to afford quinazolinones.

In another study, the reaction occurred with K_2CO_3 as a base, tetrahydropyran (THP) served as the solvent for conducting the reactions using various palladium catalysts as Pd (0) sources. Among the palladium catalysts tested, 1,1'-bis(dicyclohexylylphosphino)ferrocene-palladium (II) dichloride [$PdCl_2$(dcpf)] and 1,1'-bis(di-tert-butylphosphino)ferrocene-palladium dichloride [$PdCl_2$(dtbpf)] demonstrated superior performance, yielding products in the range 84%-95%.

2.2.4.1 Application of Kumada-cross coupling reaction

Kumada cross-coupling reaction involves the reaction of Grignard reagent with organic halides such as alkyl, vinyl, and aromatic halides in the presence of palladium or nickel as a catalyst to form Csp^2-Csp^3 bond [99]. The Kumada Coupling offers an alternative method for forming carbon-carbon bonds, utilizing environmentally friendly magnesium organometallics. The investigation focused on the Kumada cross-coupling reaction involving 6-iodo-2-phenylquinazolin-4-(3*H*)-one **65** and nine different aryl/heteroaryl Grignard reagents as substrates. $NiCl_2$(dppe) was employed as a catalyst at a concentration of 10 mol % in THF at ambient temperature. The

reaction reached completion within a 3-hour timeframe, resulting in the isolation of C-C coupled products with high yields, noteworthy advantages of this method over the Suzuki coupling reaction included significantly reduced reaction time, mild temperature conditions, and simplified workup procedures[100].

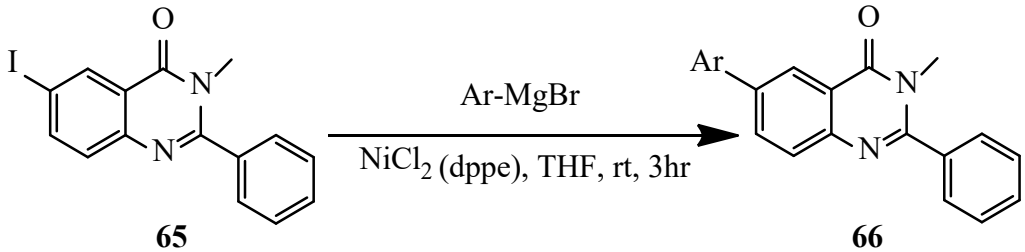

65 **66**

Scheme 2. 14: Kumada cross coupling reaction to form a quinazolinone.

A quinazolinone synthesized through Kumada cross coupling as key step, having therapeutic activity is Afloqualone (HQ-495). It is a compound that acts on GABA receptors and exhibits agonistic activity specifically at the β subtype of the GABAα receptor. Its antivertiginous effects are believed to stem from its ability to enhance the sensitivity of GABA receptors located at the LVN neuron site[101].

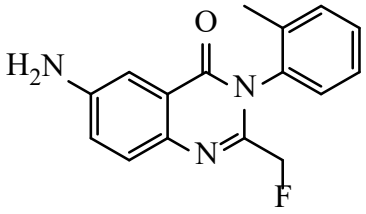

21

Figure 2. 8: Quinazolinones synthesized through Kumada cross coupling.

2.2.4.3 Application of Stille cross coupling

The Stille coupling requires the presence of a palladium catalyst, which facilitates the coupling reaction between the organotin compound and the organic electrophile. The palladium catalyst helps in breaking the carbon-halogen (C-X) bond in the electrophile and the carbon-tin (C-Sn) bond in the organotin compound. This leads to the formation of a reactive intermediate, a palladium-organic species. A study by Stelmach *et al* synthesized dihydroquinazolinones[102] through Stille cross coupling. The desired coupled product was obtained through the Stille coupling of with the vinyl tin reagent. Subsequently, the trisubstituted double bond underwent hydrogenation, and the BOC group was eliminated by acid treatment, resulting in the formation of analogues **68a–c**. These compounds were synthesized as potential inhibitors of p38 MAP kinase.

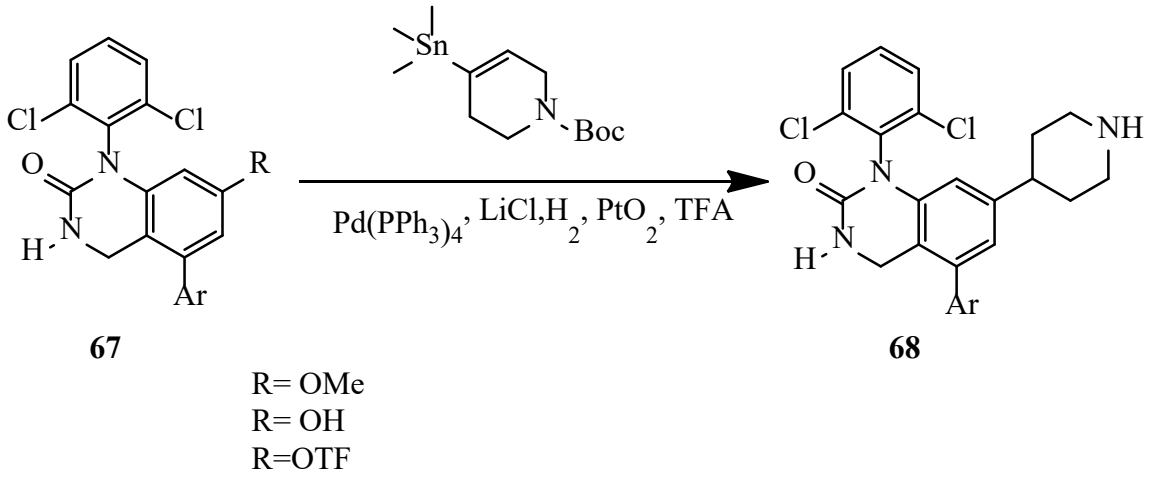

Scheme 2. 15: Stille cross coupling to afford derivatives of dihydroquinazolinones.

2.2.4.4 Application of Negishi cross coupling reaction

Negishi cross-coupling is based on the reaction between organozinc reagents and organic halides as seen in **Figure 2.16**. It is a versatile tool for carbon-carbon bond formation. The organozinc reagent and the quinazolinone are brought together in the presence of the palladium catalyst. The palladium catalyst activates the carbon-halogen (C-X) bond in the organic halide and the carbon-nitrogen (C-N) bond in the quinazolinone **69**, leading to the formation of a reactive intermediate. A study of Spiroquinazolinones as selective PDE7 inhibitors by Lorthiois *et al* used Negishi cross coupling[103] to achieve the desired derivatives spiroquinazolinones **70**.

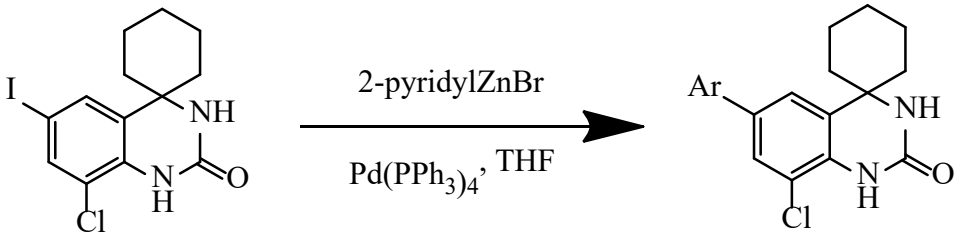

69 **70**

Ar=C_6H_4, CO_2H,4-pyridyl

Scheme 2. 16: Negishi cross coupling reaction to form quinazolinones **7**.

2.2.4.5 Sonogashira cross coupling reaction on quinazolinones

The Sonogashira cross-coupling reaction is a method for the synthesis of alkynes through the reaction of terminal alkynes with aryl or vinyl halides or triflates. This can be achieved through various methods, such as deprotonation of a terminal alkyne or transformation of a suitable precursor into the terminal alkyne form. The Sonogashira cross-coupling requires a palladium catalyst, commonly a palladium (0) species, to facilitate the coupling between the terminal alkyne and the aryl or vinyl halide present in the quinazolinone precursor. The palladium catalyst

promotes the activation of the carbon-halogen (C-X) bond in the halide and the carbon-hydrogen (C-H) bond in the terminal alkyne. A study by Poudapally *et al* investigated the C(*sp*)–C(*sp2*) bond formation using Sonogashira cross-coupling reactions on 6-halo-2-cyclopropyl-3-(pyridyl-3-ylmethyl)quinazolin-4(3*H*)-ones **71** with suitable alkynes to afford **72**. The researchers conducted optimization of reaction conditions, exploring various catalysts, ligands, bases, and solvents.

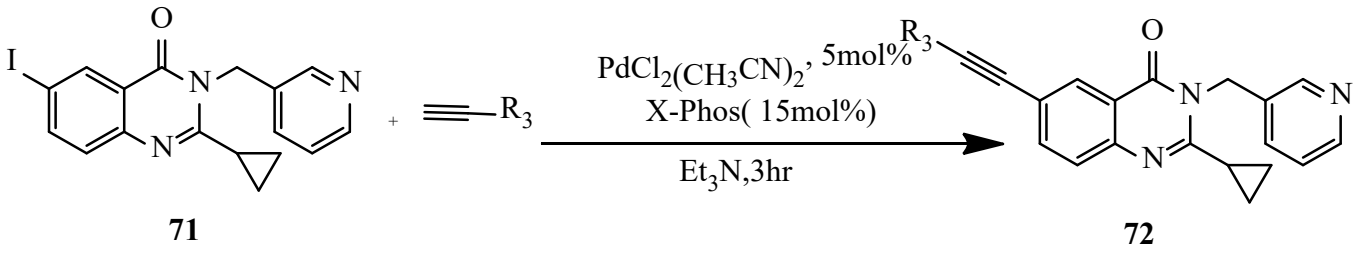

71 72

Scheme 2. 17: Sonogashira cross coupling reaction on quinazolinones.

2.3 Hypothesis

Given the increasing demand for novel and effective anticancer therapeutics, it is hypothesized that sulphonated styryl quinazolinones, structurally characterized by their fused quinazolinone core and sulphonated styryl substituents, possess inherent chemical attributes that render them promising candidates for targeted cytotoxicity against various cancer cell lines. Building upon the recognized anticancer potential of quinazolinone derivatives and the modulatory effects that sulphonated styryl moieties can confer, the central hypothesis of this study postulates that the strategic incorporation of styryl substituents onto the quinazolinone scaffold may enhances the compound’s capacity to disrupt key cellular processes implicated in cancer progression. Through their interactions with critical cellular components, including enzymes, receptors, and signaling pathways, elicit multifaceted responses within cancer cells.

2.4 Aims and objectives.

2.4.1 Aims

The aim of this study was to design, synthesize, perform molecular model studies and biologically evaluate aryl substituted 2-(4-(sulfonyl)styryl)quinazolin-4(3*H*)-ones with the intention of investigating their potential as agents for combating cancer.

2.4.2 Objectives

• Synthesize iodinated anthranilamide.

• Acetylate the resulting 2-amino-5-iodobenzamide.

• Base mediated cyclization of 2-aceto-5-iodobenzamide to yield 6-iodo-2-methylquinazolin-4(3*H*)-one.

• Sulphonate a series of hydroxybenzaldehyde.

• Condensation of the sulphonated hydroxybenzaldehyde's with 6-iodo-2-methylquinazolin-4(3*H*)-ones under Aldol reaction conditions.

• Employ Suzuki cross coupling reaction on the 6-iodo-3,4-sulphonated styryl dihydroquinazolin-4(3*H*)-ones using arylboronic acids.

• Subject the resultant aryl-substituted 2-(4-(sulfonyl)styryl)quinazolin-4(3*H*)-one derivatives to coordination with ruthenium(II) complex.

• Investigate the potential anti-cancer properties of the synthesized compounds.

• Conduct molecular docking studies to assess the binding interactions and potential binding modes of the synthesized compounds.

A series of arylsulfonamide derivatives containing 6-aryl-2-methylquinazolin-4(3*H*)-ones were obtained based on their synthetic feasibility and synthesized with moderate to good yields by the following reactions outlined in **scheme 2.18.**

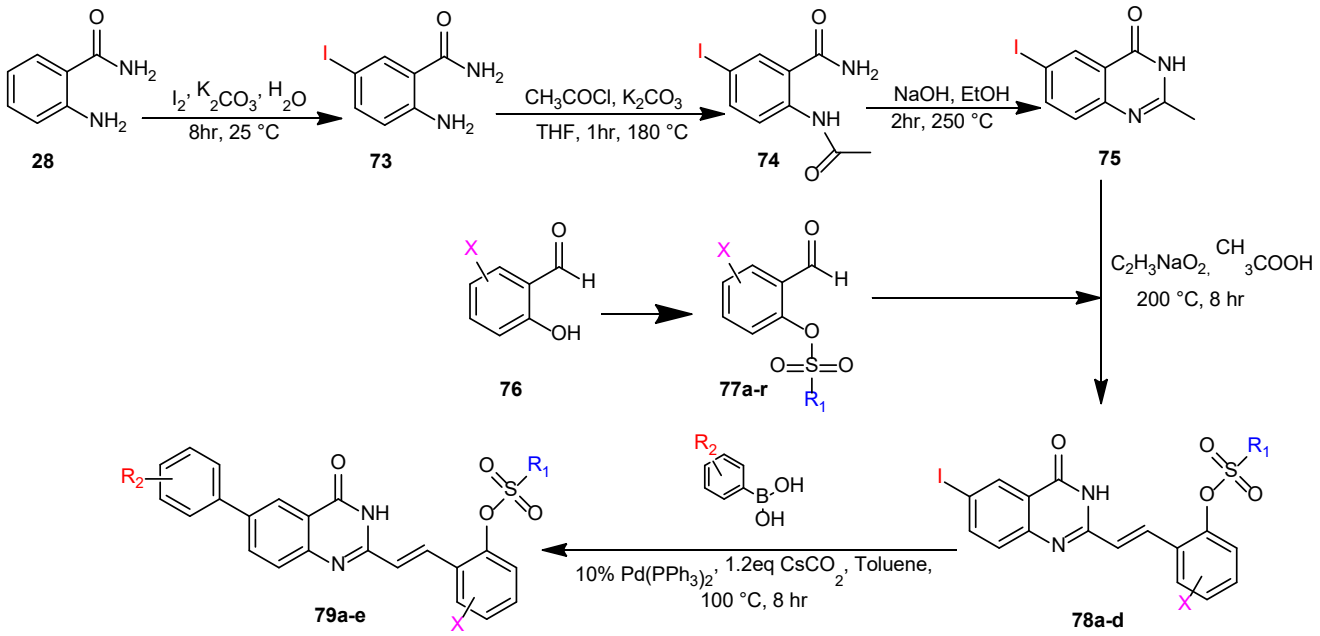

Scheme 2. 18: Methodology for synthesis of 2-(4-(sulfonyl)styryl)quinazolin-4(3*H*)-ones.

CHAPTER 3: RESULTS AND DISCUSSION

The successful synthesis and comprehensive characterization of sulfonated benzaldehydes and styryl-quinazolin-(3*H*)-ones were achieved through a rigorous experimental protocol. Utilizing a combination of spectroscopic techniques that include NMR, IR, MS, and XRD complemented with DFT. The chemical structures and properties of the synthesized compounds were elucidated with high precision. Overall, these results demonstrate the successful synthesis, laying a solid foundation for further investigations and molecular studies.

3.1 Preparation of 2-amino-5-iodobenzamide

Synthesis of 6-carbo–substituted 2-styrylquinazolin-4(3*H*)-ones was preceded by synthesis of 2-amino-5-iodobenzamide as the starting material following a literature procedure by Stein *et al.*[104]. The iodination substitution reaction of anthranilamide (2-aminobenzamide) entails the replacement of one of the hydrogen atoms attached to the benzene ring, *para* to the amine, with an iodine atom from a method reported by Stein *et al.*[105] shown below (**Scheme 3.1**). The chemical transformation is conventionally conducted by subjecting anthranilamide to iodine, utilizing sodium hydrogen carbonate as a base and water as a solvent. The reaction occurs at ambient temperature for about six hours.

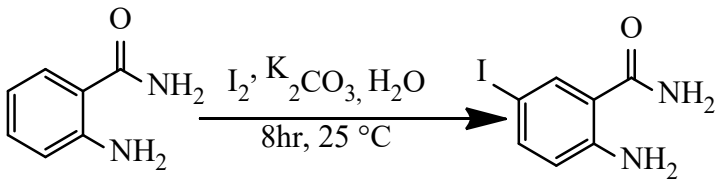

28 **73**

75%

Scheme 3. 1: Synthesis of 2-amino-5-iodobenzamide **73**

Compound (**73**) was obtained in the form of a purple crystalline product with a yield of 75%. Characterization was carried out using nuclear magnetic resonance (NMR) spectroscopy in DMSO-d_6. The ^{1}H-NMR spectrum of compound **73** displayed a decrease in multiplicities as one of the aromatic protons was replaced by an iodine atom (as illustrated in **figure 3.1**). A doublet of doublet and a doublet signal, due to coupling by ^{3}J and ^{4}J coupling constants by hydrogens on carbon 4 and 6 are observed at 7.38 ppm and 7.69 ppm, corresponding to the aromatic hydrogens on the anthranilamide ring. A doublet and singlet signals were observed at 6.54 ppm and 6.72 ppm, corresponding to the aromatic hydrogen of the anthranilamide and the two hydrogens of the amide functional group, respectively. A singlet peak at 7.03 ppm, which integrate for one proton, is attributed to one of the hydrogens of the amine functionality. Another single peak integrated for one (1) amine hydrogen proton at 7.80 ppm. The ^{13}C NMR spectrum of **73** exhibited a total of six (6) carbon peaks in the aromatic region and one (1) upfield for the carbon-Iodine (ArC-I) as seen in **figure 3.2**. The melting point was determined to be in the range of 221.09 - 230.78 °C.

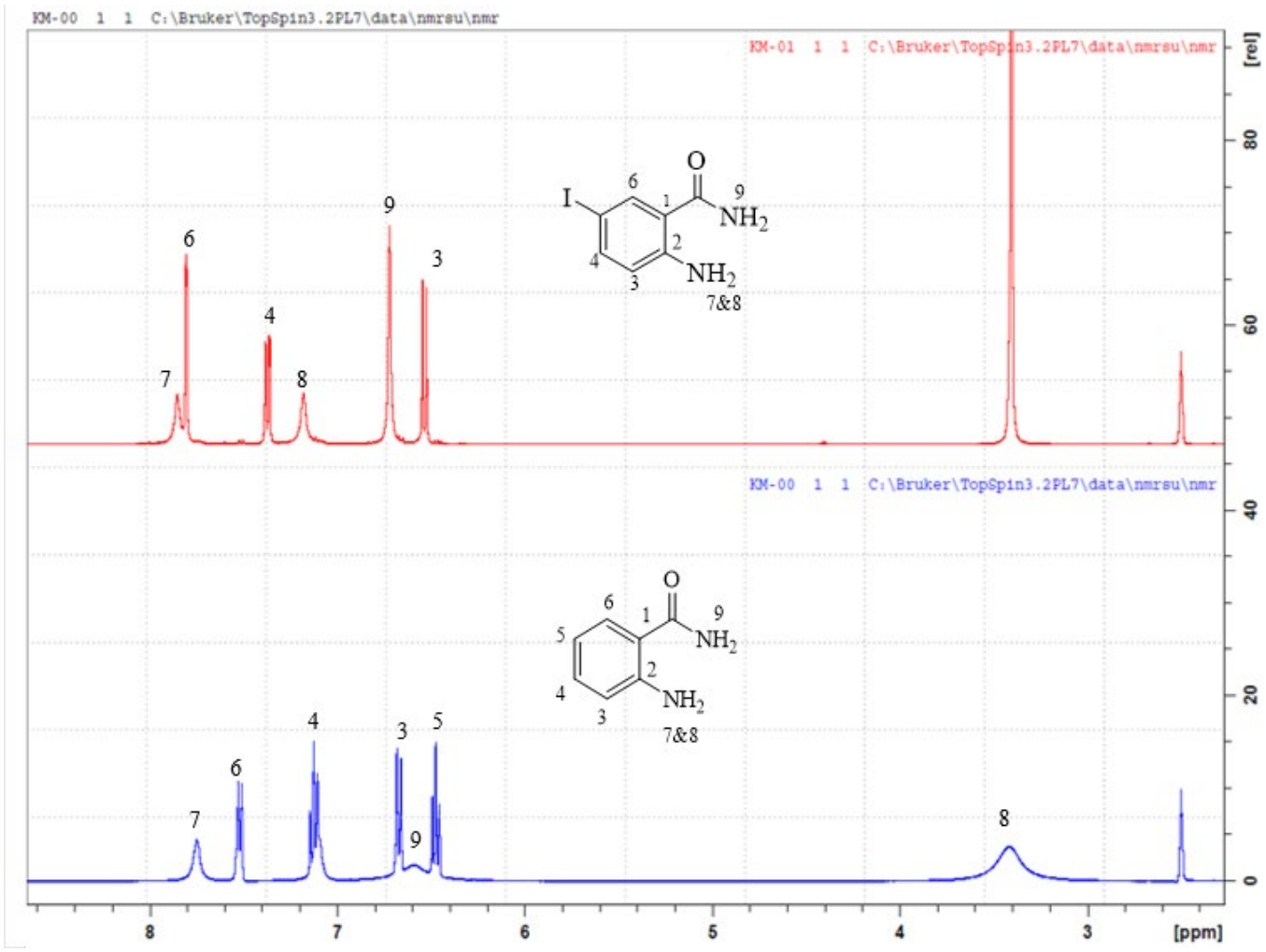

Figure 3. 1: ^{1}H NMR of **73**

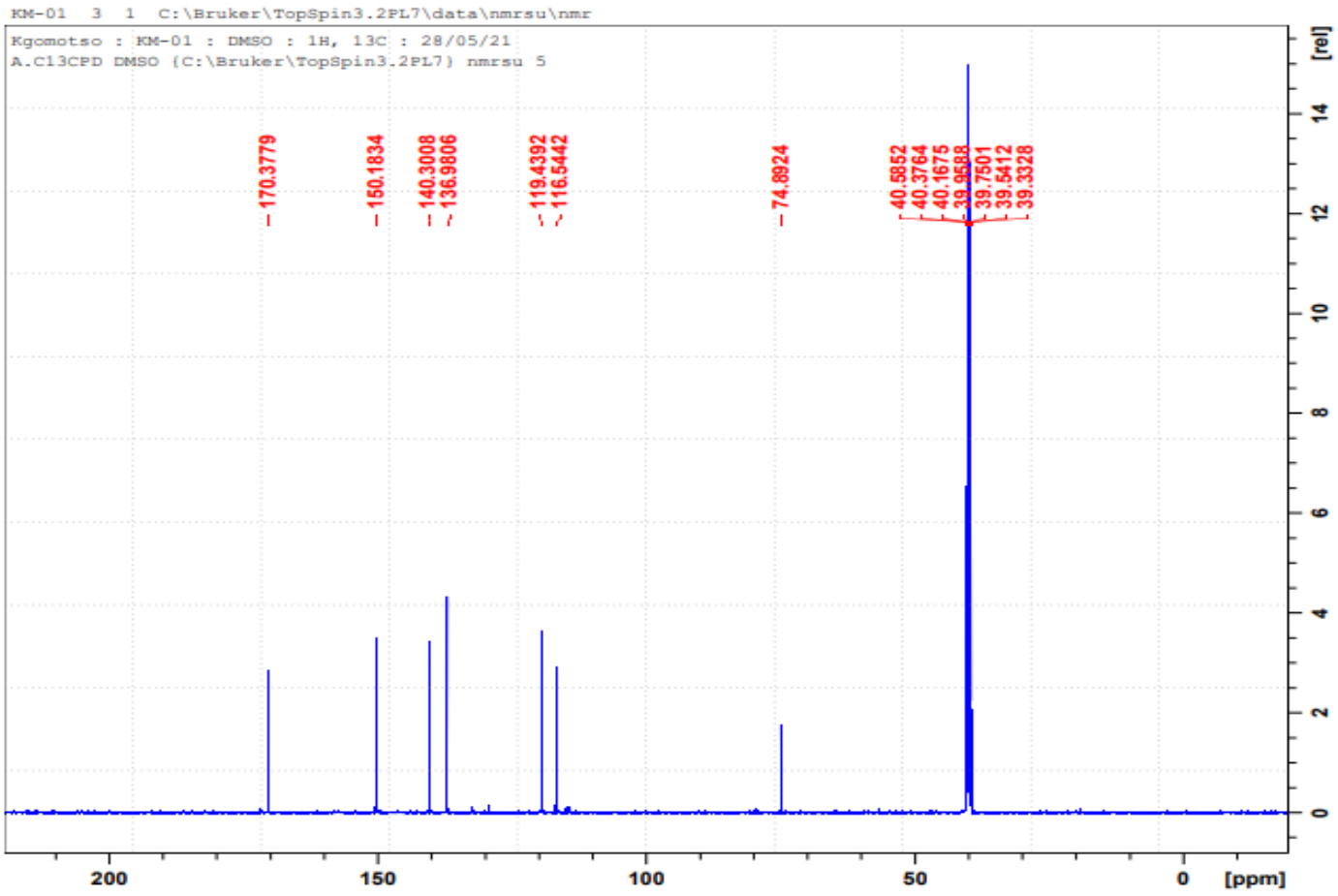

Figure 3. 2: ^{13}C NMR of **73**

3.2 Preparation of 2-acetamido-5-iodobenzamide

The next synthetic procedure involves acetylation of the 2-amino-5-iodobenzamide **73** with acetyl chloride. The synthesis began by dissolving **73** in tetrahydrofuran, followed by the addition of 1.5 stoichiometric equivalents of potassium carbonate, serving as a base, and 1.3 stoichiometric equivalents of acetyl chloride, which functions as an acetyl source to Iodinated compound as described by Kurbatov *et al*.[106]. The reaction took place under reflux conditions with continuous stirring for approximately one hour. The reaction affording 2-acetamido-5-iodobenzamide in 67% yield.

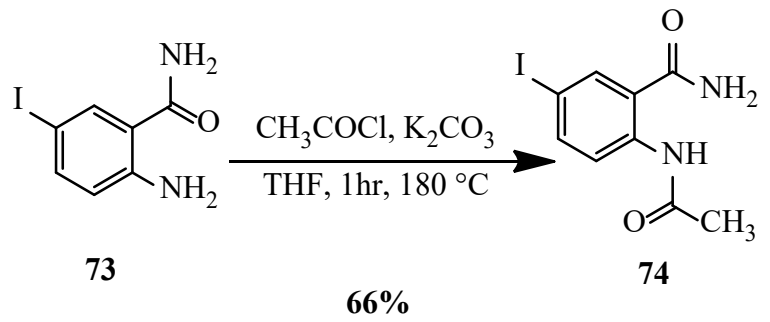

73 **74**

66%

Scheme 3. 2: Synthesis of 2-acetamido-5-iodobenzamide **74**

Compound **74** was obtained as a purple crystalline product. The acetylated product **74** was then characterized by ^{1}H and ^{13}C NMR spectroscopy, recorded in DMSO-d_6. The ^{1}H NMR spectrum shows a singlet peak at 2.38 ppm, integrating for three (3) protons of the methyl, and another singlet peak at 11.02 ppm, integrating for one (1) proton, which is attributed to the -NH proton on the secondary amine. Additionally, a doublet of doublet peak at 8.48 ppm integrating for one (1) proton and two doublets at 7.88 ppm and 8.38 ppm integrating for one (1) proton each were assigned to the ring (as illustrated in **figure 3.3**). The ^{13}C NMR spectrum displayed two (2) carbonyl carbons in the downfield region, six (6) carbons in the aromatic region and one (1) carbon in the high field region of the methyl (**figure 3.4**). The compound exhibited a melting point of 95.01-99.92 °C.

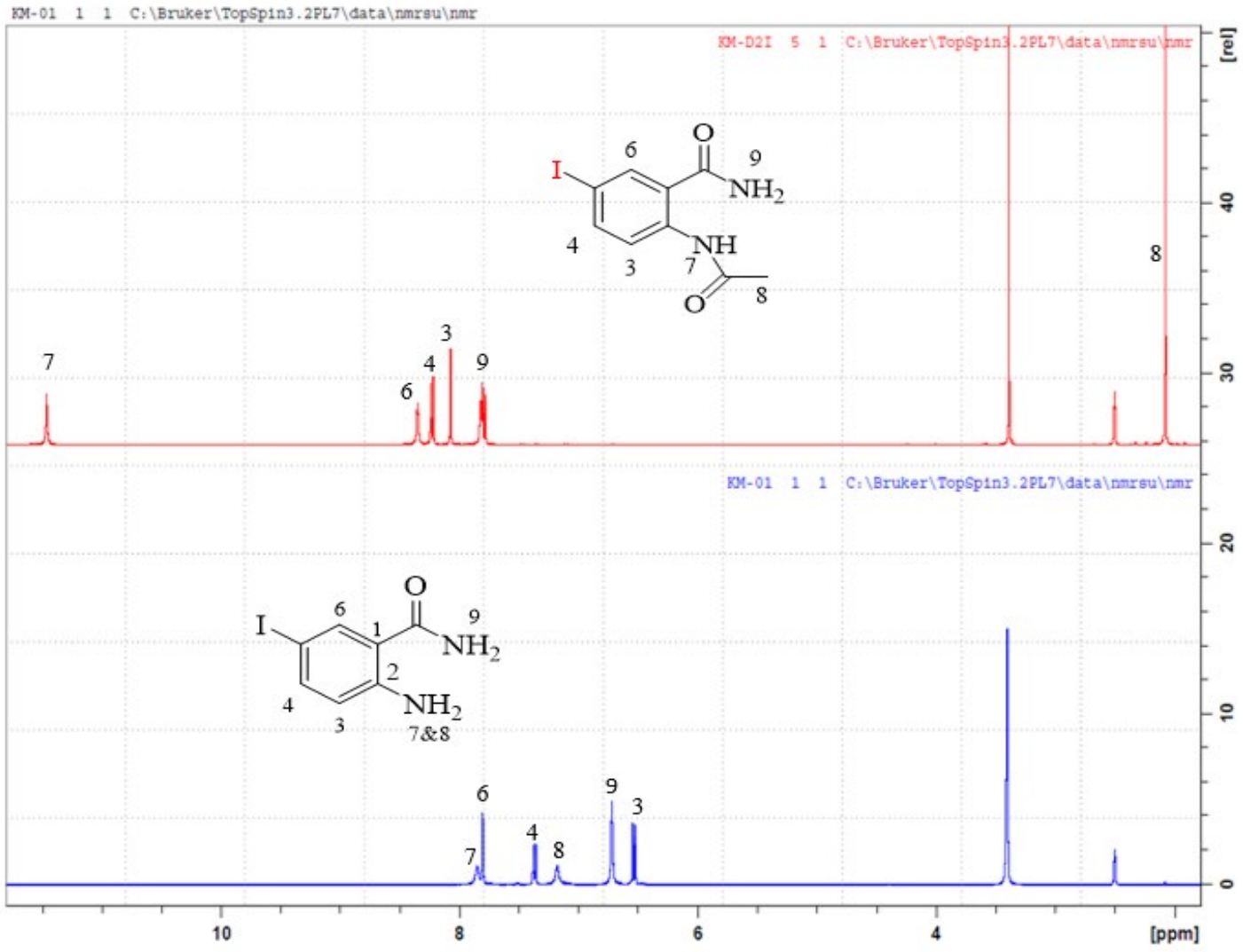

Figure 3. 3*:* ^{1}H NMR of **74**

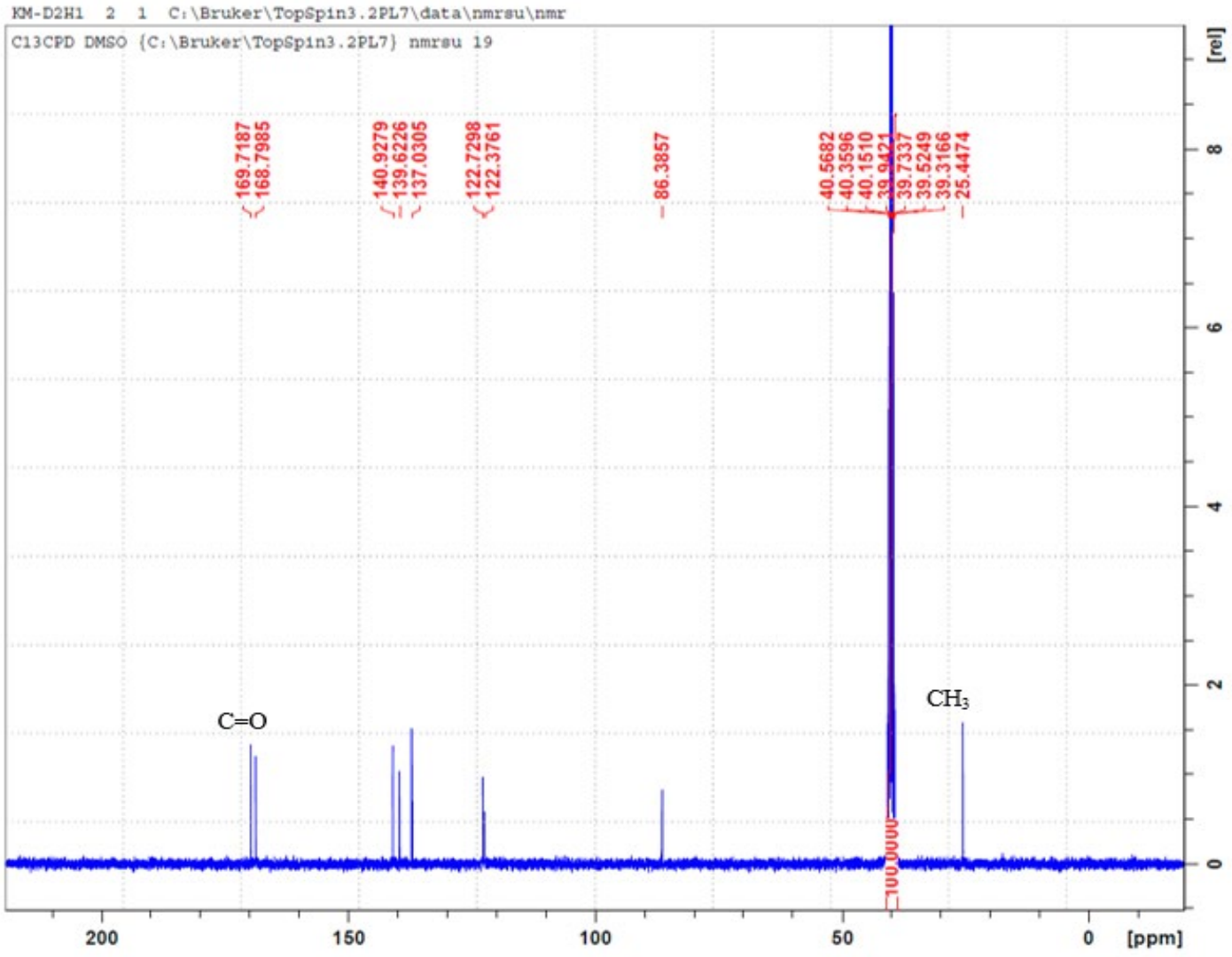

Figure 3. 4: ^{13}C NMR of **74**

3.3 Preparation of 6-iodo-2-methylquinazolin-4(3*H*)-one

The acetylated product **75** underwent a cyclisation reaction to afford a quinazolin-4(3*H*)-one, which is synthesized through a base-promoted cyclisation reaction of 2-acetamido-5-iodobenzamide following a method reported by Agbo *et al*[107]. This synthetic procedure proceeds under reflux conditions, in an ethanol: sodium hydroxide solvent system. The acetylated compound results in the formation of 6-iodo-2-methylquinazolin-4(3*H*)-one. Based on

consumption of the starting material on TLC, the solution was rapidly cooled by introducing crushed ice, effectively terminating the ongoing reaction. Sulphuric acid was then added to the reaction mixture, resulting in the formation of a milky solution with precipitates which was subsequently subjected to filtration.

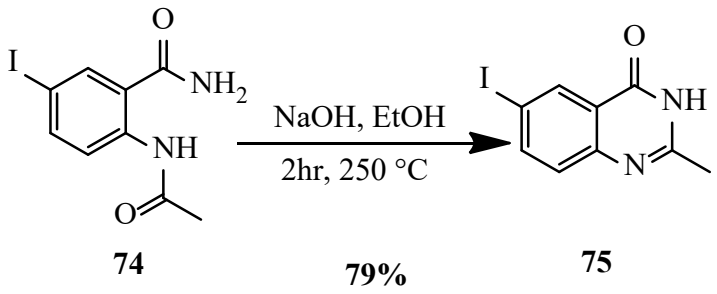

74 **79%** **75**

Scheme 3. 3: Synthesis of 6-iodo-2-methylquinazolin-4(3*H*)-one **75**

Compound **75** was obtained as a white solid product. The product was then characterized by ^{1}H NMR and FTIR. ^{1}H NMR spectrum shows a singlet peak at 2.47 ppm, integrating for three (3) protons of the methyl, and another broad singlet peak at 4.12 ppm, indicating the -OH and –NH group, which tend to appear as tautomers in DMSO (dimethyl sulfoxide), DMSO destabilizes the keto form of the compound containing these functional groups, favouring the enol or enamine tautomeric forms[108]. Additionally, the ^{1}H NMR spectrum of **88** shows a doublet resonance at 7.28 ppm integrating for one proton due to ^{3}J coupling to H-5. The ^{1}H NMR spectrum also shows a doublet of doublet resonance at 8.28 ppm integrating for one proton due to ^{3}J and ^{4}J coupling to H-5 and H-7. In the ^{1}H NMR spectrum there was also a doublet resonance at 8.45 -8.50 ppm integrating for one proton due to ^{4}J coupling to H-5 (illustrated in Figure 3.5). The compound exhibited a melting point of 95.01-99.92 °C.

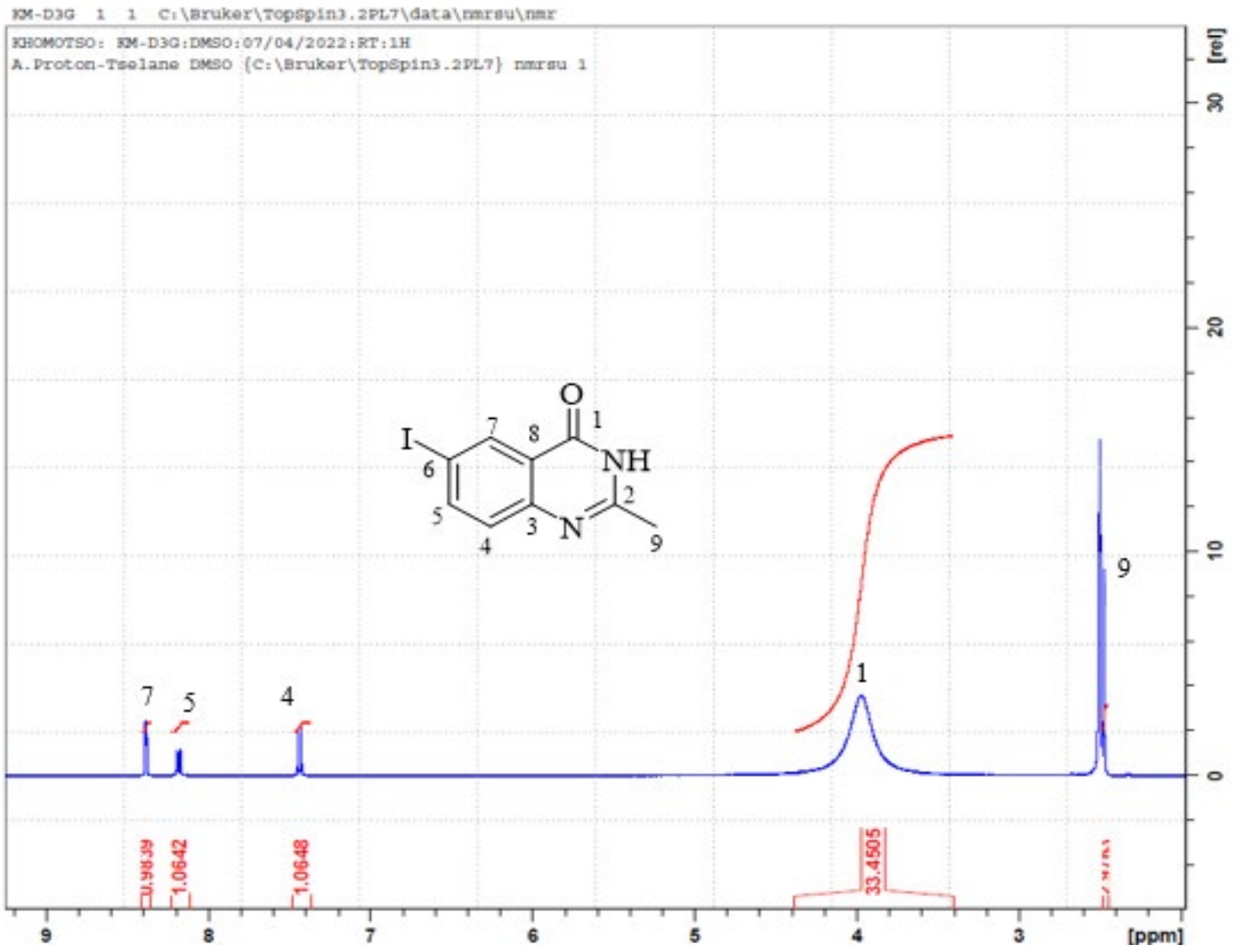

Figure 3. 5: ^{1}H NMR of **75**

3.4 Preparation of sulfonated hydroxy benzaldehydes

The sulphonation process of hydroxybenzaldehyde's entails the incorporation of derivatised sulphur moieties onto the oxygen atom of the hydroxyl group position on the benzaldehyde (**Scheme 3.4**). This chemical transformation is traditionally accomplished by subjecting two hydroxybenzaldehyde's, namely 3-methoxy-4-hydroxybenzaldehyde and 5-bromo-2-hydroxybenzaldehyde to various sulphonation agents in pyridine[109]. The reaction takes place at

low temperatures i.e. regulated by ice-filled vessel for a duration of two hours. The reaction was monitored for completion for two hours after which the reaction mixture was then quenched using crushed ice and then subjected to filtration. The resulting precipitate was subjected to recrystallization using ethanol, yielding well-defined crystals.

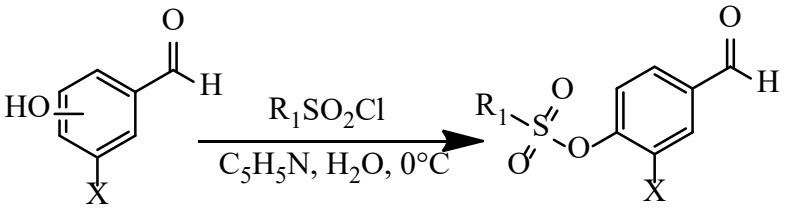

76a-r

where X is Br and OCH_3

65-89%

Scheme 3. 4: Synthesis of sulfonated benzaldehydes **76a-r**.

Table 3. 1: Derivatives of sulphonated hydroxybenzaldehyde

	R_1	%Yield	Compound number
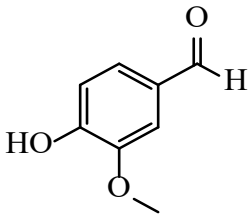	$-CH_3$	78.23	**76a**
	$-C_6H_5$	70.87	**76b**
	$--C_6H_5$-4-F	81.55	**76c**
	$-C_6H_5-NO_2$	72.14	**76d**
	$-C_6H_5-OCH_3$	89.36	**76e**
	$-C_6H_5-CH_3$	74.92	**76f**
	$-C_6H_5-CH_3F_3$	68.61	**76g**
	$-C_6H_5-OCH_3F_3$	92.05	**76h**

	-C_6H_5-$NHCOCH_3$	83.79	**76i**
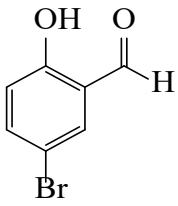	-CH_3	90.42	**76j**
	-C_6H_5	78.23	**76k**
	-C_6H_5-4-F	70.87	**76l**
	-C_6H_5-NO_2	81.55	**76m**
	-C_6H_5-OCH_3	72.14	**76n**
	-C_6H_5-CH_3	89.36	**76o**
	-C_6H_5-CH_3F_3	74.92	**76p**
	-C_6H_5-OCH_3F_3	68.61	**76q**
	-C_6H_5-$NHCOCH_3$	92.05	**76r**

Compound **76b** was obtained as a white crystalline product. The product was characterized by ^1H and ^{13}C NMR spectroscopic technique, recorded in DMSO-d_6 and X-ray diffraction. The ^1H NMR of compound **76b** displayed the presence of doublet of doublet peak in the aromatic region 7.97 ppm, representing two (2) protons brought by the benzene sulfonyl group as compared to starting material, and another doublet of doublets around 8.23 ppm, integrating for two (2) protons, were attributed to the sulfonyl ring. A distinct singlet resonance at 9.94 ppm, corresponding to a single proton, was observed, indicating the presence of an aldehyde functional group in the structure of compound **76b**. This observation serves as confirmation of the successful incorporation of the benzene sulfonyl group. The proton of the aldehyde group experiences a unique chemical environment due to its proximity to the carbonyl oxygen (strong electron withdrawing group). The methoxy protons are observed as singlets in the ^1H NMR spectrum of compound **76b** at around

3.56 - 3.76 ppm, which integrated for three (3) protons. The compound exhibited a melting point of 164.65 -165.00 °C.

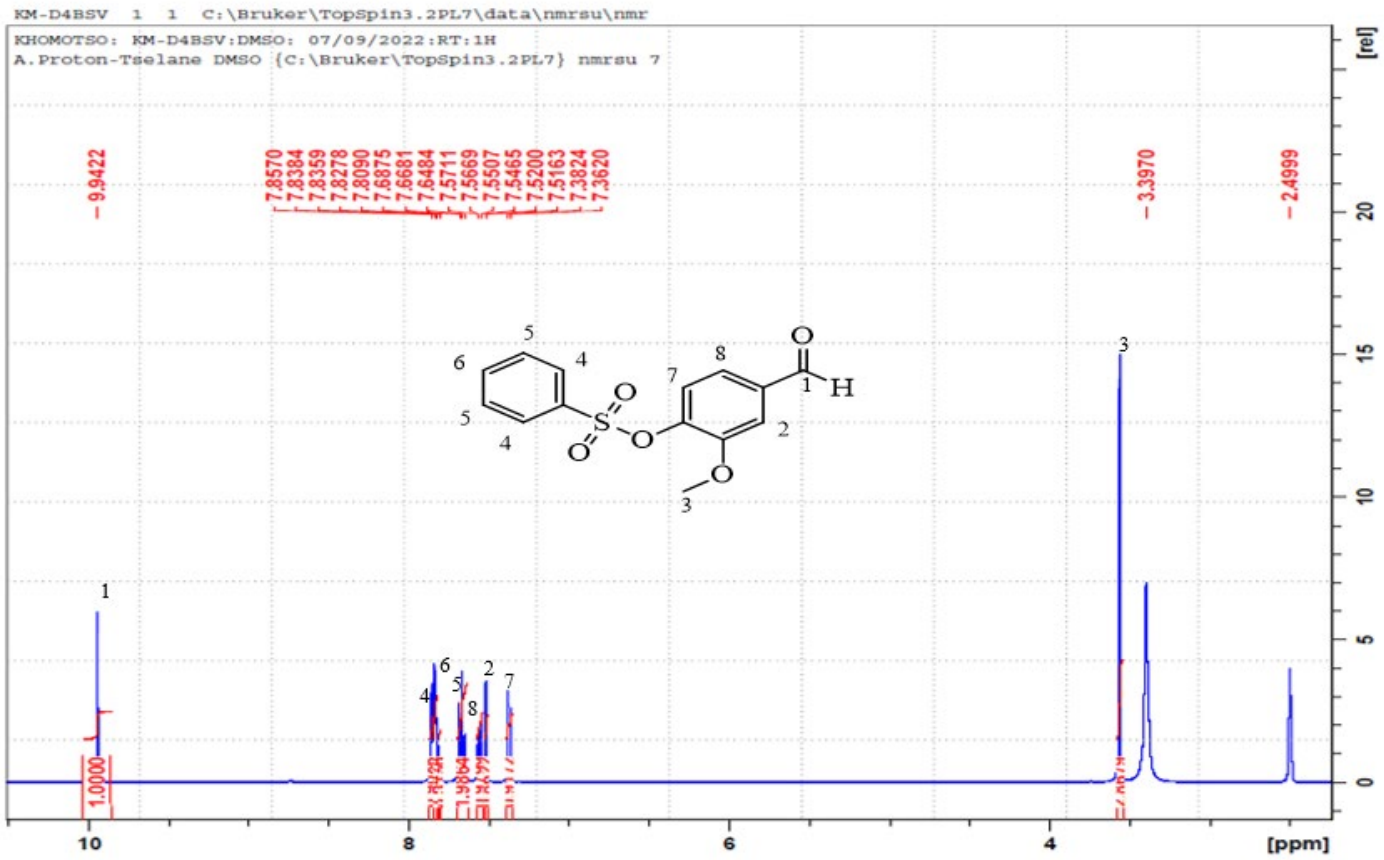

Figure 3. 6: [1]H NMR of 4-formyl-2-methoxyphenyl benzenesulfonate **76b**

3.5 X-ray studies of compounds 76a, 76b, 76k

Quality crystals suitable for X-ray diffraction of compounds **76a, 76b** and **76k** were obtained through the slow evaporation of ethanol. The molecular structure of compounds and the geometry around the C–C double bonds were unequivocally confirmed via single crystal X-ray diffraction analysis (see **Figure 3.7**). The crystal system of **76a** results in monoclinic and that of **76b** and **76k** as triclinic. Like their crystallinity, the **76a**, and **76b** and **76k** packing order results into different

space groups i.e. P21/n and P-1 respectively. Crystallographic numbering scheme has been utilized in the text for this report instead of the regular systematic numbering.

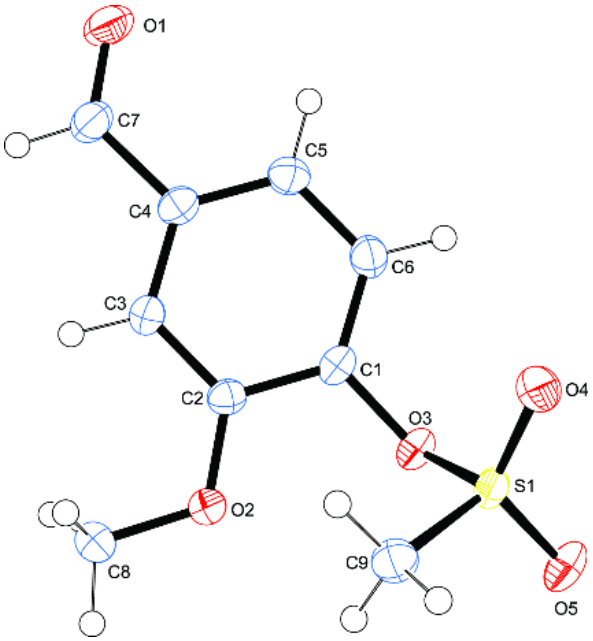

Figure 3. 7: Oak Ridge Thermal Ellipsoid Plot (ORTEP) diagram of **76a**

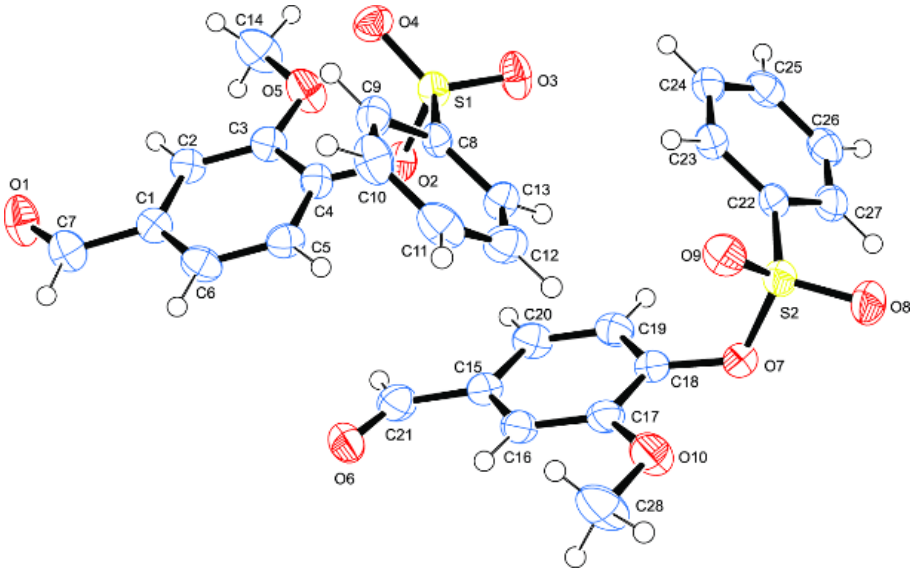

Figure 3. 8: Oak Ridge Thermal Ellipsoid Plot (ORTEP) diagram of **76b**

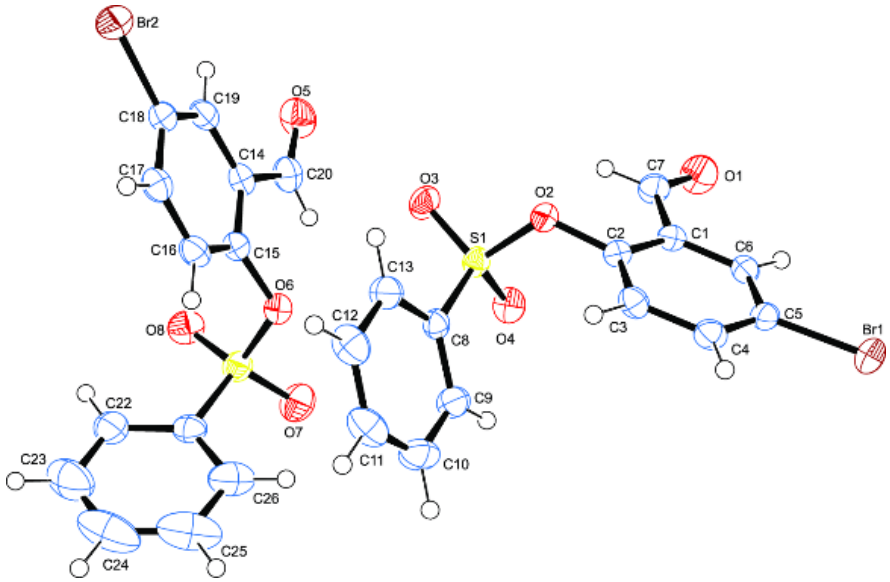

Figure 3. 9: Oak Ridge Thermal Ellipsoid Plot (ORTEP) diagram of **76k**

Table 3. 2: Crystal data and structure refinement for **76a, 76b, 76k.**

	76a	**76b**	**76k**
Empirical formula	$C_9 H_{10} O_5 S$	$C_{14} H_{12} O_5 S$	$C_{13} H_9 Br O_4 S$
Formula weight	230.23	292.30	341.17
Temperature	173(2) K	173(2) K	173(2) K
Wavelength	0.71073 Å	0.71073 Å	0.71073 Å
Crystal system	Monoclinic	Triclinic	Triclinic
Space group	P 21/n	P-1	P-1
Unit cell dimensions	a = 10.7060(4) Å b = 7.8036(3) Å c = 11.9400(5) Å α = 90°. B = 90.229(2)° γ = 90°	a = 8.5213(7) Å b = 11.3887(8) Å c = 13.8355(11) Å α= 91.516(3)° β= 101.685(4)° γ = 91.266(3)°	a = 8.0715(4) Å b = 11.2996(6) Å c = 15.0519(8) Å α = 97.029(2)° B = 92.632(2)° γ = 107.149(2)°
Volume	997.52(7) $Å^3$	1313.88(18) $Å^3$	1297.04(12) $Å^3$
Density (calculated)	1.533 Mg/m^3	1.478 Mg/m^3	1.747 Mg/m^3
Absorption coefficient	0.322 mm^{-1}	0.263 mm^{-1}	3.336 mm^{-1}
F(000)	480	608	680
Crystal size	0.337 x 0.223 x 0.140 mm^3	0.315 x 0.177 x 0.092 mm^3	0.391 x 0.365 x 0.229 mm^3
Theta range for data collection	2.550 to 27.999.	1.789 to 25.499°	1.906 to 27.000°
Index ranges	-14<=h<=14, 10<=k<=10, -15<=l<=15	-10<=h<=10, 13<=k<=13, -16<=l<=16	-10<=h<=10, 14<=k<=14, -19<=l<=19
Reflections collected	101439	40634	57553
Independent reflections	101439 [R(int) = ?]	4870 [R(int) = 0.0652]	5625 [R(int) = 0.0647]
Completeness to theta = 25.242°	100 %	99.7 %	99.0 %
Refinement method	Full-matrix least-squares on F^2	Full-matrix least-squares on F^2	Full-matrix least-squares on F^2

Data / restraints parameters	101439 / 0 / 139	4870 / 0 / 364	5625 / 0 / 343
Goodness-of-fit on F^2	1.052	1.089	1.082
Final R indices [I>2sigma(I)]	R1 = 0.0600, wR2 = 0.1364	R1 = 0.0778, wR2 = 0.2239	R1 = 0.0365, wR2 = 0.0966
R indices (all data)	R1 = 0.1111, wR2 = 0.1517	R1 = 0.0819, wR2 = 0.2267	R1 = 0.0392, wR2 = 0.0982
Largest diff. peak and hole	0.246 and -0.495 e.Å^{-3}	0.833 and -0.378 e.Å^{-3}	0.758 and -0.687 e.Å-3

Table 3. 3: Relative selected bond lengths of **76a** and **76b** crystals.

76a (A)	**76a** (B)	**76k** (A)	**76k (**B)
C(8)-S(1) = 1.759(4)	C(22)-S(2) = 1.763(5)	S(1) – C(8) = 1.752(3)	C(21)-S(2) =1.749(3)
O(2)-S(1) = 1.612(3)	O(7)-S(2) = 1.611(3)	S(1) – O(2) = 1.605(2)	O(6)-S(2) = 1.600(2)
O(3)-S(1) = 1.420(3)	O(8)-S(2) = 1.425(4)	S(1) – O(3) = 1.423(2)	O(7)-S(2) = 1.417(2)
O(4)-S(1) = 1.420(3)	O(9)-S(2) = 1.415(4)	S(1) – O(4) = 1.425(2)	O(8)-S(2) = 1.424(2)
C(4)-O(2) = 1.401(5)	C(18)-O(7) = 1.399(6)	O(2) – C(2) = 1.408(3)	C(20)-O(5) = 1.205(4)
C(1)-C(7) = 1.476(7)	C(15)-C(21) = 1.476(7)	C(5)-Br(1) = 1.890(3)	C(18)-Br(2) = 1.891(3)

3. 6 Hirshfeld fingerprint analysis of compounds 76a and 76b

The crystal structures of compound **76a** and **76b** are further discussed for clearer understanding of their packing pattern using the Hirshfeld (HF) surface analysis. This is a tool that seeks to describe the electron density distribution on the surface of molecules. Crystal Explorer software [110] was used to study the crystal packing of **76a** and **76b** and the supramolecular features of these structures by Hirshfeld surface analysis along the 2D fingerprint diagrams. The 3D HF surfaces for **76a** and **76b** were analyzed at a high standard resolution with an iso-value of 0.5 Å³. The surface volume and area for **76a** (244.26 Å³ and 236.92 Å², respectively) is lower than **76b** (322.51 Å³ and 303.35 Å², respectively). Comparing compound **76a**, which has a globularity value of 0.798, to compound **76b**, which has a globularity value of 0.750, indicates that **76a** is less spherical in shape. The molecular shapes of **76a** and **76b** are not completely symmetrical as indicated by their asphericity values of 0.133 and 0.146, respectively which means that the molecules deviate from a perfect spherical geometry and displaying a degree of distortion in their structure.

The molecular conformations of **76a** and **76b** compounds are stabilized by intramolecular or intermolecular interactions such as hydrogen to hydrogen bonds, aromatic–aromatic ($\pi\cdots\pi$, C–H$\cdots\pi$) and electrostatic interactions, as well as the weak Van der Waals interactions [111]. Variations in the intermolecular interactions observed in the crystal packing of compounds **76a** and **76b** undergo different type H---O, H---H and C---H interactions to connect each other (**Figure 3.10**). The 2D fingerprint plots provide a broad visual aid interpretation of the intermolecular interactions at play within the crystal structures of **76a** and **76b**. These fingerprints also demonstrated the specific interaction type which contributes towards establishing the 3D HF motif. **Table 1** (shown

below) shows significant points highlighted from analysis of the 2D fingerprint plots for **76a** and **76b**, which are catalogued systematically.

Table 3. 4: Hirshfeld surface values in Å for structure of **76a** and **76b**.

Interaction Mode	Minimum	Mean	Maximum		Minimum	Mean	Maximum	
Compound	**76a**				**76b**			
Di	1.011	1.633	2.264		1.04	1.683	2.432	
De	1.012	1.654	2.279		1.042	1.692	2.504	
Dnorm	-0.2	0.407	0.986		-0.152	0.438	1.244	
Shape Index (SI)	-0.989	0.275	0.997		-0.989	0.24	0.995	
Curvedness (Cr)	-3.476	-0.963	0.176		-3.658	-0.991	0.502	
Percentage Fingerprint of the total surface area for closed contact between atoms inside and outside								
	Outside Atom%				Outside Atom%			
Inside Atoms	C	H	O	S	C	H	O	S
C	4.1	5.2	2.7	.	5.5	9.8	0.8	.
F	4.6	29.8	22.3	0	6.7	33.3	18.9	.
H	2.4	26	2.9	.	2	21.4	1.6	0.1
O	.	.	.	.	0.1	.	.	.
S	11	61.1	27.9	0	14.2	64.5	21.2	0.1

The contacts that contribute significantly to the total HF surface of these compounds are the O···H/H···O and H···H contacts which contribute 29.8% and 48.3% for **76a,** and 33.3% and 40.3% for **76b** respectively. The H···C, C···O and C···C contacts also contribute to the stability of the crystal structure of **76a** (9.8%, 5.1% and 4.1% respectively), and **76b (**16.4%, 2.5% and 5.5% respectively) and to a lesser extent observed for weaker intermolecular H···H interactions. A significant part of the C···C interactions of the intramolecularly bonded hydrogen for **76a** can be rationalized as due to possible the *π*···*π* stacking interactions. The crystal structures of these

compounds are also influenced by electrostatic contacts of the type O···O between the oxygen atoms, which account for 2.9% and 1.6% of the total intermolecular forces in both **76a** and **76b**, respectively. Although these interactions are not very strong, they play a significant role in determination and maintenance of the shape and stability of these crystals[112]. In addition, compound **76b** exhibits electrostatic interactions of the type S···C/C···S and S···O/O···S which contribute 0.1% to the total surface. Although weak, non-covalent interactions are important for the structure, stability, properties and behavior of the crystal. Additionally, these interactions which may be cooperative and/or competing help to define the solubility, stability, dissolution rate and bioavailability of drug molecules, and to extrapolate structure activity relationship (SAR) [113,114].

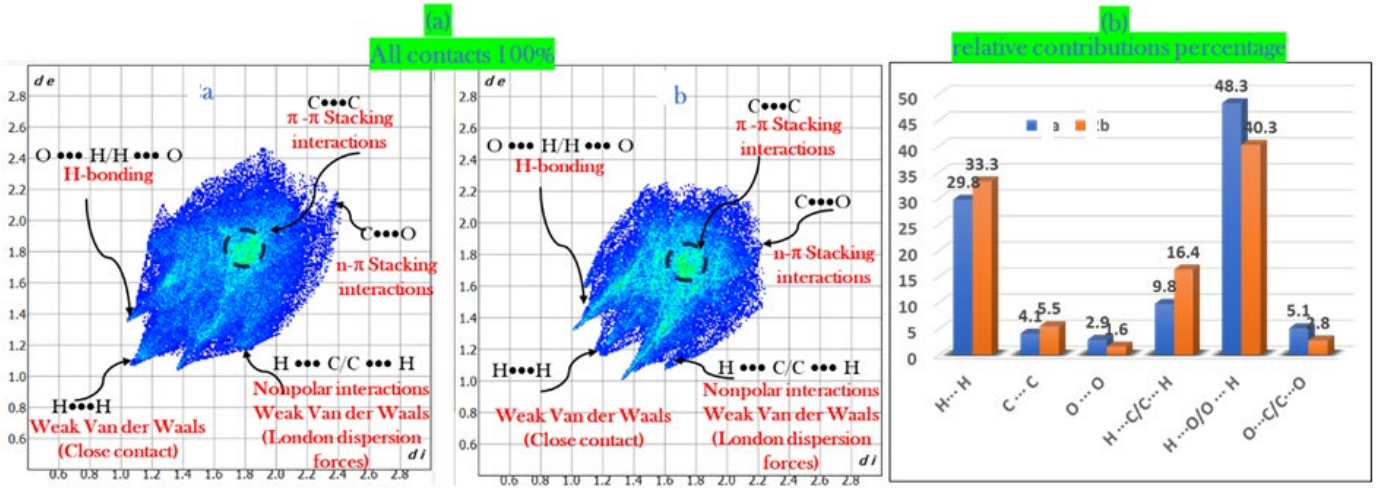

Figure 3. 10:(a) 2D HF fingerprint plots of **76a** and **76b**. The y-axis denotes 'de' (distance to the nearest external element) and the x-axis shows 'di' (distance to the nearest internal element) of the 3D Hirshfeld surface. Blue spots represent specific X···Y element pair contributions, while grey spots outline the combined contributions of all interacting pairs. (b) The relative contributions percentage of diverse intermolecular contacts to the Hirshfeld surface area in **76a** and **76b** compounds.

The comprehensive understanding of the intricate dynamics of the non-covalent interactions in this case might yield useful insights into the behaviour of the material across various conditions. Analysis of **Figure 3.10** shows a circular red spot within the contour of the HF surface, which indicates the existence of weak intermolecular interactions in the crystal structure of the compound. The dnorm values are mapped on the 3D HF surface using a color scheme of red, white and blue. The colour red indicates negative dnorm value -0.1997 (a.u) for **79a**, which is higher than **76b** with a value of about -0.1518 (a.u). The low electron density regions in this case suggest weak intermolecular interactions. White indicates zero dnorm values, which mean normal Van der Waals contacts. The blue regions suggest positive dnorm value 0.9856 (a.u) for **79a** and 1.2445 for **76b**, which mean high-electron-density regions and strong intermolecular interactions**.** **Figure 3.11** 2 shows the spatial mapping of the *de* (delocalization index outside) and *di* (delocalization index inside) surfaces for **76a** and **76b**. The colour gradient in **Figure 3.11** shows the difference between the two surfaces of **76a** and **76b**. The red colour in *de* region indicates a lower value of 1.0125 au. for **76a** than **76b** value 1.0421 au., while the blue colour represents lower values of 2.2792 au. and 2.4320 au. for **76a** and **76b**, respectively. The observed analysis means that the red spots on the *de* surface represent the regions where the electrons are most likely to be found outside the molecule, while the red spots on the *di* surface represent the regions where the electrons are most likely to be found inside the molecule, thus creating polarities within the molecule.

The hydrogen atoms H5, H8A and H9a for **76k** or H2 and H5 are situated near the external boundary of the de surface as shown in **Figure 3.10** Intriguingly, these H-atoms concurrently act as the proximate donor nuclei to the *di* surface, reflected as red contours in the figure. This therefore suggests that the H-atoms are involved in subtle intermolecular interactions. This interpretation finds alignment with insights derived from the HF surface analysis, mapped based on electrostatic potentials and dnorm. It is notable that both surfaces have conspicuously green, flat sections, suggesting the presence of *π···π* stacking interactions in the crystal packing. The *π···π* stacking interactions are a type of Van der Waals interaction that occurs between aromatic rings. This suggests that these hydrogen atoms are involved in bridging interactions between aromatic rings.

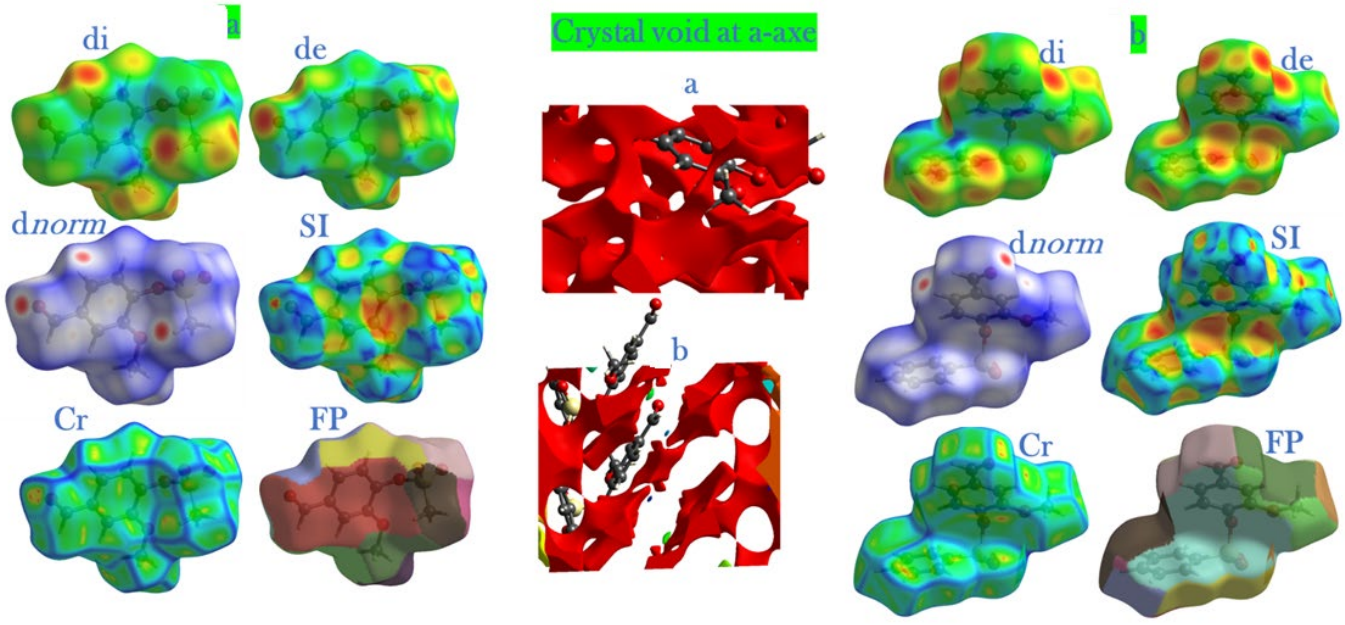

Figure 3. 11: HF 3D maps as represented in the dnorm, di, de, shape index “si”, curvedness “crv”, and fragment batch “fb”, and voids of crystal of **76a** and **76b**, respectively.

Normally, the strength of crystal packing determined the mechanical response of a material to applied stress or force. Single crystals are known for their high mechanical strength because the molecules within them are densely packed. Materials with strong molecular packing are more likely to exhibit high mechanical strength and resistance to deformation or breakage under applied stress or force [115.] The voids analysis in **Figure 3.11** reveals that the voids occupy approximately 4.23% for **76a** and 3.36% for **76k**, and of the total space within the crystal while the molecules occupy 95.76% and 96.34%, respectively. The high molecular packing order and limited voids space in the crystal structure are positive indicators of mechanical stability. The voids map crystal packing suggests that crystal **76k** is mechanically stable due to the strong packing of molecules and the limited presence of voids would make it resilient to external mechanical forces or stress.

3.5 Preparation of (*E*)-4-(2-(6-iodo-4-oxo-3,4-dihydroquinazolin-2-yl)vinyl)-2- sulfonates

Aldol condensation reaction of the sulphonated benzaldehydes with the 2-methylquinazolin-3*H*-one entails the formation of the vinylic group between the two compounds[116]. This chemical reaction is conventionally conducted by dissolving methylquinazolin-3*H*-one in 20 mL of acetic acid and 10 mL dimethylformamide for thirty minutes under reflux conditions with constant stirring until fully dissolved. Thereafter a three stochiometric equivalence of sodium acetate was added which act as a base after which two equivalences of the sulphonated salicylaldehyde was added. The reaction is refluxed at relatively high temperature for approximately six hours. After six hours of constant stirring under reflux, the mixture was quenched using crushed ice, filtered, and washed with methanol to afford crystalline product.

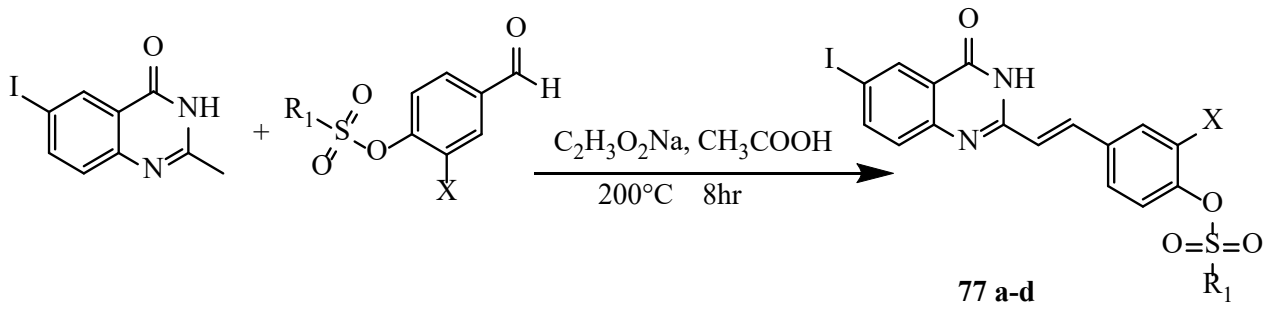

Scheme 3.5: Synthesis of (*E*)-4-(2-(6-iodo-4-oxo-3,4-dihydroquinazolin-2-yl)vinyl)-2- sulfonates **77a-d**.

Table 3. 5: Derivatives of **77a-d**

Compound number	X	R_1	Yield%
77a	Br	$-CH_3$	84
77b	Br	$-C_6H_5$	71
77c	OCH_3	$-CH_3$	93
77d	OCH_3	$-C_6H_5$	80

The aldol condensation compounds **77a-d** were obtained as white to light yellow solid powder product. The melting points ranged from 320-380 °C. The compounds were then characterized using ^1H and ^{13}C NMR spectroscopy, recorded in DMSO-d_6. The ^1H NMR displayed the merging of the distinctive peaks from the sulphonated benzaldehyde and the 6-iodo-2-methylquinazolin-(3*H*)-one, through an aldol condensation reaction. The double bond formed had *E* configuration[117] based on the coupling constant (^3J = 16 Hz). This proximity results in two doublet peaks at 6.65 ppm and 7.98 ppm, both having the same *J* coupling (illustrated in **figure 3.7**). This observation serves as confirmation of the successful aldol condensation reaction.

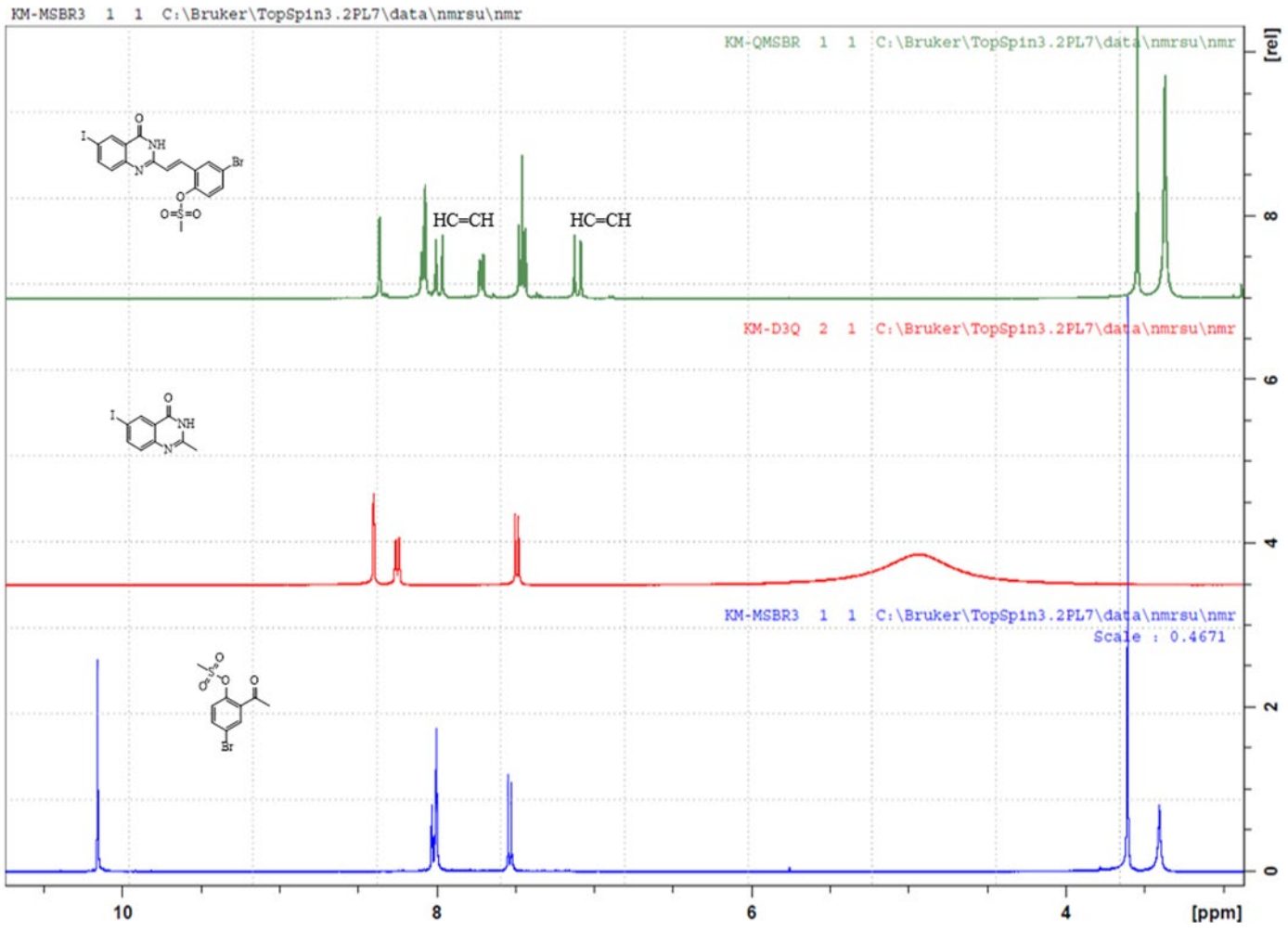

Figure 3.12: [1]H NMR of compound **77b** (*E*)-4-bromo-2-(2-(6-iodo-4-oxo-3,4-dihydroquinazolin-2-yl)vinyl)phenylmethanesulfonate.

3.6 Preparation of (*E*)-4-(2-(6-aryl-4-oxo-3,4-dihydroquinazolin-2-yl)vinyl)-2- sulfonates

Synthesis of (*E*)-2-methoxy-4-(2-(6-(4-arylphenyl)-4-oxo-3,4-dihydroquinazolin-2-yl)vinyl)phenyl sulfonates **81** followed a similar literature procedure reported by Goyal *et al*[118]. where the halogenated methylquinazolin-4(3*H*)-ones underwent Suzuki-Miyaura cross-coupling with

arylboronic acids. In our case, we followed a slightly different path whereby (*E*)-4-(2-(6-iodo-4-oxo-3,4-dihydroquinazolin-2-yl)vinyl)-2- sulfonates were reacted with palladium-tetrakis(triphenylphosphine) as the catalyst for active Pd(0) species and cesium carbonate as a base in toluene at 100°C for eight (8) hours, resulting in the formation of the novel 6-aryl–substituted derivatives **78a–e** (**Scheme 3.6** below). The following reaction conditions were adopted whereby arylboronic acids ($ArB(OH)_2$) in 1.2 equivalents, 10% $Pd[(C_6H_5)_3P]_4$, $CsCO_3$ in 1.2 equivalents in 25mL toluene was allowed to reach completion after eight (8) hours before cooling thereafter filtration, affording **80a – e** in relatively good yields.

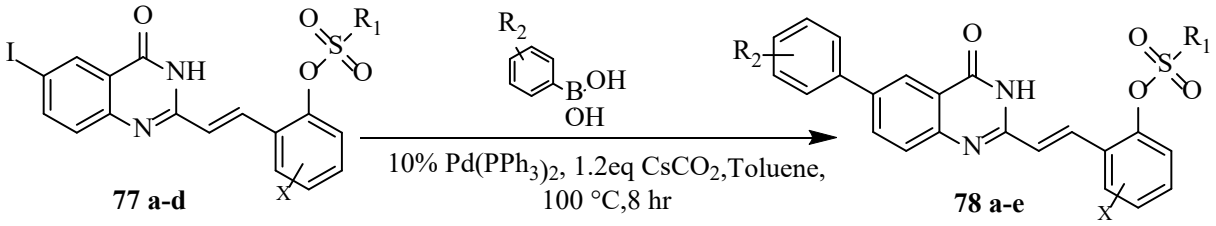

Scheme 3.6: 6-carbo–substituted 2-styrylquinazolin-4(3*H*)-ones **78a-e**.

Table3.6: Derivatives of (*E*)-(2-(6-(4-aryl)-4-oxo-3,4-dihydroquinazolin-2-yl)vinyl)phenylsulfonate.

Compound number	R_1	R_2	X	%Yield
78a	$-CH_3$	4-OCH_3	$-OCH_3$	71.29
78b	$-CH_3$	4-F	- OCH_3	88.03
78c	$-C_6H_5$	4-OCH_3	$-OCH_3$	75.48
78d	$-C_6H_5$	4-H	$-OCH_3$	93.61
78e	$-OCH_3$	4-OCH_3	-Br	71.29

Compounds **78a-e** were achieved bearing different substituents in varying yields and characterized as illustrated in the tabulated result (**Table 3.6**). It is noteworthy to observe that 6-carbo–substituted 2-styrylquinazolin-4(3*H*)-one's derivatives exhibit limited solubility in the

commonly used deuterated solvents. Their solubility in DMSO-d_6 allowed for the acquisition of ^{1}H-NMR spectra within a few minutes. However, all the compounds, precipitated from DMSO-d_6 at room temperature, affecting the quality of their ^{13}C-NMR spectra. Despite these challenges, the distinct proton signals in the aromatic region of the ^{1}H-NMR spectra and accurate calculated m/z values confirmed the assigned structures.

Compound **78f** was obtained in the form of a brownish solid product. The product was then characterized through ^{1}H and ^{13}C NMR spectroscopy, recorded in DMSO-d_6. The ^{1}H NMR displayed the presence of an increased number of protons in the aromatic region arising from the Suzuki coupling reaction. Specifically, a set of two doublet of doublet peaks in the aromatic region 7.66 ppm and 8.22 ppm, integrating for two (2) protons. A distinct singlet peak at 12.61 ppm, corresponding to a single proton, was observed, indicating the proton resonance of the –NH group in the lower field region. The vinylic group shifted position but still had *E* configuration[119] based on the coupling constant (^3J = 16 Hz). This proximity results in two doublet peaks, one around 7.18 ppm and another around 7.85 ppm, both having the same *J* coupling constant. This observation serves as confirmation of the successful coupling in the position of Iodine atom. The methoxy and methyl protons observed as singlets in the spectrum around 3.67 ppm and 3.73 ppm, where they integrate for three (3) protons. The compound exhibited a melting point of 180.65-200.00 °C.

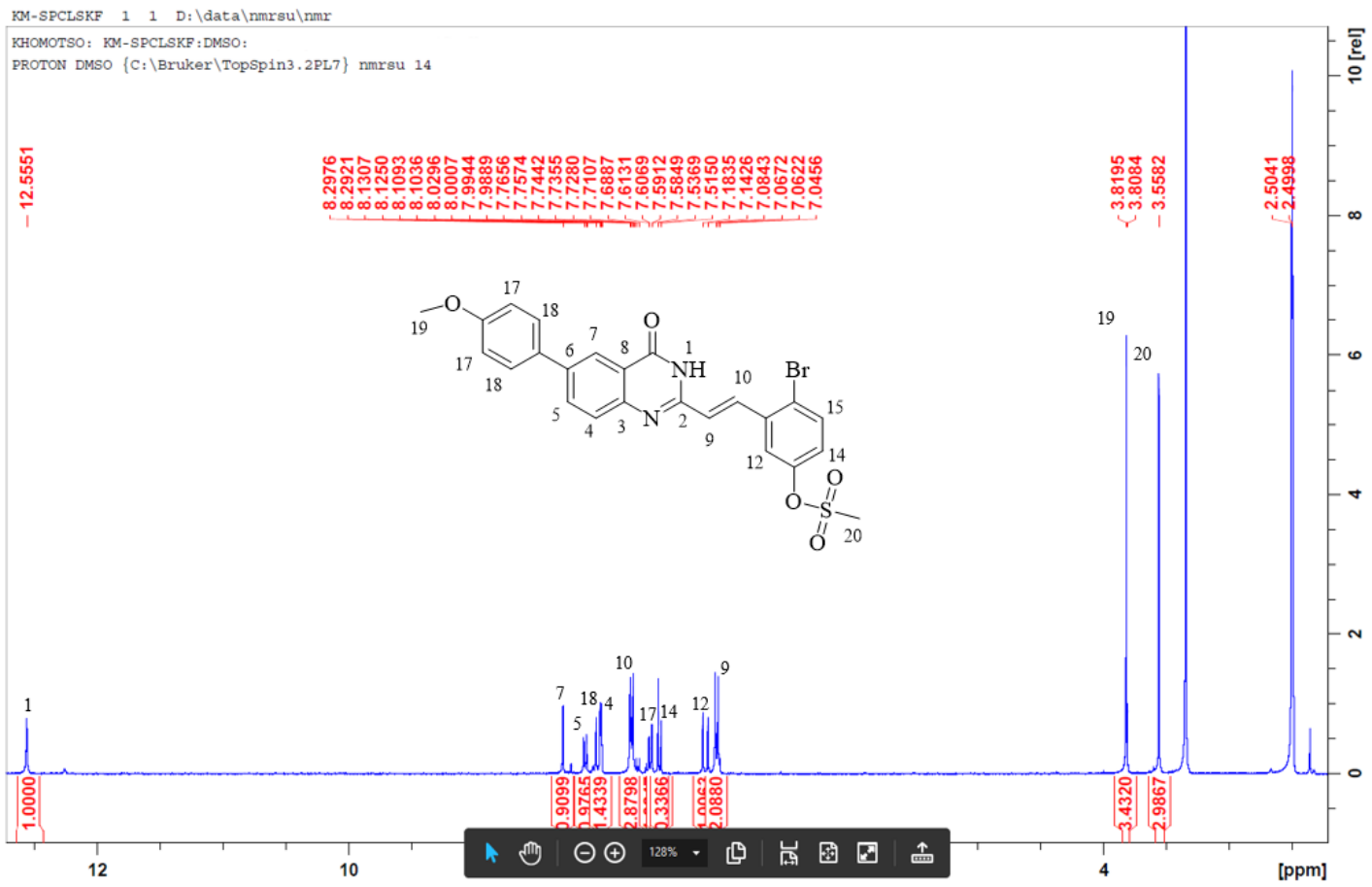

Figure 3.13: ^{1}H NMR of (*E*)-4-bromo-3-(2-(6-(4-methoxyphenyl)-4-oxo-3,4-dihydroquinazolin-2-yl)vinyl)phenylmethanesulfonate **78e**.

3.7 Biological toxicity evaluation

Styrylquinazolinones are renowned for their diverse pharmacological properties, they have garnered substantial attention due to their ability to inhibit key pathways implicated in cancer progression. Moreover, sulfonated hydroxybenzaldehyde derivatives have emerged as potent anticancer agents, exhibiting remarkable efficacy in targeting specific molecular targets involved in tumorigenesis. This section will delve into the biological activity of these compounds, elucidating their mechanisms of action and highlighting their therapeutic potential in combating cancer. Research into cell viability and antioxidant properties using chemically synthesized drugs helps elucidate the complex signaling pathways involved in cell death and survival[120]. Testing drugs synthesized by organic chemists in cell culture[121] allows researchers to assess their efficacy and safety profiles.

When synthesizing our target compounds, we discovered that the precursors, sulphonated benzaldehydes **76a-r**, were novel and had not been previously reported. This novelty prompted us to perform biological evaluations of these precursors together with the target compound, Styrylquinazolinones. Evaluating the biological properties of precursors alongside the target compounds is crucial for comprehending their distinct biological characteristics, refining the synthesis process, evaluating safety aspects, and meeting regulatory requirements. This comprehensive approach not only streamlines compound synthesis but also strengthens our capability to create compounds that are safe and efficacious for their intended uses.

3.7.1 Cell viability analysis of compounds 77a-d and 78a-e against MCF-7, HeLa and HEK293-T.

The biological activity of the synthesized compounds against the (MCF-7) cell line **figure 3.14**, (HeLa) human cell lines **figure 3.15**, and (HEK293-T) human embryonic kidney cells **figure 3.16** was investigated using MTT (3-(4,5-dimethylthiazol-2-yl)-2,5-diphenyltetrazolium bromide) assay based on protocol established by Mosman[122]. Cells were treated at a concentration of 100 µM of the synthesized active compounds, dissolved in a culture medium containing 0.5% DMSO, with curcumin serving as the standard.

The preliminary results indicate promising biological activity against the cell lines tested, more comprehensive studies are needed to fully assess the therapeutic potential of the synthesized compounds. This includes determining IC_{50} values, conducting additional biological evaluations, testing smaller concentrations, and performing comparative studies. These steps will provide a more thorough understanding of the compounds' efficacy, safety profile, and potential for further development as anticancer agents.

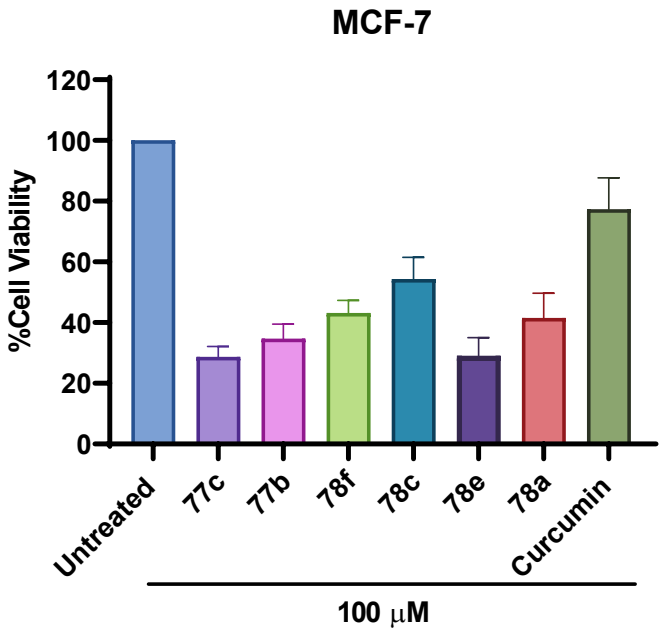

Figure 3. 14: %Cell viability of compounds against MCF-7 at 100 μM

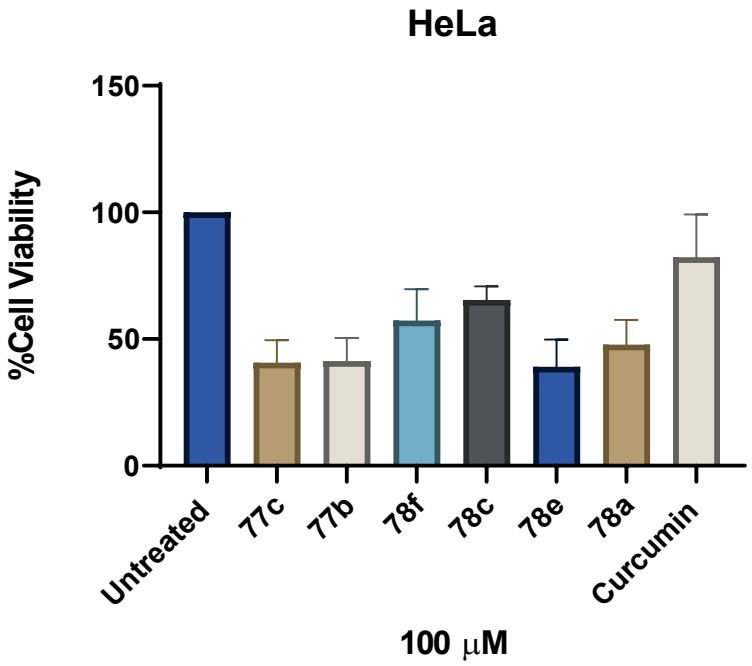

Figure 3. 15: %Cell viability of compounds against HeLa at 100 μM

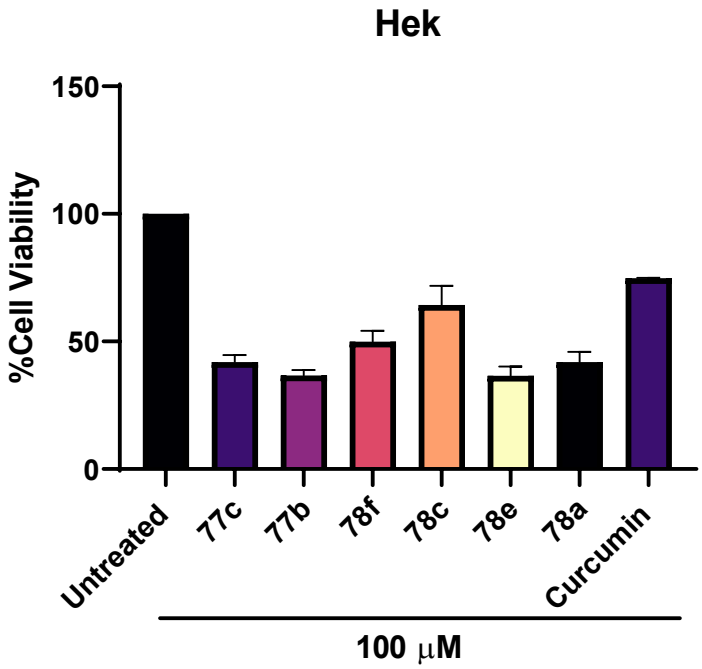

Figure 3. 16: %Cell viability of compounds against Hek at 100 μM

The (*E*)-4-(2-(6-iodo-4-oxo-3,4-dihydroquinazolin-2-yl)vinyl)-2-sulfonates displayed promising activity with %cell viability when compared with the positive control, curcumin. From the preliminary tests, the most active compound, **77c** showed 30% cell viability when compared with curcumin (90%) cell viability at 100 μM against MCF-7. Compound **77b** and **77c** and **77e** had the most activity against the HeLa cells with a percentage viability of 50%, 51%, and 55% respectively, compared to curcumin at 90%. Compound **77b** and **78e** resulted in similar %viability of 40% against the HEK293-T cells where curcumin was 90% at 100 μM but the **77b** would be most preferred since adhering to ADMET properties.

3.7.2 DPPH assay of compounds 76a-76i

Series of the sulphonated hydroxybenzaldehyde derivatives were evaluated through enzymatic assays in vitro for radical scavenging potential. DPPH (2,2′-diphenyl-1-picrylhydrazyl) radical scavenging assay was conducted by testing the compounds alongside ascorbic acid as a positive control.

Table 3. 7: The vanillin series subjected to the DPPH radical scavenging assay in the presence of ascorbic acid.

Vanillin	R	$1C_{50}$ VALUES (μM ± SD)	Compound number
2a	$-CH_3$	1.083± 3.914	**76a**
2b	$-C_6H_5$	13.64± 2.839	**76b**
2c	$--C_6H_5$-4-F	8.228± 1.470	**76c**
2d	$-C_6H_5-NO_3$	0.0001248± 1.911	**76d**
2e	$-C_6H_5-OCH_3$	29.26 ± 2.368	**76e**
2f	$-C_6H_5-CH_3$	3.406e-16 ± 2.024	**76f**
2g	$-C_6H_5-CH_3F_3$	24.88± 3.351	**76g**
2h	$-C_6H_5-OCH_3F_3$	2.732e-020± 11.400	**76h**
2i	$-C_6H_5-NHCOCH_3$	1.617e-018± 2.255	**76i**

	Ascorbic acid	5.87 ± 0.88	

Compounds **79a-79i** were tested for antioxidant activity using the DPPH assay, compounds **79d, 79f, 79h** and **79i** have been found to have more scavenging activity (IC_{50} = 0.29 µM, 0.67 µM, 0.0273 µM and 0.0617 µM) than ascorbic acid (IC_{50} = 5.87 ± 0.88 µM). This can be seen in **Figure 3.17.**

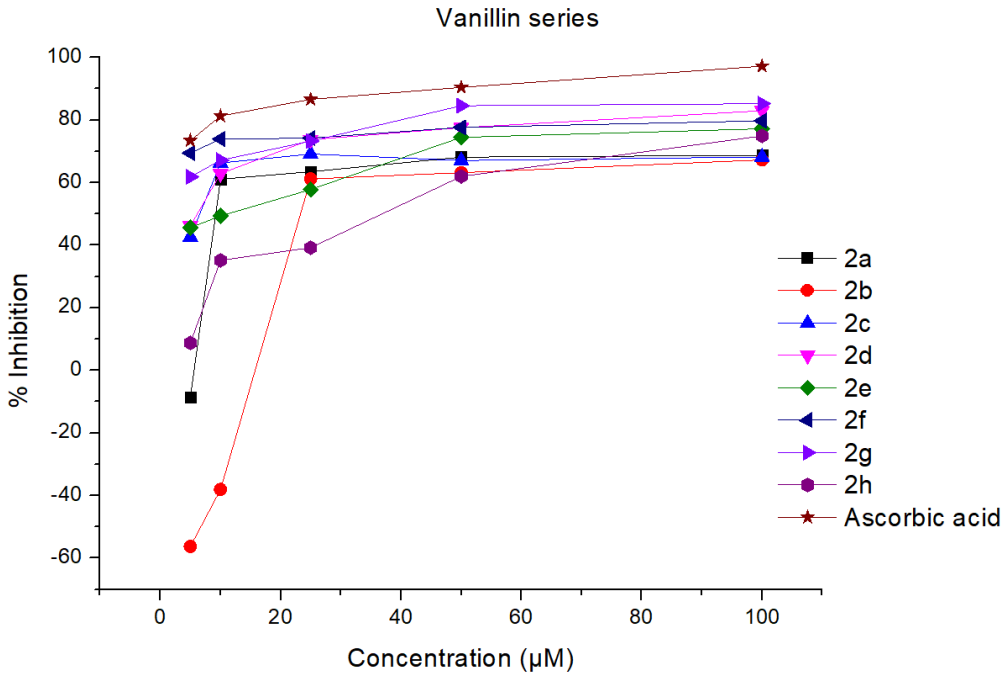

Figure 3. 17: Line plot of **76aj-76i** antioxidant activity

Table 3. 8: The bromo series subjected to the DPPH radical scavenging assay in the presence of ascorbic acid.

5-Bromo	R	IC_{50} VALUES (μM ± SD)	Compound number
2a	$-CH_3$	0.6798± 14,29	**76j**
2b	$-C_6H_5$	0.007719± 7,439	**76k**
2c	$-C_6H_5$-4-F	49.39± 3,512	**76l**
2d	$-C_6H_5-NO_3$	56300990± 1,823	**76m**
2e	$-C_6H_5-OCH_3$	0.7021± 5,004	**76n**
2f	$-C_6H_5-CH_3$	444633208 ± 7,748	**76o**
2g	$-C_6H_5-CH_3F_3$	5.216e-007± 2,957	**76p**
2h	$-C_6H_5-OCH_3F_3$	3.215e+016± 1,022	**76q**
2i	$-C_6H_5$-NHCOCH$_3$	1.617e-018± 2,255	**76r**
	Ascorbic acid	5.87 ± 0.88	

Compounds **76j** to **76r** were assessed for their inhibitory activity against the specified target using IC_{50} values. Notably, compounds **76k**, **76p**, and **76r** demonstrated particularly potent activity with IC_{50} values of 0.007719 μM, 5.216e-007 μM, and 1.617e-018 μM, respectively. These results indicate that these compounds are highly effective inhibitors compared to the standard, ascorbic acid, which had an IC50 value of 5.87 ± 0.88 μM. Conversely, compounds

76m, **76o**, and **76q** showed very high IC_{50} values, suggesting limited inhibitory activity under the tested conditions. This can be seen in **Figure 3.18**.

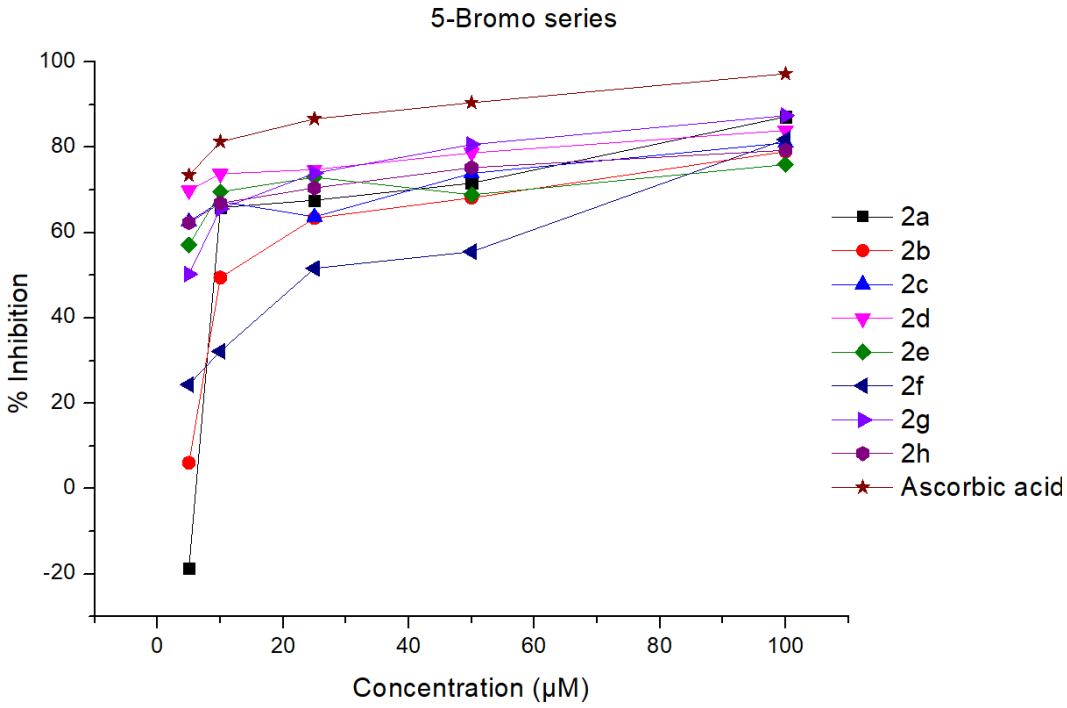

Figure 3. 18: Line plot of **79j-79q** antioxidant activity

3.7.3 MTT assay of sulphonated benzaldehydes against lung cancer cell (A459) with camptothecin as a positive control.

In this study, we assessed the cell viability of sulphonated benzaldehydes against (A549) lung cancer cells using the MTT assay. Leveraging camptothecin as a positive control, we aimed to elucidate the potential of these compounds in inhibiting cancer cell proliferation.

Table 3. 9: IC_{50} values of sulphonated benzaldehydes against A549 cells.

IC_{50} (100 µM)	Compound number
5.28	**76b**
4.60	**76c**
3.67	**76d**
3.77	**76e**
6.05	**76f**
15.36	**76g**
7.91	**76h**
0.042	**76i**
5.79	**76n**
6.30	**76o**
114.30	**76p**
3.21	**76q**
6,32	**Camptothecin**

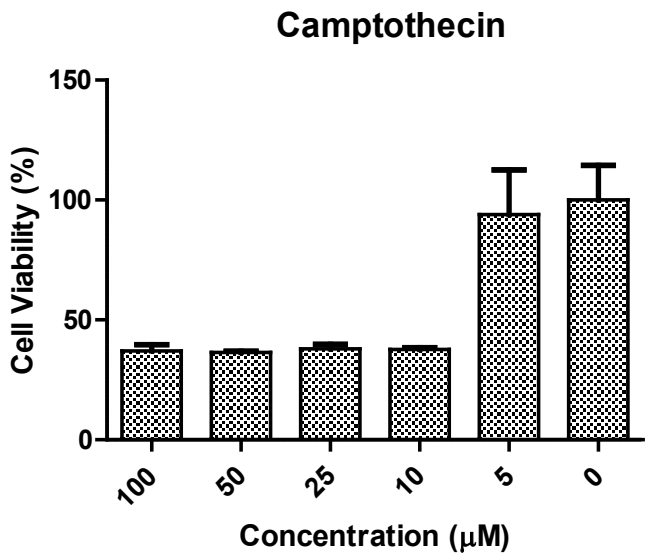

Figure 3. 19: %Percentage cell viability of standard camptothecin

Compound **76i** was found to be most active with the IC_{50} value of 0.042 100 μM compared to camptothecin of an IC_{50} value of 6.32 100 μM. This indicates its greater potency, as lower concentrations of the compound are needed to achieve the desired level of inhibition.

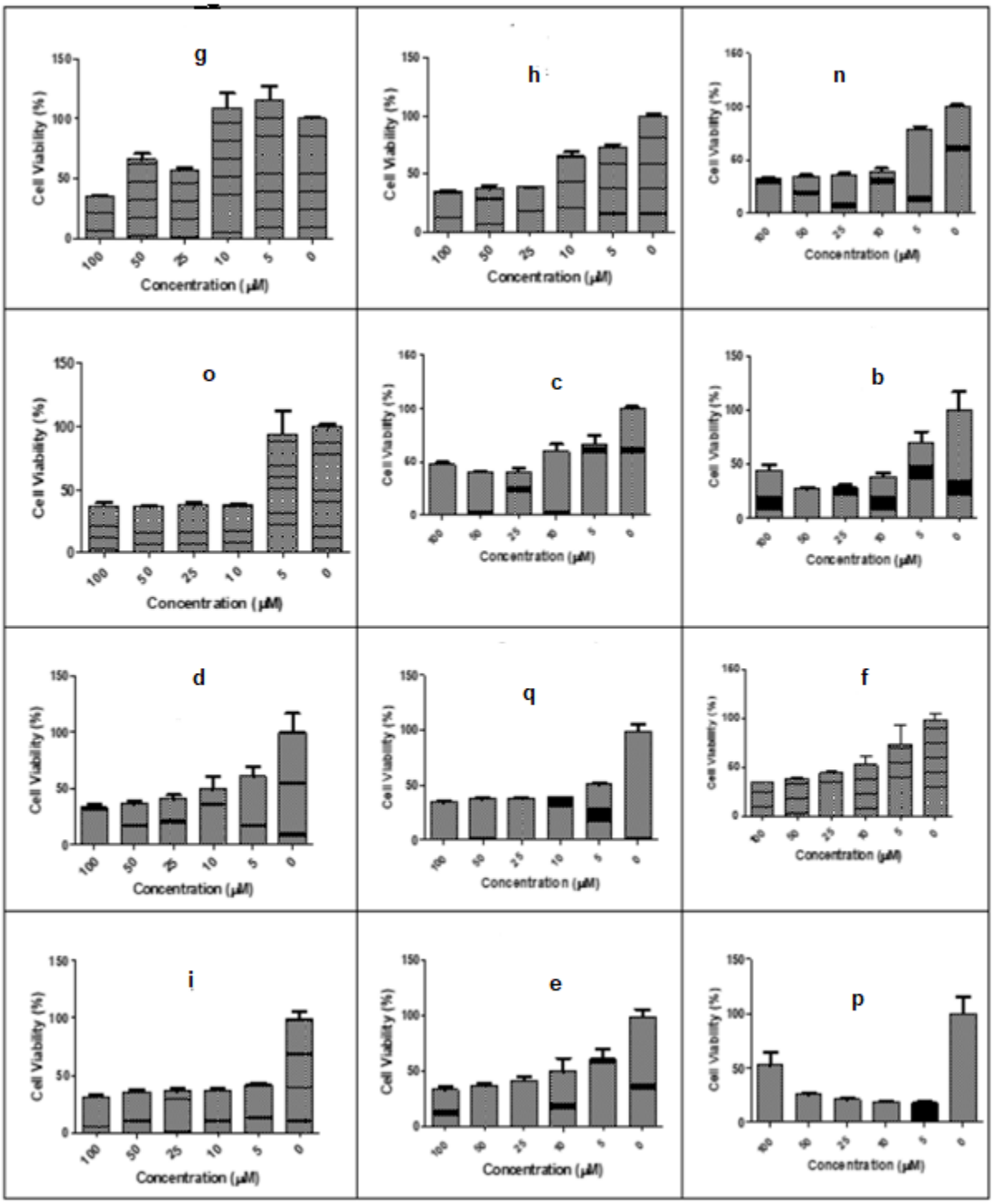

Figure 3. 20: Bar plot of sulphonated benzaldehydes (**76** series) against camptothecin.

3.8. Molecular docking studies

Molecular docking has been performed to evaluate the interaction between the enzyme and the potential ligands to reveal the site of action and possible interaction modes with the key residues of the receptors. The docking analysis was performed i*n silico* studies of the possible potency of these desirable molecules *in-vitro* against the tyrosine Kinase and peroxidase proteins, respectively utilizing their respective crystallized frameworks (PDB: 2OH4 [123] and 2X08[124]. The docking investigation procedures were studied through Glide's module® [125,126,127,128,129]. The preliminary inhibitors [benzimidazole, and Ascorbic] were redocked into the examined crystal frameworks as reference standards to verify the efficiency of docking methodology. In addition, the efficacious performance of the targeted molecules was authenticated *via* the low values of Root Mean Square Deviation (RMSD) of tyrosine kinase (2.05 and 0.231Å), and for peroxidase (2.01 and 0.201 A), respectively. They were each acquired through the root mean square deviation (RMSD) between the native and re-docked poses of the co-crystallized inhibitor. The established inhibition behaviour in binding-energy BE terms for the tested compounds **76a-76r** with the receptor are herein reported in **Table 3.9**

The initial inhibitors have been adequately installed into their binding sites to attain their crystal configurations. The hetero-nuclear ring for benzimidazole centered on the tyrosine Kinase VEGFR-2 adenine-pocket and interacted with ALA868, LYS 868, CYS917, GLU883, VAL914, VAL916, CYS 1045, ASP1046, and PHE1047 while the Ascorbic acid seem to be capped with ARG48, TRP51, MET 172, HIS 175, HIS177, LYS179, THR180, HIS181, ARG184, SER185 and

PHE191 in peroxidase. It is known that these amino acids interact with the ligands of tyrosine Kinase and peroxidase that are essential for its catalytic activity.

We observed in our experiments that almost all conformations of all compounds **76a-76r** showed interactions with important residues within the protein pocket. The molecules seem to dock efficiently into the active sites in a similar mechanism as the control inhibitors. The overlay for most active compounds and reference inhibitor was figured for further validation of the molecular docking experiment, then the ligand efficacy (LE) and inhibition constant (Ki) were then calculated. The binding mode and stability of the docked poses were evaluated by the Glide ΔG score, which estimates the free energy of binding between the ligand and the receptor protein (**Table 3.9)**. The lowest score poses and RMSD suggest a more stable orientation in the binding pocket. The data herein quoted was used to rank the docked poses and to select the most stable docked conformation of each compound **76a-76i**. The docking energy details are shown in **Table 3.9**. The interactions between the active compounds and the active site residues were mainly polar, H-H, π−π, π−H, π−S, and π−cation interactions, which contributed to a strong alignment with the enzyme backbone.

Table 3. 10: The binding-affinity for compounds **76a-76i** with docking score (kcal/mol) against VEGFR-2 and hCAII.

No.	***ΔG***	**RMSD**	**H. B**	**EInt.**	**Eele**	**Ki**	**LE**
2OH4							
76a	-5.485	0.673	7.872	-14.297	-8.963	-24.617	8.146
76b	-7.998	1.768	12.534	-24.123	-8.089	-37.175	4.523
76c	-7.448	1.683	74.747	-19.257	-7.798	-31.488	4.425
76d	-6.734	0.919	44.431	-17.328	-8.091	-31.825	7.330

76e	-7.694	1.091	66.703	-16.857	-8.060	-34.290	7.055
76f	-8.199	1.575	67.062	-27.120	-8.914	-38.804	5.207
76g	-7.799	1.030	107.068	-22.125	-8.595	-32.641	7.568
76h	-7.532	1.716	69.264	-25.980	-8.837	-33.094	4.388
76i	-7.078	1.268	74.977	-25.153	-8.707	-29.583	5.583
Benzimidazole	-5.324	0.891	73.874	-7.862	-8.636	-19.834	5.976
2X08							
1	-5.159	1.149	8.095	-14.889	-8.471	-22.254	4.491
76a	-7.199	1.195	75.685	-24.680	-8.938	-36.498	6.024
76b	-6.793	1.580	73.531	-23.907	-7.906	-32.323	4.300
76c	-6.358	1.128	45.054	-16.324	-8.479	-32.319	5.639
76d	-7.087	1.399	68.823	-24.418	-8.905	-30.697	5.065
76e	-7.219	0.981	66.333	-22.314	-7.836	-30.191	7.357
79f	-7.648	1.909	103.146	-18.185	-8.957	-35.952	4.006
76g	-7.055	1.320	71.832	-18.153	-7.439	-26.001	5.345
76h	-7.330	1.745	103.927	-17.811	-8.540	-35.402	4.201
76i	-7.671	1.202	24.351	-19.568	-7.434	-33.917	6.383
Ascorbic	-5.16	1.52	77.69	-11.52	-7.96	-23.80	4.70

Where, *ΔG*: Free binding energy of the ligand; RMSD: root-mean-square deviation; *H*.B.: H-bonding energy between protein and ligand; EInt.: Binding affinity of H-bond interaction with receptor; Eele: Electrostatic interaction over the receptor, LE: ligand efficacy and Ki: inhibition constant in μM.

3.8.1 Docking of VEGFR-2 protein

All compounds **76a-76j** demonstrated higher binding affinities (ΔG = -5.4 to -8.1 kcal/mol) than benzimidazole (ΔG = -5.3 kcal/mol [130]), which substantiated their promising potencies. The most active molecules **76a, 76e** and **76i** revealed a relatively strong attachment within the protein binding pockets, interacting with the vital hydrophobic VAL 916, LEU 889 and VAL 899 residues in the same manner as benzimidazole (**Figure 3.19**).

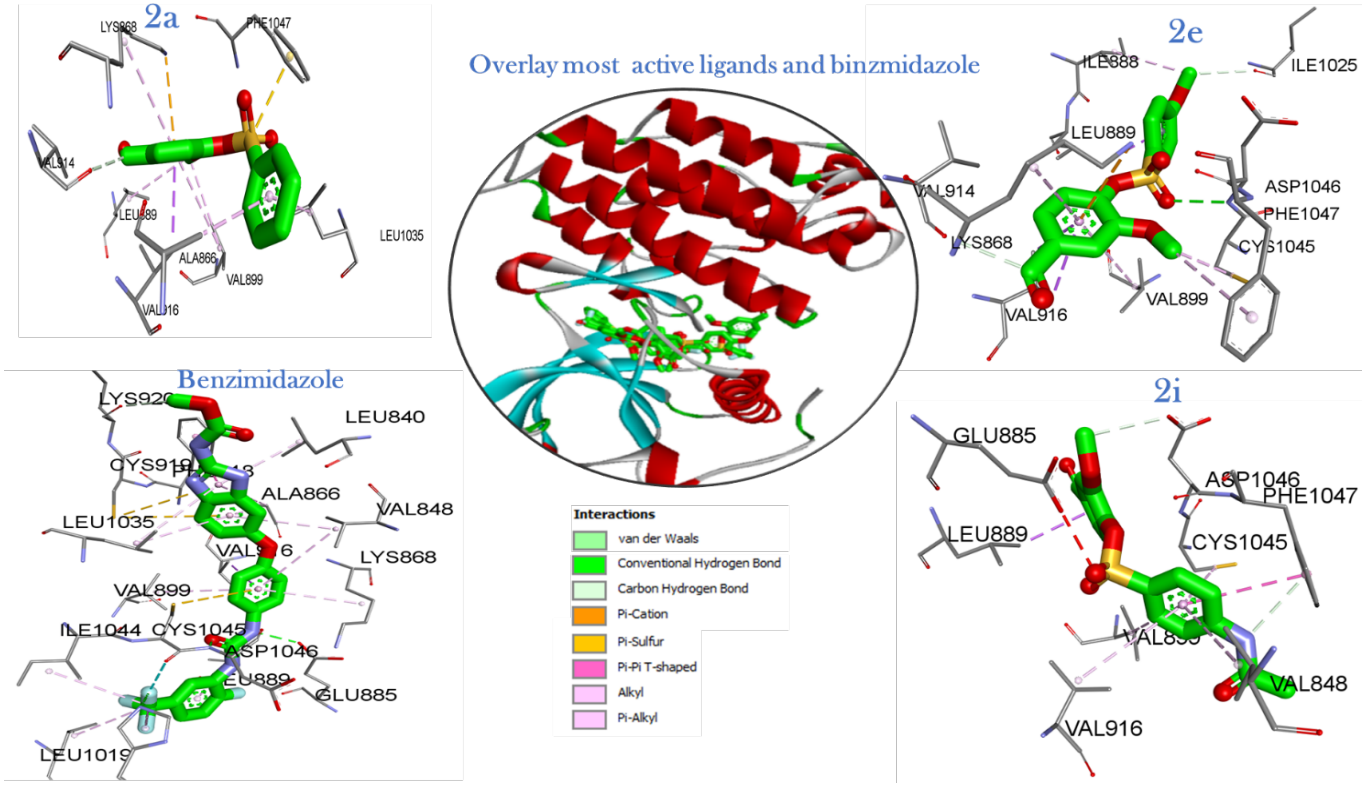

Figure 3. 21: 3D mapping surface of three most active compounds **76a, 76e, 76i** and benzimidazole inside 2OH4.

The most active molecule **76i** with IC_{50} = 0,0422 had binding energy equivalent to -8.035 Kcal/mol, comfortable within the binding pocket by interacting with the important hydrophilic binding pocket GLU885, ASP 1045 and ASP 1046 that led to an increase in activity against VEGFR-2. The second most active compound **76a** with ∆G = -7.998 Kcal/mol was docked in the VEGFR-2 binding pocket *via* interaction with hydrophilic binding pocket LYS 868 and PHE 1047, while interacting with hydrophobic part VAL 914, ALA886, and LEU 1035. Compound **76e** has the third most binding affinity -8.199 Kcal/mol and interacts with LYS 868, GLU885, CYS1045 and ASP1046 and hydrophobic part VAL 848, and PHE 1047 (Figure 3). It is therefore inferred that the formation of strong interactions with the selected residues pinpoint to the VEGFR-2 binding pocket.

3.8.2 Docking profile into 2X08 peroxidase active site.

Among the nine investigated compounds **76a-76i,** five compounds **76d, 76e, 76f, 76h and 76i** have been found to have more scavenging activity (IC_{50} = 0.29μM, 0.67 μM, 0.0273 μM and 0.0617 μM) than ascorbic acid (IC_{50} = 5.87 ± 0.88 μM) and showed strong peroxidase interactions (-7.219 Kcal/mol., -7.087 Kcal/mol., -7.648 Kcal/mol., -7.330 Kcal/mol., and -7.671 Kcal/mol.). It can be concluded that four hybrids exhibited scavenging efficacy most comparable to the reference inhibitor, showing the highest binding efficacy with an inhibitory activity of **ΔG =** -5.16 Kcal/mol **(Table 3.9).**

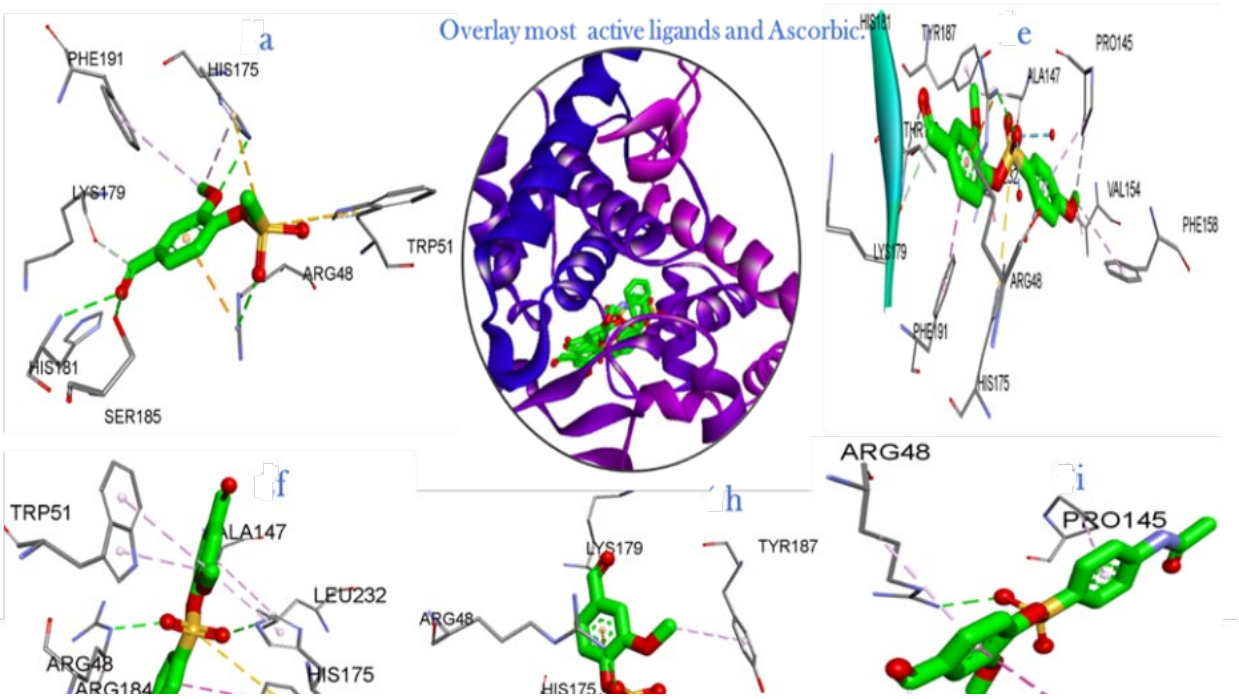

Figure 3. 22: 3D mapping surface of four most active compounds **76a, 76e, 76f, 76h, 76i** and ascorbic acid inside 2X08.

The most active inhibitors of peroxidase were found to be compounds **76h** and **76i**, which demonstrated different binding modes around the protein's active site. Compound **76h** formed strong O---H interactions with both hydrophilic (ARG 48, PRO 145, HIS 175, LYS 179, THR 234, TYR 187) and hydrophobic (PHE 147) residues, while compound **76i** interacted with hydrophilic residues (ARG 48, PRO 145, LYS 179) and one *π-π* interaction with hydrophobic residue (PHE 191). Compounds **76d** and **76e** showed the same inhibitory activity, but also differed in their binding energies of -7.087 Kcal/mol. and -7.219 Kcal/mol., as mentioned in (**Table 3.9**). Compound **76e** showed the best potent binding energy which interacted with hydrophilic residues (TYR 187, HIS 181, LYS 179, HIS 175, PRO 145, ARG 48) and one *π-π* interaction with residue (PHE 191and PHE 158), but also interacted with VAL 154 and ALA 147 through alkyl bond, **Figure 3.20**. Compound **76f** had a similar binding mode to ascorbic acid[131] and interacted with TRP 51

and ARG 184. The identified active compounds are assumed to disrupt the catalytic function of peroxidase by forming stable interactions with key amino acids in the active site (Figure-4).

3.8.3 *In silico* Toxicological Profile

In silico cytotoxicity screening were checked through ADMET (absorption, distribution, metabolism, and excretion - toxicity) parameters acting as a fundamental route in therapeutic bioactive molecules. SwissADME [132] and admet-SAR mode [133]were used to predict parameters for seven investigated molecules **76a-76i**, which are shown in **Table 3.10**. The physicochemical and ADME parameters stated that these ligands are suitable for all investigated rules as Lipinski, Ghose, Veber, Egan, Muegge rule*s* with no violations. All seven investigate compounds **76a-76i** and ascorbic acid were subjected to Lipinski, Ghose, Muegge, and Golden Triangle rules and pass via Veber, Egan, Pfizer, GSK without any alerts in PAINS crtria. While benzamidazole rejected all their tested rules. The tested compound **76a-76i** and ascorbic acid exhibited promising bioavailability scores (0.55) compared to benzimidazole which has (0.17).

The synthesized compounds **76a-76r** were then subjected to drug-likeliness conditions such as good oral bioavailability and resistance to biodegradation or commonly defined as ADMET following Lipinski's rule of five. All the molecules in the **76a-76i** showed good oral bioavailability and resistance to biodegradation, as shown by the data in **Table 3.10**. The Radar for Bioavailability plot (**Figure-5**) illustrates the drug-likeness analysis based on the balance of polarity, size, lipophilicity, solubility, saturation, and flexibility [[134]]. The reader indicates the ideal ranges for each feature with a pink color.

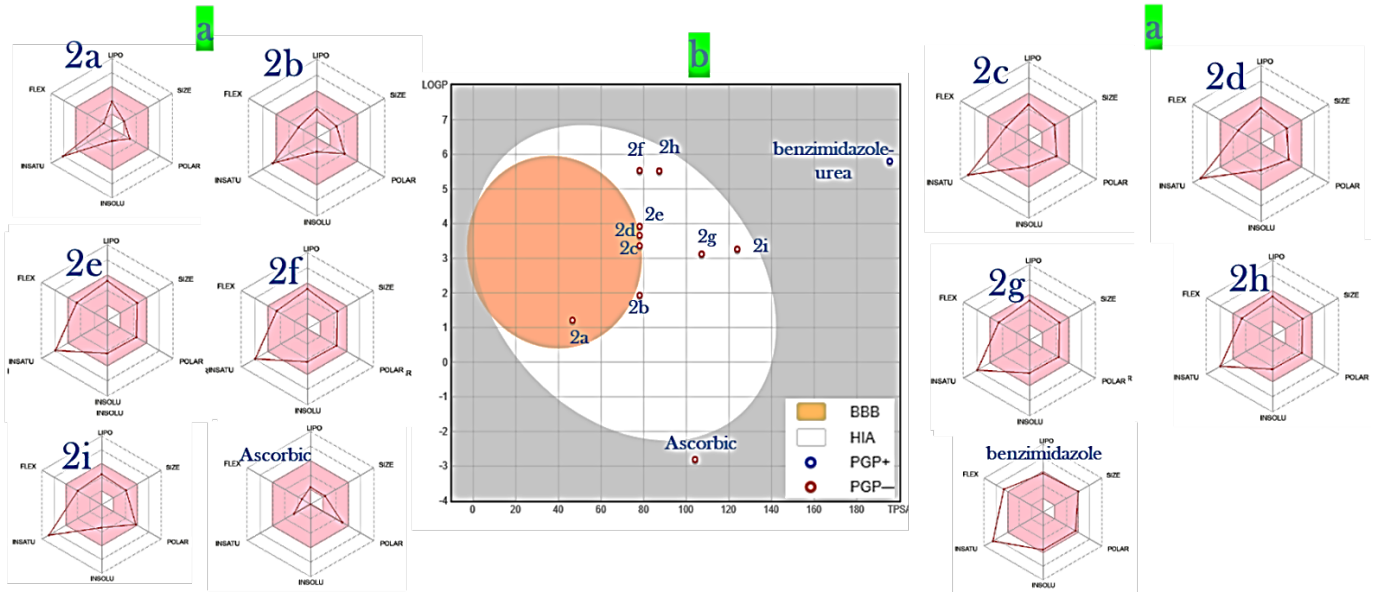

Figure 3. 23: a) The optimal range as red color for; Lipophilicity: −0.7 ≤ XLOGP3 ≤ +5.0, size: 150 ≤ MW ≤ 500 g/mol, polarity: TPSA ≤ 140 Å2, solubility: log S ≤ 6, saturation fraction of carbons in the hybridization sp3 ≥ 0.25, and flexibility: rotatable bonds ≤ 9**.**

b) Boiled-egg plot, White and yellow color represented highly probable for HIA (GI) absorption and BBB permeation, respectively, grey outside for molecules is low absorption and not brain penetration, blue and red points represented as P-gp substrate (PGP+) and P-gp non-substrate (PGP−), respectively.

All compounds **76a-76r** and ascorbic acid had low *Csp3* Fraction values ranging from 0.07 to 0.17 (passing value *Csp3* < 0.25) [[135]], which indicate a low degree of saturation of the carbon atoms. Another important factor for absorption *in silico* is water solubility [[136]]. All the synthesized compounds **76a-76r** exhibited strong absorption as with ADMET-sar pharmacokinetic characteristics i.e. mutagenic, tumorigenic, reproductively effective, irritant, and human intestinal absorption which were also examined *in silico* [[137]].

Table 3. 11: *In silico* ADMET and drug likeness assessment for the seven investigated compounds, **76a-76i** including ascorbic acid (As) and benzimidazole (Bi) as control inhibitor.

	1	**76a**	**76b**	**76c**	**76d**	**76e**	**76f**	**76g**	**76h**	**76i**	**As**	**Bi**
Fraction Csp3	0.12	0.22	0.07	0.07	0.13	0.13	0.13	0.13	0.07	0.75	0.09	
H-bond acceptors	3	5	5	6	5	6	8	9	7	6	6	13
H-bond donors	1	0	0	0	0	0	0	0	0	3	1	3
MR	40.34	53.78	72.62	72.58	77.59	79.11	77.62	79.3	81.44	86.93	33.81	253.68
TPSA	46.53	78.05	78.05	78.05	78.05	87.28	78.05	87.28	123.87	107.15	104.06	195.43
%ABS	92.95	82.07	82.07	82.07	82.07	78.89	82.07	78.89	66.26	72.03	73.1	68.78
iLOGP	1.57	1.42	2.38	2.62	2.66	2.26	2.38	2.47	1.7	2.06	-0.3	6.37
XLOGP3	3.9	4.75	4.66	4.26	3.94	4.72	4.63		-1.42			
Consensus Log P	1.2	1.12	2.44	2.78	2.78	2.36	3.47	3.29	1.66	2.02	-1.61	4.57
ESOL Log S	-1.82	-1.8	-3.25	-3.4	-3.54	-3.31	-4.15	-4.36	-3.36	-2.94	0.08	-8.9
GI absorption	High	High	High	High	High	High	High	High	High	High	Low	Low
BBB permeant	Yes	No	Yes	No	Yes	No	No	No	No	No	No	No
BBB	0.745	0.378	0.11	0.08	0.07	0.057	0.196	0.111	0.071	0.096	0.073	0.064
PPB	79.00%	78.34%	97.70%	98.46%	98.06%	98.44%	98.24%	99.86%	97.79%	91.77%	63.23%	97.54%
Pgp substrate	No	No	No	No	No	No	No	No	No	No	No	Yes
CYP1A2 inhibitor	No	No	Yes	Yes	Yes	No	Yes	No	No	No	No	No
CYP2C19 inhibitor	No	No	Yes	Yes	Yes	Yes	Yes	Yes	Yes	Yes	No	No
CYP2C9 inhibitor	No	No	No	No	No	No	Yes	Yes	Yes	No	No	No
CYP2D6 inhibitor	No	No	No	No	No	No	No	No	No	No	No	No
CYP3A4 inhibitor	No	No	No	No	No	No	No	No	Yes	No	No	No
log Kp (cm/s)	-6.37	-7.14	-6.41	-6.45	-6.24	-6.62	-6.13	-6.01	-6.74	-7.27	-8.37	-7.6
SkinSen	0.26	0.5	0.235	0.134	0.182	0.186	0.041	0.118	0.836	0.111	0.837	0.951
Lipinski violations	0	0	0	0	0	0	0	0	0	0	0	2
Ghose #violations	2	0	0	0	0	0	0	0	0	0	2	4
Veber #violations	0	0	0	0	0	0	0	0	0	0	0	1

Egan #violations	0	0	0	0	0	0	0	0	0	0	0	1
Muegge #violations	1	0	0	0	0	0	0	0	0	0	1	4
PAINS #alerts	0	0	0	0	0	0	0	0	0	0	0	0
Pfizer	Accepted	Accepted	Accepted	Accepted	Accepted	Accepted	Rejected	Accepted	Accepted	Accepted	Accepted	Accepted
GSK	Accepted	Accepted	Accepted	Accepted	Accepted	Accepted	Accepted	Accepted	Accepted	Accepted	Accepted	Rejected
GoldenTriangle	Rejected	Accepted	Accepted	Accepted	Accepted	Accepted	Accepted	Accepted	Accepted	Accepted	Rejected	Rejected
Bioavailability score	0.55	0.55	0.55	0.55	0.55	0.55	0.55	0.55	0.55	0.55	0.55	0.17
Leadlikeness #violations	1	1	0	0	0	0	1	2	0	0	1	2
Synthetic Accessibility	1.15	2.36	2.77	2.77	2.88	2.91	2.85	2.94	2.84	2.73	3.16	10
HIA	0.012	0.009	0.007	0.005	0.004	0.006	0.004	0.004	0.007	0.008	0.069	0.944
Caco-2	-4.484	-4.684	-4.699	-4.612	-4.664	-4.652	-4.753	-4.92	-4.649	-4.913	-5.917	-4.858
MDCK	1.37E-05	1.75E-05	2.50E-05	2.35E-05	2.38E-05	2.15E-05	2.33E-05	2.51E-05	7.44E-05	1.40E-05	0.000143	1.28E-05
Carcinogenicity	0.119	0.732	0.856	0.935	0.921	0.909	0.724	0.93	0.926	0.685	0.266	0.041
hERG	0.035	0.013	0.128	0.157	0.179	0.307	0.138	0.47	0.528	0.124	0.015	0.261
H-HT	0.019	0.817	0.083	0.76	0.128	0.171	0.264	0.974	0.829	0.318	0.168	0.99
DILI	0.033	0.783	0.954	0.937	0.949	0.942	0.954	0.975	0.94	0.946	0.936	0.867
Ames	0.067	0.611	0.014	0.015	0.015	0.016	0.032	0.153	0.962	0.028	0.027	0.009
Pgp-inh	0	0.001	0.012	0.076	0.007	0.065	0.058	0.358	0.004	0.011	0.001	1
Pgp-sub	0.082	0.002	0	0	0.001	0	0.001	0	0	0.019	0.089	0.862
IGC50	3.177	2.92	3.388	3.492	3.565	3.637	3.835	3.698	3.853	3.279	1.489	5.106
LD50	3.863	4.119	4.287	4.419	4.361	4.329	4.904	4.867	4.485	4.21	2.389	2.009

To assess the potential of these compounds as substrates or non-substrates for different biological barriers and transporters, we applied another support vector machine algorithm to predict their permeability for skin permeation (Log Kp), Caco-2, blood brain barrier (BBB) and p-glycoprotein (P-gp). We also used the same algorithm to evaluate their inhibition effects on the main cytochromes P450 isoenzymes (CYP1A2, CYP2C19, CYP2C9, CYP2D6 and CYP3A4). The predictions from (**Table 3.10**) indicated that none of these compounds had the ability to inhibit any of the P450 types.

The permeability of the compounds **76a-76r** across skin and intestinal cells was low, as indicated by their low (Log Kp) and Caco-2 values. The BOILED-Egg model was applied to plot the WLOGP and TPSA values of these compounds (**Figure 3.21**) which revealed that the compounds **76a-76r** had high BBB permeability, high GI absorption, high brain penetration, weak inhibition of (hERG) ranging from (0.013-0.52) and no resistance to P-gp protein. The compounds were also non-carcinogenic, non-mutagenic and non-tumorigenic when compared with 981 carcinogenic chemicals from the “Carcinogenic Potency Database (CPDB)” [138].

CHAPTER 4: EXPERIMENTAL

4.1 General

Reagents and solvents used in this study were procured from commercial sources, mainly Sigma-Aldrich and Merck (South Africa). All materials were utilized without further purification, unless clearly mentioned. Reactions involving moisture-sensitive substances were conducted under a nitrogen (N_2) atmosphere, employing oven-dried glassware. Tetrahydrofuran (THF) was distilled freshly over sodium/benzophenone under a N_2 atmosphere prior to its application. All experiments were carried out at room temperature unless specifically indicated. Thin-layer chromatography was performed using self-cut Merck silica gel F254 plates with a thickness of 0.255 mm, and when necessary, visualization of spots was achieved through ultraviolet fluorescence at wavelengths of 254 or 297 nm. Flash column chromatography was executed using Merck Kiesel silica gel 60 (230–400 mesh). Analytical preparative thin-layer chromatography (TLC) on silica gel plates was also employed for purification in some instances.

The structural characteristics of the compounds were documented and confirmed through various analytical techniques: High-resolution mass spectra were acquired using a Waters Synapt G2 instrument with an ESI probe, operating in ESI Positive mode with a Cone Voltage of 15 V (Waters Corp., Milford, MA, USA); Melting points were determined using a Lasec/SA-melting point apparatus from Lasec company, SA (Johannesburg, South Africa), and reported without correction; IR spectra were recorded using a Bruker Alpha platinum-ATR FTIR spectrometer and Nuclear Magnetic Resonance (NMR) data were collected on a Bruker Ascend 400 MHz Topspin 3.2 spectrometer. Chemical shifts are presented in parts per million (ppm) relative to tetramethylsilane

(TMS). Peak multiplicities are indicated as brs (broad singlet), s (singlet), d (doublet), t (triplet), q (quartet), quin (quintet), sex (sextet), and m (multiplet), or combinations thereof (e.g., dd for doublet of doublet), with coupling constants (*J*) reported in hertz (Hz). ^{1}H NMR and ^{13}C NMR spectra were internally referenced using solvent signals as follows: ^{1}H NMR: 7.25 ppm for $CDCl_3$, 2.50 ppm for DMSO-d_6, 3.31 ppm for MeOD; ^{13}C NMR: 77.0 ppm for $CDCl_3$, 39.9 ppm for DMSO-d_6, and 49.1 ppm for MeOD, all recorded at room temperature."

4.2 Synthesis of substrates

4.2.1 Synthesis of 5-iodo-2-aminobenzamide 73

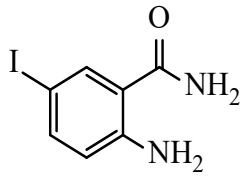

A mixture of 2-aminobenzamide (5.00 g,37,72 mmol), I_2 (11.13 g, 44.06 mmol), $NaHCO_3$ (3.70 g, 44.06 mmol) and H_2O (1 L) was allowed to stir at room temperature for 6 hr. The mixture was quenched in $Na_2S_2O_3$ solution in a beaker containing crushed ice. The precipitate formed was filtered, then recrystallized in ethanol which afforded a purple crystalline solid. **73** (6.46 g; 75.33%) M.p. (221.09 °C); FTIR ($\nu_{max,}$ cm^{-1}) 504, 836, 1158, 1381, 1618, 3188, 3315, 3376 cm^{-1}. ^{1}H NMR: (400 MHz, DMSO-$d_{6,}$ ppm), 7.85 (s, 1H, N<u>H</u>), 7.81 (d, 1H, Ph, *J* = 4.0 Hz), 7.38 (dd, 1H, Ph, *J* = 2.0 Hz and *J* = 8.4 Hz) 7.17 (s, 1H, N<u>H</u>) 6.72 (s, 2H, N<u>H</u>$_2$), 6.54 (d, 1H, Ph, *J* = 3.0 Hz); ^{13}C NMR: (100 MHz, DMSO-d_6, ppm) 40.1, 40.3, 40.5, 74.8, 116.5, 119.4, 136.9, 140.3, 150.1, 170.3; HRMS (ESI): calculated 261.96 $[M]^+$ $C_7H_7IN_2O^+$ 262.9956.

4.2.2 Synthesis of 2-acetamido-5-iodobenzamide 74

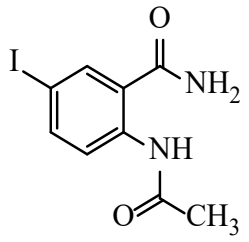

A stirred mixture of 5-iodo-2-aminobenzamide (6.00 g, 22.89 mmol), K_2CO_3 (9.15 g, 34.35 mmol) and CH_3COCl was allowed to reflux at 66 ˚C for a 1 hr in THF (200 mL). The reaction was cooled for 10 min, then quenched using crushed ice. Thereafter the residue is partitioned between dichloromethane DCM and water (H_2O), the layers of the filtrate were separated and the organic phase is washed with 1M sodium carbonate solution (Na_2CO_3), dried with magnesium sulphate (MgSO4), and evaporated to afford a greyish solid **74** (4.62 g, 66.57 %) M.p (326.58 °C); FTIR ($V_{max,}$ cm^{-1}) 413, 423, 455, 505, 545, 625, 725, 844, 1297, 1372, 1400, 1498, 1565, 1663, 2046, 2163, 2920, 3166, 3341 cm^{-1}; ^{1}H NMR: (400 MHz, DMSO-d_6, ppm) 11.46 (s, 1H, N<u>H</u>) 8.35 (d, 1H, Ph, *J* = 3.0 Hz), 8.23 (d, 1H, Ph, *J* = 8.8 Hz) 8.07 (s, 2H,N<u>H</u>$_2$), 8.23 (dd, 1H, Ph, *J* = 8.8 Hz and *J* = 2.0 Hz); ^{13}C NMR: (100 MHz, DMSO-d_6, ppm) 25.4, 86.3, 122.3, 122.7, 137.0, 139.6, 140.9, 168.7, 169.7; HRMS (ESI): calculated 285.96 $[M]^+$ $C_9H_7IN_2O^+$,287.9788.

4.2.3 Synthesis of 6-iodo-2-methylquinazolin-4(*3H*)-one 75

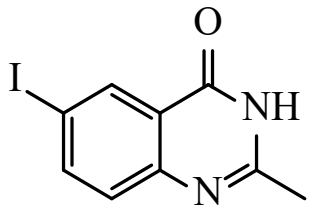

A stirred mixture of 2-acetamido-5-iodobenzamide (1.00 g, 3.29 mmol) in an aqueous solution of 99% NaOH in ethanol 8:2 (20 mL) was allowed to reflux for 2 hr. The solution was quenched using crushed ice, then followed by addition of sulphuric acid for neutralization. The solution was then filtered and afforded a white-greyish solid **75** (0.69 g, 79.24%), M.p. (312.91 °C); FTIR ($V_{max,}$ cm^{-1}) 420, 494, 530, 574, 590, 783, 1077, 1302, 1467, 1559, 1656, 1704, 2573 CM^{-1}; ^{1}H NMR: (400 MHz, DMSO-d_6, ppm) 8.41 (d, 1H, Ph, *J* = 3.6 Hz), 8.27 (dd, 1H, Ph, *J* = 2.0 Hz and *J* = 8.8 Hz), 7.50 (d, 1H, Ph, *J* = 8.4 Hz) 5.23 (s, N<u>H</u>) 2.58 (s, 3H, C<u>H</u>$_3$), ^{13}C NMR: (100 MHz, DMSO-d_6, ppm) 24.5, 98.4, 126.3, 128.2, 139.8, 139.9, 145.1, 149.4, 163.9, 164.9 HRMS (ESI): calculated 285.96 $[M]^+$ $C_9H_7IN_2O^+$,286.9609.

4.2.4 Synthesis of 4-formyl-2-methoxyphenyl aryl sulfonates (76a-i)

4.2.4.1

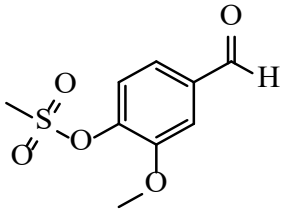

Synthesis of 4-formyl-2-methoxyphenylmethanesulfonate **76a**

To a stirring solution of 4-hydroxy-3-methoxysalicyladehyde (1.00 g, 6.57 mmol) and pyridine (5mL) in an ice bath, methane sulfonyl chloride (0.88 g, 7.67 mmol) 0.59 mL was added in a dropwise manner and the reaction was allowed to stir for 2 hr at 0 °C. After the TLC had shown the complete consumption of the starting material, the reaction was quenched with crushed ice and then filtered. The resulting precipitate was then recrystallized in ethanol to afford compound **76a** (1.03 g, 69.66%),as white crystals M.p. (60.57 °C); FTIR ($V_{max,}$ cm^{-1}) 503, 519, 543, 567, 595, 690, 776, 824, 852, 932, 978, 1025, 1104, 1150, 1173, 1264, 1286, 1356, 1452, 1505, 1588, 1694 cm^{-1}; 1H NMR: (400 MHz, DMSO-d_6, ppm) 9.98 (s, 1H, CO<u>H</u>), 7.67 (d, 1H, Ph, *J* = 4.5 Hz), 7.61 (dd, 1H, Ph, *J* = 2.6 Hz and *J* = 8.6 Hz), 7.56 (d, 1H, Ph, *J* = 8.4 Hz), 3.96 (s, 3H, OC<u>H</u>$_3$), 3.24 (s, 3H, C<u>H</u>$_3$); ^{13}C NMR: (100 MHz, DMSO-d_6, ppm) 56.2, 111.3, 124.67, 125.0, 135.9, 142.6, 152.4; HRMS (ESI): calculated 230.02 $[M]^+$ $C_9H_{10}O_5S^+$ 231.0389.

4.2.4.2

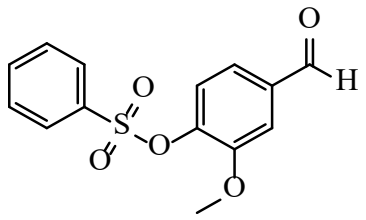

Synthesis of 4-formyl-2-methoxyphenylbenzenesulfonate **(76b)**

To a stirring solution of 4-hydroxy-3-methoxysalicyladehyde (1.00 g, 6.57 mmol) and pyridine (5mL) in an ice bath, benzene sulfonyl chloride (1.35 g, 7.67 mmol) 0.98 mL was added in a dropwise manner and the reaction was allowed to stir for 2 hr at 0 °C. After the TLC had shown the complete consumption of the starting material, the reaction was quenched with crushed ice and then filtered.

The resulting precipitate was then recrystallized in ethanol to afford compound **76b** (1.71 g, 86.80%) as yellow crystals M.p. (138.35 °C); FTIR ($V_{max,}$ cm^{-1}) 438, 520, 562, 586, 625, 683, 704, 725, 750, 836, 892, 1069, 1161, 1189, 1250, 1370, 1466, 1590, 1687 cm^{-1}; ^{1}H NMR: (400 MHz, DMSO-d_6, ppm) 9.94 (s, 1H, CO<u>H</u>), 7.84- 7.86 (m, 1H, Ph), 7.83- 7.87 (m, 2H, Ph), 7.67 (t, 2H, Ph, *J* = 8.0 Hz), 7.56 (dd, 1H, *J* = 2.6 Hz and *J* = 8.0 Hz), 7.52 (d, 1H, *J* = 6.6 Hz), 7.37 (d, 1H, *J* = 8.4 Hz), 3.65 (s, 3H, OC<u>H</u>$_3$); ^{13}C NMR: (100 MHz, DMSO-d_6, ppm) 55.9, 112.7, 123.2, 124.4, 128.2, 129.6, 134.8, 135.1, 135.9, 141.8, 152.0, 192.0; HRMS (ESI): calculated 292.04 $[M]^+$, $C_{14}H_{12}O_5S^+$ 293.0723.

4.2.4.3

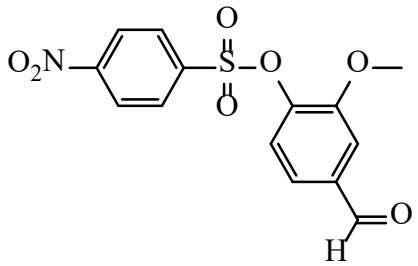

Synthesis of 4-formyl-2-methoxyphenyl 4-nitrobenzenesulfonate **(76c)**

To a stirring solution of 4-hydroxy-3-methoxysalicyladehyde (1.00 g, 6.57 mmol) and pyridine (5mL) in an ice bath, 4-nitrobenzenesulfonyl chloride (3.68 g, 15.77 mmol) was added manner and the reaction was allowed to stir for 2 hr at 0 °C. After the TLC had shown the complete consumption of the starting material, the reaction was quenched with crushed ice and then filtered. The resulting precipitate was then recrystallized in ethanol to afford compound **76c** (1.89 g, 85.52%) as purple crystal, M.p. (160.77 °C); FTIR ($v_{max,}$ cm^{-1}) cm^{-1} 562, 666, 709, 827, 1019, 1087, 1141, 1266, 1360, 1495, 1592, 1689; ^{1}H NMR: (400 MHz, DMSO-d_6, ppm) 9.9 (s, 1H, CO<u>H</u>), 7.77 (d, 1H, Ph, *J* = 8.8

Hz), 7.35 (dd, 1H, Ph, *J* = 6.6 Hz and *J* = 2.6 Hz), 7.34 (d, 1H, Ph, *J* = 3 Hz), 6.94 (d, 2H, Ph, *J* = 9.0 Hz), 3.86 (s, 3H, C<u>H</u>$_3$); ^{13}C NMR: (100 MHz, DMSO-d$_6$, ppm) 55.7, 110.9, 114.0, 124.4, 127.0, 130.8, 135.6, 142.9, 152.5, 164.1, 190.8; HRMS (ESI): calculated 337.30 $[M]^+$, $C_{14}H_{11}NO_7S^+$ 338.8911.

4.2.4.4

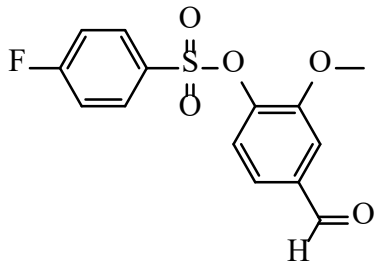

Synthesis of 4-formyl-2-methoxyphenyl 4-fluorobenzenesulfonate **(76d)**

To a stirring solution of 4-hydroxy-3-methoxysalicyladehyde (1.00 g, 6.57 mmol) and pyridine (5mL) in an ice bath, 4-fluorobenzenesulfonyl chloride (3.068 g, 15.77 mmol) was added manner and the reaction was allowed to stir for 2 hr at 0 °C. After the TLC had shown the complete consumption of the starting material, the reaction was quenched with crushed ice and then filtered. The resulting precipitate was then recrystallized in ethanol to afford compound **76d** (1.50 g, 73.89%) as white crystal, M.p. (151.49 °C), FTIR (V_{max}, cm^{-1}) 156, 611, 627, 769, 832, 898, 1045, 1127, 1245, 1339, 1442, 1525, 1627; ^{1}H NMR: (400 MHz, DMSO-d$_6$, ppm) 9.91 (s, 1H, CO<u>H</u>), 7.88 (m, 2H, Ph), 7.43

(dd, 1H, Ph, *J* = 6.4 Hz and *J* = 2.6 Hz), 7.35 (d, 1H, Ph, *J* = 4.6 Hz), 7.19 (m, 2H, Ph), 3.62 (s, 3H, OC$\underline{H}_3$); ^{13}C NMR: (100 MHz, DMSO-d_6, ppm) 55.7, 110.9, 116.1, 116.3, 124.3, 124.6, 135.8, 142.5, 152.3, 164.7, 167.3, 190.7; HRMS (ESI): calculated 310.30 $[M]^+$, $C_{14}H_{11}FO_5S^+$, 311.9813.

4.2.4.5

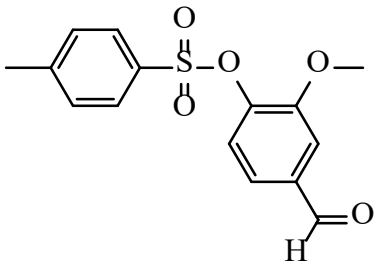

Synthesis of 4-formyl-2-methoxyphenyl 4-methylbenzenesulfonate **(76e)**

To a stirring solution of 4-hydroxy-3-methoxysalicyladehyde (1.00 g, 6.57 mmol) and pyridine (5mL) in an ice bath, toluenesulfonyl chloride (3.00 g, 15.77 mmol) was added and the reaction was allowed to stir for 2 hr at 0 °C. After the TLC had shown the complete consumption of the starting material, the reaction was quenched with crushed ice and then filtered. The resulting precipitate was then recrystallized in ethanol to afford compound **76e** (1.42 g, 69.65%) as white crystal, M.p. (161.67 °C),FTIR (V_{max}, cm^{-1}) 547, 598, 661, 709, 751, 780, 839, 1029, 1055, 1152, 1178, 1290, 1363, 1502, 1593, 1697; ^{1}H NMR: (400 MHz, DMSO-d_6, ppm) 9.90 (s, 1H, CO$\underline{H}$), 7.73 (d, 2H, Ph, *J* = 8 Hz), 7.41 (dd, 1H, Ph, *J* = 6.8 Hz and *J* = 2.4 Hz), 7.32 (d, 2H, Ph, *J* = 7.6 Hz), 7.19 (d, 2H, Ph, *J* = 8.6) 3.61 (s, 3H, OC$\underline{H}_3$), 2.43 (s, 3H, C$\underline{H}_3$); ^{13}C NMR: (100 MHz, DMSO-d_6, ppm) 55.8, 55.7, 110.9, 124.3, 124.4, 128.5, 129.4, 132.8, 135.6, 142.9, 145.4, 152.5, 190.8 HRMS (ESI): calculated 306.06 $[M]^+$, $C_{15}H_{14}O_5S^+$, 307.1156.

4.2.4.6

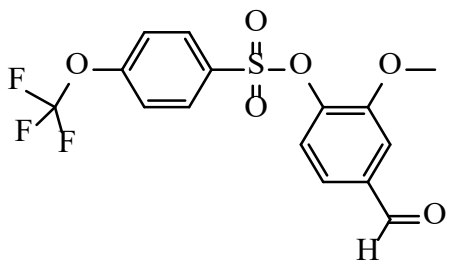

Synthesis of 4-formyl-2-methoxyphenyl 4-(trifluoromethoxy)benzenesulfonate **(76f)**

To a stirring solution of 4-hydroxy-3-methoxysalicyladehyde (1.00 g, 6.57 mmol) and pyridine (5mL) in an ice bath, 4-trifluoromethoxybenzenesulfonyl chloride (4.11 g, 15.77 mmol) was added manner and the reaction was allowed to stir for 2 hr at 0 °C. After the TLC had shown the complete consumption of the starting material, the reaction was quenched with crushed ice and then filtered. The resulting precipitate was then recrystallized in ethanol to afford compound **76f** (1.98 g, 80.16%) as white crystal, M.p. (162.14 °C), FTIR ($\nu_{max,}$ cm^{-1}) 542, 593, 714, 752, 836, 1024, 1147, 1375, 1499, 1553, 1694; ^{1}H NMR: (400 MHz, DMSO-d_6, ppm) 9.90 (s, 1H, CO<u>H</u>), 7.89 (d, 2H, Ph, *J* = 8.4 Hz), 7.34 (d, 2H, Ph, *J* = 8.8 Hz), 7.33 (d, 3H, Ph, *J* = 6.6 Hz), 3.54 (s, 3H, OC<u>H</u>$_3$); ^{13}C NMR: (100 MHz, DMSO-d_6, ppm) 30.8, 55.5, 110.9, 118.7, 124.7, 130.7, 142.3, 152.1, 153.2, 190.6, 207.0; HRMS (ESI): calculated 376.02 $[M]^+$, $C_{15}H_{11}F_3O_6S^+$, 377.7678.

4.2.4.7

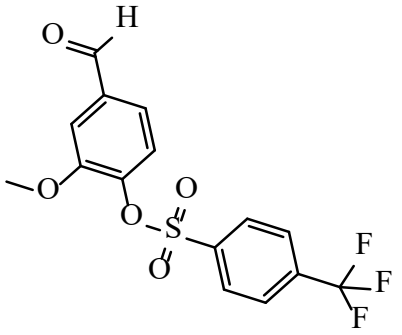

Synthesis of 4-formyl-2-methoxyphenyl 4-(trifluoromethyl)benzenesulfonate **(76g)**

To a stirring solution of 4-hydroxy-3-methoxysalicyladehyde (1.00 g, 6.57 mmol) and pyridine (5mL) in an ice bath, 4-trifluoromethylsulfonyl chloride (2.00 g, 15.77 mmol) was added and the reaction was allowed to stir for 2 hr at 0 °C. After the TLC had shown the complete consumption of the starting material, the reaction was quenched with crushed ice and then filtered. The resulting precipitate was then recrystallized in ethanol to afford compound **76g** (1.76 g, 74.57%) as white crystal, M.p. (166.33 °C), FTIR (ν_{max}, cm^{-1}) 428, 539, 596, 719, 825, 1059, 1140, 1271, 1316, 1370, 1496, 1656; ^{1}H NMR: (400 MHz, DMSO-d_6, ppm) 9.95 (s, 1H, CO<u>H</u>), 8.06 (dd, 4H, Ph, *J* = 8.4 Hz and *J* = 3.3 Hz), 7.58 (dd, 1H, Ph, *J* = 6.5 Hz and *J* = 2.4 Hz), 7.54 (d, 1H, Ph, *J* = 6.1 Hz), 3.52 (s, 3H, OC<u>H</u>$_3$), 3.46 (s, 3H, C<u>H</u>$_3$); ^{13}C NMR: (100 MHz, DMSO-d_6, ppm) 55.6, 111.0, 125.9, 126.0, 129.3, 135.8, 135.9, 139.1, 139.2, 142.3, 152.1, 192.6; HRMS (ESI): calculated 360.30 $[M]^+$, $C_{15}H_{11}F_3O_5S^+$, 361.7681.

4.2.4.8

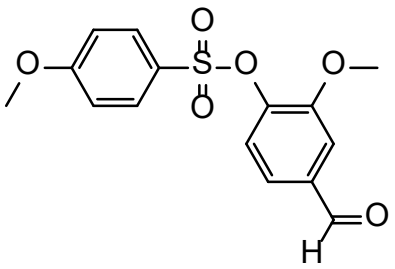

Synthesis of 4-formyl-2-methoxyphenyl 4-methoxybenzenesulfonate **(76h)**

To a stirring solution of 4-hydroxy-3-methoxysalicyladehyde (1.00 g, 6.57 mmol) and pyridine (5mL) in an ice bath, 4-methoxybenzenesulfonyl chloride (3.06 g, 15.77 mmol) was added and the reaction was allowed to stir for 2 hr at 0 °C. After the TLC had shown the complete consumption of the

starting material, the reaction was quenched with crushed ice and then filtered. The resulting precipitate was then recrystallized in ethanol to afford compound **7**6h (1.45 g, 68.72%) as white crystal, M.p. (184.25 °C); FTIR ($V_{max,}$ cm^{-1}) 561, 665, 708, 826, 1019, 1087, 1140, 1265, 1360, 1495, 1592, 1689; ^{1}H NMR: (400 MHz, DMSO-d_6, ppm) ^{1}H NMR: (400 MHz, DMSO-d_6, ppm) 9.88 (s, 1H, COH), 7.74 (d, 2H, Ph, *J* = 8.8 Hz), 7.38 (dd, 1H, Ph, *J* = 6.4 Hz and *J* = 1.6 Hz), 7.33 (d, 1H, *J* = 3.6 Hz), 7.32 (d, 1H, Ph, *J* = 3.2 Hz), 7.93 (d, 2H, Ph, *J* = 8.8 Hz), 3.84 (s, 3H, OCH3), 3.61 (s, 3H, OCH3);; ^{13}C NMR: (100 MHz, DMSO-d_6, ppm) 30.8, 55.6, 55.7, 110.9, 113.9, 124.1, 124.4, 126.8, 130.7, 135.5, 142.8, 152.4, 164.1, 190.8; HRMS (ESI): calculated 322.33 $[M]^+$, $C_{15}H_{14}O_6S^+$, 323.6788.

4.2.4.9

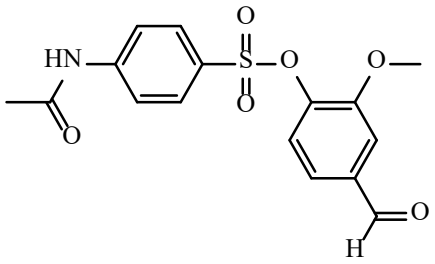

Synthesis of 4-formyl-2-methoxyphenyl 4-acetamidobenzenesulfonate **(76i)**

To a stirring solution of 4-hydroxy-3-methoxysalicyladehyde (1.00 g, 6.57 mmol) and pyridine (5mL) in an ice bath, 4-acetamidebenzenesulfonyl chloride (3.68 g, 15.77 mmol) was added and the reaction was allowed to stir for 2 hr at 0 °C. After the TLC had shown the complete consumption of the starting material, the reaction was quenched with crushed ice and then filtered. The resulting precipitate was then recrystallized in ethanol to afford compound **76i** (1.49 g, 65.06%) as white crystal,M.p. (300.65 °C); FTIR (v_{max}, cm^{-1}, 432, 566, 627, 704, 737, 795, 893,1048, 1127, 1213,

1333, 1436, 1551, 1619, 1740; ^{1}H NMR: (400 MHz, DMSO-d_6, ppm) 9.89 (s, 1H, CO<u>H</u>), 8.58 (s, 1H, N<u>H</u>), 7.73 (m, 4H, Ph), 7.41 (d, 1H, Ph, *J* = 6.0 Hz), 7.89 (dd, 1H, Ph, *J* = 8.6 Hz and *J* = 2.4 Hz), 7.31 (d, 1H, Ph, *J* = 8.0 Hz), 3.60 (s, 3H, OC<u>H</u>$_3$), 2.20 (s, 3H, C<u>H</u>$_3$); ^{13}C NMR: (100 MHz, DMSO-d_6, ppm) 23.3, 56.0, 112.8, 118.8, 123.3, 124.4, 127.8, 129.9, 135.9, 142.0, 145.1, 152.1, 169.6, 192.2; HRMS (ESI): calculated 349.36 $[M]^+$, $C_{16}H_{15}NO_6S^+$ 356.7845.

4.2.5 Synthesis of 4-bromo-2-formylphenyl arylsulfonates 76j-r

4.2.5.1

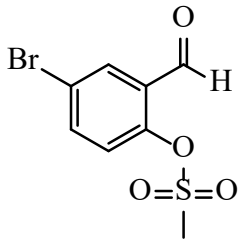

Synthesis of 4-bromo-2-formylphenyl methanesulfonate **(76j)**

To a stirring solution of 5-bromosalicyladehyde (1.00 g, 4.96 mmol) and pyridine (5mL) in an ice bath, methanesulfonyl chloride (1.14 g, 9.95 mmol) 0.77 mL was added in a dropwise manner and the reaction was allowed to stir for 2 hr at 0 °C. After the TLC had shown the complete consumption of the starting material, the reaction was quenched with crushed ice and then filtered. The resulting precipitate was then recrystallized in ethanol to afford compound **76j** (1.10 g, 80.29%) as white crystal, M.p. (81.88 °C); FTIR ($\nu_{max,}$ cm^{-1}) 526, 610, 833, 1306, 1461, 1619, 1678 cm^{-1}; ^{1}H NMR: (400 MHz, DMSO-d_6, ppm) 3.66 (s, 3H, C<u>H</u>$_3$), 7.53 (d, 1H, Ph, *J* = 8 Hz), 8.00 (dd, 1H, Ph, *J* = 6.64 and *J* = 2.8 Hz), 8.03 (d, 1H, Ph, *J* = 3.4 Hz), 10.15 (s, 1H, CO<u>H</u>); ^{13}C NMR: (100 MHz, DMSO-d_6, ppm) 96.0, 125.6, 128.1, 130.2, 130.5, 134.4, 135.7, 135.8, 138.3, 139.5, 147.7, 151.1, 153.9, 156.3; HRMS (ESI): calculated $[M]^+$ 277.92, $C_8H_7BrO_4S^+$ 278.9843.

4.2.5.2

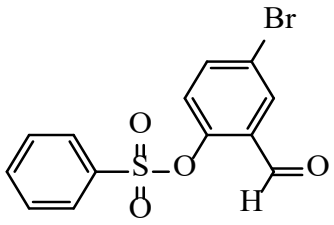

Synthesis of 4-bromo-2-formylphenyl benzenesulfonate **(76k)**

To a stirring solution of 5-bromosalicyladehyde (1.00 g, 4.96 mmol) and pyridine (5mL) in an ice bath, benzene sulfonyl chloride (1.14 g, 9.95 mmol) 0.77 mL was added in a dropwise manner and the reaction was allowed to stir for 2 hr at 0 °C. After the TLC had shown the complete consumption of the starting material, the reaction was quenched with crushed ice and then filtered. The resulting precipitate was then recrystallized in ethanol to afford compound **76k** (1.20 g, 71.42%) as white crystal, M.p. (164.65 °C); FTIR ($\nu_{max,}$ cm^{-1}) 438, 520, 562, 586, 625, 682, 703, 724, 750, 836, 891, 1088, 1160, 1198, 1249, 1372, 1449, 1466, 1590, 1687 cm^{-1}; ^{1}H NMR: (400 MHz, DMSO-d_6, ppm) 9.81 (s, 1H, COH), 7.95 (d, 1H, Ph, *J* = 6.6 Hz), 7.91 (dd, 2H, Ph, *J* = 6.0 Hz and *J* = 2.0 Hz), 7.88-7.89 (m, 1H, Ph), 7.87 (dd, 1H, Ph, *J* = 1.2 Hz and *J* = 5.2 Hz), 7.69 (t, 2H, Ph, *J* = 6.0 Hz), 7.17 (d, 1H, Ph, *J* = 8 Hz); ^{13}C NMR: (100 MHz, DMSO-d_6, ppm) 121.5, 125.5, 130.5, 131.5, 133.9, 135.2, 138.0, 149.8, 185.8; HRMS (ESI): calculated 339.94 $[M]^+$, $C_{13}H_9BrO_4S^+$ 340.2356.

4.2.5.3

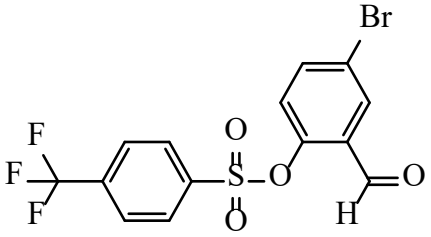

Synthesis of 4-bromo-2-formylphenyl 4-(trifluoromethyl)benzenesulfonate **(76l)**

To a stirring solution of 5-bromosalicyladehyde (1.00 g, 4.96 mmol) and pyridine (5mL) in an ice bath, trifluoromethylbenzenesulfonyl chloride (1.45 g, 6.00 mmol) was added and the reaction was allowed to stir for 2 hr at 0 °C. After the TLC had shown the complete consumption of the starting material, the reaction was quenched with crushed ice and then filtered. The resulting precipitate was then recrystallized in ethanol to afford compound **76l** (1.69 g, 83.36%) as white crystal, M.p. (192.51 °C); FTIR (ν_{max}, cm^{-1}) 427, 558, 599, 709, 747, 839, 893, 1059, 1090, 1135, 1164, 1316, 1382, 1466, 1690; ^{1}H NMR: (400 MHz, DMSO-d_6, ppm); 9.95 (s, 1H, CO<u>H</u>), 7.98 (d, 2H, Ph, *J* = 4.4 Hz), 7.91 (dd, 2H, Ph, *J* = 4.0 Hz and *J* = 2.4 Hz), 7.68 (dd,1H, Ph, *J* = 6.8 Hz and *J* = 2.8 Hz), 7.38 (d, 2H, Ph, *J* = 8 Hz), 7.05 (d, 1H, Ph, *J* = 8 Hz); ^{13}C NMR: (100 MHz, DMSO-d_6, ppm); 121.8, 125.1, 126.7, 126.8, 129.1, 130.4, 132.1, 138.1, 149.1, 185.5; HRMS (ESI): calculated 409.17 $[M]^+$, $C_{14}H_8BrF_3O_4S^+$, 410.5578.

4.2.5.4

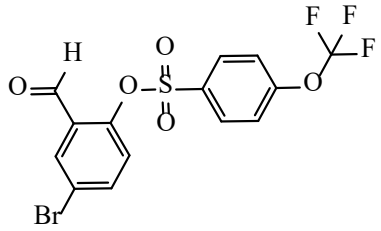

Synthesis of 4-bromo-2-formylphenyl 4-(trifluoromethoxy)benzenesulfonate **(76m)**

To a stirring solution of 5-bromosalicyladehyde (1.00 g, 4.96 mmol) and pyridine (5mL) in an ice bath, trifluoromethoxybenzenesulfonyl chloride (1.55 g, 6.00 mmol) was added and the reaction was allowed to stir for 2 hr at 0 °C. After the TLC had shown the complete consumption of the

starting material, the reaction was quenched with crushed ice and then filtered. The resulting precipitate was then recrystallized in ethanol to afford compound **76m** (1.69 g, 83.36%) as white crystal, M.p. (214.86); FTIR (ν_{max}) cm^{-1} 542, 554, 597, 715, 749, 838, 1089, 1158, 1249, 1380, 1467, 1590, 1691, 2909, 3108; ^{1}H NMR: (400 MHz, DMSO-d_6, ppm) 9.95 (s, 1H, CO<u>H</u>), 7.98 (d, 2H, Ph, *J* = 6.4 Hz), 7.91 (dd, 2H, Ph, *J* = 6.0 Hz and *J* = 2.0 Hz), 7.68 (dd,1H, Ph, *J* = 6 Hz and *J* = 1.8 Hz), 7.38 (dd, 2H, Ph, *J* = 8 Hz), 7.05 (d, 1H, Ph, *J* = 8 Hz); ^{13}C NMR: (100 MHz, DMSO-d_6, ppm) 121.0, 121.7, 125.3, 130.4, 130.8, 131.9, 132.0, 138.1, 185.6; HRMS (ESI): calculated 425.17 $[M]^+$, $C_{14}H_8BrF_3O_5S^+$, 425.6790.

4.2.5.5

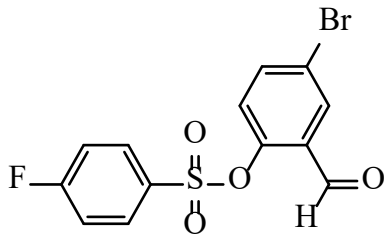

Synthesis of 4-bromo-2-formylphenyl 4-fluorobenzenesulfonate **(76n)**

To a stirring solution of 5-bromosalicyladehyde (1.00 g, 4.96 mmol) and pyridine (5mL) in an ice bath, 4-fluorobenzenesulfonyl chloride (1.15 g, 6.00 mmol) was added and the reaction was allowed to stir for 2 hr at 0 °C. After the TLC had shown the complete consumption of the starting material, the reaction was quenched with crushed ice and then filtered. The resulting precipitate was then recrystallized in ethanol to afford compound **76n** (1.41 g, 79.21%) as white crystal, M.p. (177.76 °C); FTIR (ν_{max}, cm^{-1}) 444, 555, 622, 717, 832, 888, 1087, 1161, 1257, 1378, 1467, 1587, 1678, 2913., 3075; ^{1}H NMR: (400 MHz, DMSO-d_6, ppm); 9.87 (s, 1H, CO<u>H</u>), 8.65 (dd, 2H, Ph, *J* = 8.4 Hz), 8.11 (dd, 2H, Ph, *J* = 8.4 Hz and *J* = 2.0 Hz), 8.20 (d, 1H, Ph, *J* = 2.3 Hz), 7.65 (dd, 1H, *J* =

4.0 Hz and *J* = 8.0 Hz), 7.16 (d, 1H, *J* = 8.0 Hz)^{13}C NMR: (100 MHz, DMSO-d_6, ppm) 110.9, 118.7, 121.3, 124.2, 124.7, 130.7, 142.3, 152.1, 153.2, 190.6. HRMS (ESI): calculated 359.17 $[M]^+$, 360.017.

4.2.5.6

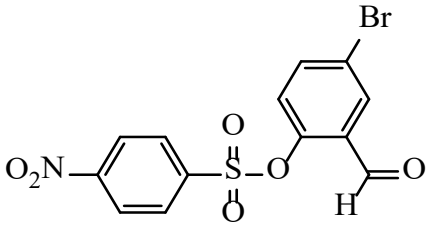

Synthesis of 4-bromo-2-formylphenyl 4-nitrobenzenesulfonate **(76o)**

To a stirring solution of 5-bromosalicyladehyde (1.00 g, 4.96 mmol) and pyridine (5mL) in an ice bath, 4-nitrobenzenesulfonyl chloride (1.32 g, 6.00 mmol) was added and the reaction was allowed to stir for 2 hr at 0 °C. After the TLC had shown the complete consumption of the starting material, the reaction was quenched with crushed ice and then filtered. The resulting precipitate was then recrystallized in ethanol to afford compound **76o** (1.60 g, 84.29%) as white crystal, M.p. (235.67 °C); FTIR ($\nu_{max,}$ cm^{-1}) 3118, 2888, 1690, 1609, 1591, 1535, 1466, 1405, 1383, 1362, 1349, 1319, 1289, 1253, 1201, 977, 965, 850, 763.03, 746, 731, 623, 603, 562, 462 cm^{-1}; ^{1}H NMR: (400 MHz, DMSO-d_6, ppm) 9.97 (s, 1H, CO<u>H</u>), 8.42 (dd, 2H, Ph, *J* = 8.0 Hz), 8.09 (dd, 2H, Ph, *J* = 8.8 Hz and *J* = 8.4 Hz), 8.00 (d, 1H, Ph, *J* = 3.4 Hz), 7.71 (dd, 1H, *J* = 4.0 Hz and *J* = 8.0 Hz), 7.06 (d, 1H, *J* = 8.0 Hz); ^{13}C NMR: (100 MHz, DMSO-d_6, ppm) 122.0, 124.7, 125.1, 129.9, 130.3, 132.5, 138.2, 139.8, 148.3, 151.1, 185.4; HRMS (ESI): calculated 386.17 $[M]^+$, 387.9978.

4.2.5.7

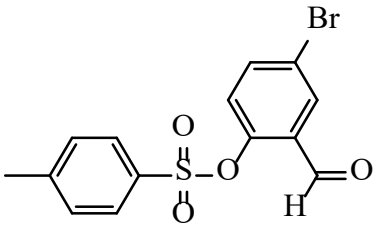

Synthesis of 4-bromo-2-formylphenyl 4-methylbenzenesulfonate **(76p)**

To a stirring solution of 5-bromosalicyladehyde (1.00 g, 4.96 mmol) and pyridine (5mL) in an ice bath, 4-toluenesulfonyl chloride (1.13 g, 6.00 mmol) was added and the reaction was allowed to stir for 2 hr at 0 °C. After the TLC had shown the complete consumption of the starting material, the reaction was quenched with crushed ice and then filtered. The resulting precipitate was then recrystallized in ethanol to afford compound **76p** (1.21 g, 68.75%) as white crystal, M.p. (188.32 °C); FTIR (ν_{max} cm^{-1}) 551, 661, 707, 736, 822, 885, 1084, 1167, 1376, 1466, 1559, 1690, 2880, 3067; ^{1}H NMR: (400 MHz, DMSO-d_6, ppm) 9.82 (s, 1H, CO<u>H</u>), 7.88 (d, 1H, Ph, *J* = 4.2 Hz), 7.59-7.63 (m, 3H, Ph), 7.29 (dd, 2H, Ph, *J* = 8.6 Hz), 6.97 (d, 1H, Ph, *J* = 8.2 Hz), 2.39 (s, 3H, C<u>H</u>$_3$); ^{13}C NMR: (100 MHz, DMSO-d_6, ppm) 30.5, 57.4, 121.1, 125.3, 128.2, 130.1, 130.3, 130.5, 131.1, 137.8, 146.5, 149.7, 185.9; HRMS (ESI): calculated 355.20 $[M]^+$, $C_{14}H_{11}BrO_4S^+$, 356.4590.

4.2.5.9

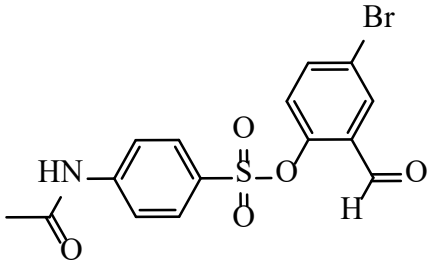

Synthesis of 4-bromo-2-formylphenyl 4-acetamidobenzenesulfonate **(76q)**

To a stirring solution of 5-bromosalicyladehyde (1.00 g, 4.96 mmol) and pyridine (5mL) in an ice bath, 4-acetamidebenzenesulfonyl chloride (1.39 g, 6.00 mmol) was added and the reaction was allowed to stir for 2 hr at 0 °C. After the TLC had shown the complete consumption of the starting material, the reaction was quenched with crushed ice and then filtered. The resulting precipitate was then recrystallized in ethanol to afford compound **76q** (1.64 g, 83.24%) as white crystal, M.p. (223.98); FTIR (ν_{max} cm^{-1}) 421, 462, 577, 661, 782, 867, 926, 1125, 1225, 1225, 1285, 1335, 1424, 1556, 1621; ^{1}H NMR: (400 MHz, DMSO-d_6, ppm) 9.89 (s, 1H, CO<u>H</u>), 8.58 (s, 1H, N<u>H</u>), 7.73 (m, 4H, Ph), 7.41 (d, 1H, Ph, *J* = 4.9 Hz), 7.89 (dd, 1H, Ph, *J* = 4.4 Hz and *J* = 2.0 Hz), 7.31 (d, 1H, Ph, *J* = 8.4 Hz), 3.60 (s, 3H, OC<u>H</u>$_3$), 2.20 (s, 3H, C<u>H</u>$_3$); ^{13}C NMR: (100 MHz, DMSO-d_6, ppm) 24.7, 119.2, 121.4, 125.5, 127.6, 129.9, 130.4, 131.5, 138.1, 144.3, 149.8, 169.1, 186.1; HRMS (ESI): calculated 398.23 $[M]^+$, 399.9032.

4.2.5.10

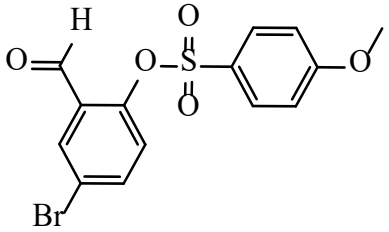

Synthesis of 4-bromo-2-formylphenyl 4-methoxybenzenesulfonate **(76r)**

To a stirring solution of 5-bromosalicyladehyde (1.00 g, 4.96 mmol) and pyridine (5mL) in an ice bath, 4-methoxybenzenesulfonyl chloride (1.23 g, 6.00 mmol) was added and the reaction was allowed to stir for 2 hr at 0 °C. After the TLC had shown the complete consumption of the starting material, the reaction was quenched with crushed ice and then filtered. The resulting precipitate was then recrystallized in ethanol to afford compound **76r** (1.23 g, 66.84%) as white crystal, M.p.

(210.67 °C); FTIR (ν_{max}, cm^{-1}) 557, 664, 705, 830, 1019, 1087, 1166, 1267, 1374, 1464, 1589, 1688; ^{1}H NMR: (400 MHz, DMSO-d_6, ppm) 9.88 (s, 1H, CO<u>H</u>), 7.93 (d, 1H, Ph, *J* = 4.9 Hz), 7.71 (dd, 2H, Ph, *J* = 4.2 Hz and *J* = 2.0 Hz), 7.69 (dd, 2H, Ph, *J* = 4.8 Hz), 7.03 (d, 1H, Ph, *J* = 8.6 Hz), 6.96 (dd, 2H, Ph, *J* = 8 Hz and *J* = 1.2 Hz), 3.24 (s, 3H, OC<u>H</u>$_3$); ^{13}C NMR: (100 MHz, DMSO-d_6, ppm) 30.8, 55.8, 114.7, 121.2, 124.8, .125.5, 137.9, 150.0, 164.7, 185.8, 206.9; HRMS (ESI): calculated 371.20 $[M]^+$, 372.6554.

4.2.6 Synthesis of (*E*)-4-(2-(6-iodo-4-oxo-3,4-dihydroquinazolin-2-yl)vinyl)-2- sulfonates

4.2.6.1

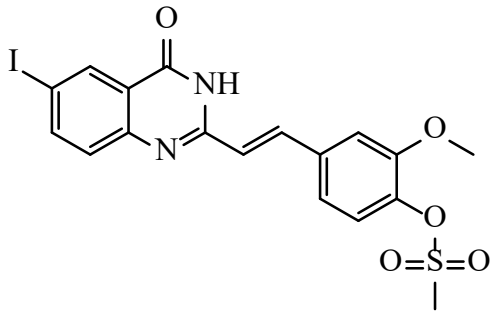

Synthesis of (E)-4-(2-(6-iodo-4-oxo-3,4-dihydroquinazolin-2-yl)vinyl)-2-methoxyphenyl methanesulfonate **(78a)**

A mixture of 6-iodo-2-methylquinazolin-4(3*H*)-one (2.00 g, 12.49 mmol) and 4-formyl-2-methoxyphenyl methanesulfonate (3.44 g, 14.99 mmol) with sodium acetate (2.04 g, 24.98 mmol) in 100 mL of acetic acid was allowed to stir for 8 hr at 117 °C. The reaction was quenched with ice, filtered and washed with methanol to afford compound **78a** (5.23 g, 84.21%) as a yellow powder. M.p. (340.23 °C); FTIR ($\nu_{max,}$ cm^{-1}) 510, 531, 602, 682, 788, 812, 853, 967, 1030, 1114, 1150, 1174, 1257, 1295, 1354, 1459, 1503, 1574, 1643, 1673, 2845, 2918 cm^{-1} ^{1}H NMR: (400 MHz,

DMSO-d_6, ppm) 12.49 (s, 1H, NH), 8.36 (d, 1H, Ph, *J* = 4.0 Hz), 8.07 (dd, 1H, Ph, *J* = 2.0 Hz and *J* = 8.8 Hz), 7.94 (d, 1H, Ph, *J* = 6.4 Hz), 7.15 (m, 1H, Ph), 7.43 (d, 1H, Ph, *J* = 8.4 Hz), 7.38 (d, 1H, Ph, *J* = 8.4 Hz), 7.27 (d, 1H, Ph, *J* = 8.4 Hz), 7.05 (d, 1H, Ph, *J* = 6.0 Hz), 7.00 (d, 1H, CH=CH, *J* = 16.0 Hz), 3.92 (s, 3H, OCH_3), 3.39 (s, 3H, CH_3); ^{13}C NMR: (100 MHz, DMSO-d_6, ppm) 56.6, 113.2, 123.7, 125.0, 136.2, 142.6, 150.0, 152.5, 164.7, 192.5, 187.8, 189.4; HRMS (ESI): calculated 497.97 $[M]^+$, $C_{18}H_{15}IN_2O_5S^+$.498.3309.

4.2.6.2

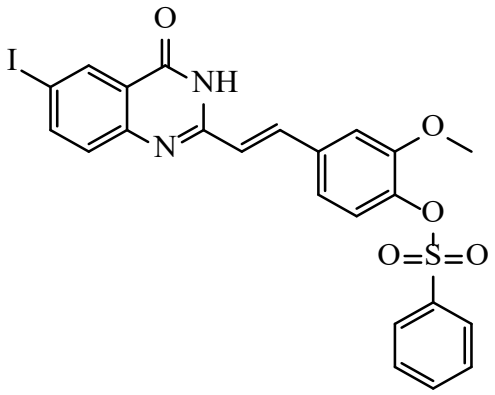

Synthesis of (E)-4-(2-(6-iodo-4-oxo-3,4-dihydroquinazolin-2-yl)vinyl)-2-methoxyphenyl benzenesulfonate **(78b)**

A mixture of 6-iodo-2-methylquinazolin-4(3*H*)-one (2.00 g, 12.49 mmol) and 4-formyl-2-methoxyphenyl benzenesulfonate (4.43 g, 14.99 mmol) with sodium acetate (2.04 g, 24.98 mmol) in 100 mL of acetic acid was allowed to stir for 8 hr at 117 °C. The product was quenched with ice, filtered then washed with methanol which afforded a yellow solid **78b** (5.02 g, 71.81%), M.p. (378.65 °C); FTIR ($\nu_{max,}$ cm^{-1}) 456, 652, 683, 712, 789, 843, 955, 1007, 1186, 1332, 2778, 2889, 2956 ^1H NMR: (400 MHz, DMSO-d_6, ppm) 8.23 (s, 1H, NH), 8.36 (d, 1H, Ph, *J* = 5.0 Hz), 8.33 (d,

1H, Ph, *J* = 3.0 Hz), 8.03 (m, 1H, Ph), 7.89 (d, 1H, Ph, *J* = 8.4 Hz), 7.84 (m, 1H, Ph), 7.67 (m, 1H, Ph), 7.52 (dd, 1H, Ph, *J* = 8.2 Hz and *J* = 2.0 Hz), 7.44 (d, 1H, Ph, *J* = 8.8 Hz), 7.37 (dd, 1H, *J* = 3.0 Hz and *J* = 8.4 Hz), 7.15 (m, 1H, Ph), 7.00 (d, 1H, C<u>H</u>=C<u>H</u>, *J* = 16.0 Hz), 3.54 (s, 3H, C<u>H</u>$_3$); ^{13}C NMR: (100 MHz, DMSO-d$_6$, ppm) 55.5, 122.9, 123.0, 124.7, 128.4, 129.4, 129.7, 130.5, 132.7, 133.2, 133.5, 133.8, 134.1, 139.9, 144.3, 144.5, 187.3, 187.8, 189.4, HRMS (ESI): calculated 559.99 $[M]^+$, $C_{23}H_{17}IN_2O_5S^+$ 560.8706.

4.2.6.3

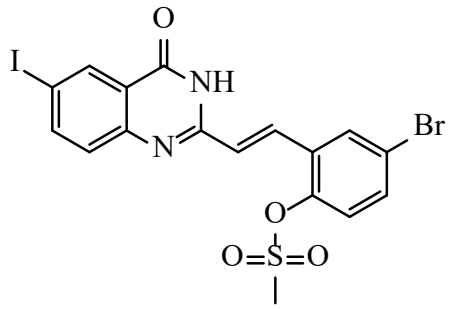

Synthesis of (E)-4-bromo-2-(2-(6-iodo-4-oxo-3,4-dihydroquinazolin-2-yl)vinyl)phenyl methanesulfonate **(78c)**

A mixture of 6-iodo-2-methylquinazolin-4(3*H*)-one (2.00 g, 12.49 mmol) and 4-bromo-2-formylphenyl methanesulfonate (4.18 g, 14.99 mmol) with sodium acetate (2.04 g, 24.98 mmol) in 100 mL of acetic acid was allowed to stir for 8 hr at 117 °C. The product was quenched with ice, filtered then washed with methanol which afforded a white solid powder. **78c** (6.39 g, 93.83%) M.p. (356.67 °C); FTIR ($\nu_{max,}$ cm^{-1}) 420, 504, 554, 702, 838, 865, 903, 2927, 3755, 3768; ^{1}H NMR: (400 MHz, DMSO-d$_6$, ppm) 12.06 (s, 1H, N<u>H</u>), 8.07 (dd, 1H, Ph, *J* = 2.0 Hz and *J* = 8.3 Hz), 7.96 (m,

1H, Ph), 7.71 (dd, 1H, Ph, *J* = 2.0 and *J* = 8.6 Hz), 7.45 (t, 2H, Ph, *J* = 6.3 Hz and *J* = 2.7 Hz), 7.10 (d, 1H, C<u>H</u>=C<u>H</u>, *J* = 16.0 Hz), 3.25 (s, 3H, C<u>H</u>$_3$); ^{13}C NMR: (100 MHz, DMSO-d$_6$, ppm) 30.8, 91.9, 120.6, 123.1, 125.5, 125.7, 129.6, 130.2, 130.2, 131.1, 133.8, 134.3, 143.3, 146.2, 148.1, 151.6, 160.7; HRMS (ESI): calculated 545.87 $[M]^+$, $C_{17}H_{12}BrIN_2O_4S^+$ 546.6777.

4.2.6.4

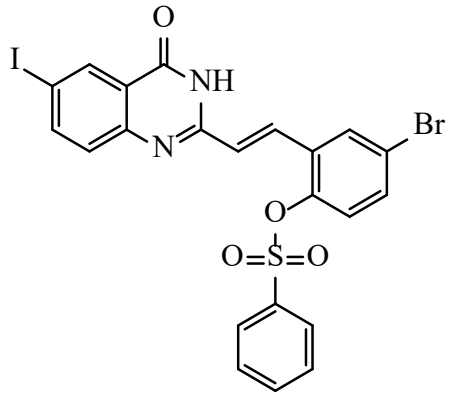

Synthesis of (E)-4-bromo-2-(2-(6-iodo-4-oxo-3,4-dihydroquinazolin-2-yl)vinyl)phenyl benzenesulfonate **(78d)**

A mixture of 6-iodo-2-methylquinazolin-4(3*H*)-one (2.00 g, 12.49 mmol) and of 4-bromo-2-formylphenyl benzenesulfonate (5.35 g, 14.99 mmol) with sodium acetate (2.04 g, 24.98 mmol) in 100 mL of acetic acid was allowed to stir for 8 hr at 117 °C. The product was quenched with ice, filtered then washed with methanol which afforded a yellow solid powder. **78d** (6.09 g, 80.03%) M.p. (320.98 °C); FTIR ($\nu_{max,}$ cm^{-1}) 452, 521, 557, 577, 594, 622, 634, 699, 747, 800, 829, 969, 1084, 1183, 1298, 1354, 1298, 1354, 1456, 1579, 1648 cm^{-1}; ^{1}H NMR: (400 MHz, DMSO-d$_6$, ppm) 12.44 (s, 1H, N<u>H</u>), 8.12 (dd, 1H, Ph, *J* = 1.6 Hz and *J* = 8.8 Hz), 7.90 (d, 1H, Ph, *J* = 2.0 Hz), 7.70 (dd, 1H, Ph, *J* = 2.4 Hz and *J* = 8.8 Hz), 7.63 (m, 1H, Ph), 7.56 (d, 1H, Ph, *J* = 16.0 Hz), 7.51 (m, 4H, Ph), 7.24 (d, 1H, Ph, *J* = 8.8 Hz), 6.74 (d, 1H, C<u>H</u>=C<u>H</u>, *J* = 16.0 Hz); ^{13}C NMR: (100 MHz,

DMSO-d_6, ppm) 91.9, 120.9, 123.0, 124.7, 125.9, 128.4, 129.5, 129.7, 129.8, 130.0, 131.0, 133.6, 133.8, 134.3, 165.4, 173.1, 186.2, 191.1; HRMS (ESI): calculated 609.23 $[M]^+$, $C_{22}H_{14}BrIN_2O_4S^+$ 610.4599.

4.2.7 Synthesis of (*E*)-2-methoxy-4-(2-(6-(4-arylphenyl)-4-oxo-3,4-dihydroquinazolin-2-yl)vinyl)phenyl sulfonates

4.2.7.1

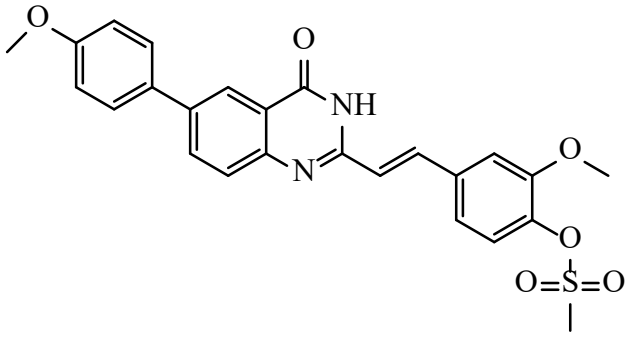

Synthesis of (E)-2-methoxy-4-(2-(6-(4-methoxyphenyl)-4-oxo-3,4-dihydroquinazolin-2-yl)vinyl)phenyl methanesulfonate **(79a)**

A stirred mixture of (*E*)-4-(2-(6-iodo-4-oxo-3,4-dihydroquinazolin-2-yl)vinyl)-2-methoxyphenylmethanesulfonate (0.30 g, 0.60 mmol) , 10% Palladium-tetrakis(triphenylphosphine) (0.07 g, 0.06 mmol) and cesium carbonate (0.23 g, 0.72 mmol) in toluene (25 mL) was purged with argon gas for 30 minutes. 4-methoxyphenylboronic acid (0.11 g, 0.72 mmol) was added to the mixture. The reaction was stirred at 100 °C for 8 h. Thereafter reaction was cooled for 10 min then filtered to afford **79a** (0.28 g, 77.11%), as a brown powder, M.p. (367.87 °C); FTIR ($v_{max,}$ cm^{-1}) 515, 823, 861, 973, 103.5, 1113, 1148, 1180, 1251, 1357, 1475, 1574, 1657 cm^{-1}; ^1H NMR: (400 MHz,

DMSO-d_6, ppm) 8.24 (d, 1H, Ph, *J* = 4.4 Hz), 7.95 (m, 1H, Ph), 7.71 (dd, 1H, Ph, *J* = 8.4 Hz and *J* = 2.2 Hz), 7.63 (m, 2H, Ph), 7.50 (d, 1H, Ph, *J* = 4.8 Hz), 7.32 (dd, 1H, Ph, *J* = 8.8 Hz and *J* = 1.2 Hz), 7.26 (d, 1H, Ph, *J* = 4.0 Hz), 7.23 (d, 1H, *J* = 4.8 Hz), 7.05 (dd, 2H, *J* = 3.0 Hz and *J* =8.4 Hz), 7.03 (d, 1H, C<u>H</u>=C<u>H</u>, *J* = 16.2 Hz), 3.93 (d, 3H, OC<u>H</u>$_3$), 3.79 (d, 3H, OC<u>H</u>$_3$), 3.37 (d, 3H , C<u>H</u>$_3$); ^{13}C NMR: (100 MHz, DMSO-d_6, ppm) 27.3, 56.5, 127.9, 123.0, 125.7, 129.4, 129.5, 129.7, 131.5, 133.7, 134.2, 135.5, 136.8, 137.1, 139.6, 153.2, 164.9, 178.1, 188.8, 189.4; HRMS (ESI): calculated 609.23 $[M]^+$, $C_{22}H_{14}BrIN_2O_4S^+$, 479.7777.

4.2.7.2

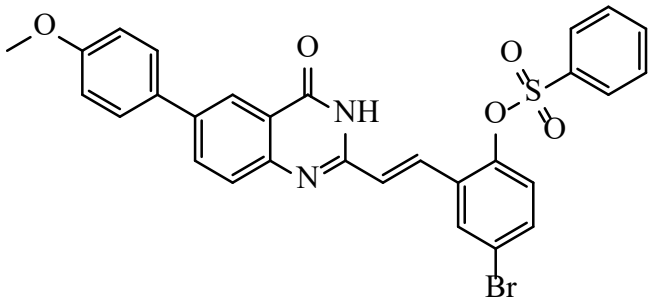

Synthesis of (E)-4-bromo-2-(2-(6-(4-methoxyphenyl)-4-oxo-3,4-dihydroquinazolin-2-yl)vinyl)phenyl benzenesulfonate **(79b)**

A stirred mixture of (*E*)-4-bromo-2-(2-(6-iodo-4-oxo-3,4-dihydroquinazolin-2-yl)vinyl)phenyl benzenesulfonate (0.30 g, 0.60 mmol), 10% Palladium-tetrakis(triphenylphosphine) (0.07 g, 0.06 mmol) and of cesium carbonate (0.23 g, 0.72 mmol) in 25 mL toluene was purged with argon gas for 30 minutes. 4-methoxyphenylboronic acid (0.11 g, 0.72 mmol) was then added to the mixture. The reaction was stirred at 100 °C for 8 h. The reaction was then cooled for 10min and filtered to afford **79b** (0.24 g, 68.50% as a brown powder. M.p. (309.67 °C); FTIR ($\nu_{max,}$ cm^{-1}) 515, 682, 817,

1176, 1353, 1568, 3178; ^{1}H NMR: (400 MHz, DMSO-d_6, ppm) 8.27 (dd, 1H, Ph, *J* = 4.0 Hz and *J* = 2.0 Hz), 7.99 (d, 1H, Ph, *J* = 3.4 Hz), 7.92 (d, 1H, Ph, *J* = 8.0 Hz), 7.63 (m, 2H, Ph), 7.60 (m, 2H, Ph), 7.25 (d, 1H, Ph, *J* = 8.0 Hz), 7.18 (d, 1H, Ph, *J* = 8.8 Hz), 7.08 (m, 2H, Ph), 6.35 (s, 1H, N<u>H</u>), 3.93 (d, 3H, OC<u>H</u>$_3$) ^{13}C NMR: (100 MHz, DMSO-d_6, ppm) 55.5, 121.2, 122.9, 123.0, 124.3, 124.6, 124.7, 128.4, 128.7, 129.4, 129.7, 130.5, 130.8, 132.7, 133.2, 133.5, 133.8, 134.1, 138.5, 139.1, 139.9, 141.7, 142.8, 144.3, 184.5, 184.9, 195.2, 196.1, 197.3; HRMS (ESI): calculated 590.23 $[M]^+$, $C_{29}H_{21}BrN_2O_5S^+$, 591.2388.

4.2.7.3

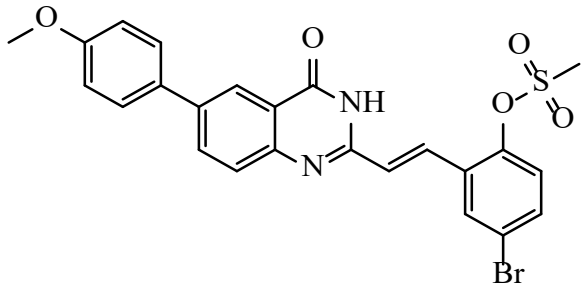

Synthesis of (E)-4-bromo-2-(2-(6-(4-methoxyphenyl)-4-oxo-3,4-dihydroquinazolin-2-yl)vinyl)phenyl methanesulfonate **(79c)**

A stirred mixture of (*E*)-4-bromo-2-(2-(6-iodo-4-oxo-3,4-dihydroquinazolin-2-yl)vinyl)phenyl benzenesulfonate (0.30 g, 0.49 mmol), 10% Palladium-tetrakis(triphenylphosphine) (0.07 g, 0.06 mmol) and cesium carbonate (0.23 g, 0.72 mmol) in 25 mL toluene was purged with argon gas for 30 minutes. 4-methoxyboronic acid (0.11 g, 0.72 mmol) was added to the mixture. The reaction was stirred at 100 °C for 8 h. The reaction was then cooled for 10min and filtered to afford **79c** (0.22 g, 78.56%), as a reddish powder, M.p. (347.71 °C); FTIR ($\nu_{max,}$ cm^{-1}) 557, 591, 607, 634, 695, 748,

801, 828, 968, 1084, 1186, 1353, 1456, 1575, 1652 cm^{-1}; ^{1}H NMR: (400 MHz, DMSO-d_6, ppm) 9.52 (s, 1H, NH), 8.39 (d, 1H, Ph, *J* = 6.0 Hz), 8.12 (dd, 1H, Ph, *J* = 6.0 Hz and *J* = 2.4 Hz), 7.91 (d, 1H, Ph, *J* = 6.0 Hz), 7.82 (m, 5H, Ph), 7.71 (dd, 1H, Ph, *J* = 8.4 Hz and *J* = 2.0 Hz), 7.75 (m, 1H, Ph), 7.50 (m, 3H, Ph), 7.24 (d, 1H, Ph, *J* = 8.8 Hz), 6.74 (d, 1H, Ph, *J* = 6.0 Hz) 6.33 (d, 1H, CH=CH, *J* = 16.0 Hz); ^{13}C NMR: (100 MHz, DMSO-d_6, ppm) 120.2, 121.5, 123.8, 125.4, 127.1, 128.6, 129.3, 130.7, 132.0, 133.5, 134.8, 135.2, 136.7, 137.4, 138.1, 139.6, 121.9, 123.3, 124.6, 126.2, 127.7, 149.0, 150.5, 171.8, 183.2, 184.5, 196.0, 197.6, 199.1; HRMS (ESI): calculated 577.42$[M]^+$, $C_{28}H_{18}BrFN_2O_4S^+$,527.4306.

4.2.7.4

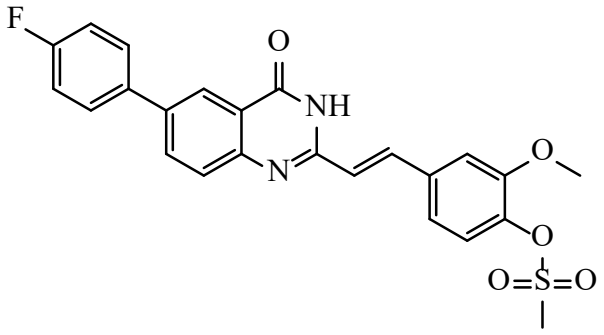

Synthesis of (E)-4-(2-(6-(4-fluorophenyl)-4-oxo-3,4-dihydroquinazolin-2-yl)vinyl)-2-methoxyphenyl methanesulfonate **(79d)**

A stirred mixture of (*E*)-4-bromo-2-(2-(6-iodo-4-oxo-3,4-dihydroquinazolin-2-yl)vinyl)phenyl benzenesulfonate (0.30 g, 0.49 mmol), 10% Palladium-tetrakis(triphenylphosphine) (0.07 g, 0.06 mmol) and cesium carbonate (0.23 g, 0.72 mmol) in 25 mL toluene was purged with argon gas for 30 minutes. 4-methoxyboronic acid (0.11 g, 0.72 mmol) was added to the mixture. The reaction

was stirred at 100 °C for 8 h. The reaction was then cooled for 10min and filtered to a afford a green powder **79d** (0.16 g, 72.72%), M.p. (352.12 °C); FTIR (ν_{max}) 509, 603, 682, 788, 812, 832, 867, 968, 1032, 1115, 1149, 1174, 1268, 1297, 1356, 1461, 1574, 1668 cm^{-1}; ^{1}H NMR: (400 MHz, DMSO-d_6, ppm) 8.37 (d, 1H, Ph, *J* = 2 Hz), 8.31 (d, 1H, Ph, *J* = 2 Hz), 8.11 (m, 2H, Ph), 7.96 (m, 1H, Ph), 7.83 (dd, 1H, Ph, *J* = 2 Hz and *J* = 5.6 Hz), 7.75 (d, 1H, Ph, *J* = 8.0 Hz), 7.52 (dd, 1H, Ph, *J* = 1.6 Hz and *J* = 7.2 Hz), 7.26-7.40 (m, 3H, Ph), 7.04 (d, 1H, *J* = 16.0 Hz), 6.57 (s, 1H, NH) 6.22 (d, 1H, CH=CH, *J* = 16.0 Hz), 3.93 (s, 3H, OCH_3), 3.92 (s, 3H, CH_3); ^{13}C NMR: (100 MHz, DMSO-d_6, ppm) 26.5, 56.7, 120.4, 121.7, 123.1, 124.5, 125.8, 127.3, 128.9, 130.2, 131.6, 133.0, 134.3, 135.7, 137.1, 138.6, 140.0, 151.3, 182.6, 194.0, 195.4, 196.8HRMS (ESI): calculated 466.10 $[M]^+$, $C_{24}H_{19}FN_2O_5S^+$, 467.9856.

4.2.7.5

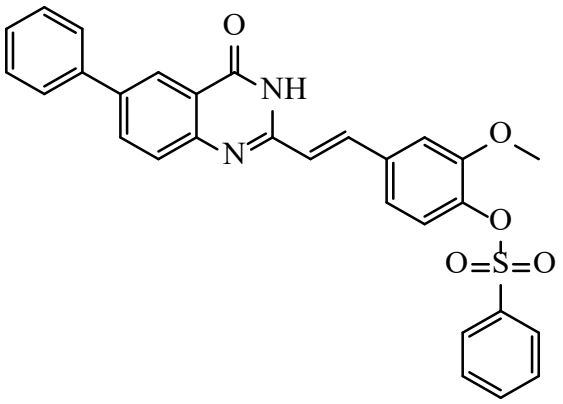

Synthesis of (E)-2-methoxy-4-(2-(4-oxo-6-phenyl-3,4-dihydroquinazolin-2-yl)vinyl)phenyl benzenesulfonate **(79e)**

A stirred mixture of (E)-4-bromo-2-(2-(6-iodo-4-oxo-3,4-dihydroquinazolin-2-yl)vinyl)phenyl benzenesulfonate (0.30 g, 0.49 mmol), 10% Palladium-tetrakis(triphenylphosphine) (0.07 g, 0.06 mmol) and cesium carbonate (0.23 g, 0.72 mmol) in 25 mL toluene was purged with argon gas for 30 minutes. Phenylboronic acid (0.11 g, 0.72 mmol) was added to the mixture. The reaction was stirred at 100 °C for 8 h. The reaction was then cooled for 10min and filtered to a afford **79e** (0.14 g, 58.76%) as a red powder, M.p. (322.11 °C); FTIR ($v_{max,}$ cm^{-1}) 572, 607, 637, 695, 736, 750, 804, 836, 1080, 1187, 1350, 1460, 1657, 3364 cm^{-1}; ^{1}H NMR: (400 MHz, DMSO-d_6, ppm) 8.26 (d, 1H, Ph, *J* = 3.0 Hz), 7.98 (m, 1H, Ph), 7.63 (m, 7H, Ph), 7.53 (dd, 1H, Ph, *J* = 2.4 Hz and *J* = 8.8 Hz), 7.31 (m, 5H, Ph), 7.23 (d, 1H, Ph, *J* = 8.8 Hz), 7.07 (d, 1H, Ph, *J* = 8.8 Hz), 6.85 (d, 1H, Ph, *J* = 6.0 Hz), 6.32 (d, 1H, C<u>H</u>=C<u>H</u>, *J* = 16.0 Hz), 3.88 (s, 3H, OC<u>H</u>$_3$); ^{13}C NMR: (100 MHz, DMSO-d_6, ppm) 55.4, 120.2, 121.1, 122.5, 124.0, 125.3, 126.7, 128.0, 129.4, 130.6, 132.1, 133.5, 134.7, 136.2, 137.6, 138.9, 140.2, 120.8, 122.3, 123.7, 125.1, 126.4, 127.9, 129.3, 130.7, 132.0, 133.4, 134.9, 136.3, 137.7HRMS (ESI): calculated 510.12 $[M]^+$, $C_{29}H_{22}N_2O_5S^+$, 512.3497.

4.3 X-Ray diffraction method

Intensity measurements were conducted using a Bruker D8 Venture Microfocus instrument equipped with a Photon III CCD area detector diffractometer. The radiation source employed was graphite-monochromated MoKα1 (wavelength, λ = 0.71073 Å), and the data collection occurred at a temperature of 173 K, facilitated by the Oxford Cryostream 600 cooler. Data processing was performed using the SAINT+ software (version 6.021), and empirical absorption corrections were implemented using SADABS[139]. The assignment of the space group was accomplished using XPREP. Subsequently, the structure determination involved the WinGX[140] Suite of programs, with intrinsic phasing carried out via SHELXT. The refinement phase utilized full-matrix least-squares and difference Fourier techniques applied to F2 values, with the refinement conducted using SHELXL-2018/3[141]. Throughout the refinement process, carbon-bound hydrogen atoms were positioned at idealized locations and refined as riding atoms, with isotropic parameters set at 1.2 times those of their parent atoms. Diagrams and materials intended for publication were generated using ORTEP-32 and PLATON[142].

4.4 Hirshfield analysis method

Utilizing the Crystal Explorer software[143], we conducted a comprehensive study on the crystal packing of compounds, incorporating Hirshfeld surface analysis and 2D fingerprint diagrams. The 3D Hirshfeld (HF) surfaces of the compounds were meticulously examined at a high standard resolution, with an isovalue set at 0.5. During this analysis, crucial parameters such as surface volume and area were precisely determined. The globularity value for compounds was identified, indicating a distinctive shape characteristic. Furthermore, the conformation of the molecules was stabilized through a diverse array of intramolecular and intermolecular interactions.

4.5 Cell viability assays

The synthesized compounds were tested for anti-proliferative activity against the human breast[144] cancer cells (MCF-7), cervical[145] cancer cells (HeLa) and embryonic kidney[146] cells (HEK-293) using the 3-(4,5-dimethylthiazol-2-yl)-2,5-diphenyltetrazolium bromide (MTT) assay. The cells were treated for 24 hours with the synthesized compounds at 200 μM or, with a culture medium containing 0.5% DMSO and curcumin 200 μM, as the positive control, for 24 hr. Subsequently, 20 μL of 5 mg/mL of MTT was introduced into each well of the plate and the plate incubated in a CO_2 incubator at 37ºC for 2 hr. Afterward, the cell culture medium was replaced with 100 μL of DMSO to dissolve the blue formazan crystals. The absorbance was measured at 560 nm using a BioRad microplate reader. The percentage cell viability was calculated using the formula [(Abs sample/Abs control) × 100%] and the IC_{50} values of the compounds were calculated using the GraphPad application.

4.6 DPPH antioxidant assay

The 2,2′-diphenyl-1-picrylhydrazyl (DPPH) radical scavenging assay[147] was conducted to test the antioxidant capacity of the compounds alongside ascorbic acid[148] as a positive control. In a 96-well plate, 40 μL of 0.20 mM DPPH in methanol was combined with varying concentrations (5, 10, 25, 50, and 100 μM) of the test compounds and the positive control, with each combination replicated three times. The reaction mixtures were then shielded from light and incubated for 45 min at room temperature. Subsequently, absorbance readings were taken at a wavelength of 512 nm using a Varioskan flash microplate spectrophotometer reader and utilized to estimate the DPPH radical scavenging activity of the compounds using the equation (%) = [(A0 – A1)/A0) × 100]

4.7 Molecular Docking method

GOLD (version 5.2)[149] was employed for a molecular docking investigation. The initial inhibitors have been effectively incorporated into their respective binding sites to achieve their crystal configurations. The benzimidazole-centered hetero-nuclear ring, targeting the tyrosine kinase VEGFR-2 adenine pocket, establishes interactions with ALA868, LYS 868, CYS917, GLU883, VAL914, VAL916, CYS 1045, ASP1046, and PHE1047. Simultaneously, Ascorbic acid appears to be enclosed by ARG48, TRP51, MET 172, HIS 175, HIS177, LYS179, THR180, HIS181, ARG184, SER185, and PHE191 within the peroxidase. Subsequently, the ligands were redocked into the vacant active site after the standard inhibitor had been eliminated. The ChemPLP scoring function was applied to ascertain the necessary affinity, and charges were assigned using the CHARMM force field[150]. The structure exhibiting the lowest RMSD score was employed to generate a diverse set of ligand poses. The ChemPLP scoring function was specifically designed to calculate binding affinity, while the CHARMM force field was used for charge assignment. The structure with the lowest RMSD score was selected to generate multiple ligands poses.

CHAPTER 5: CONCLUSION AND FUTURE WORK

The sulfonated benzaldehydes and styryl-quinazolin-(3*H*)-ones were successfully synthesized and comprehensively characterized through a rigorous experimental protocol by utilizing a combination of spectroscopic techniques including NMR, IR and XRD, and spectrometric technique, UPHLC-MS. Chemical structures and properties of the synthesized compounds were therefore elucidated with high precision. The synthesized compounds were tested for anti-proliferative and cytotoxicity activity against the breast cancer cells (MCF-7), cervical cancer cells (HeLa) and human embryonic kidney cells (HEK293-T), along with tests for antioxidative activity by DPPH assay. It has been established that medications targeting oxidative stress and exhibiting cytotoxic effects present a potential avenue for the creation of innovative multifunctional treatments for inflammation and cancer.

The x-ray crystallography studies provided valuable insights into the structural characteristics of three sulphonated benzaldehydes (**76a**, **76b**, and **76k**). The analysis revealed distinct crystal systems and packing arrangements, with **89a** exhibiting a monoclinic crystal system and **76b** and **76k** displaying triclinic crystal systems. Notably, the crystal structures showcased a robust intramolecular hydrogen bonding pattern, indicative of an *α, β*-unsaturated framework. Further investigation of compounds **76a** and **76b** through Hirshfeld surface analysis elucidated differences in surface volume, area, and globularity, underscoring variations in their molecular packing patterns. Moving beyond structural elucidation, the synthesized compounds underwent comprehensive evaluation for their biological activities. In anti-proliferative assays against various cancer cell lines, particularly MCF-7, HeLa, and HEK293-T, several compounds demonstrated promising activity, with compound **77c** exhibiting notable efficacy against MCF-7

cells. Moreover, compound **76i** emerged as a potent candidate with significant anti-proliferative and antioxidative activities, showcasing potential for further development as therapeutic agents against cancer. These findings contribute to the growing body of knowledge on the structural properties and pharmacological potential of sulphonated benzaldehydes, offering avenues for future exploration and drug discovery endeavors the findings from this research indicate the potential for continued exploration of derivatives of sulphonated benzaldehydes and styrylquinazolin-(3*H*)-ones as promising candidates for anti-inflammatory and anti-cancer agents.

Additionally, the evaluation of antioxidative activity using the DPPH assay revealed that compounds **76d, 76e**, **76f**, **76h**, and **76i** exhibited potent scavenging activity, surpassing that of ascorbic acid. Furthermore, strong peroxidase interactions were observed for these compounds, indicating their potential as antioxidants. Overall, the comprehensive characterization of sulphonated benzaldehydes in this study sheds light on their structural features, biological activities, and therapeutic potential.

Further research at reduced concentrations is necessary to ascertain the complete efficacy of these compounds. While the preliminary findings suggest promising activity, further exploration at lower concentrations is justified. Testing drugs at high concentrations may present disadvantages such as potential toxicity or exaggerated effects that do not accurately represent their performance at therapeutic levels.

In future investigations, the synthesized aryl-substituted 2-(4-(sulfonyl)styryl)quinazolin-4(3*H*)-one derivatives will be subjected to coordination with ruthenium(II) complexes, exploiting the unique properties of this transition metal. This step aims to explore the potential synergistic effects between the quinazolinone derivatives and ruthenium (II) complexes, with the anticipation

of enhancing their biological activities, particularly in the context of anticancer properties. Coordination with ruthenium (II) complexes offers a promising avenue to modulate the physicochemical properties and biological behaviors of the quinazolinone derivatives, potentially leading to the development of novel therapeutic agents with improved efficacy and selectivity against cancer cells.

References

[1] Hassanpour, S. H., & Dehghani, M. (2017). Review of cancer from perspective of molecular. *Journal of Cancer Research and Practice*, 4(4), 127-129.

[2] Khan, M. N., Wang, Q., Idrees, B. S., Xiangli, W., Teng, G., Cui, X., Wei, K., Zhao, Z. & Abrar, M. (2022). A review on laser-induced breakdown spectroscopy in different cancers diagnosis and classification. *Frontiers in Physics*, 10, 10.

[3] Das, P., Delost, M. D., Qureshi, M. H., Smith, D. T., & Njardarson, J. T. (2018). A survey of the structures of US FDA approved combination drugs. *Journal of medicinal chemistry*, 62(9), 4265-4311.

[4] Pasqual, E., Schonfeld, S., Morton, L. M., Villoing, D., Lee, C., de Gonzalez, A. B., & Kitahara, C. M. (2022). Association between radioactive iodine treatment for pediatric and young adulthood differentiated thyroid cancer and risk of second primary malignancies. *Journal of Clinical Oncology*, 40(13), 1439.

[5] Li, J., & Kataoka, K. (2020). Chemo-physical strategies to advance the in vivo functionality of targeted nanomedicine: the next generation. *Journal of the American Chemical Society*, 143(2), 538-559.

[6] Demaria, M., O'Leary, M. N., Chang, J., Shao, L., Liu, S. U., Alimirah, F., Koenig, k.,Catherine Le, C., Mitin, N., Deal, A. M., Alston, S., Academia, E. C., Kilmarx, S., Valdovinos, A., Wang, B.,

de Bruin, A., Kennedy.,B. K., Melov, S., Zhou, W., Sharpless, N. E., Muss, H. & Campisi, J. (2017). Cellular senescence promotes adverse effects of chemotherapy and cancer relapse. *Cancer discovery*, 7(2), 165-176.

[7] Amjad, M. T., Chidharla, A., & Kasi, A. (2023, February 27). Cancer Chemotherapy. In StatPearls [Internet]. Treasure Island, FL: StatPearls Publishing.

[8] Hajdu, S. I. (2016). Pathfinders in oncology from ancient times to the end of the M iddle A ges. Cancer, 122(11), 1638-1646.

[9] Raffa, D., Edler, M. C., Daidone, G., Maggio, B., Merickech, M., Plescia, S., Schillaci, D., Bai, R., & Hamel, E. (2004). Tubulin polymerization inhibition and antiproliferative activity of analogs of 2,5-dideoxy-2,5-imino-d-glucitol (DAB). *European Journal of Medicinal Chemistry*, 39, 299.

[10] Liu, J.-F., Kaselj, M., Isome, Y., Ye, P., Sargent, K., Sprague, K., Cherrak, D., Wilson, C. J., Si, Y., Yohannes, D., & Ng, S.-C. (2006). Design, synthesis, and biological activity of a new class of tubulin polymerization inhibitors. *Journal of Combinatorial Chemistry*, 8, 7.

[11] Sgobba, M., & Rastelli, G. (2009). Hsp90 inhibitors: a new avenue to the treatment of cancer. *Chemical Medicinal Chemistry*, 4, 1399.

[12] Bhandari, S. V., Deshmane, B. J., Dangare, S. C., Gore, S. T., Raparti, V. T., Khachane, C. V., & Sarkate, A. P. (2008). Synthesis and anticonvulsant activity of some new 2-styryl benzimidazole derivatives. *Pharmacology Online*, 2.

[13] Jatav, V., Mishra, P., Kashaw, S., & Stables, J. P. (2008). Synthesis, pharmacological evaluation and docking studies of 2-styryl benzoxazinone derivatives as potential anticonvulsant agents. *European Journal of Medicinal Chemistry*, 43.

[14] Mrozek-Wilczkiewicz, A., Kalinowski, D. S., Musiol, R., Finster, J., Szurko, A., Serafin, K., Knas, M., Kamalapuram, S. K., Kovacevic, Z., Jampilek, J., Ratuszna, A., Rzeszowska-Wolny, J., Richardson, D. R., & Polanski, J. (2010). Novel 2-styryl-4(3*H*)-quinazolinone derivatives: Design, synthesis, cytotoxicity and structure-activity relationships. *Bioorganic & Medicinal Chemistry*, 18.

[15] Gupta, V., Kashaw, S. K., Jatav, V., & Mishra, P. (2008). Design, synthesis and antimicrobial screening of novel 2-styryl benzoxazinone derivatives. *Medicinal Chemistry Research*, 17, 205.

-

[16] Radhakrishnan, S., Syed, R., Takei, H., Kobayashi, I. S., Nakamura, E., Sultana, F., Kamal, A., Tenen, D. G., & Kobayashi, S. S. (2019). Styryl quinazolinones and its ethynyl derivatives induce myeloid differentiation. *Bioorganic & Medicinal Chemistry Letters*, 29(16), 2286-2289.

[17]Satpute, D. P., Shirwadkar, U., Tharalla, A. K., Shinde, S. D., Vaidya, G. N., Joshi, S., Vatsa, P. P., Jain, A., Singh, A. A., Garg, R., Mandoli, A., & Kumar, D. (2023). Discovery of fluorinated 2-Styryl 4(3*H*)-quinazolinone as potential therapeutic hit for oral cancer. *Bioorganic & Medicinal Chemistry*, 81, 117193

[18] Jatav, V., Mishra, P., Kashaw, S., & Stables, J. P. (2008). CNS depressant and anticonvulsant activities of some novel 3-[5-substituted 1,3,4-thiadiazole-2-yl]-2-styryl quinazoline-4(3*H*)-ones. *European journal of medicinal chemistry*, 43(9), 1945–1954.

[19] Jain, N., Jaiswal, J., Pathak, A., & Singour, P. K. (2018). Synthesis, molecular docking and evaluation of 3-{4-[2-amino-4-(substitutedphenyl)-2*H*-[1, 3] oxazin/thiazin-6-yl} 2-phenyl-3H-quinazolin-4-one derivatives for their anticonvulsant activity. Central Nervous System Agents in Medicinal Chemistry (Formerly Current Medicinal Chemistry-Central Nervous System Agents), 18(1), 63-73.

[20] Seifu, G. W., Birhan, Y. S., Beshay, B. Y., Hymete, A., & Bekhit, A. A. (2022). Synthesis, antimalarial, antileishmanial evaluation, and molecular docking study of some 3-aryl-2-styryl substituted-4(3*H*)-quinazolinone derivatives. *Biomedical Central chemistry*, 16(1), 107.

[21] Birhan, Y. S., Bekhit, A. A., & Hymete, A. (2014). Synthesis and antileishmanial evaluation of some 2,3-disubstituted-4(3H)-quinazolinone derivatives. *Organic and medicinal chemistry letters*, 4(1), 10.

[22]A. Radwan, A., & K. Alanazi, F. (2020). Biological Activity of Quinazolinones. *IntechOpen*.

[23]Zhao, C., Rakesh, K. P., Ravidar, L., Fang, W. Y., & Qin, H. L. (2019, January 15). Pharmaceutical and medicinal significance of sulfur (SVI)-Containing motifs for drug discovery: A critical review. *European Journal of Medicinal Chemistry*, 162, 679-734.

[24] Ali, A., Reddy, G. S., Nalam, M. N., Anjum, S. G., Cao, H., Schiffer, C. A., & Rana, T. M. (2010). Structure-based design, synthesis, and structure-activity relationship studies of HIV-1 protease inhibitors incorporating phenyloxazolidinones. *Journal of Medicinal Chemistry*, 53(21), 7699-7708.

[26] Jampilek, J. (2019). Heterocycles in Medicinal Chemistry. *Molecules*, 24(21), 3839.

[27] Kumar, N., & Goel, N. (2022). Heterocyclic Compounds: Importance in Anticancer Drug Discovery. *Anticancer Agents Medicinal Chemistry*, 22(19), 3196-3207.

[28] Chen, X. W., Rao, L., Chen, J. L., & Zou, Y. (2022). Unexpected assembly machinery for 4(3*H*)-quinazolinone scaffold synthesis. *Nature Communications*, 13(1), 6522.

[29]Srivastava, S., & Srivastava, S. (2015). Biological activity of Quinazoline: A Review. *International Journal of Pharma Sciences and Research.*

[30] Ranawat, M. S., Amrutkar, S. V., & Phargharmol, P. (2011). Synthesis and pharmacological evaluation of 3-alkyl/aryl−2-methylquinazolin-4-one derivatives. *International Journal of Drug Design and Discovery*, 2, 453–457.

[31] Asif, M. (2014). Chemical characteristics, synthetic methods, and biological potential of quinazoline and quinazolinone derivatives*. International Journal of Medicinal Chemistry*, 12, 111.

32 Mahato, A. K., Srivastava, B., & Nithya, S. (2011). Chemistry, structure-activity relationship, and biological activity of quinazoline-4(3*H*)-one derivatives. Inventi Rapid: *Medicinal Chemistry*, 2, 400–402.

[33] Alsibaee, A. M., Al-Yousef, H. M., & Al-Salem, H. S. (2023). Quinazolinones, the Winning Horse in Drug Discovery. *Molecules*, 28(3), 978.

[34] Kamel, M., Zaghary, W., Al-Wabli, R., & Anwar, M. (2016). Synthetic approaches and potential bioactivity of different functionalized quinazoline and quinazolinone scaffolds. *Egyptian Pharmaceutical Journal*, 15, 98–131.

[35] Faisal, M., & Saeed, A. (2021). Chemical Insights into the Synthetic Chemistry of Quinazolines: Recent Advances. *Frontiers in Chemistry*, 8, 594717.

[36] Shang, X.-F., Morris-Natschke, S. L., Yang, G.-Z., Liu, Y.-Q., Guo, X., Xu, X.-S., Goto, M., Li, J.-C., Zhang, J.-Y., & Lee, K.-H. (2018). Biologically active quinoline and quinazoline alkaloids part II. *Medicinal Research Reviews*, 38(5), 1614-1660.

[37] Jafari, E., et al. (2016). Quinazolinone and quinazoline derivatives: recent structures with potent antimicrobial and cytotoxic activities. *Research in Pharmaceutical Sciences*, 11(1), 1–14.

[38] Dholakia, S. P., Suhagia, B. N., Patel, A. K., Kapupara, P. P., & Sureja, D. K. (2011). novel target for cancer therapy. *Journal of Chemistry*, 3(4), 315-332.

[39] Zhang, J., Liu, J., Ma, Y., Ren, D., Cheng, P., Zhao, J., et al. (2016). One-pot synthesis and antifungal activity against plant pathogens of quinazolinone derivatives containing an amide moiety. *Bioorganic & Medicinal Chemistry Letters*, 26(9), 2273-2277.

[40] Li, H., Fu, G., & Zhong, W. (2023). Natural quinazolinones: From a treasure house to promising anticancer leads. *European Journal of Medicinal Chemistry*, 245(Part 1), 114915.

[41] Amin, K. M., Kamel, M. M., Anwar, M. M., Khedr, M., & Syam, Y. M. (2010). Synthesis, biological evaluation and molecular docking of novel series of spiro[(2H,3H)quinazoline-2,1'-cyclohexan]-4(1*H*)-one derivatives as anti-inflammatory and analgesic agents. *European Journal of Medicinal Chemistry*, 45(6), 2117-2131.

[42]Griess, P. (1869). Ueber die Einwirkung des Cyans auf Anthranilsäure. *Berichte der Deutschen Chemischen Gesellschaft,* 2, 415-417.

[43] He, D., Wang, M., Zhao, S., Shu, Y., Zeng, H., Xiao, C., Lu, C. & Liu, Y. (2017). Pharmaceutical prospects of naturally occurring quinazolinone and its derivatives. *Fitoterapia*, 119, 136-149.

[44] Sridhar, R., Takei, H., Syed, R., Kobayashi, I. S., Hui, L. B., Kamal, A., Tenen, D. G., & Kobayashi, S. S. (2018). Styryl Quinazolinones as Potential Inducers of Myeloid Differentiation via Upregulation of C/EBPα. *Molecules*, 23(8), 1938.

[45] Senerovic, L., Opsenica, D., Moric, I., Aleksic, I., Spasić, M., & Vasiljevic, B. (2020). Quinolines and quinolones as antibacterial, antifungal, anti-virulence, antiviral and anti-parasitic agents. Advances in Microbiology, *Infectious Diseases and Public Health*: Volume 14, 37-69.

[46] Bouley, R., Ding, D., Peng, Z., Bastian, M., Lastochkin, E., Song, W., Suckow, M. A., Schroeder, V. A., Wolter, W. R., Mobashery, S., & Chang, M. (2016). Structure–Activity Relationship for the 4(3*H*)-Quinazolinone Antibacterials. *Journal of Medicinal Chemistry*, 59, 5011–5021.

[47] Moradi, M., Mousavi, A., Emamgholipour, Z., Giovannini, J., Moghimi, S., Peytam, F., Honarmand, A., Bach, S., & Foroumadi, A. (2023). Quinazoline-based VEGFR-2 inhibitors as potential anti-angiogenic agents: A contemporary perspective of SAR and molecular docking studies. *European Journal of Medicinal Chemistry*, 259, 115626.

[48] Radomska, H. S., Jernigan, F., Nakayama, S., Jorge, S. E., Sun, L., Tenen, D. G., & Kobayashi, S. S. (2015). A Cell-Based High-Throughput Screening for Inducers of Myeloid Differentiation. *Journal of Biomolecular Screening*, 20, 1150–1159.

[49] Pathak, S., Malhotra, V., Nath, R., & Shanker, K. (2014). Synthesis and Antihypertensive Activity of Novel Quinazolin-4(3*H*)-one Derivatives. *Central Nervous System Agents in Medicinal Chemistry*, 14, 10.

[50]Mishra, S., Das, D., Sahu, A., Verma, E., Patil, S., Agarwal, R. K., & Gajbhiye, A. (2020). Electronegativity in Substituted-4(*H*)-quinazolinones Causes Anxiolysis without a Sedative-hypnotic Adverse Reaction in Female Wistar Rats. *Central Nervous System Agents in Medicinal Chemistry*, 20(1), 26-40.

[51]Gatadi, S., Lakshmi, T. V., & Nanduri, S. (2019). 4(3*H*)-Quinazolinone derivatives: Promising antibacterial drug leads. *European Journal of Medicinal Chemistry*, 170, 157-172.

[52] Ghodge, B., Kshirsagar, A., & Navghare, V. (2020). Synthesis, characterization, and investigation of the anti-inflammatory effect of 2,3-disubstituted quinazoline-4(1*H*)-one. *Beni-Suef University Journal of Basic and Applied Sciences*, 9, 30.

[53] Hameed, A., Al-Rashida, M., Uroos, M., Ali, S. A., Arshia, Ishtiaq, M., & Khan, K. M. (2018). Quinazoline and quinazolinone as important medicinal scaffolds: a comparative patent review (2011–2016). *Expert opinion on therapeutic patents*, 28(4), 281-297.

[54] Crown, J. P., Burris, H. A., III, Boyle, F., et al. (2008). Pooled analysis of diarrhea events in patients with cancer treated with lapatinib. *Breast Cancer Research and Treatment*, 112(2), 317–325.

[55] Chau, N. G., & Haddad, R. I. (2013). Vandetanib for the treatment of medullary thyroid cancer. *Clinical Cancer Research*, 19(3), 524–529.

[56] Degrauwe, N., Sosa, J. A., Roman, S., & Deshpande, H. A. (2012). Vandetanib for the treatment of metastatic medullary thyroid cancer. Clinical Medicine Insights. *Oncology*, 6, 243-252.

[57] Hirsh, V. (2011). Managing treatment-related adverse events associated with EGFR tyrosine kinase inhibitors in advanced non-small-cell lung cancer. *Current Oncology*, 18(3), 126–138.

[58]Von Hoff, D., Rozencweig, M., Soper, W., Helman, L., Penta, J., Davis, H., & Muggia, F. (1977). Whatever happened to NSC–? An analysis of clinical results of discontinued anticancer agents. *Cancer Treatment Reports*, 61, 759–768.

[59] Wu, P., Nielsen, T.E., & Clausen, M.H. (2015). FDA-Approved Small-Molecule Kinase Inhibitors. *Trends in Pharmacological Sciences*, 36, 422–439.

[60] Zhang, S., Zeng, Q., Gettayacamin, M., Tungtaeng, A., Wannaying, S., Lim, A., Hansukjariya, P., Okunji, C. O., Zhu, S., & Fang, D. (2005). Antimalarial activities and therapeutic properties of febrifugine analogs. *Antimicrobial Agents and Chemotherapy*, 49(3), 1169-1176.

[61] Grudzien, M. M., Low, P. S., Manning, P. C., Arredondo, M., Belton, R. J. Jr, & Nowak, R. A. (2010). The antifibrotic drug halofuginone inhibits proliferation and collagen production by human leiomyoma and myometrial smooth muscle cells. *Fertility and Sterility*, 93(4), 1290-1298.

[62] Jain, P. P., Zhao, T., Xiong, M., Song, S., Lai, N., Zheng, Q., Chen, J., Carr, S. G., Babicheva, A., Izadi, A., Rodriguez, M., Rahimi, S., Balistrieri, F., Rahimi, S., Simonson, T., Valdez-Jasso, D., Thistlethwaite, P. A., Shyy, J. Y., Wang, J., Makino, A., … Yuan, J. X. (2021). Halofuginone, a promising drug for treatment of pulmonary hypertension. *British journal of pharmacology*, 178(17), 3373–3394.

[63] Liu, Z., Zeng, L. Y., Li, C., Yang, F., Qiu, F., Liu, S., & Xi, B. (2018). "On-Water" Synthesis of Quinazolinones and Dihydroquinazolinones Starting from o-Bromobenzonitrile. *Molecules* (Basel, Switzerland), 23(9), 2325.

[64] Hekal, M.H., & Abu El-Azm, F.S.M. (2018). New potential antitumor quinazolinones derived from dynamic 2-undecyl benzoxazinone: Synthesis and cytotoxic evaluation. *Synthetic Communications*, 48, 2391–2402.

[65] Kavitha, K., Yahoob, N., Vijayakumar, B., & Fathima, K. R. (2017). Synthesis and evaluation of quinazolinone derivatives. *Asian Journal of Research in Chemistry*, 10(4), 577-581.

[66]El-Hashash, M., Morsy, J., Azab, M., & Mahmoud, N. (2016). Design, synthesis and anticancer activity of novel 2,3-and 2,4-disubstituted quinazoline and quinazolinone derivatives. *Heterocycles*, 92, 316–329.

[67] Abuelizz, H. A., Marzouk, M., Ghabbour, H., & Al-Salahi, R. (2017). Synthesis and anticancer activity of new quinazoline derivatives. *Saudi Pharmaceutical Journal*, 25(7), 1047-1054.

[68] Maddali, N. K., Viswanath, I. V. K., Murthy, Y. L. N., Bera, R., Takhi, M., Rao, N. S., & Gudla, V. (2019). Design, synthesis, and molecular docking studies of quinazolin-4-ones linked to 1,2,3-triazol hybrids as Mycobacterium tuberculosis H37Rv inhibitors besides antimicrobial activity. *Medicinal Chemistry Research*, 28, 559–570.

[69] Banu, S., Bollu, R., Nagarapu, L., Nanubolu, J. B., Yogeswari, P., Sriram, D., Gunda, S. K. & Vardhan, D. (2018). Design, Synthesis, and in vitro antitubercular activity of 1, 2, 3-triazolyl-dihydroquinoline derivatives. *Chemical Biology & Drug Design*, 92(1), 1315-1323.

[70] Bashir, A. D., Akshya, K. S., Praveen, P., Jyoti, P., Parveen, S., Meena, S., & Baldev, S. (2012). An easy and efficient protocol for the synthesis of 2,3-dihydroquinazolinones using a low cost and reusable heterogeneous catalyst. *American Journal of Chemistry*, 2, 248-254.

[71]Kiaee, S., Masoumnia, A., & Maghsoodlou, M. (2012). A facile synthesis of 2,3-dihydroquinazolin-4(1*H*)-ones catalyzed by fumaric acid. *Research in Pharmaceutical Sciences*, 7, S508.

[72] Shaabani, A., Ali Maleki, A., & Mofakham, H. (2008). Click reaction: highly efficient synthesis of 2, 3-dihydroquinazolin-4(1*H*)-ones. *Synthetic Communications*, 38, 3751-3751.

[73] Yoo, C. L., Fettinger, J. C., & Kurth, M. J. (2005). Stannous chloride in alcohol: a one-pot conversion of 2-nitro-N-arylbenzamides to 2, 3-dihydro-1 H-quinazoline-4-ones. *The Journal of Organic Chemistry*, 70(17), 6941-6943.

[74] Labade, V. B., Shinde, P. V., & Shingare, M. S. (2013). A facile and rapid access towards the synthesis of 2, 3-dihydroquinazolin-4 (1*H*)-ones. *Tetrahedron Letters*, 54(43), 5778-5780.

[75] Lopez, S. E., Rosales, M. E., Urdaneta, N., Godoy, M. V., & Charris, J. (2000). The synthesis of substituted 2-aryl 4(3*H*)-quinazolinones using NaHSO3/DMA. Steric effect upon the cyclisation-dehydrogenation step. *Journal of Chemical Research Synopses*, 6, 258−259.

[76] Ghashang, M., Azizi, K., Moulavi-Pordanjani, H., & Shaterian, H. R. (2011). Eco-friendly and Efficient Synthesis of 2,3-Dihydroquinazolin-4(1*H*)-ones. *Chinese Journal of Chemistry*, 29, 1617−1623.

[77] Wang, M., Gao, J. J., Song, Z. G., Wang, L. (2011). Cerium(IV) ammonium nitrate catalyzed green synthesis of 2-substituted 2,3-dihydro-quinazolin-4(1*H*)-ones using a grinding technique. *Chemical Heterocyclic Compounds*, 47, 851−854.

[78] Badolato, M., Aiello, F., Neamati, N. (2018). 2,3-Dihydroquinazolin-4(1*H*)-one as a privileged scaffold in drug design. *Royal Society of Chemistry*, 8, 20894-20921.

[79] Shi, D., Rong, L., Wang, J., Zhuang, Q., Wang, X., Hu, H. (2003). A facile synthesis of 1,2-dihydroquinazolin-4(3*H*)-ones with the aid of a low-valent titanium reagent. *Tetrahedron Letters*, 44, 3199-3201.

[80] Dutta, A., Sarma, D. (2021). Base promoted metal-free approach towards synthesis of quinazolin-4(3H)-ones and 2,3-dihydroquinazolin-4(1*H*)-ones under microwave irradiation. *Sustainable Chemistry and Pharmacy*, 20, 100402.

[81]Romero, A., Salazar, J., Lopez, S. (2013). ChemInform Abstract: A Simple One-Pot Synthesis of 2-Substituted Quinazolin-4(3H)-ones from 2-Nitrobenzamides by Using Sodium Dithionite. *Synthesis*, 45, 2043-2050.

[82] Wang, S., Yin, S., Xia, S., Shi, Y., Tu, S., Rong, L. (2012). An efficient synthesis of 3-benzylquinazolin-4(1*H*)-one derivatives under catalyst-free and solvent-free conditions. *Green Chemistry Letters and Reviews*, 5, 603-607.

[83] Brown, D. J. (1984). Pyrimidines and their Benzo Derivatives. In A. R. Katritzky, & C. W. Rees (Eds.), *Comprehensive Heterocyclic Chemistry* (pp. 57-155). Pergamon.

[84]Faghih, Z., Rahmannejadi, N., Sabet, R., Zomorodian, K., Asad, M., Khabnadideh, S. (2019). Synthesis of some novel dibromo-2-arylquinazolinone derivatives as cytotoxic agents. *Research in Pharmaceutical Sciences*, 14(2), 115-121.

[85] Nayl, A. A., Aly, A. A., Arafa, W. A. A., Ahmed, I. M., Abd-Elhamid, A. I., El-Fakharany, E. M., Abdelgawad, M. A., Tawfeek, H. N., & Bräse, S. (2022). Azides in the Synthesis of Various Heterocycles. *Molecules*, 27(12), 3716.

[86] Jiang, X., Tang, T., Wang, J., Chen, Z., Yong-Ming, Z., & Shun-Jun, J. (2014). Palladium Catalyzed One-Pot Synthesis of Quinazolinones via tert-Butyl Isocyanide Insertion. *Journal of Organic Chemistry*, 79, 5082–5087.

[87] Refaie, F., Esmat, A., Gawad, S., Ibrahim, A., & Mohamed, M. (2005). The antihyperlipidemic activities of 4(3H) quinazolinone and two halogenated derivatives in rats. *Lipids in Health and Disease*, 4, 22.

[88] Baudoin, B., Ribeill, Y., & Vicker, N. (1993). A facile preparation of quinazolin-4-(3*H*)-ones from O-amido benzonitriles using sodium perborate. 2833-2837.

[89] Cabrera-Rivera, F. A., Ortíz-Nava, C., Román-Bravo, P., Leyva, M., Jaime, A., & Escalantea. (2012). Direct halogenation reaction in 2,3-dihydro-4(1*H*)-quinazolinones. *Heterocycles*, 9, 2173-2195.

[90] Mmonwa, M. M., Mphahlele, M. J., Morad, M. El-Hendawy, M. M., El-Nahas, A., & Koga, N. (2014). Synthesis and photophysical properties of the 2-(3-(2-alkyl-6,8-diaryl-4-oxo-1,2,3,4-tetrahydroquinazolin-2-yl)propyl)-6,8-diarylquinazolin-4(3*H*)-ones. *Molecules*, 19, 9712-9735.

[91] Mphahlele, M. J., Nwamadi, M. S., & Mabeta, P. (2006). Synthesis and further studies of chemical transformation of the 2-aryl-3-halogenoquinolin-4(1*H*)-one derivatives. *Heterocyclic Chemistry*, 43, 255–260.

[92] Sayyed, M. A., Mokle, S. S., & Vibhute, Y. B. (2006). Synthesis of 6-iodo/bromo-3-amino-2-methylquinazolin-4(3*H*)-ones by direct halogenation and their Schiff base derivatives. 221-226.

[93] Liu, M., Shu, M., Yao, C., Yin, G., Wang, D., & Huang, J. (2016). Synthesis of pyrido-fused quinazolinone derivatives via copper-catalyzed domino reaction. *Organic letters*, 18(4), 824-827.

[94] Akazome, M.; Kondo, T.; Watanabe, Y. Transition-metal complex-catalyzed reductive N-heterocyclization: synthesis of 4(3H)-quinazolinone derivatives from N-(2-nitrobenzoyl) amides. *Journal of Organic Chemistry*, 1993, 58, 310–312.

[95] Okuro, K., Gurnham, J., & Alper, H. (2012). Ionic diamine rhodium complex catalyzed reductive N-heterocyclization of N-(2-nitroarylidene) amines. *Tetrahedron Letters*, 53(6), 620-622.

[96] Bhat, B. A., & Sahu, D. P. (2004). One Pot Synthesis of 4(3H)-Quinazolinones. *Synthetic Communications*, 34(12), 2169–2176.

[97] Gurram, V., Garlapati, R., Thulluri, C., et al. (2015). Design, synthesis, and biological evaluation of quinazoline derivatives as α-glucosidase inhibitors. Medicinal Chemistry Research, 24, 2227–2237.

[98] Surber, B. W., Cross, J. L., & Hannick, S. M. (2010). Tenth international symposium on the synthesis and applications of isotopes and isotopically labelled compounds—poster presentations Session 19. *Journal of Labelled Compounds and Radiopharmaceuticals*, 53, 468–670.

[99] Mantovani, A. C., & Lüdtke, D. S. (2022). Pyridines and Their Benzo Derivatives: Reactivity of Substituents. In D. StC Black, J. Cossy, & C. V. Stevens (Eds.), *Comprehensive Heterocyclic Chemistry IV* (pp. 62-91). Elsevier.

[100] Shankaraiah, P., Veeresham, S., & Bhavani, A.K.D. (2016). Kumada cross coupling reaction-based synthesis, antimicrobial and computational studies of 6-aryl-2-phenyl-3-methylquinazolin-4(3*H*)-ones. *Russian Journal of General Chemistry*, 86, 368–375.

[101] Ankireddy, A. R., Syed, R., Gundla, R., Manasa, K. L., Reddy, C. V. R., Yatam, S., & Paidikondala, K. (2019). Kumada Cross Coupling Reaction for the Synthesis of Quinazoline

Derivatives, Evaluation of Their Antibacterial Activity and Docking Studies. *Russian Journal of General Chemistry*, 89(12), 2544–2557.

[102] Stelmach, J. E., Liu, L., Patel, S. B., Pivnichny, J. V., Scapin, G., Singh, S. & Doherty, J. B. (2003). Design and synthesis of potent, orally bioavailable dihydroquinazolinone inhibitors of p38 MAP kinase. *Bioorganic & Medicinal Chemistry Letters*, 13(2), 277-280.

[103] Lorthiois, E., Bernardelli, P., Vergne, F., Oliveira, C., Mafroud, A. K., Proust, E., Heuze, L., Moreau, F., Idrissi, L., Tertre, A., Bertin, B., Coupe, M., Wrigglesworth R., Descours A., Soulard P., Berna, P. (2004). Spiroquinazolinones as novel, potent, and selective PDE7 inhibitors. Part 1. *Bioorganic & Medicinal Chemistry Letters*, 14(18), 4623-4626.

[104] Steinberg, S. M., Emerson, D. W., & Cerefice, G. (2003). Immobilization of Fission Iodine by Reaction with a Fullerene-Containing Carbon Compound and Insoluble Natural Organic Matrix, 1-26.

[105] Wiklund, P. (2004). Synthesis of Heterocycles from Anthranilic acid and its Derivatives. Biovetenskaper och näringslära/Biosciences and Nutrition.

[106] Kurbatov, E. R., Korkodinova, L. M., Gol'dshtein, A. G., Yarygina, T. I., Mardanova, L. G., & Botalova, A. S. (2015). Synthesis, Properties, and Biological Activity of N-Acyl(Alkenyl)-5-Iodo(*H*)Anthranilic Acid Amides. *Pharmaceutical Chemistry Journal*, 48(9), 791–794.

[107] Agbo, E. N., Makhafola, T. J., Choong, Y. S., Mphahlele, M. J., & Ramasami, P. (2015). Synthesis, Biological Evaluation and Molecular Docking Studies of 6-Aryl-2-Styrylquinazolin-4(3*H*)-Ones. *Molecules*, 20(12), 23577–23591.

[108] Abraham, R. J., Byrne, J. J., Griffiths, L., & Perez, M. (2006). 1H chemical shifts in NMR: Part 23, the effect of dimethyl sulphoxide versus chloroform solvent on 1H chemical shifts. *Magnetic resonance in chemistry*, 44(5), 491–509.

[109] Tanc, M., Carta, F., Bozdag, M., Scozzafava, A., & Supuran, C. T. (2013). 7-Substituted-sulfocoumarins are isoform-selective, potent carbonic anhydrase II inhibitors. *Bioorganic & Medicinal Chemistry*, 21(15), 4502-4510.

[110] Turner, M. J., McKinnon, J. J., Wolff, S. K., Grimwood, D. J., Spackman, P. R., Jayatilaka, D., Spackman, M. A., & Crystal Explorer17. (2017). *CrystalExplorer17*. University of Western Australia.

111 Al-Hamdani, Y. S., and Tkatchenko, A. (2019). Understanding non-covalent interactions in larger molecular complexes from first principles. Chemical Physics, 150, 010901.

[112] Asad, M., Arshad, M. N., Asiri, A. M., Marwani, H. M., Alamry, K. A., Alam, M. M., Nazreen, S., Elhenawy, A. A., and Rahman, M. M. (2023). Synthesis of N-acylated pyrazolines: Spectroscopic, crystallographic, Hirshfeld Surface, lead sensing and theoretical studies. *Journal of Molecular Liquids*, 122340.

[113] Alsehli, M. H., Al-Harbi, L. M., Okasha, R. M., Fouda, A. M., Ghabbour, H. A., Amr, A. E. G., Elhenawy, A. A., and El-Agrody, A. M. (2022). Synthesis, Cytotoxic Activity, Crystal Structure, DFT, Molecular Docking Study of β-Enaminonitrile Incorporating 1 H-Benzo [f] Chromene Moiety. *Crystals*, 13(1), 24.

[114] Okasha, R. M., Fouda, A. M., Bajaber, M. A., Ghabbour, H. A., Amr, A. E. G., Naglah, A. M., Almehizia, A. A., Elhenawy, A. A., and El-Agrody, A. M. (2022). The Crystal Structure of 3-Amino-1-(4-Chlorophenyl)-9-Methoxy-1 H-Benzo [f] Chromene-2-Carbonitrile: Antimicrobial Activity and Docking Studies. *Crystals*, 12(7), 982.

[115] Turner, M. J., McKinnon, J. J., Jayatilaka, D., and Spackman, M. A. (2011). Visualisation and characterisation of voids in crystalline materials. Crystal Engineering Communications, 13, 1804–1813.

[116] Rathman, T. L., Sleevi, M. C., Krafft, M. E., & Wolfe, J. F. (1980). Functionalization of 2-methyl-3-o-tolyl-4(3*H*)-quinazolinone and related compounds through carbanion reactions at the 2-methyl group. *Journal of Organic Chemistry*, 45(11), 2169–2176.

[117] Takeuchi, Y., Oshige, M., Azuma, K., Abe, H., & Harayama, T. (2005). Concise synthesis of dl-febrifugine. *Chemical and pharmaceutical bulletin*, 53(7), 868-869.

[118] Goyal, R., Sharma, M., Ahuja, D., & Jain, A. (2019). Synthesis and Anti-Oxidant Activity of Phenol and Aldehyde Derivatives of Sulfonyl Chloride Quinoxaline. *Journal of Drug Delivery and Therapeutics*, 9(4-s), 1240-1244.

[119] Takeuchi, Y., Oshige, M., Azuma, K., Abe, H., & Harayama, T. (2005). Concise synthesis of dl-febrifugine. *Chemical and pharmaceutical bulletin*, 53(7), 868-869.

[120] Adan, A., Kiraz, Y., & Baran, Y. (2016). Cell Proliferation and Cytotoxicity Assays. *Current pharmaceutical biotechnology*, 17(14), 1213–1221.

[121] Segeritz, C. P., & Vallier, L. (2017). Cell Culture: Growing Cells as Model Systems In Vitro. *Basic Science Methods for Clinical Researchers*, 151–172.

[123] Freimoser, F. M., Jakob, C. A., Aebi, M., & Tuor, U. (1999). The MTT [3-(4, 5-dimethylthiazol-2-yl)-2, 5-diphenyltetrazolium bromide] assay is a fast and reliable method for colorimetric determination of fungal cell densities. Applied and environmental microbiology, 65(8), 3727-3729.

[123] Hasegawa, M., Nishigaki, N., Washio, Y., Kano, K., Harris, P. A., Sato, H., Mori, I., West, R. I., Shibahara, M., Toyoda, H., and Wang, L. (2007). Discovery of novel benzimidazoles as potent inhibitors of TIE-2 and VEGFR-2 tyrosine kinase receptors. *Journal of Medicinal Chemistry*, 50(18), 4453-4470.

[124] Murphy, E. J., Metcalfe, C. L., Basran, J., Moody, P. C., and Raven, E. L. (2008). Engineering the substrate specificity and reactivity of a heme protein: creation of an ascorbate binding site in cytochrome c peroxidase. *Biochemistry*, 47(52), 13933-13941.

[125] Ahmad, R., Alam, A., Khan, M., Ali, T., Elhenawy, A. A., and Ahmad, M. (2023). Antioxidant Activity, Molecular Docking and Quantum Studies of New Bis-Schiff Bases Based on Benzyl Phenyl Ketone Moiety. *Chemistry Select*, 8, e202302338.

[126] Feng, Y., Likos, J. J., Zhu, L., Woodward, H., Munie, G., McDonald, J. J., Stevens, A. M., Howard, C. P., De Crescenzo, G. A., Welsch, D., and Shieh, H. S. (2002). Solution structure and backbone dynamics of the catalytic domain of matrix metalloproteinase-2 complexed with a hydroxamic acid inhibitor. *Biochemistry. Biophysics*. Acta (BBA)-Proteins and Proteomics, 1598, 10-23.

[127] Barqi, M. M., Abdellah, I. M., Eletmany, M. R., Ali, N. M., Elhenawy, A. A., Abd El Latif, F. M. (2023). Synthesis, Characterization, Bioactivity Screening and Computational Studies of Diphenyl− malonohydrazides and Pyridines Derivatives. *Chemistry Select*, 8, e202203913.

[128] Nazreen, S., Elbehairi, S. E. I., Malebari, A. M., Alghamdi, N., Alshehri, R. F., Shati, A. A., Ali, N. M., Alfaifi, M. Y., Elhenawy, A. A., Alam, M. M. (2023, May 15). New Natural Eugenol Derivatives as Antiproliferative Agents: *Synthesis, Biological Evaluation, and Computational Studies*. ACS Omega.

[129] Alam, M. M., Elbehairi, S. E. I., Shati, A. A., Hussien, R. A., Alfaifi, M. Y., Malebari, A. M., Asad, M., Elhenawy, A. A., Asiri, A. M., Mahzari, A. M., Alshehri, R. F. (2023). Design, synthesis, and biological evaluation of new eugenol derivatives containing 1, 3, 4-oxadiazole as novel inhibitors of thymidylate synthase. *New Journal of Chemistry*, 10, 5021-5032.

[130] Synthesis and Characterization of a New Class of Chromene-Azo Sulfonamide Hybrids as Promising Anticancer Candidates with the Exploration of their EGFR, hCAII and MMP-2 Inhibitors based on Molecular Docking Assays. (2023). *Accepted International Journal of Molecular Sciences*.

[131] Ardjani, T. E. A., & Alvarez-Idaboy, J. R. (2018). Radical scavenging activity of ascorbic acid analogs: Kinetics and mechanisms. *Theoretical Chemistry Accounts*, 137, 1-8.

[132] Daina, A., Michielin, O., & Zoete, V. (2017). SwissADME: a free web tool to evaluate pharmacokinetics, drug-likeness, and medicinal chemistry friendliness of small molecules. *Scientific Reports*, 7(1), 42717.

[133] Yang, H., Lou, C., Sun, L., Li, J., Cai, Y., Wang, Z., Li, W., Liu, G., & Tang, Y. (2019). admetSAR 2.0: web-service for prediction and optimization of chemical ADMET properties. *Bioinformatics*, 35(6), 1067-1069.

[134] Ahmad, R., Alam, A., Khan, M., Ali, T., Elhenawy, A. A., & Ahmad, M. (2023). Antioxidant Activity, Molecular Docking and Quantum Studies of New Bis-Schiff Bases Based on Benzyl Phenyl Ketone Moiety. *ChemistrySelect*, 8(35), e202302338.

[135] Zhao, Y. H., Abraham, M. H., Le, J., Hersey, A., Luscombe, C. N., Beck, G., Sherborne, B., & Cooper, I. (2002). *Pharmaceutical research*, 19, 1446-1457.

[136] Wang, H., Ye, W., Yin, B., Wang, K., Riaz, M. S., Xie, B. B., Zhong, Y., & Hu, Y. (2023). Modulating Cation Migration and Deposition with Xylitol Additive and Oriented Reconstruction of Hydrogen Bonds for Stable Zinc Anodes. Angewandte Chemie, 62(10), e202218872.

[137] Banerjee, P., Eckert, A. O., Schrey, A. K., & Preissner, R. (2018). ProTox-II: a webserver for the prediction of toxicity of chemicals. *Nucleic acids research*, 46(W1), W257–W263.

[138] Cheng, F., Li, W., Zhou, Y., Shen, J., Wu, Z., Liu, G., Lee, P. W., & Tang, Y. (2012). admetSAR: a comprehensive source and free tool for assessment of chemical ADMET properties. *Journal of chemical information and modelling*, 52(11), 3099–3105.

[139] Bruker, APEX-3, SAINT+, Version 6.02 (Includes XPREP and SADABS), Bruker AXS Inc., Madison, Wisconsin, USA, 2016.

[140] Farrugia, L. J. (2012). *Journal of Applied Crystallography*, 45(5), 849-854.

[141] Sheldrick, G. M. (2015). Acta Crystallographica Section C: *Structural Chemistry*, 71(1), 3-8.

[142] Spek, A. L. (2009). Acta Crystallographica Section D: Biological *Crystallography*, 65(2), 148-155.

[143] Hassanain, H. M., Al-Sharif, S., Al-Ghamdi, H. A., Nahari, L. M., Al-Sulami, A. I., Mousally, S. M., & Al-Zaydi, K. M. (2024). Synthesis, Crystal Structure, Hirshfeld Surface Analysis, Energy Framework Calculations, and Halogen Bonding Investigation of Benzene-1,3,5-triyltris((4-chlorophenyl)methanone). *Crystals,* 14(1), 17.

[144] Aziz, M. W., Kamal, A. M., Mohamed, K. O., & Elgendy, A. A. (2021). Design, synthesis and assessment of new series of quinazolinone derivatives as EGFR inhibitors along with their cytotoxic evaluation against MCF7 and A549 cancer cell lines. *Bioorganic & Medicinal Chemistry Letters*, 41, 127987.

[145] Alkhatib, F. M., & Alsulami, H. M. (2023). Synthesis, characterization, DFT calculations and biological activity of new Schiff base complexes. *Heliyon*, 9(8), e18988

[146] Taayoshi, F., Iraji, A., Moazzam, A., et al. (2022). Synthesis, molecular docking, and cytotoxicity of quinazolinone and dihydroquinazolinone derivatives as cytotoxic agents. *Chemistry Central Journal*, 16(1), 35

[147]Wołosiak, R., Drużyńska, B., Derewiaka, D., Piecyk, M., Majewska, E., Ciecierska, M., Worobiej, E., & Pakosz, P. (2022). Verification of the conditions for determination of antioxidant activity by ABTS and DPPH assays—A practical approach. *Molecules*, 27(1), 5

[148] Saravanan, G. O. V. I. N. D. A. R. A. J., Alagarsamy, V. E. E. R. A. C. H. A. M. Y., & Prakash, C. R. (2010). Synthesis and evaluation of antioxidant activities of novel quinazoline derivatives. *International Journal of Pharmacy and Pharmaceutical Sciences*, 2(4), 83-86.

[149] Hostetler, M. J., Wingate, J. E., Zhong, C.-J., Harris, J. E., Vachet, R. W., Clark, M. R., Londono, J. D., Green, S. J., Stokes, J. J., & Wignall, G. D. (1998). *Langmuir*, 14(1), 17-30.

[150] Brooks, B. R., Bruccoleri, R. E., Olafson, B. D., States, D. J., Swaminathan, S. A., & Karplus, M. (1983). *Journal of Computational Chemistry*, 4(2), 187-217.

SUPPLEMENTARY DATA

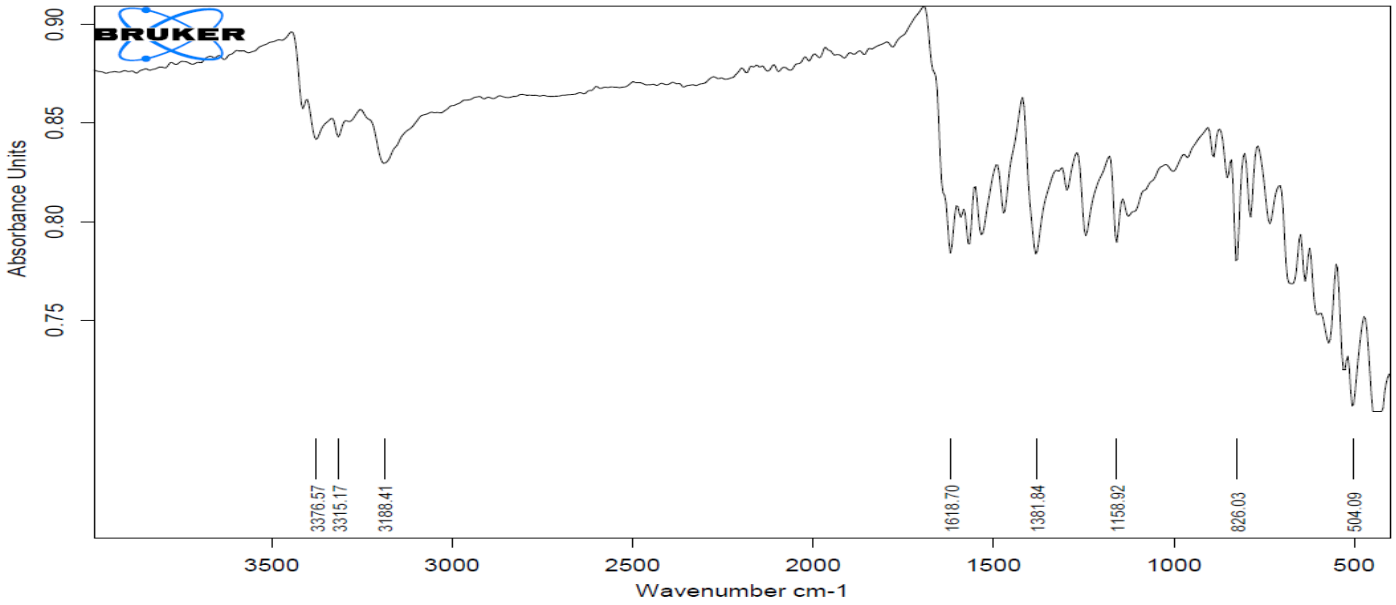

Figure 1: FTIR of **73**

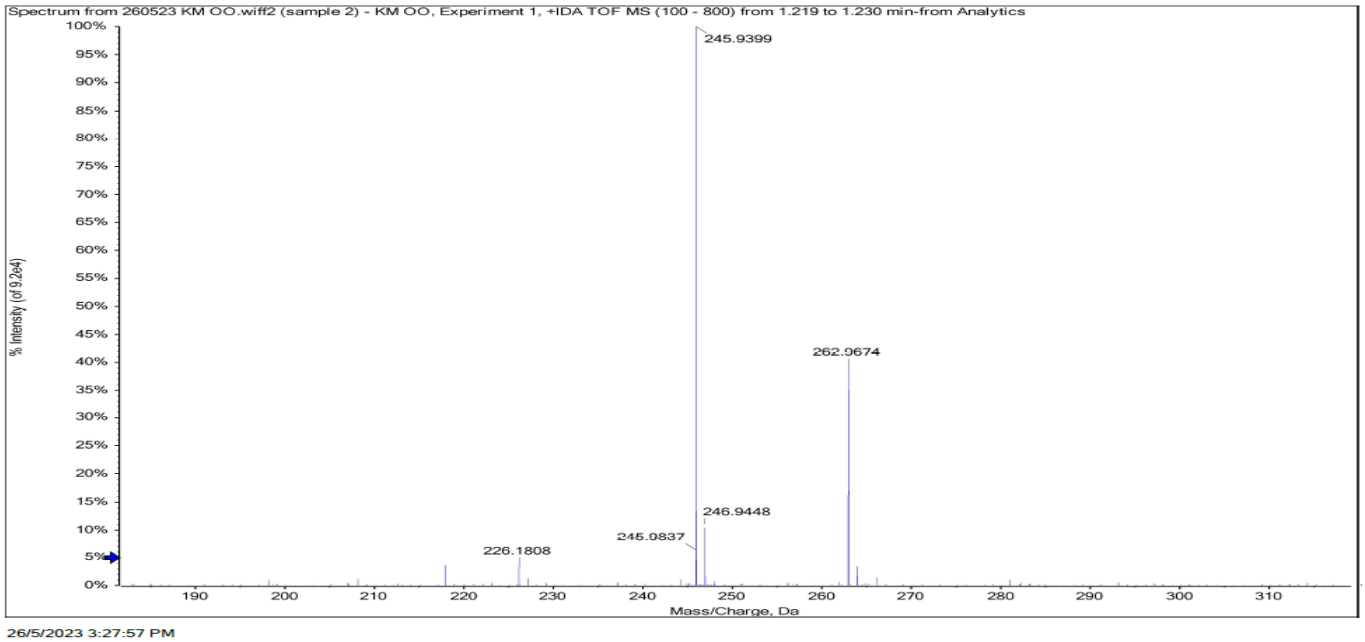

Figure 2: MS of **73**

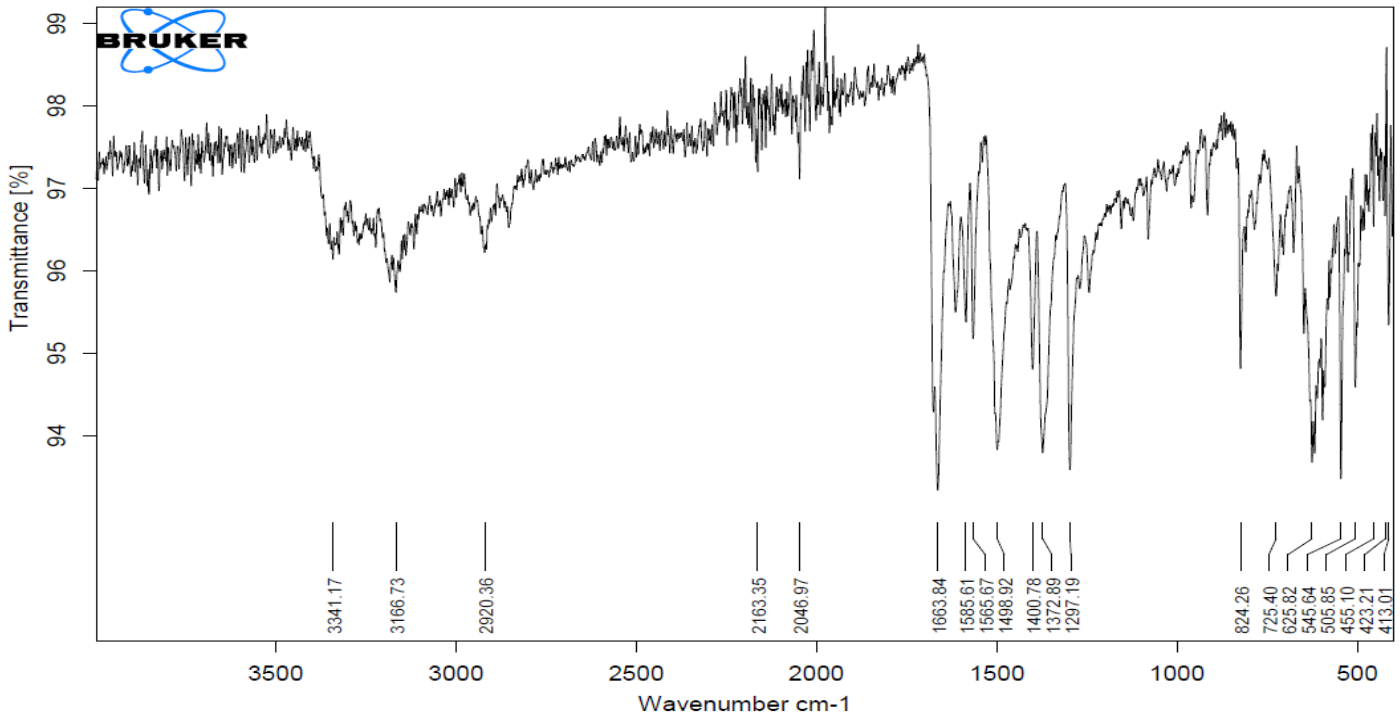

Figure 3: FTIR of **74**

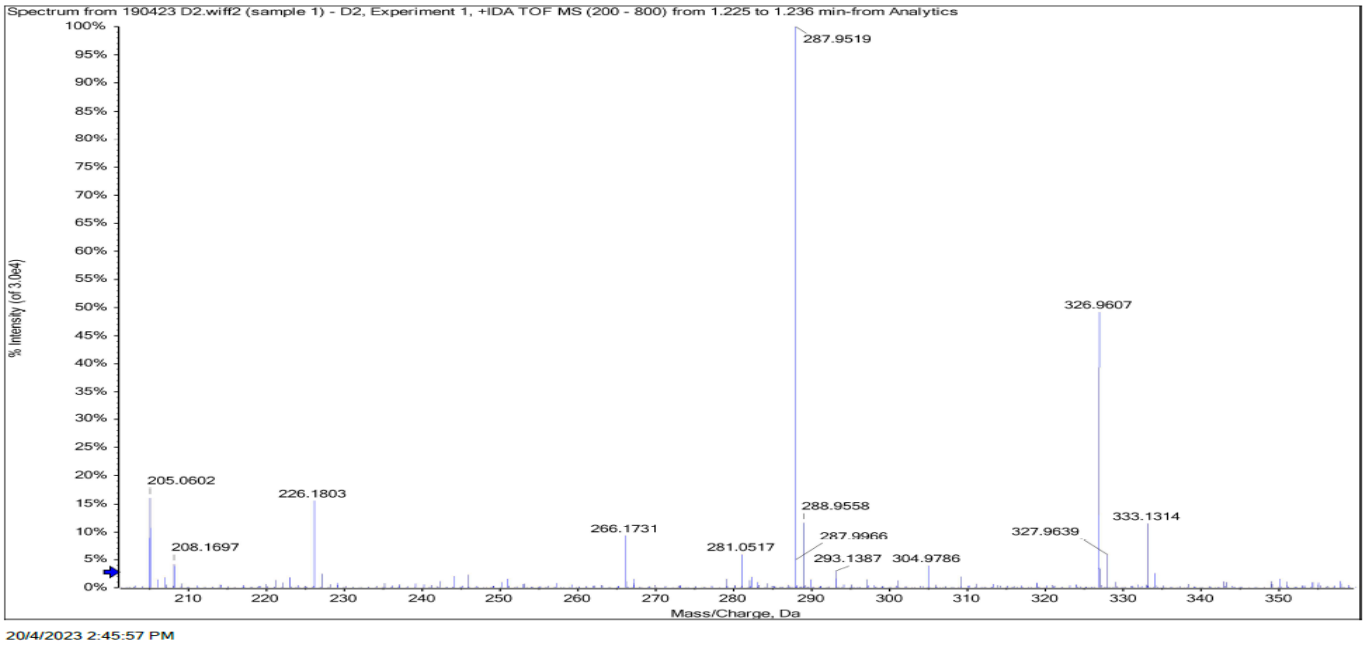

Figure 4: MS of **74**

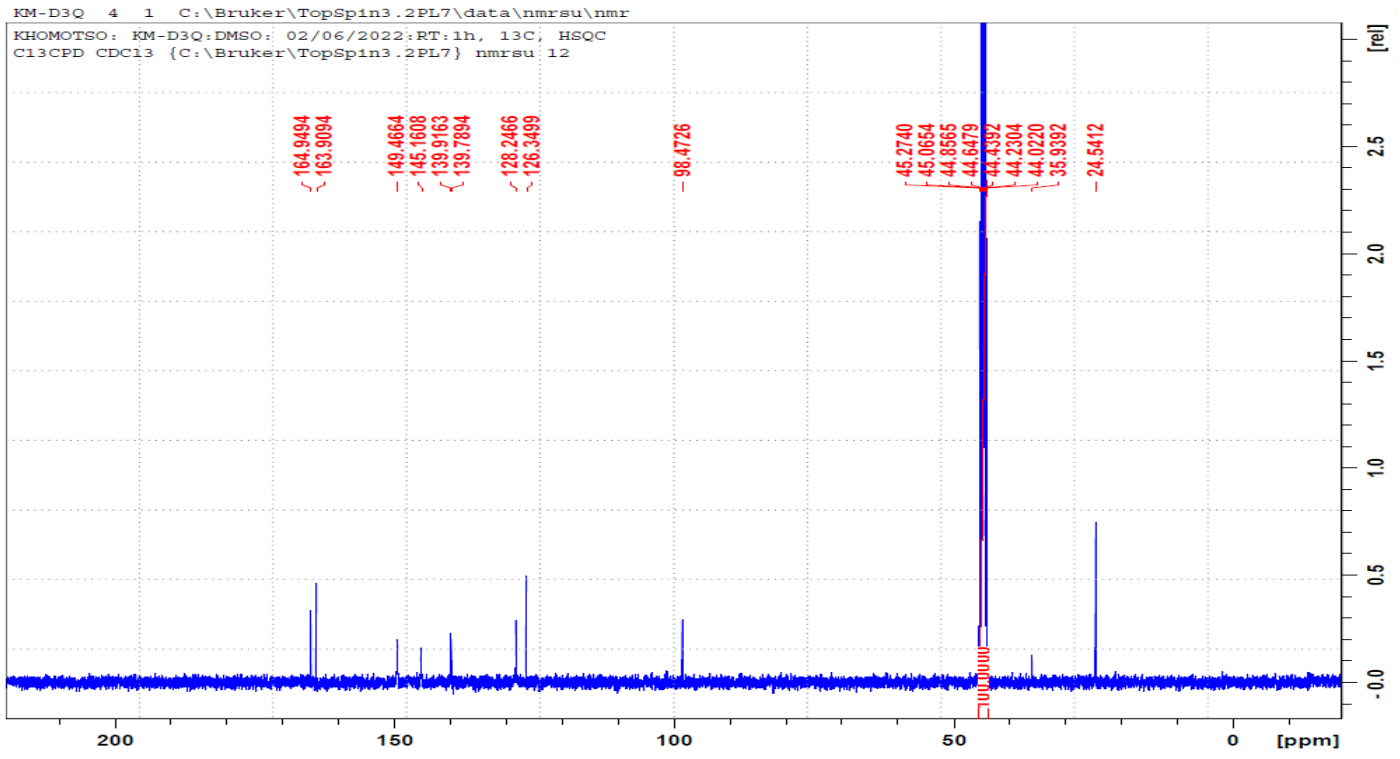

Figure 5: ^{13}C NMR of **74**

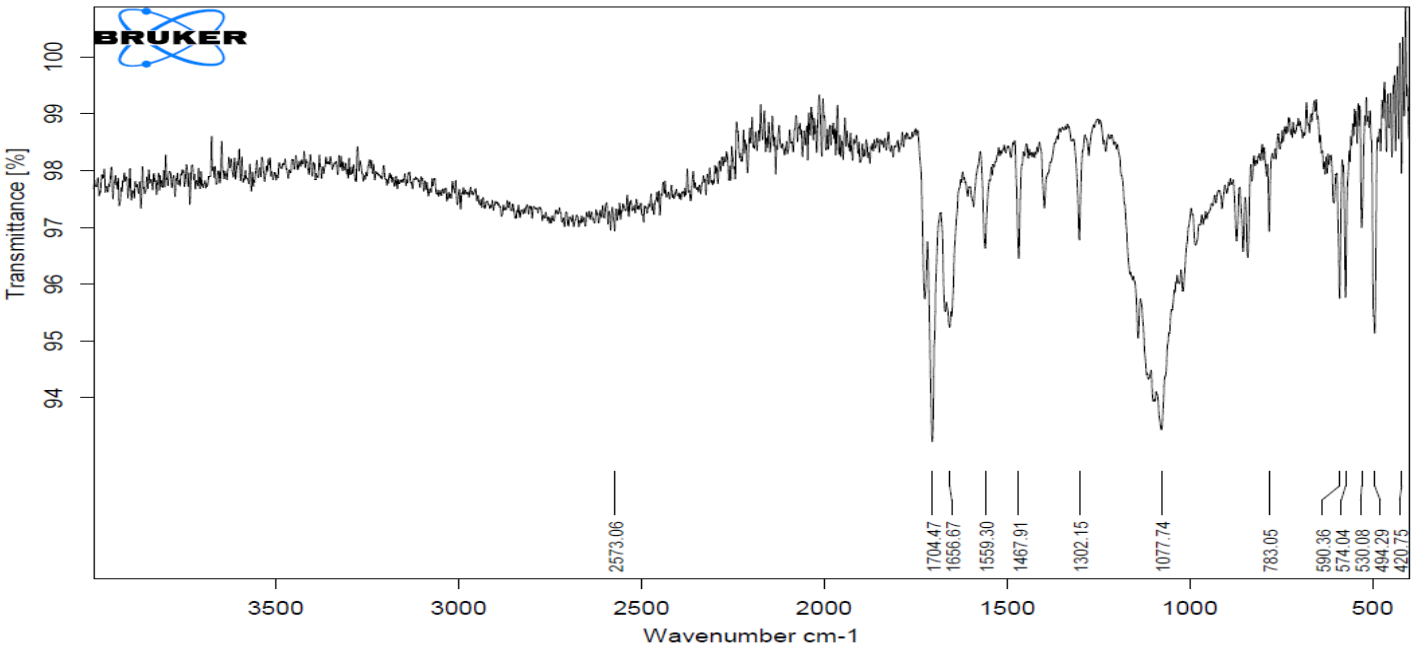

Figure 6: FTIR of **75**

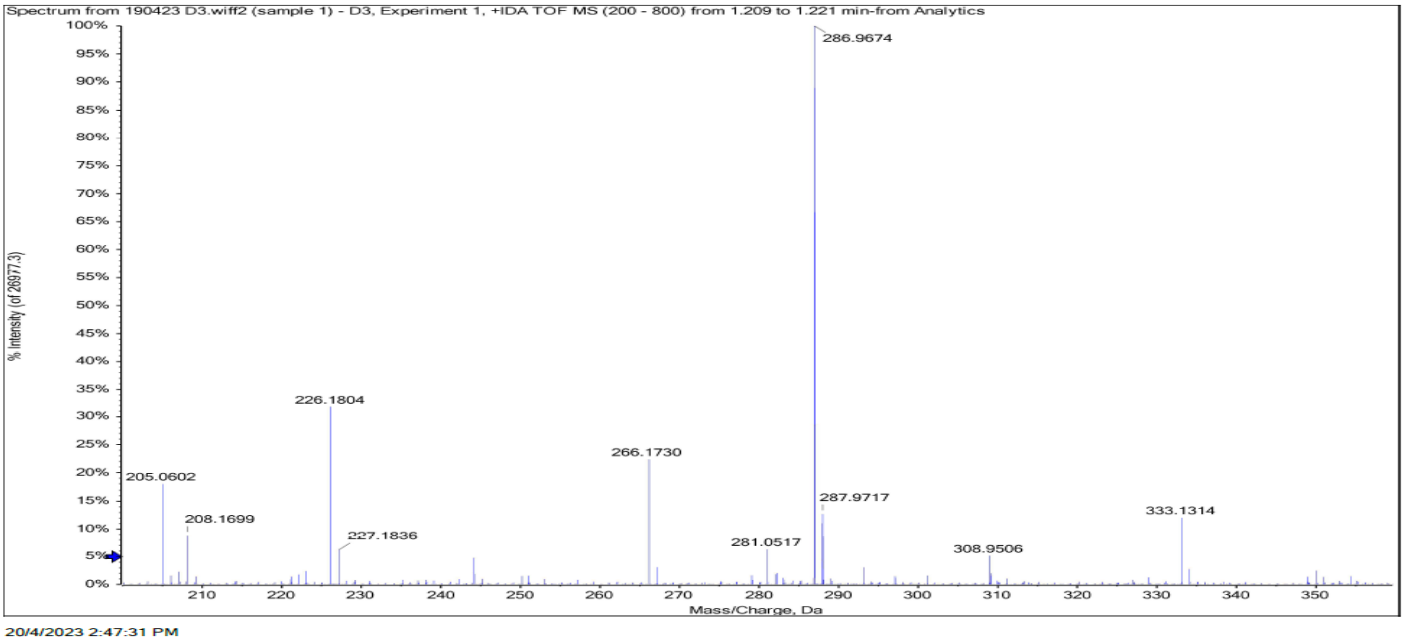

Figure 7: MS of **75**

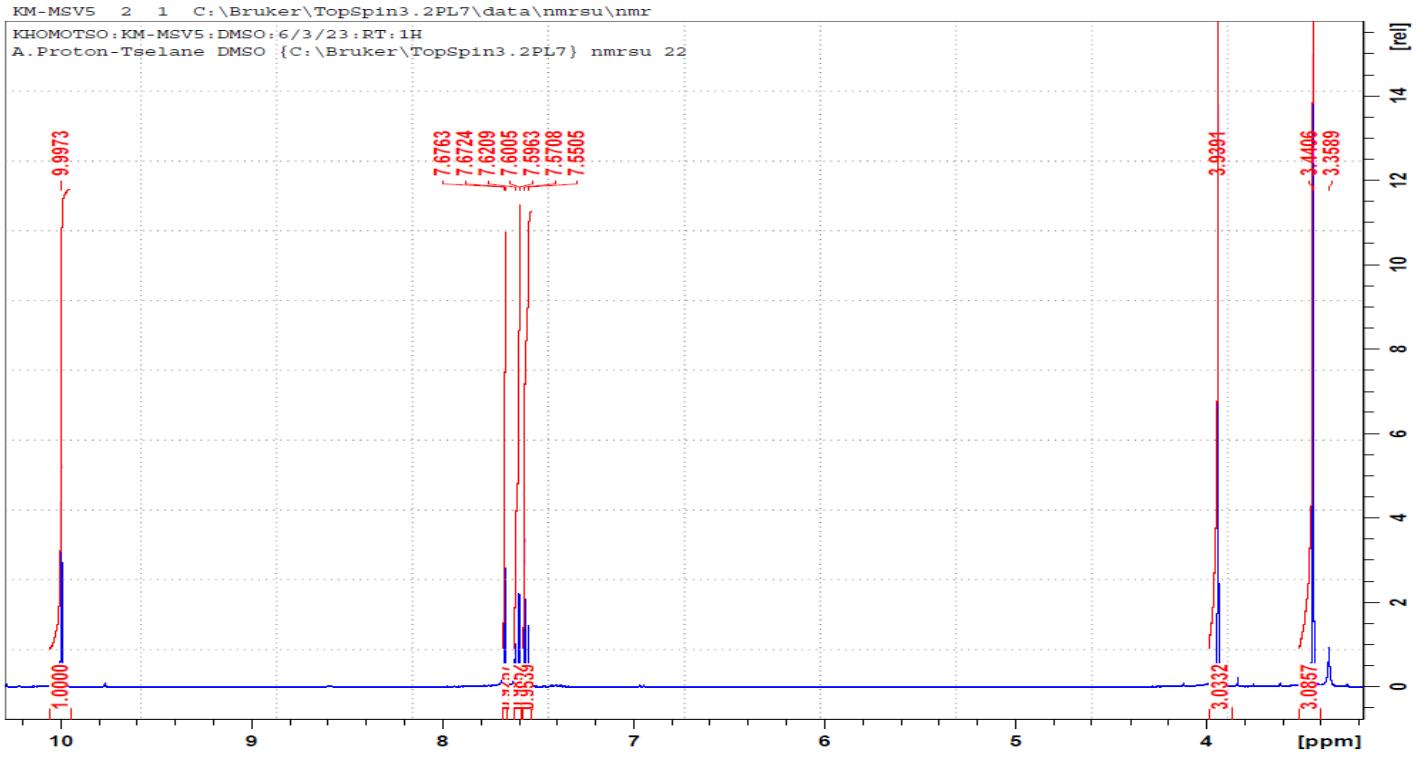

Figure 8: ^{1}H NMR of **76a**

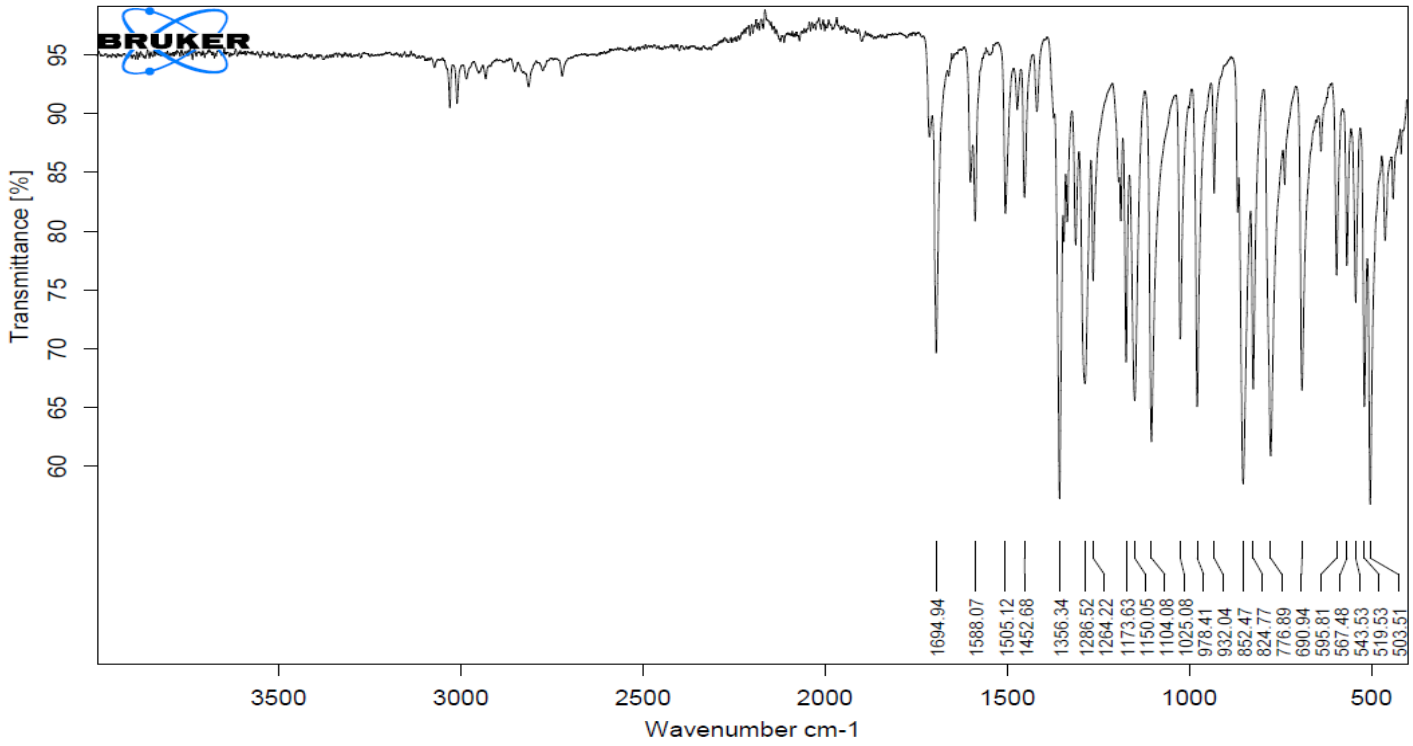

Figure 9: FTIR of **76a**

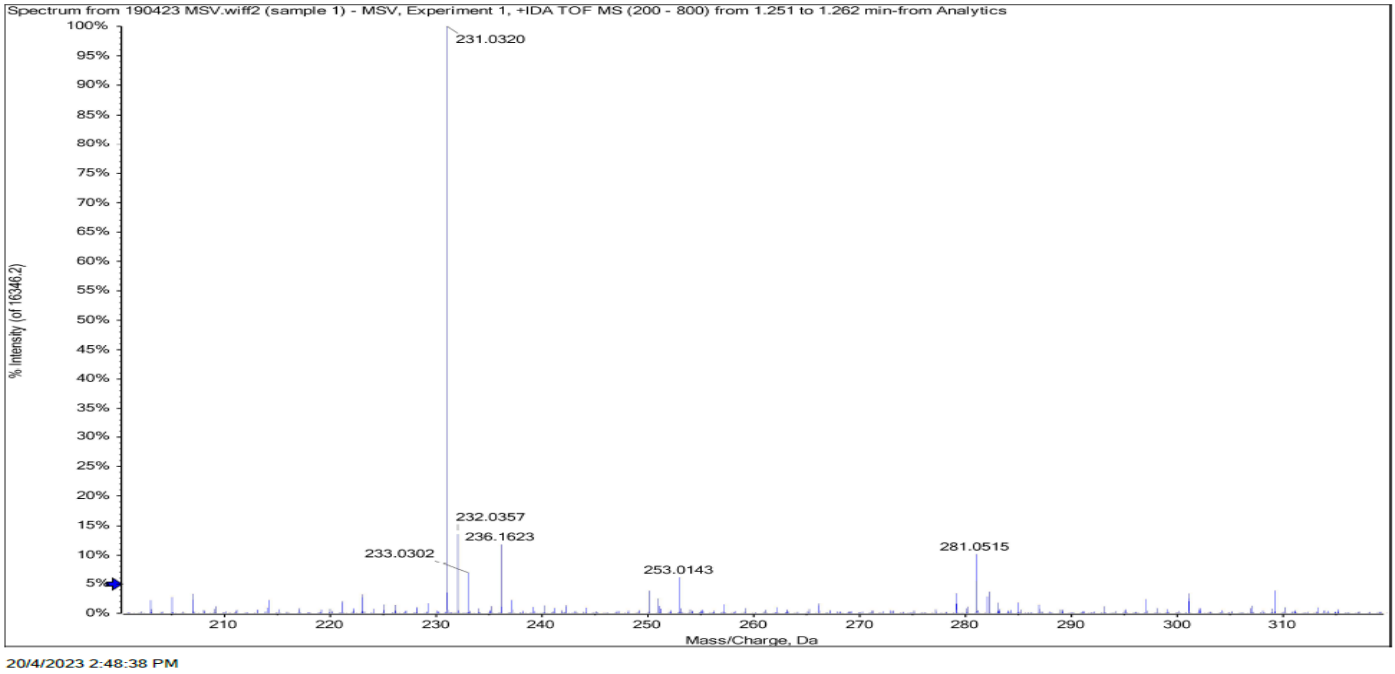

Figure 10: MS of **76a**

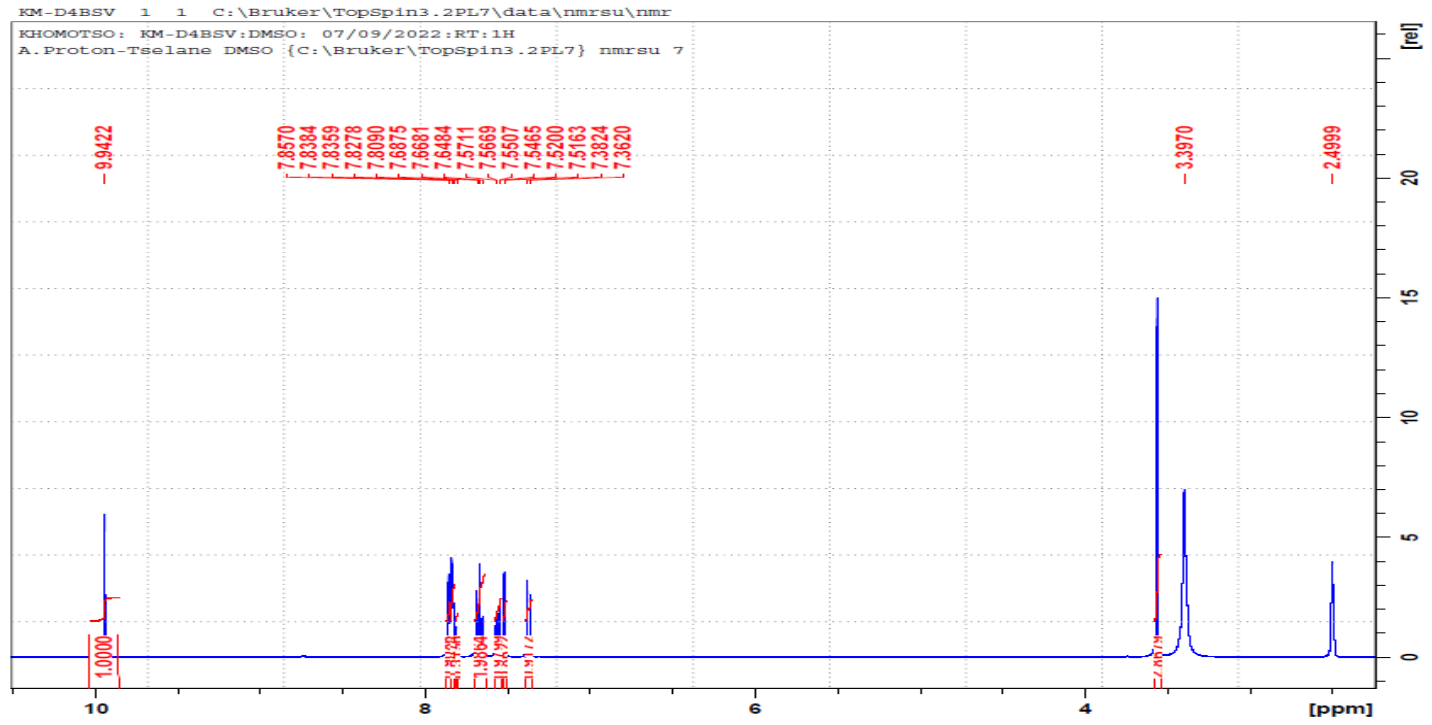

Figure 11: ^{1}H NMR of **76b**

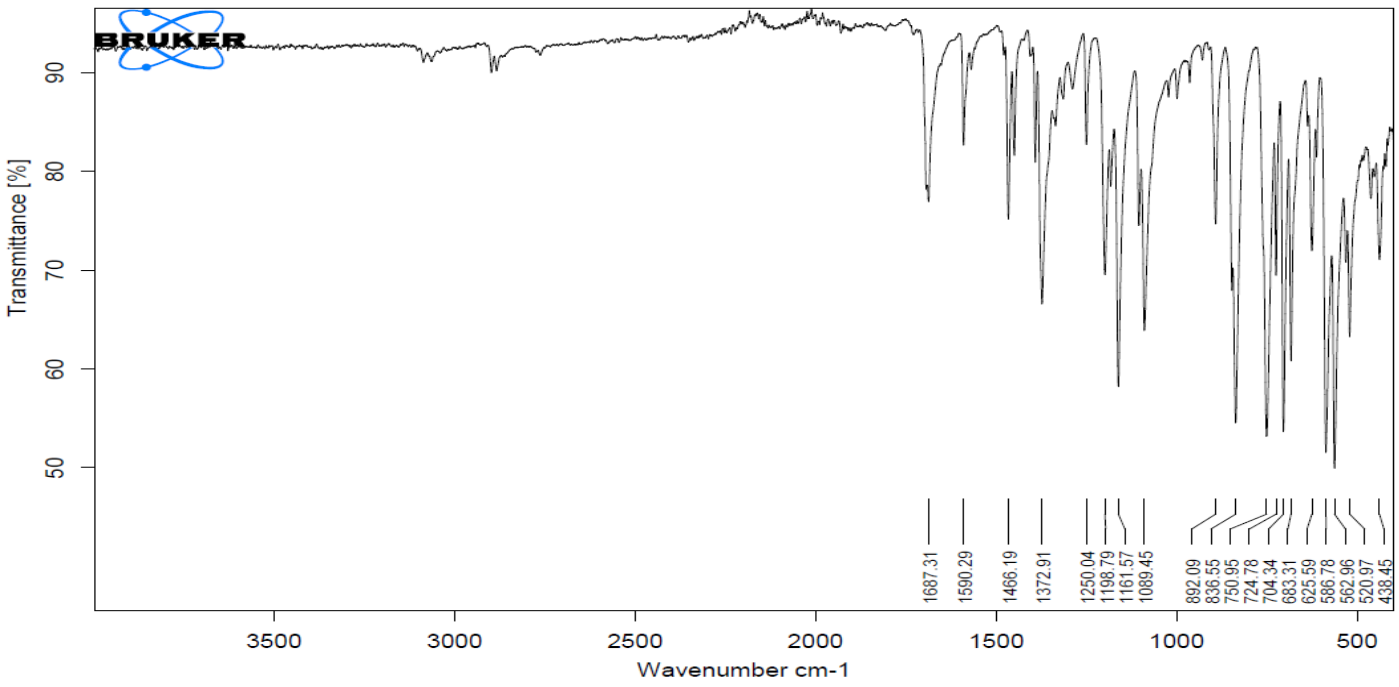

Figure 12: FTIR of **76b**

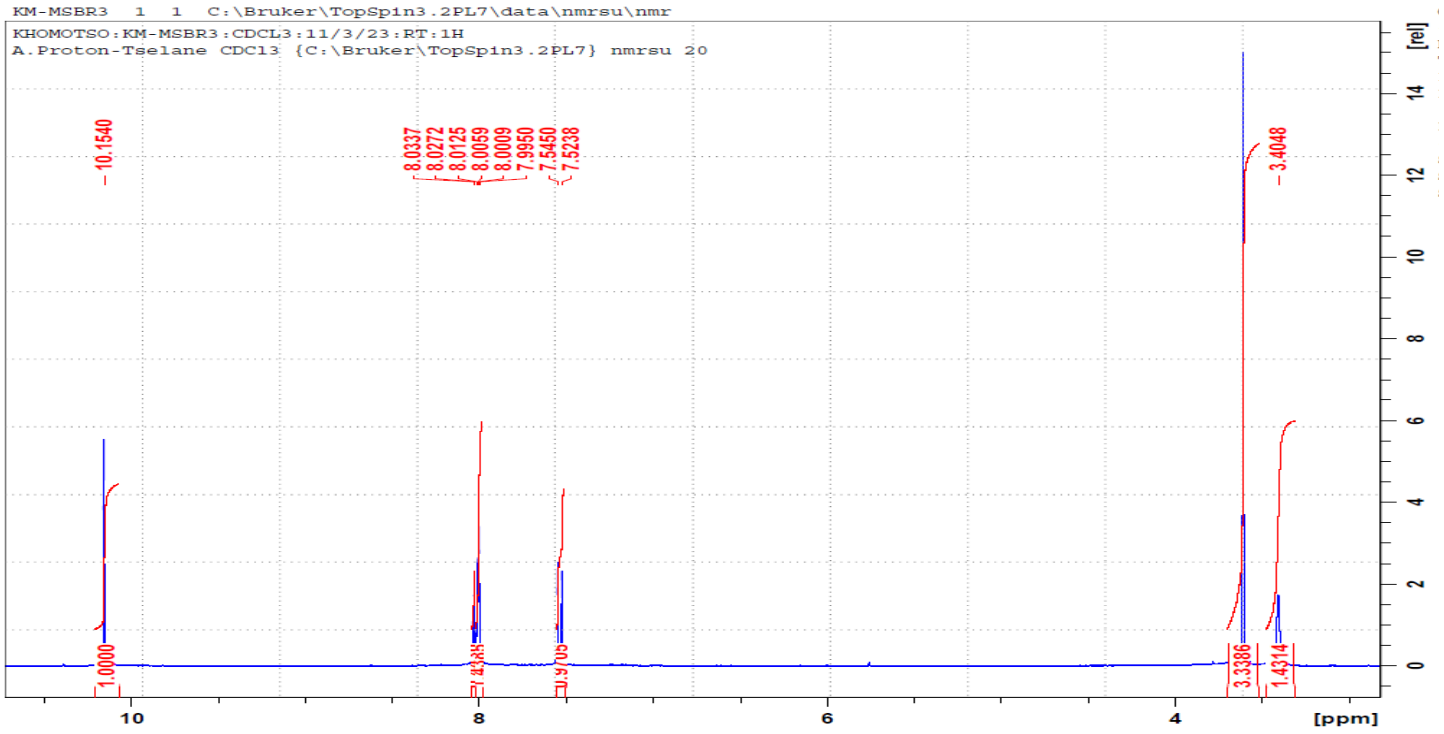

Figure 13: ^{1}H NMR of **76c**

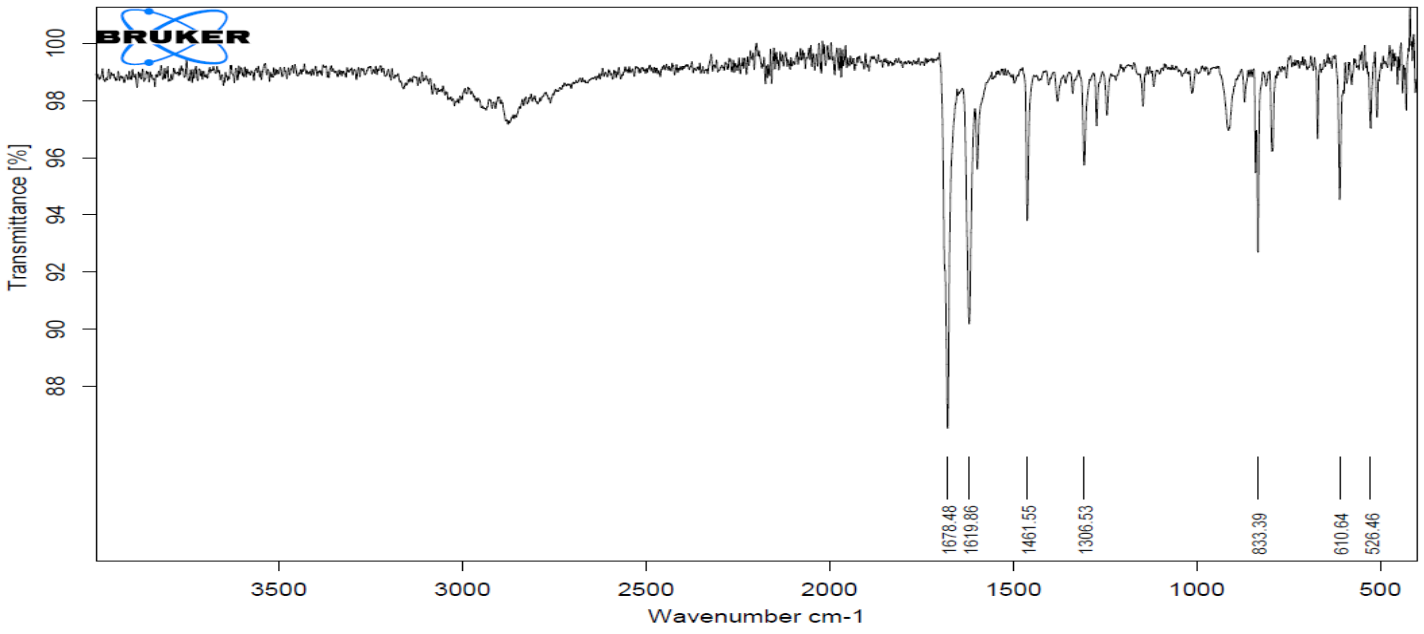

Figure 14: FTIR of **76c**

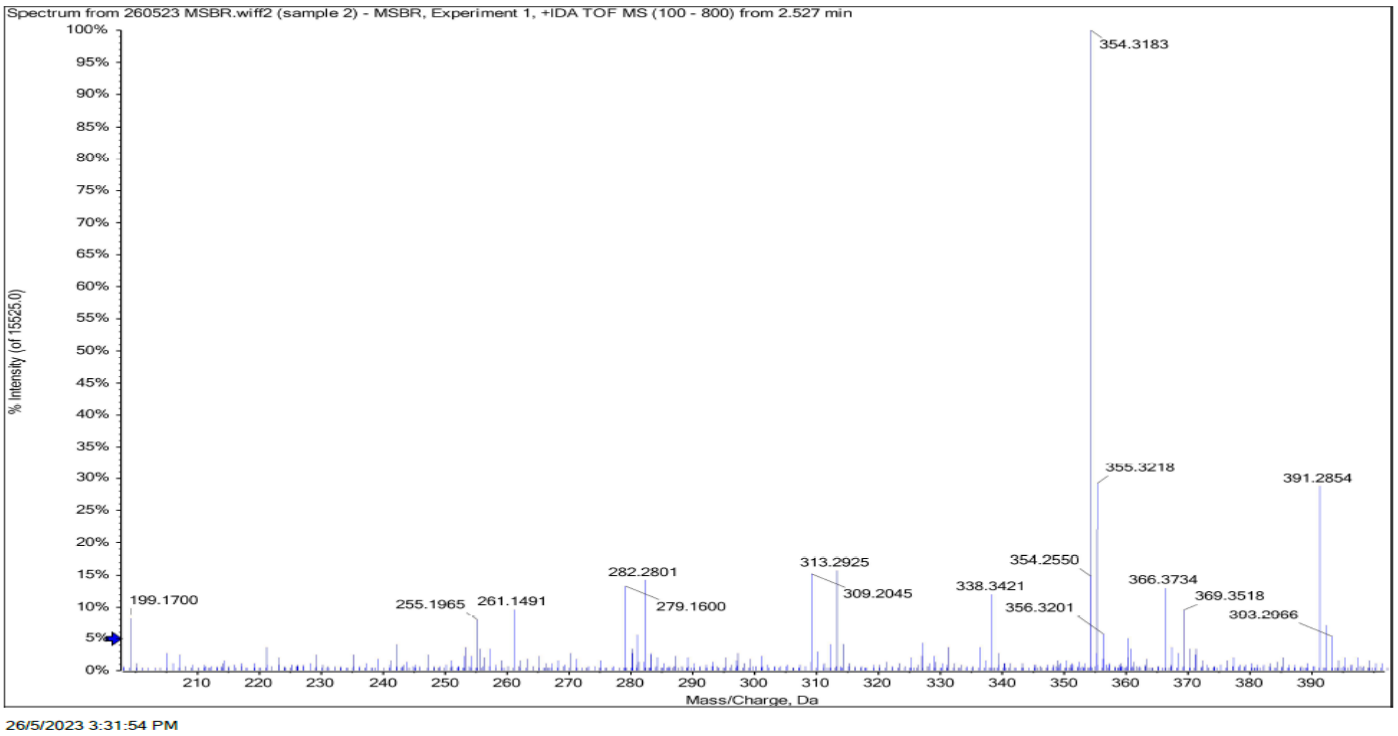

Figure 15: MS of **76c**

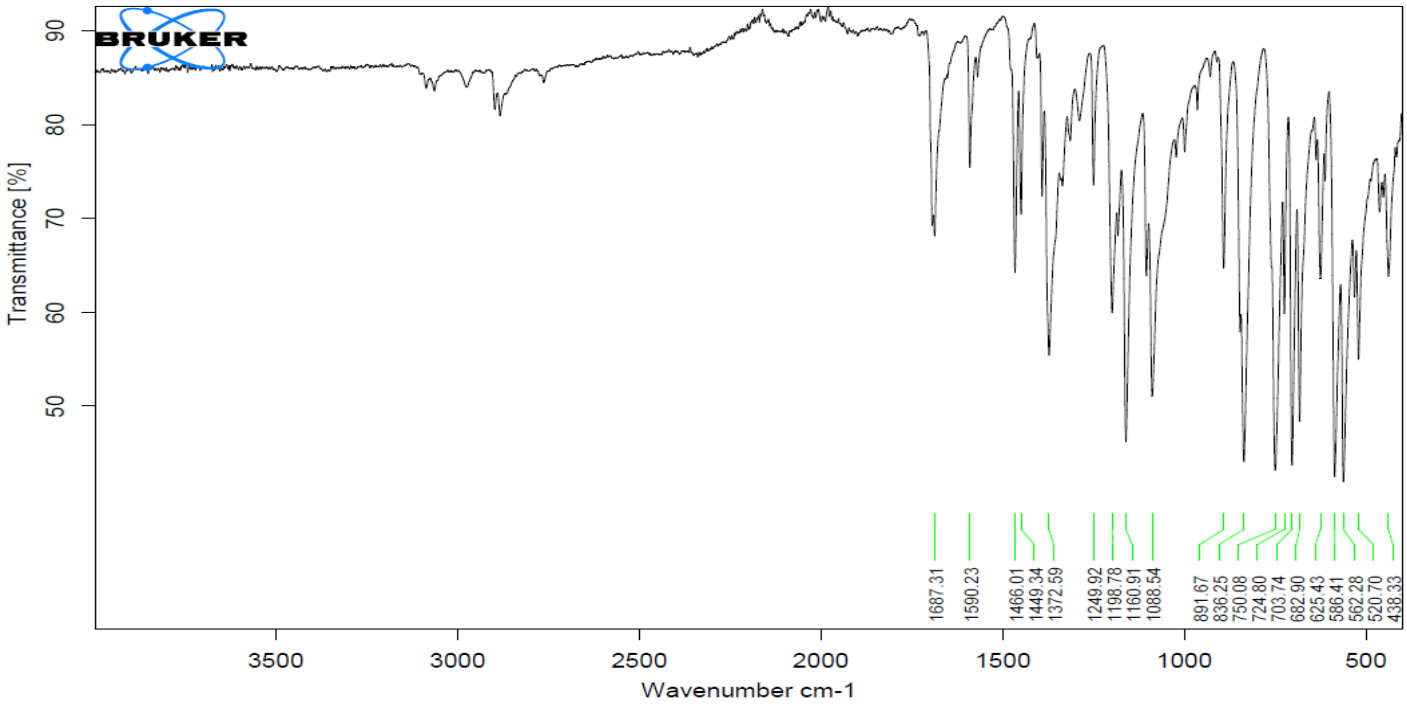

Figure 16: FTIR of **76c**

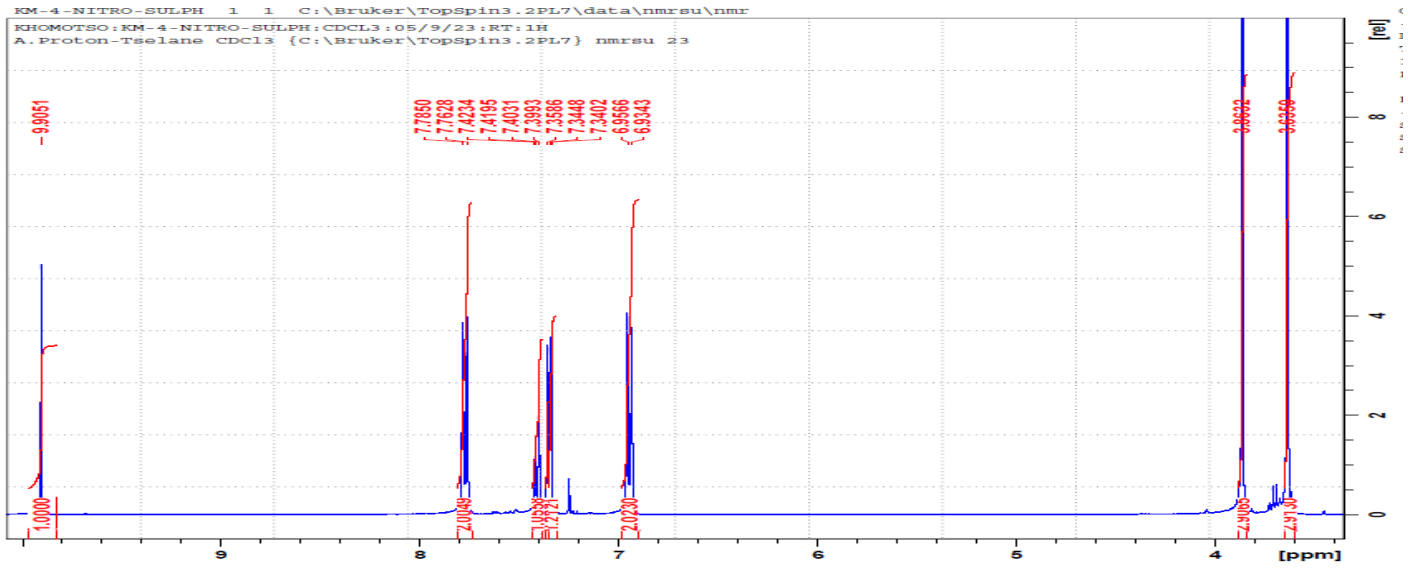

Figure 17: ^{1}H NMR of **76d**

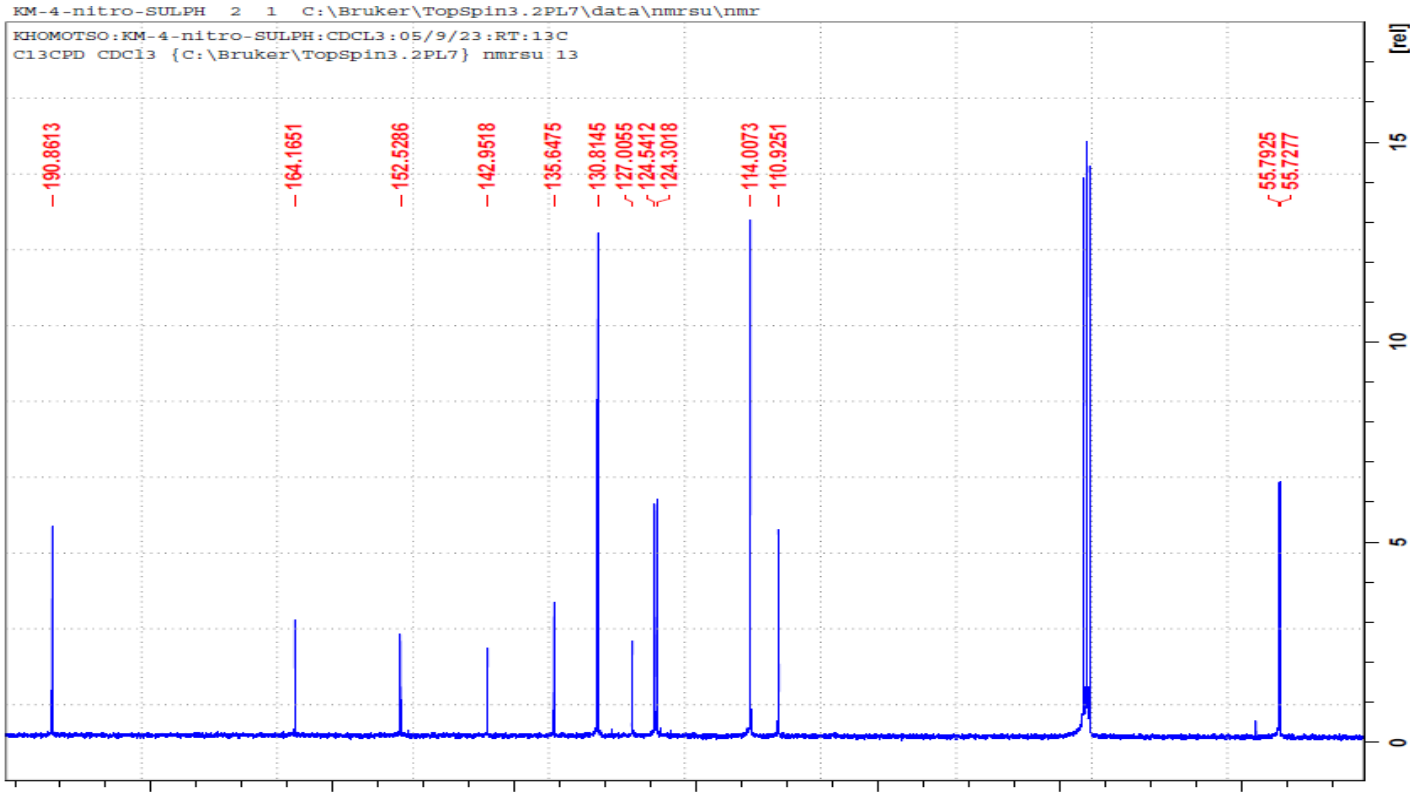

Figure 18: ^{13}C NMR of **76d**

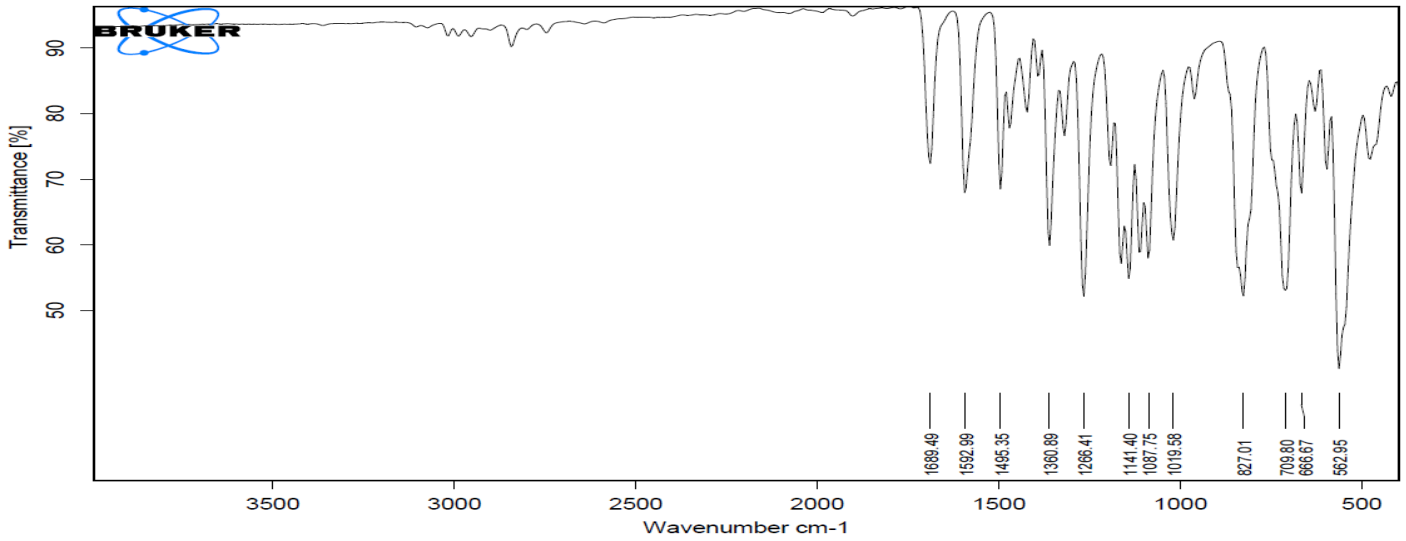

Figure 19: FTIR of **76d**

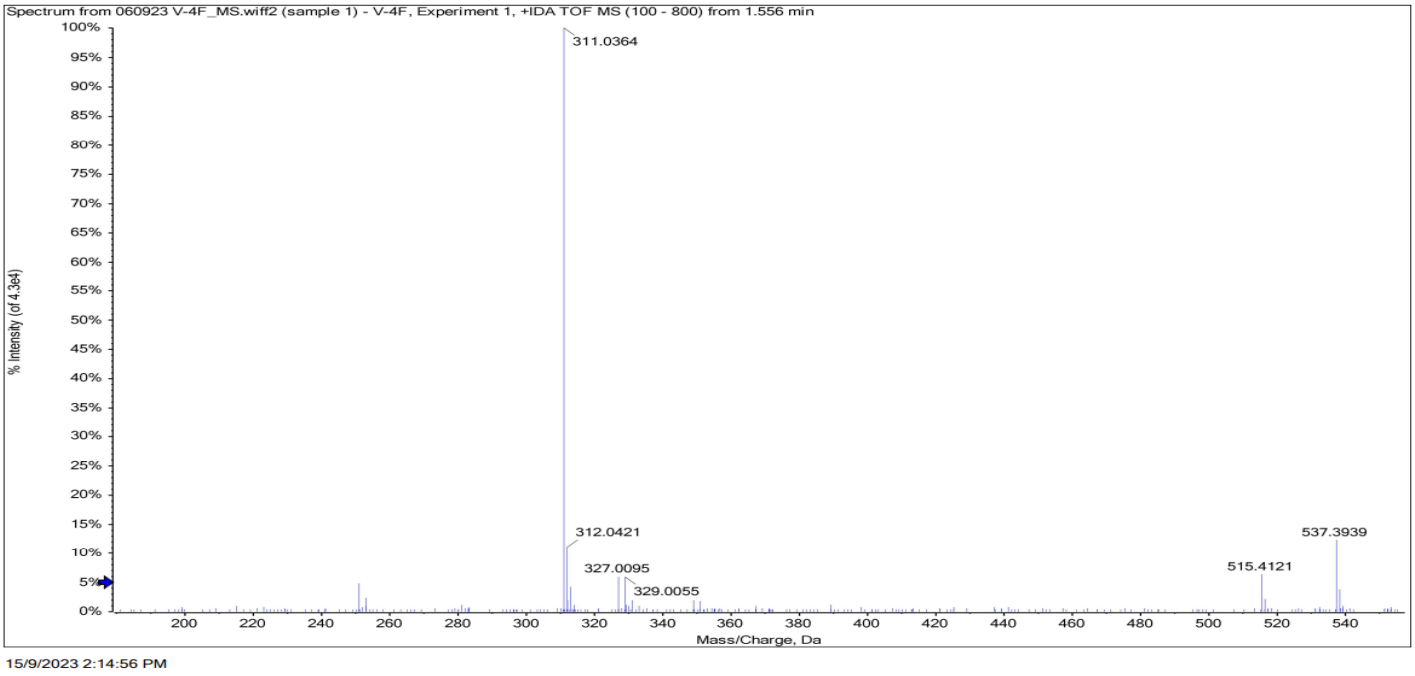

Figure 20: MS of **76d**

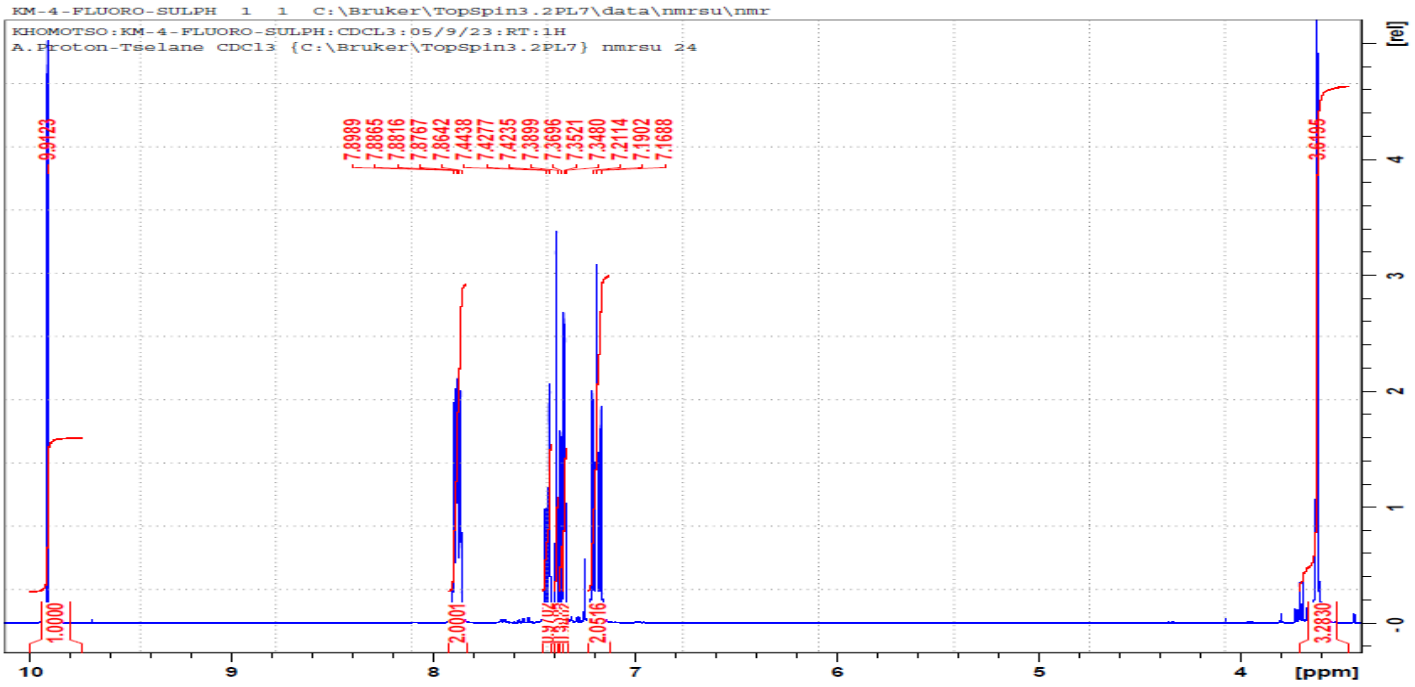

Figure 21: ^{1}H NMR of **76e**

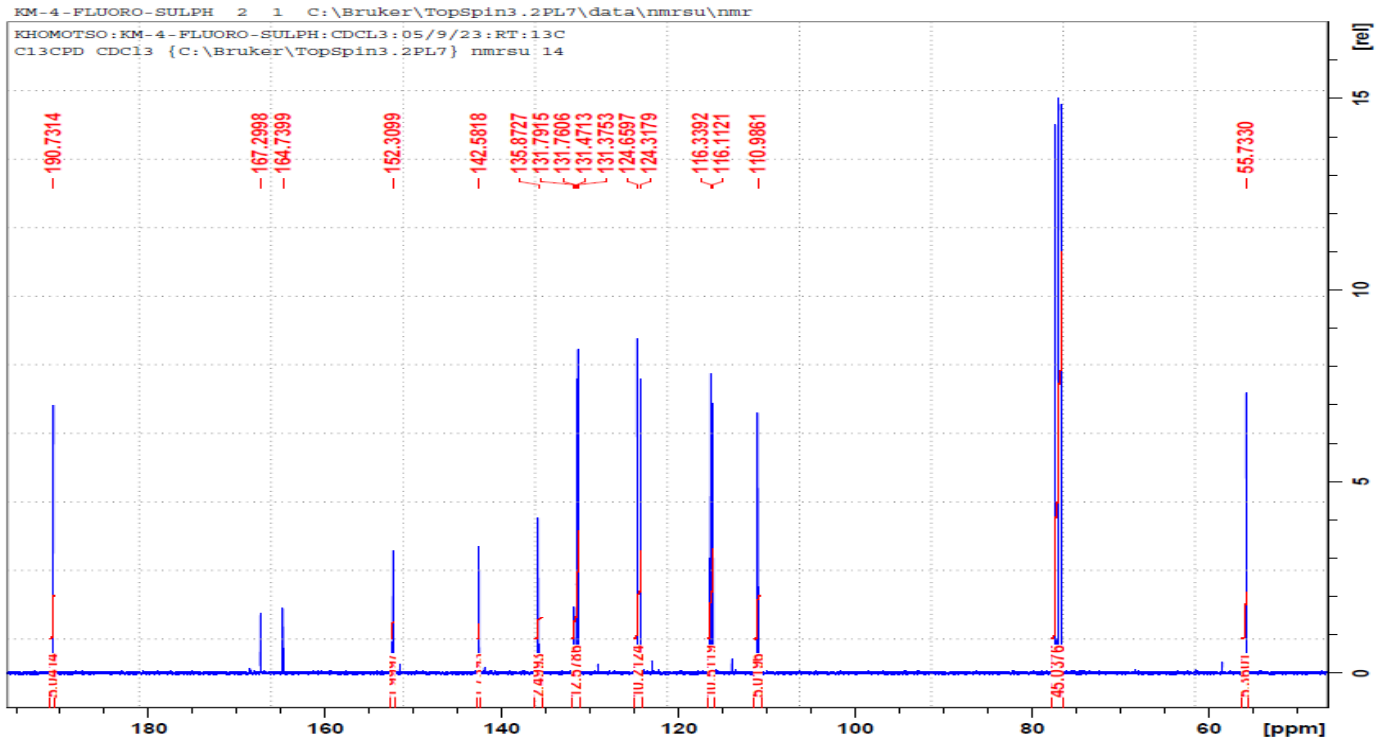

Figure 22: ^{13}C NMR of **76e**

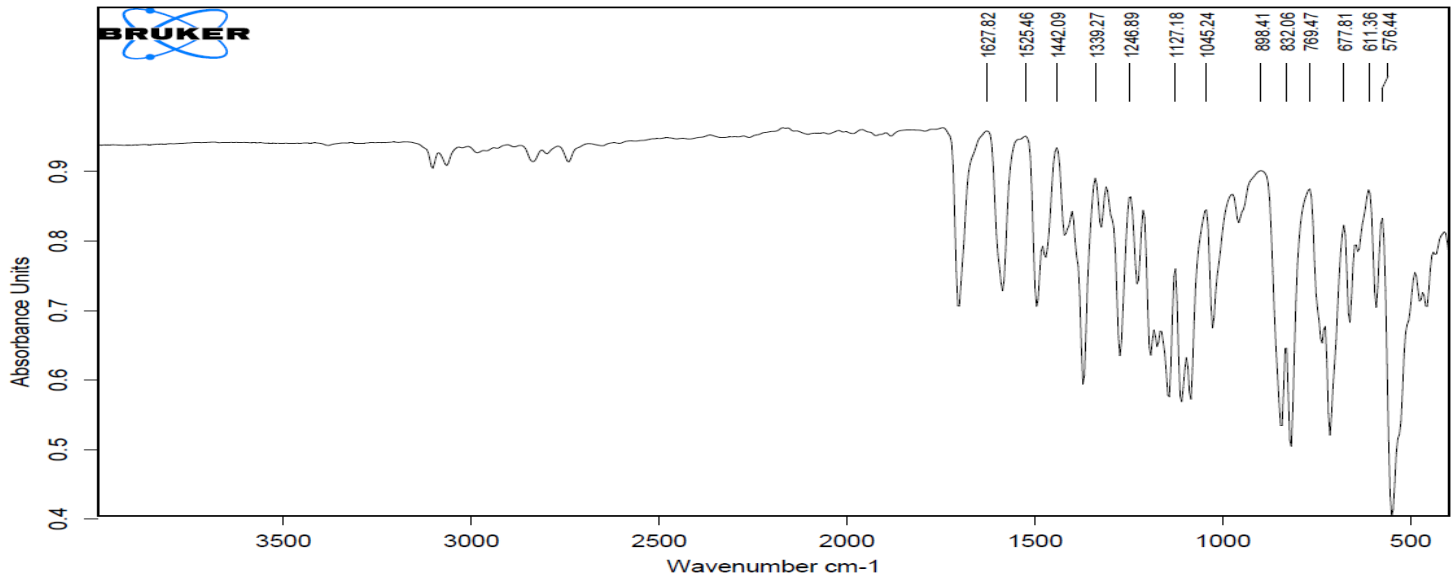

Figure 23: FTIR of **76e**

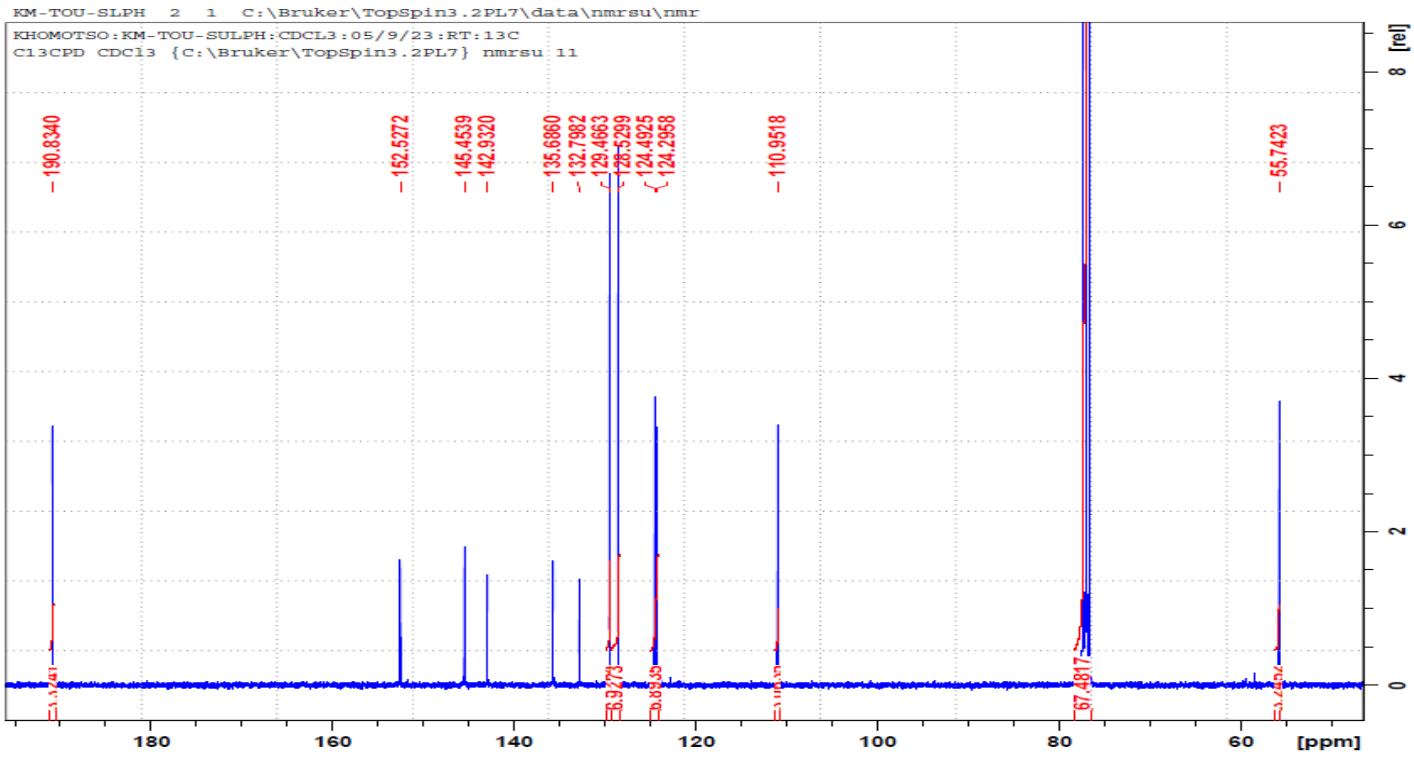

Figure 24: ^{13}C NMR of **76e**

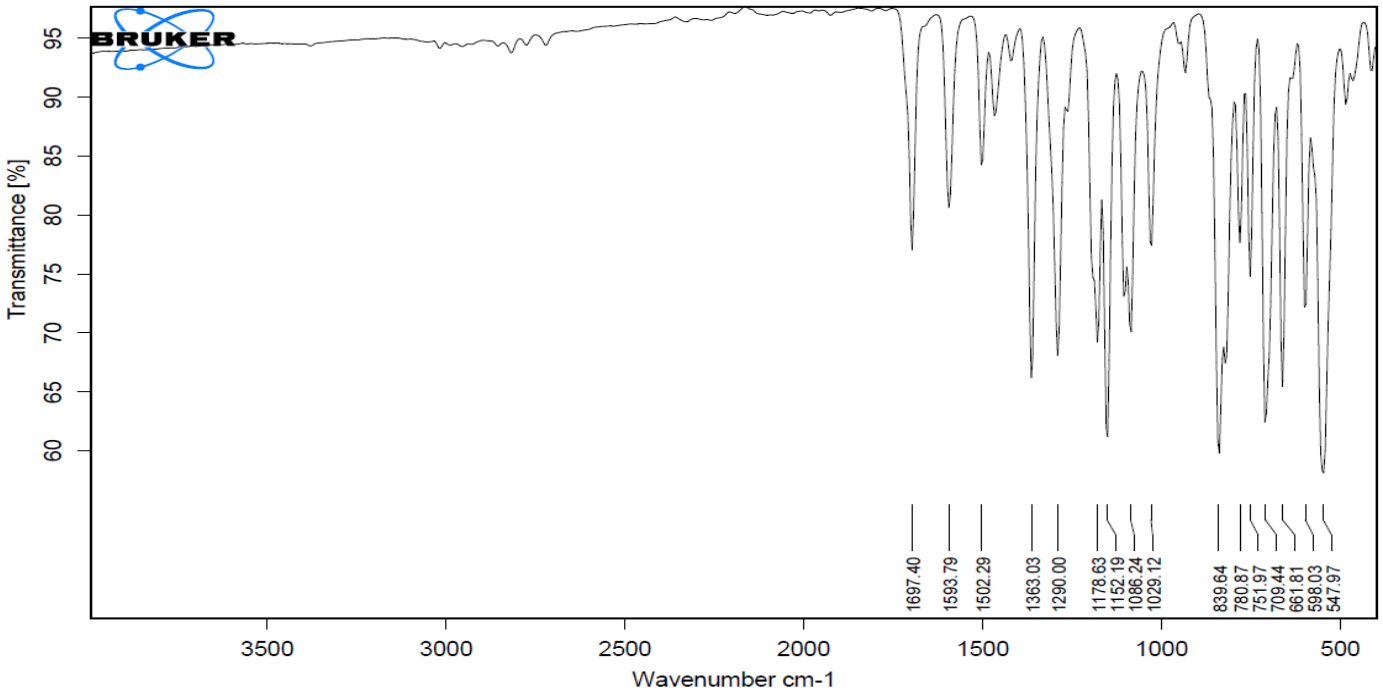

Figure 25: FTIR of **76e**

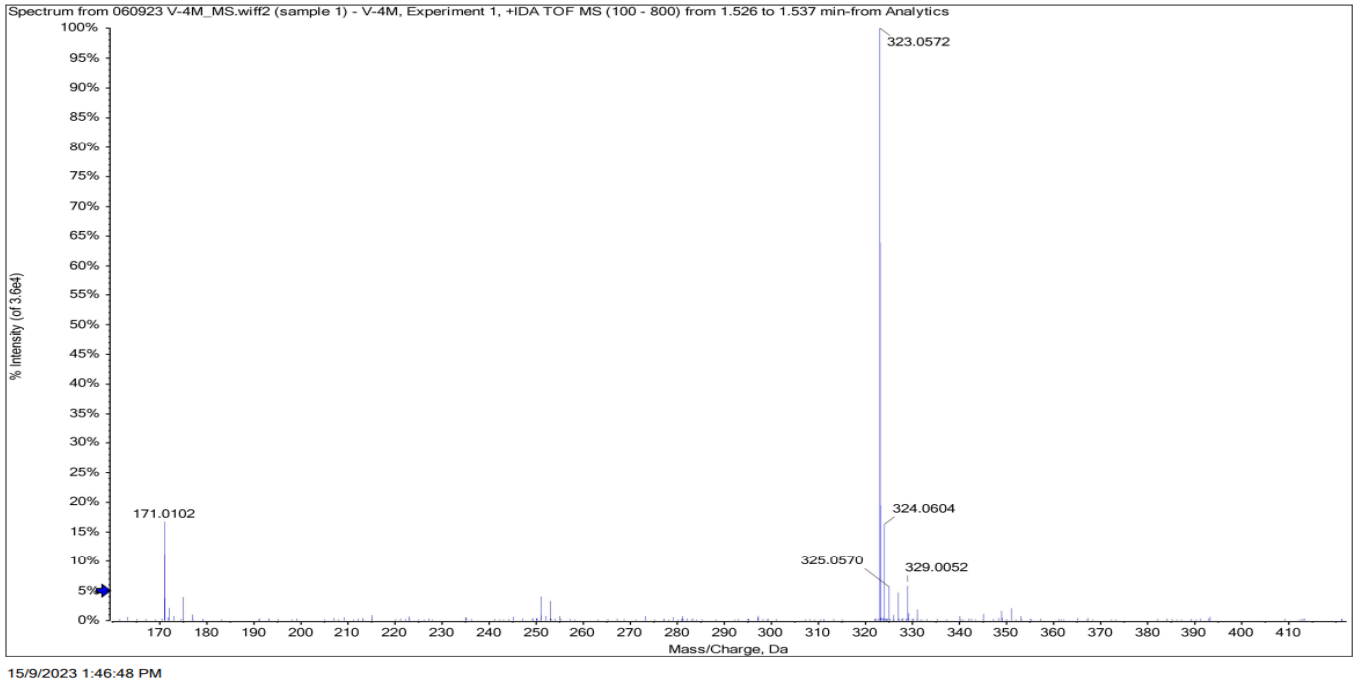

Figure 26: MS of **76e**

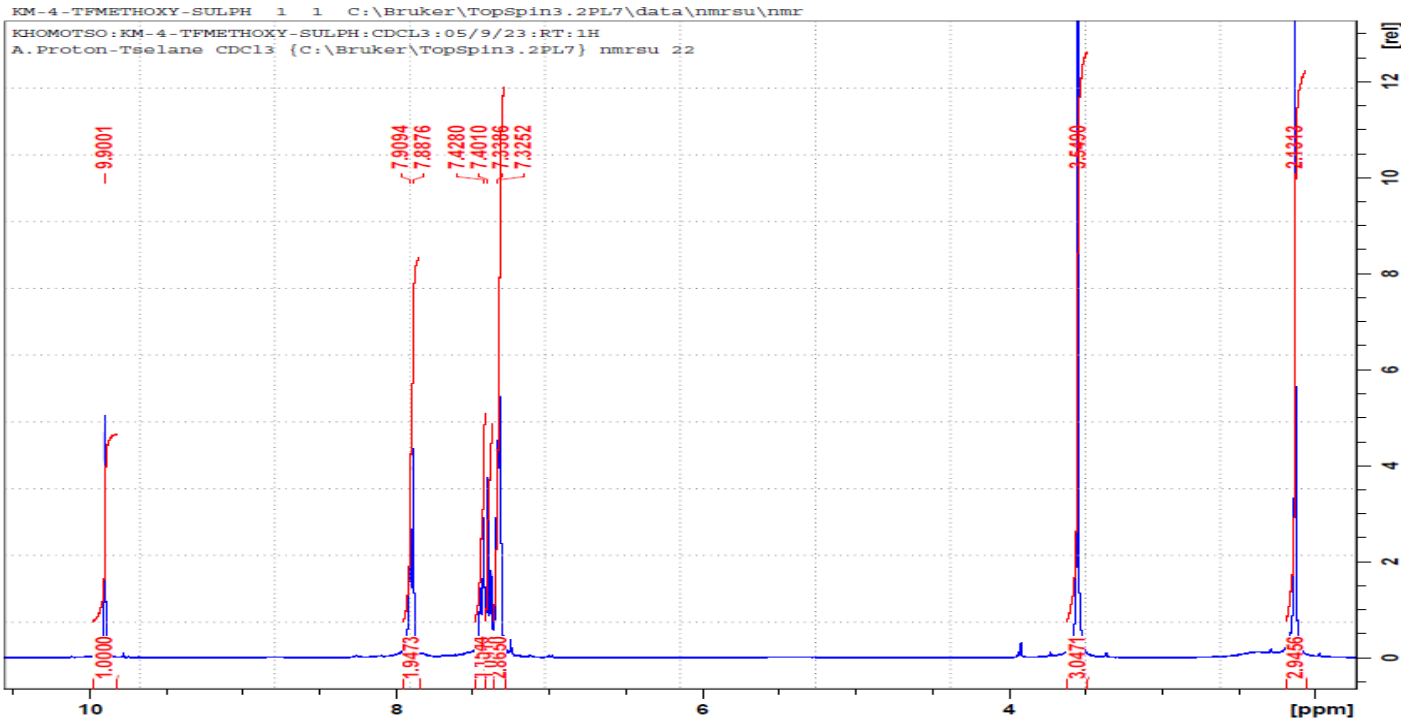

Figure 27: ^{1}H NMR of **76f**

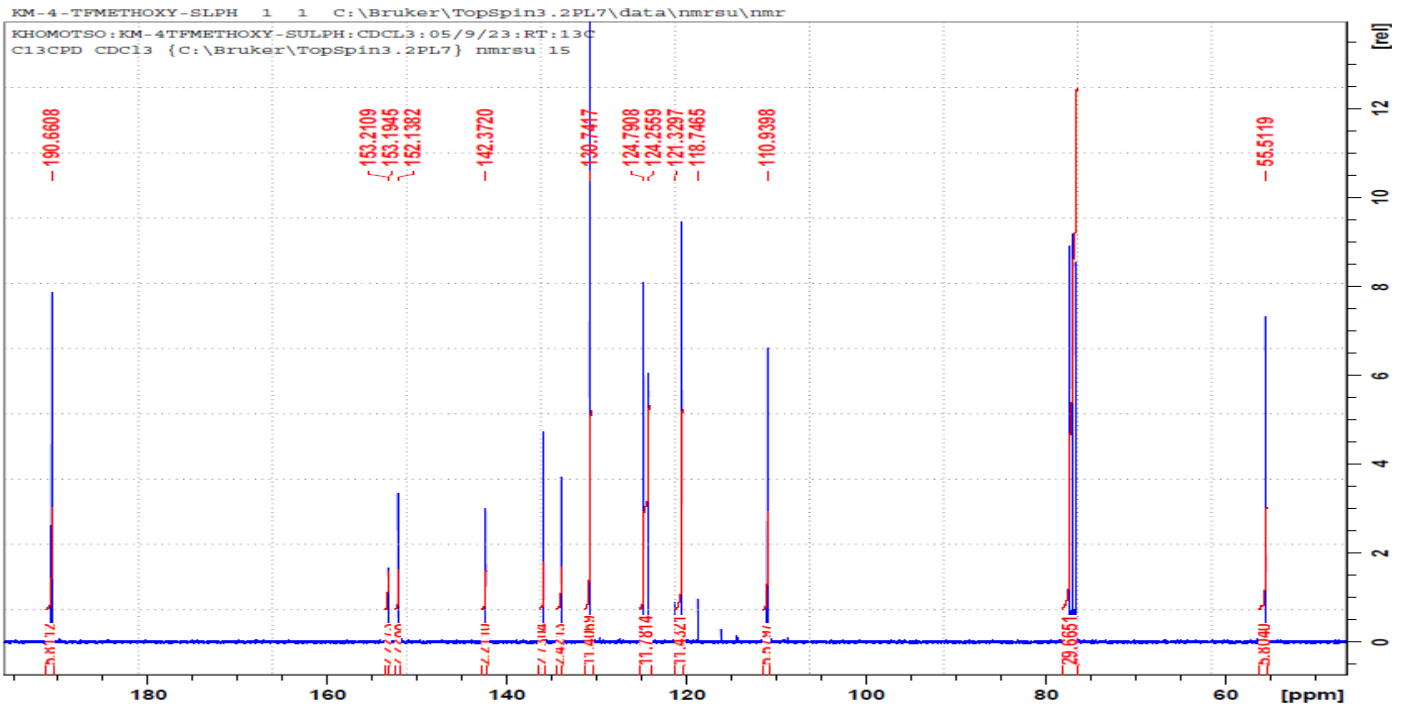

Figure 28: ^{13}C NMR of **76f**

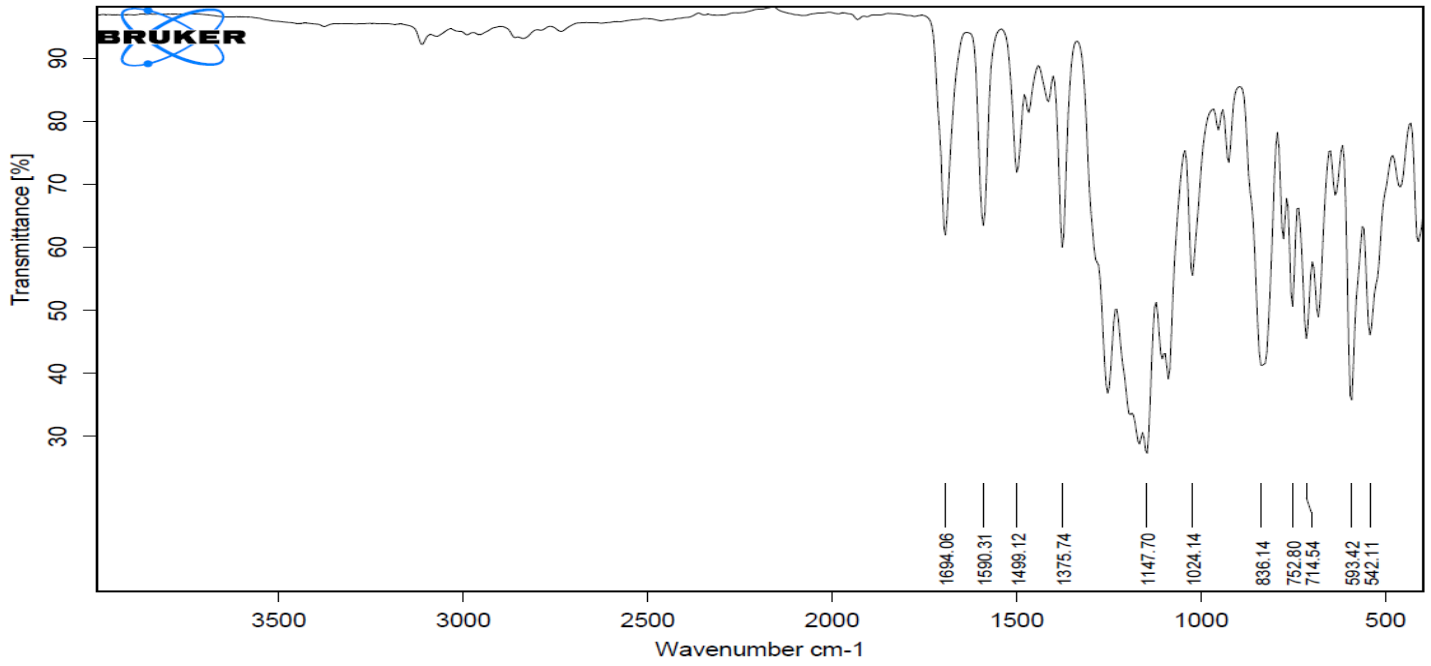

Figure 29: FTIR of **76f**

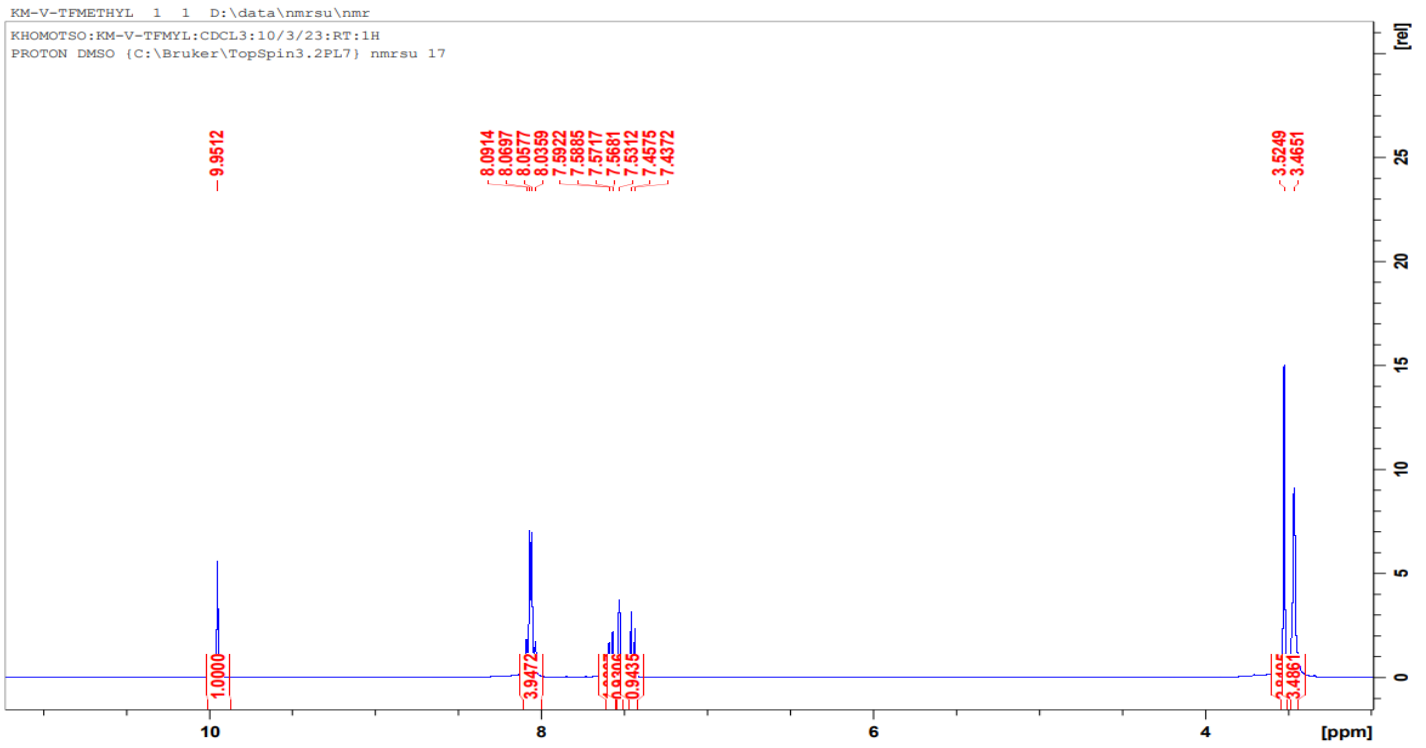

Figure 30: ^{1}H NMR of **76g**

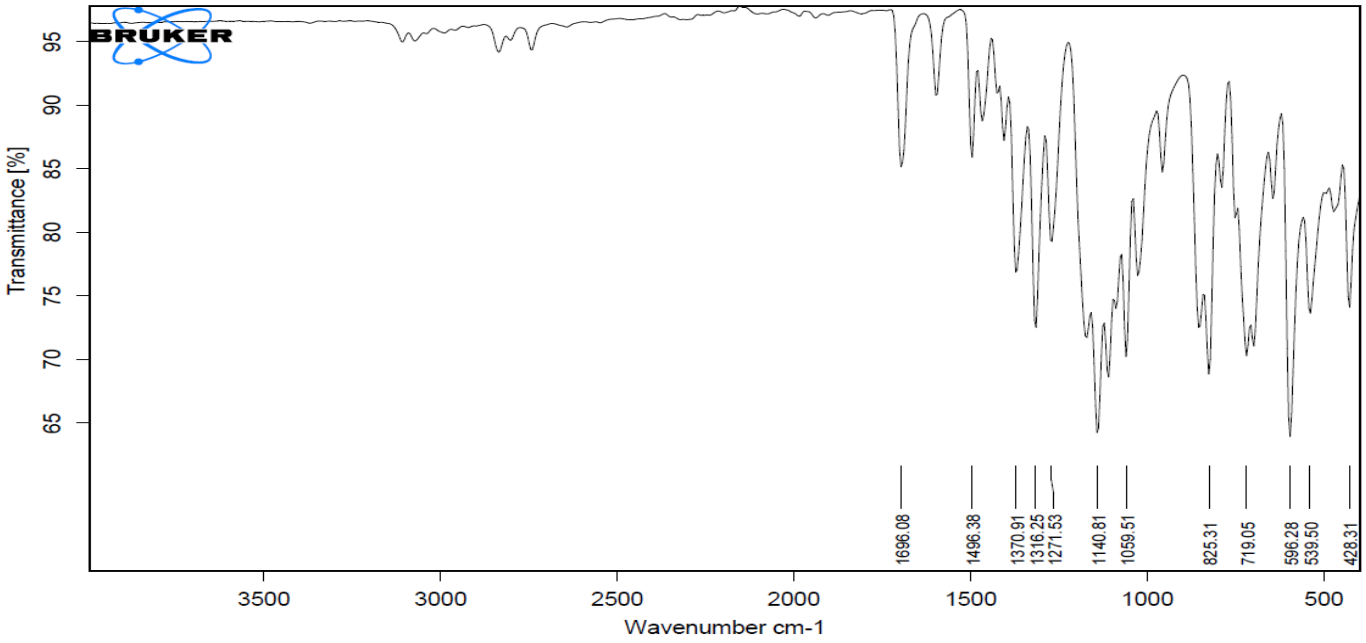

Figure 31: FTIR of **76g**

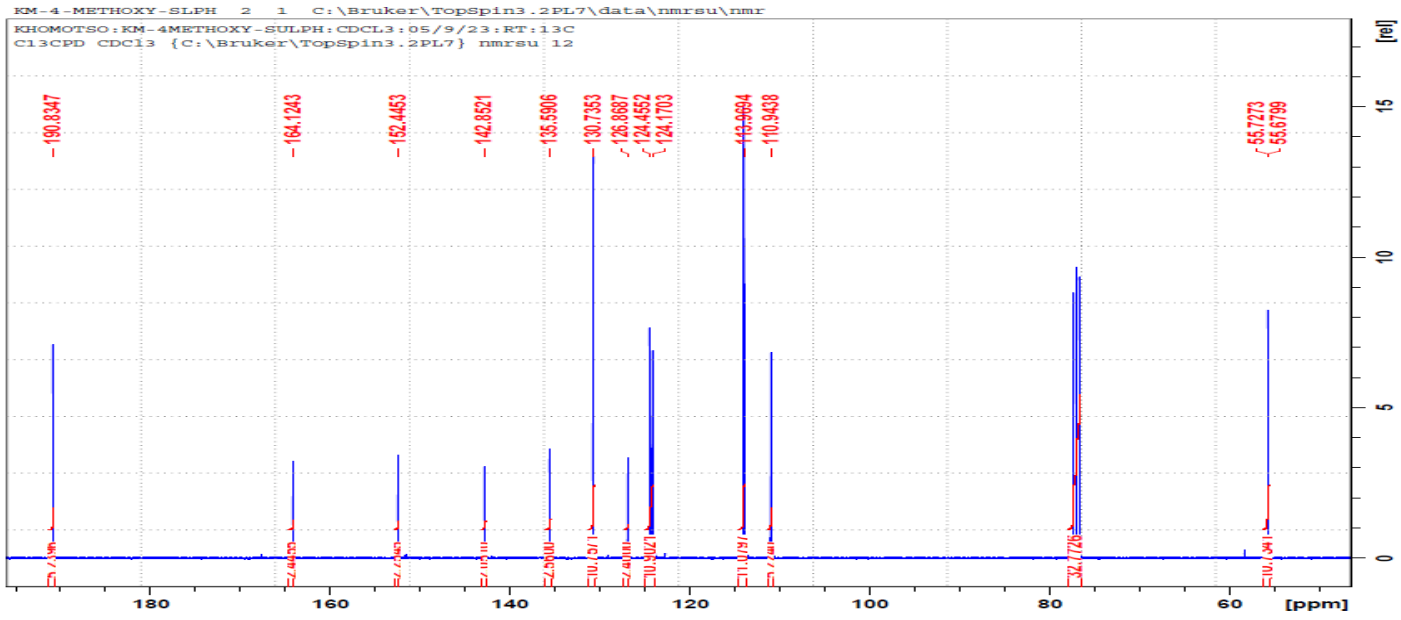

Figure 32: $^{1\,3}$C NMR of **76g**

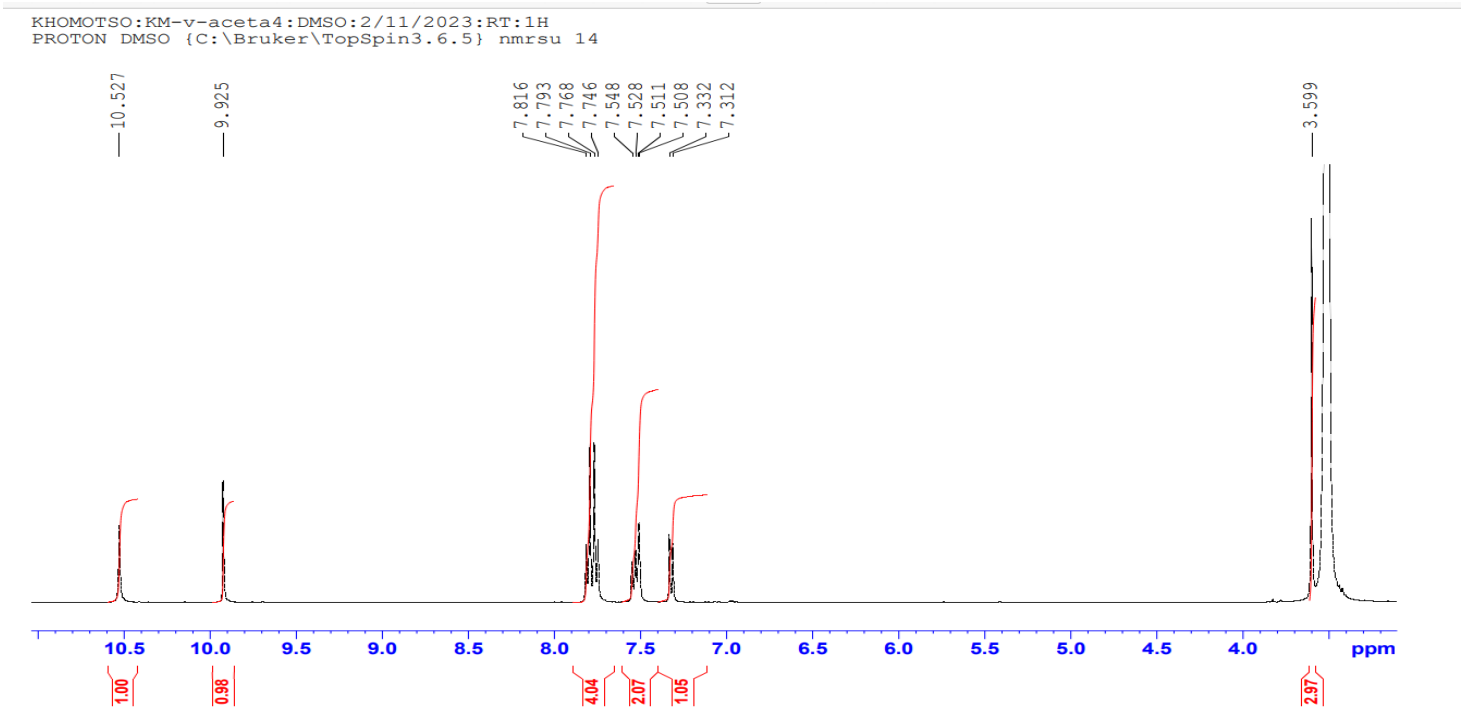

Figure 33: ^{1}H NMR of **76h**

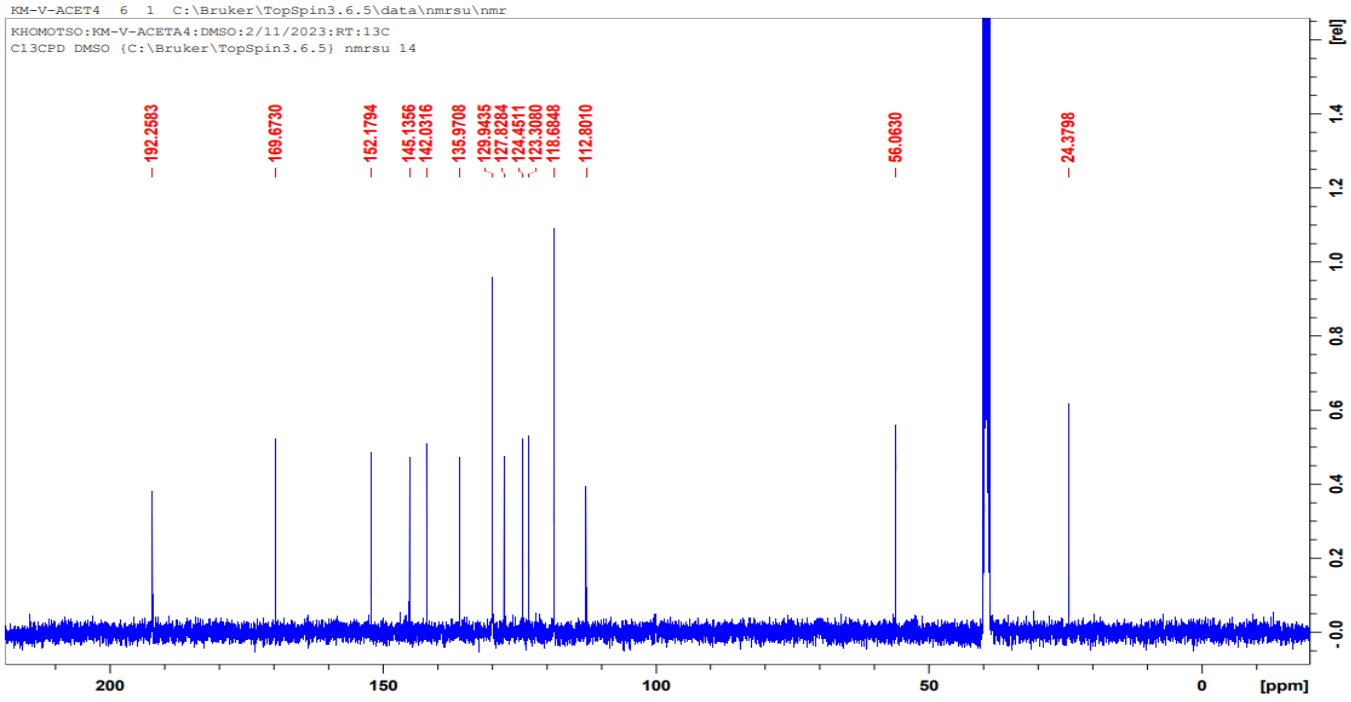

Figure 34: $^{1\,3}$C NMR of **76h**

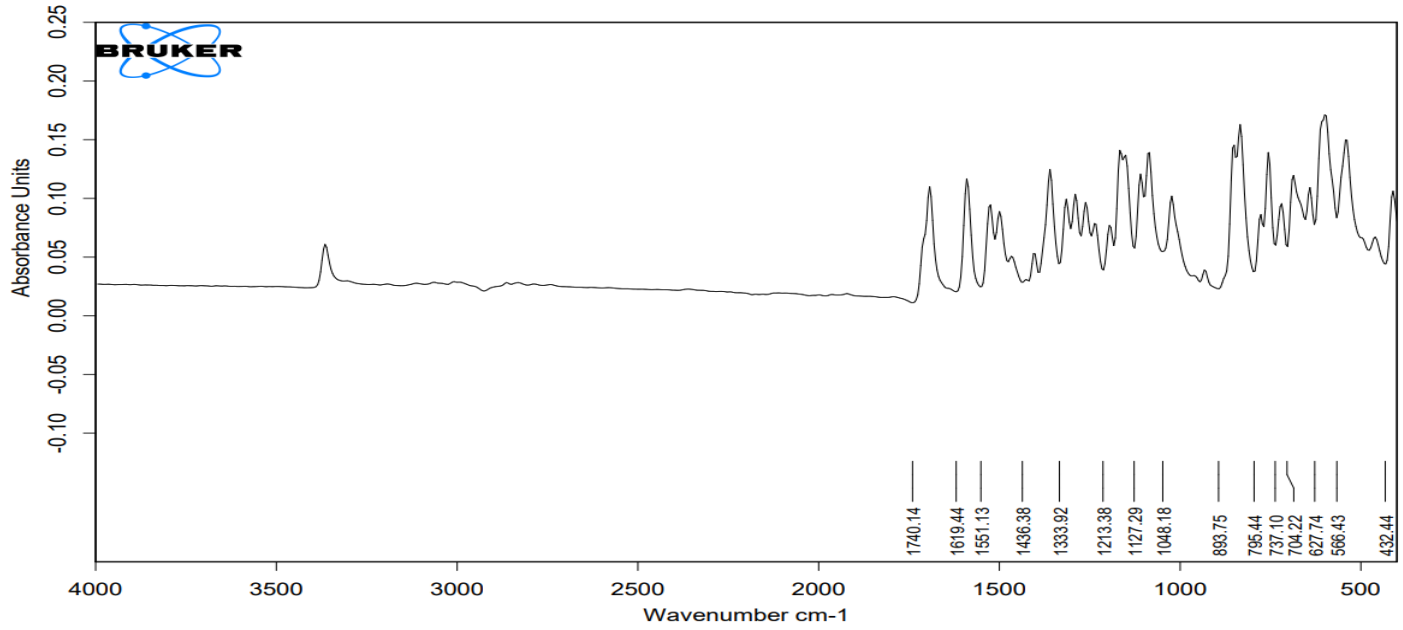

Figure 35: FTIR of **76h**

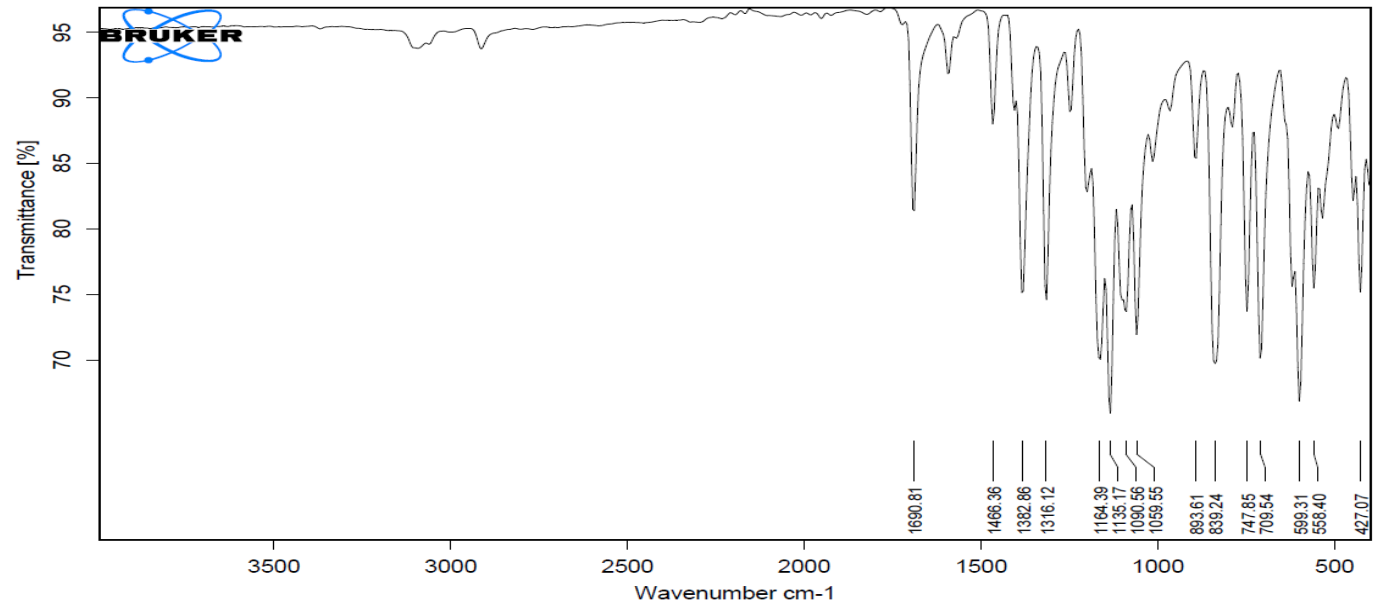

Figure 35: FTIR of **76h**

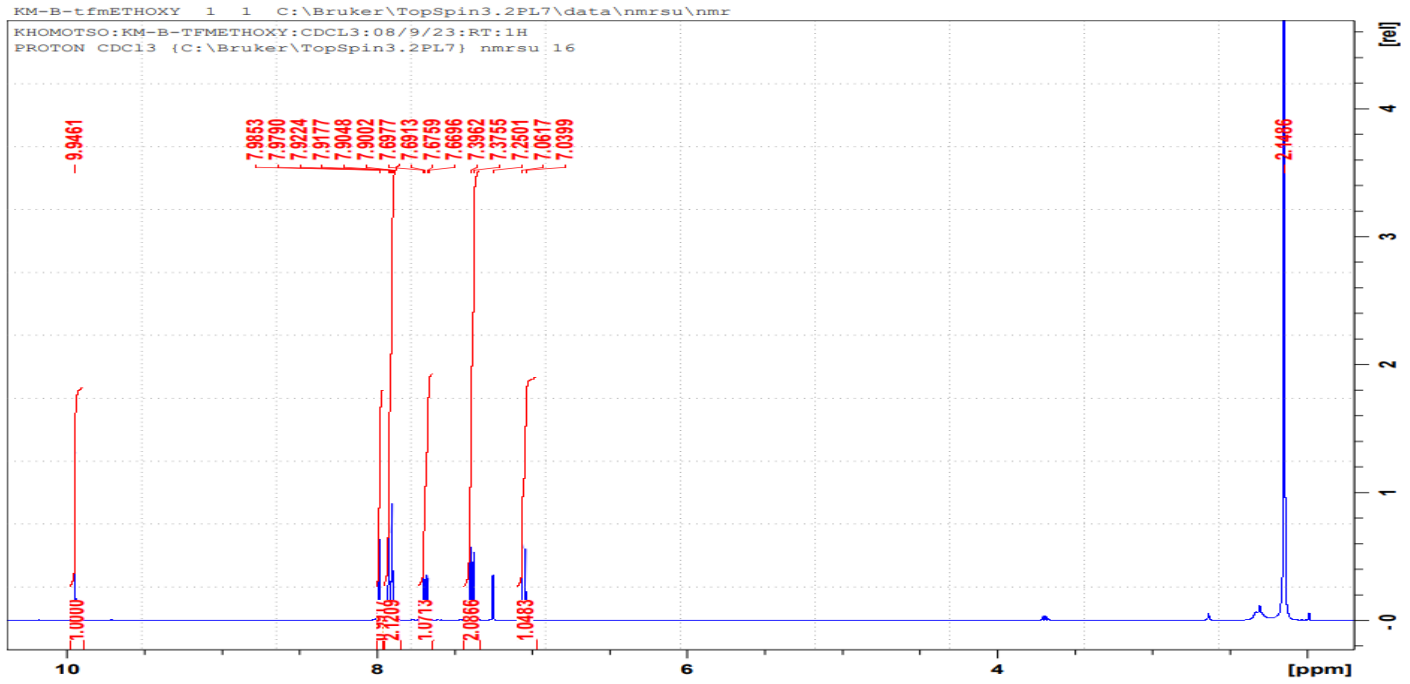

Figure 36: ^{1}H NMR of **76i**

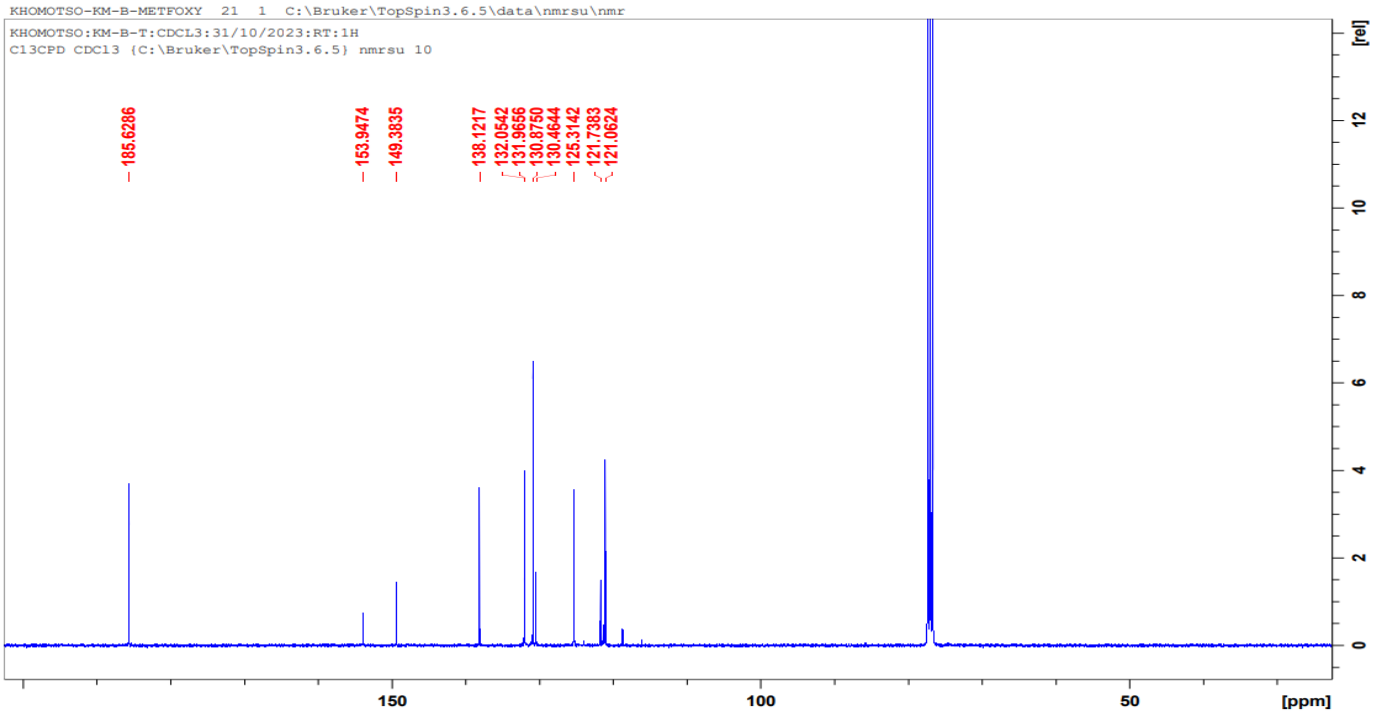

Figure 37: $^{1\,3}$C NMR of **76i**

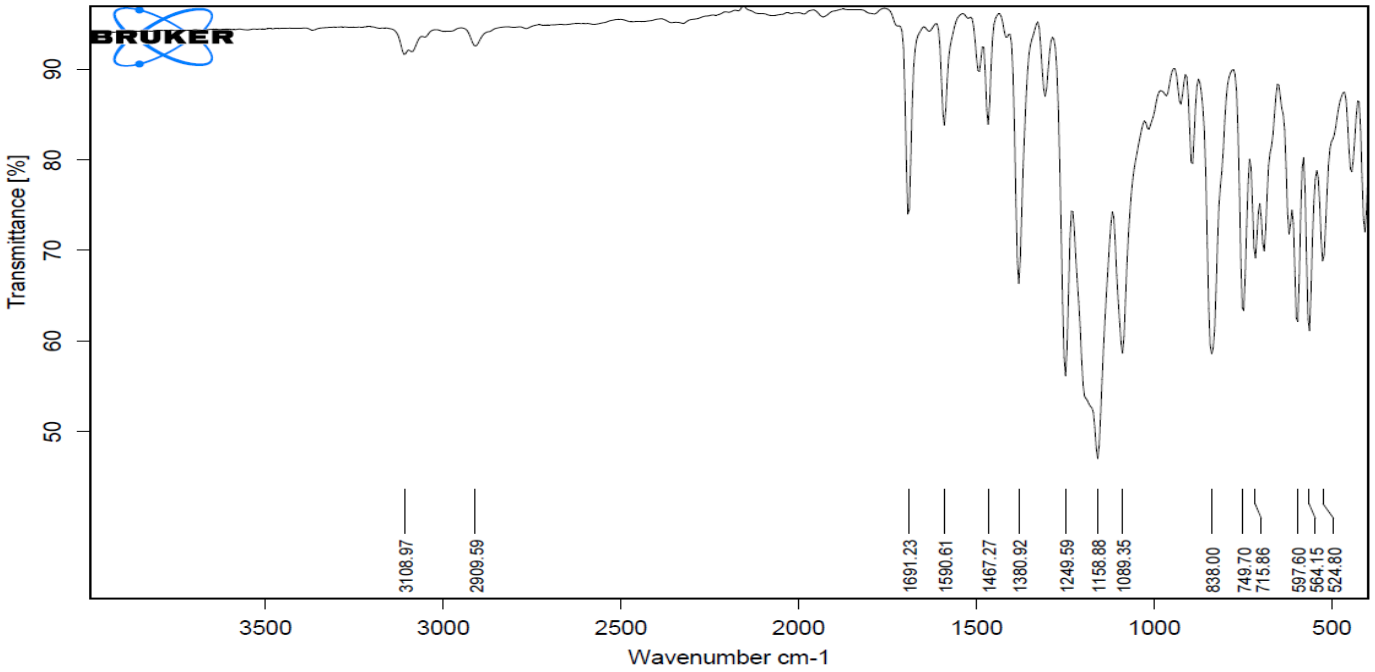

Figure 38: FTIR of **76i**

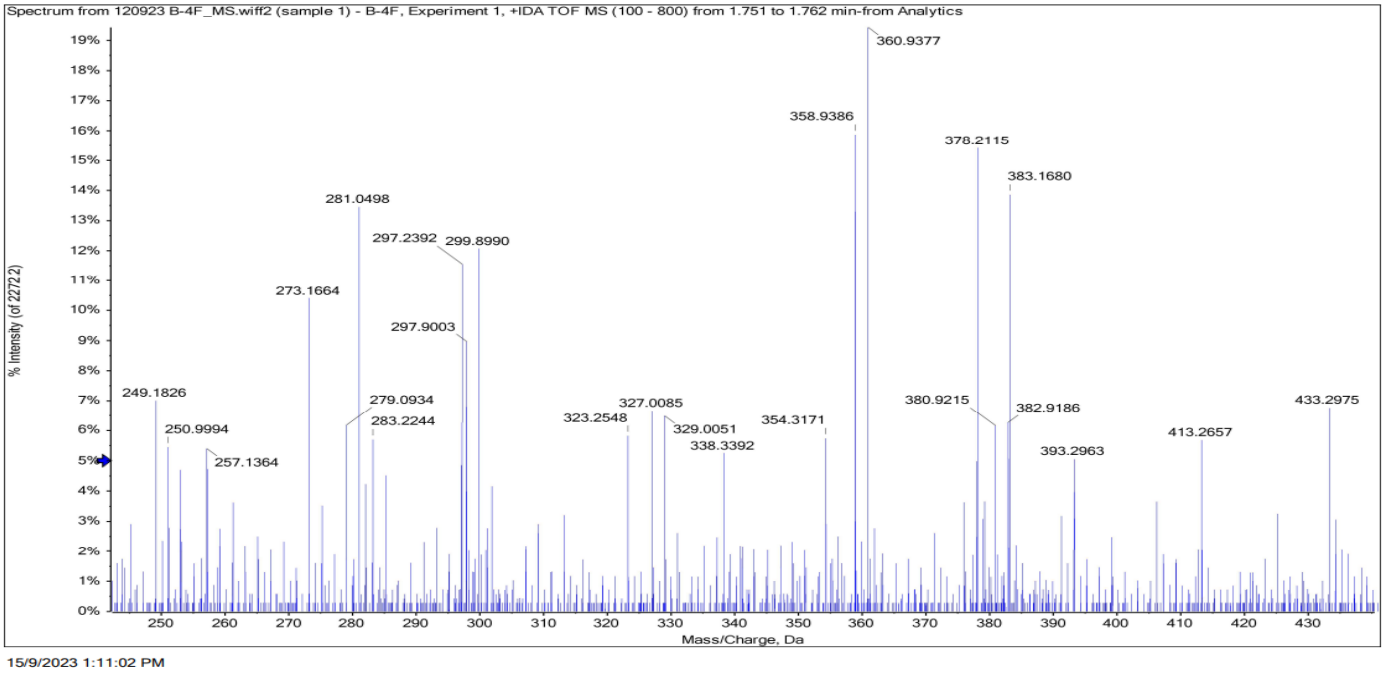

Figure 39: MS of **76j**

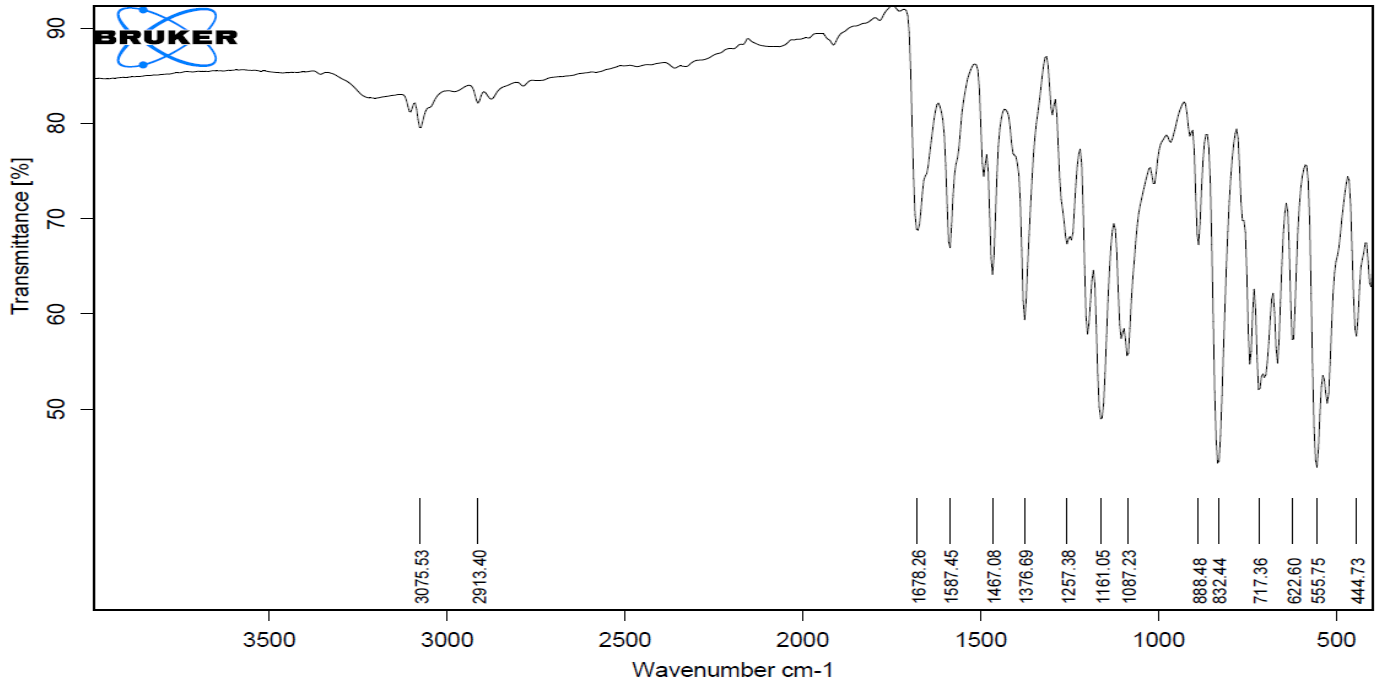

Figure 40: FTIR of **76j**

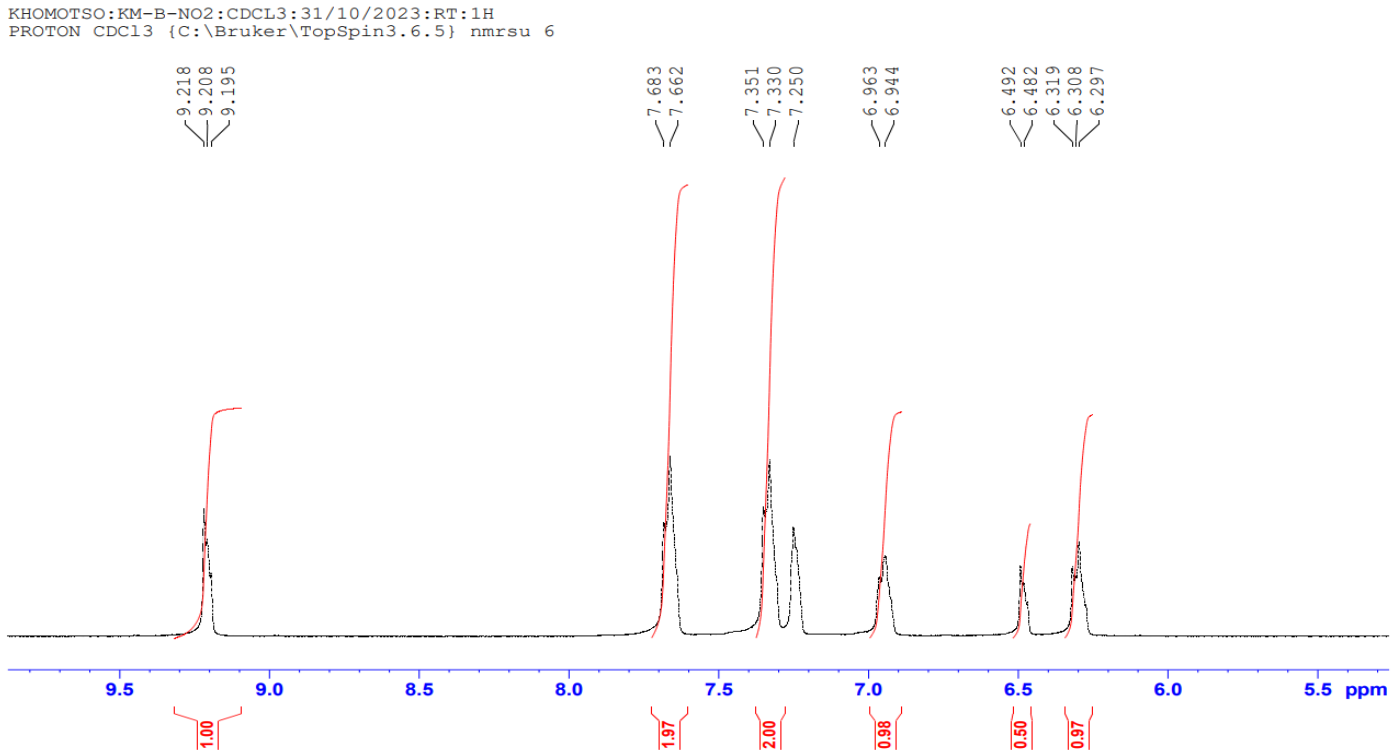

Figure 41: ^{1}H NMR of **76k**

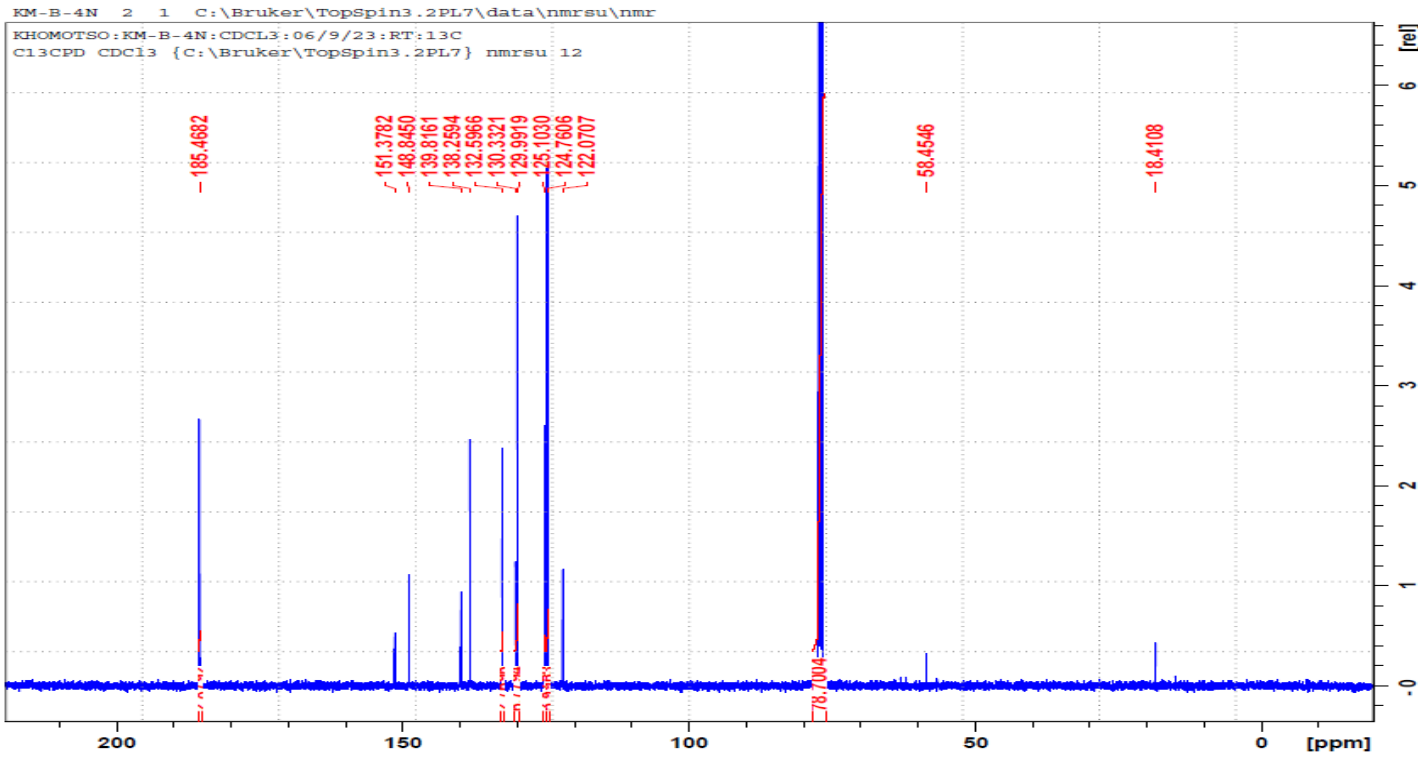

Figure 42: $^{1}{}^{3}C$ NMR of **89k**

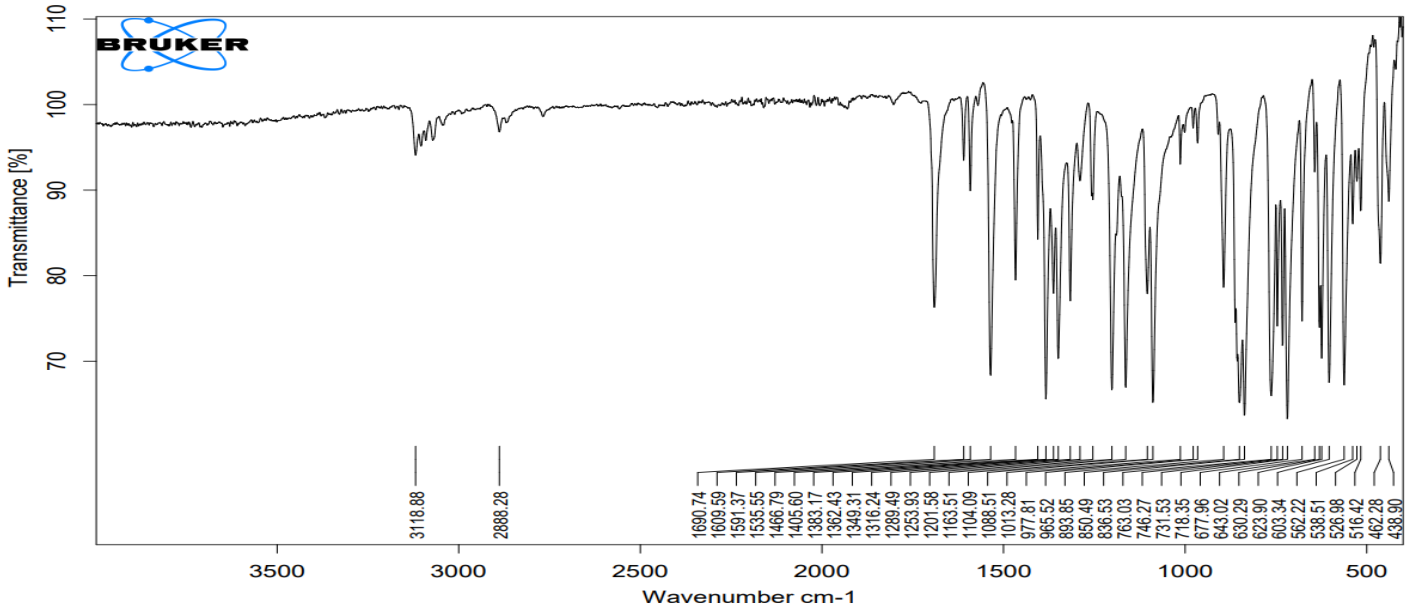

Figure 43: FTIR of **76k**

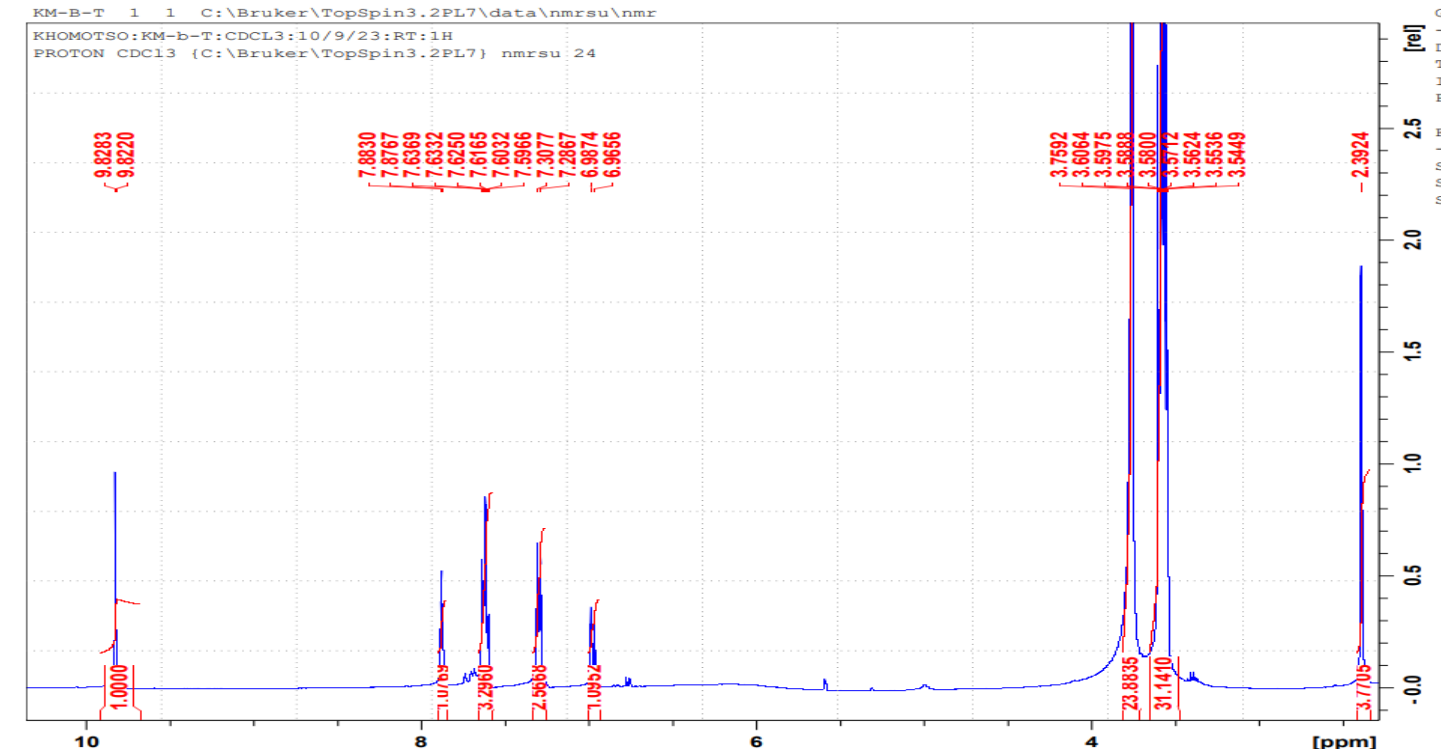

Figure 44: ^{1}H NMR of **76l**

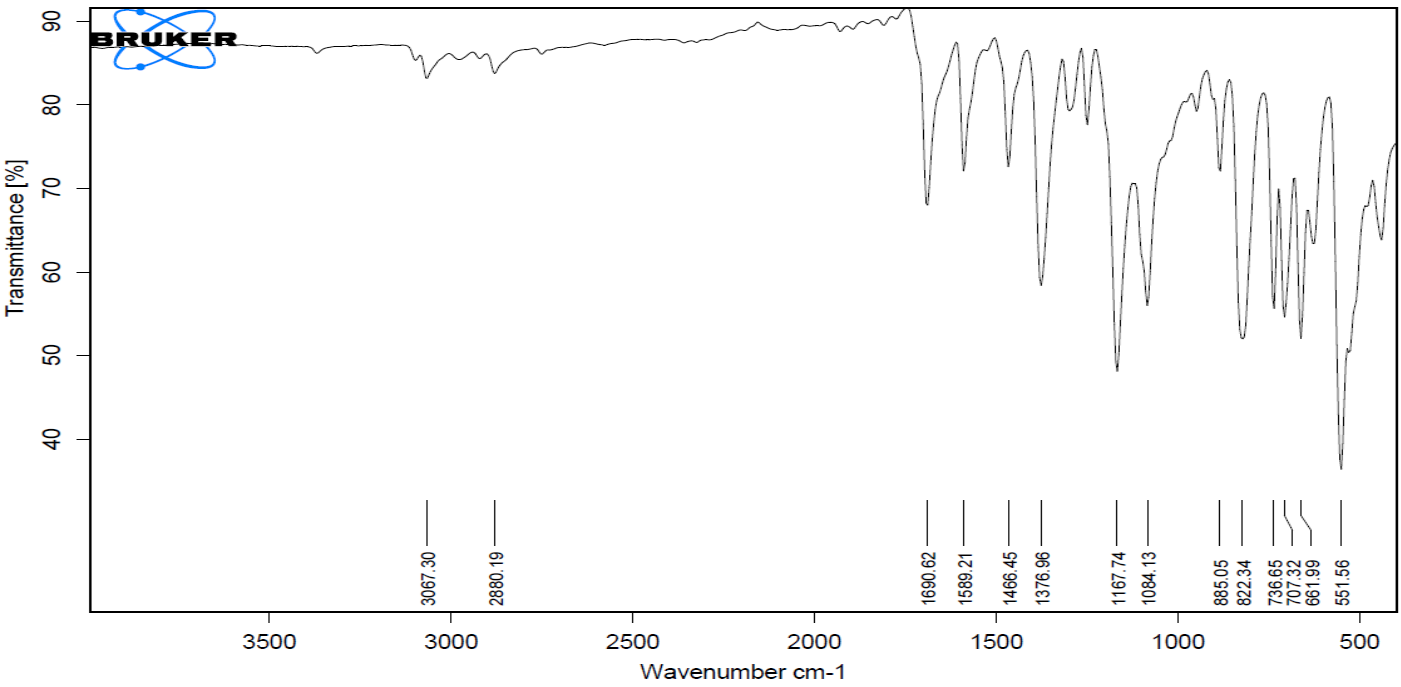

Figure 45: FTIR of **76l**

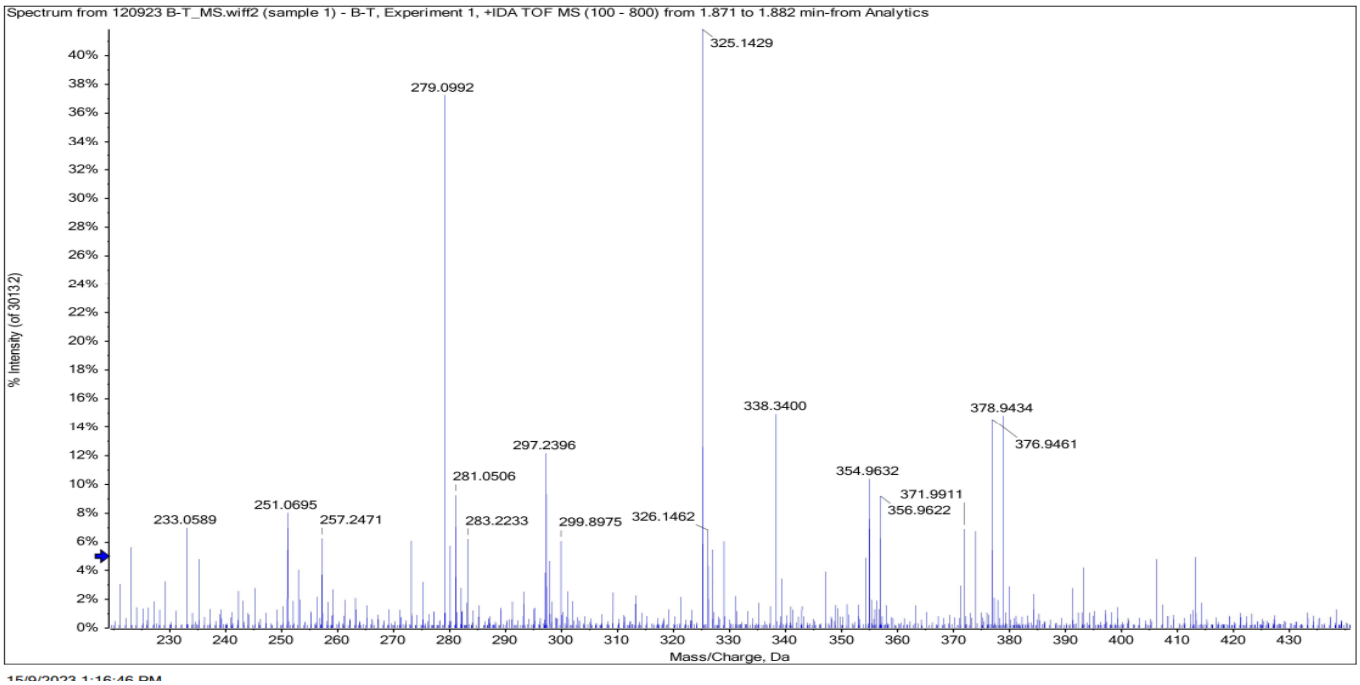

Figure 46: MS of **76l**

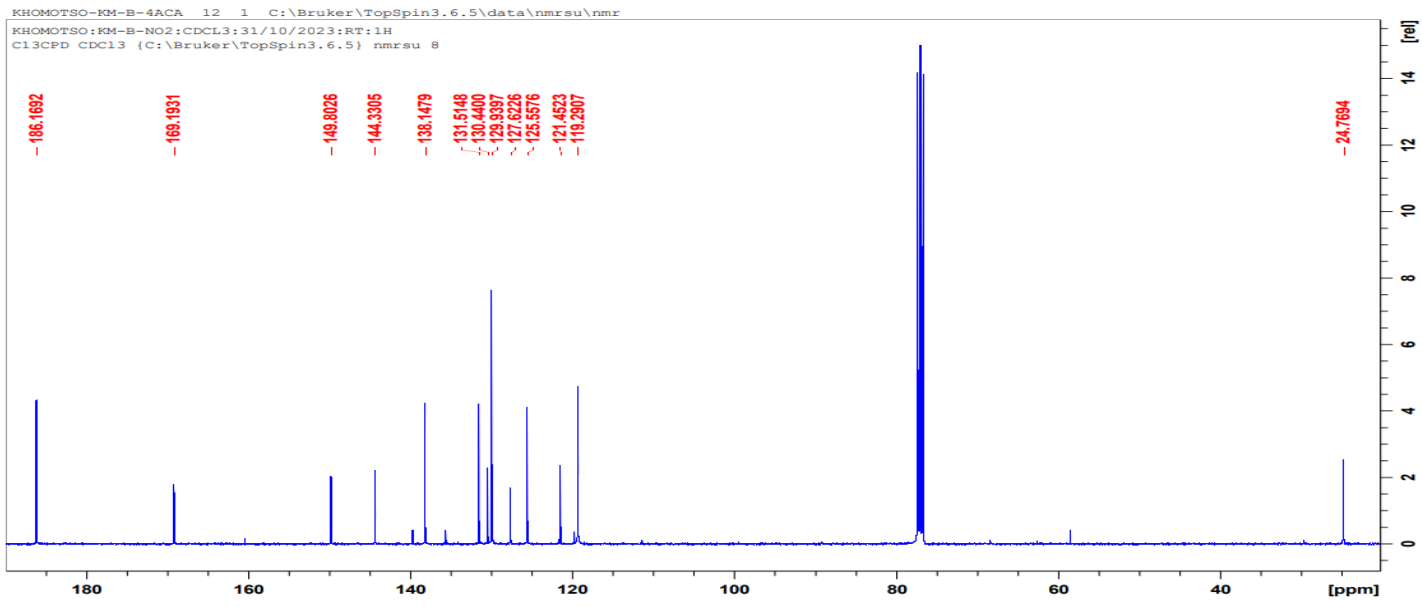

Figure 47: ^{13}C NMR of **76m**

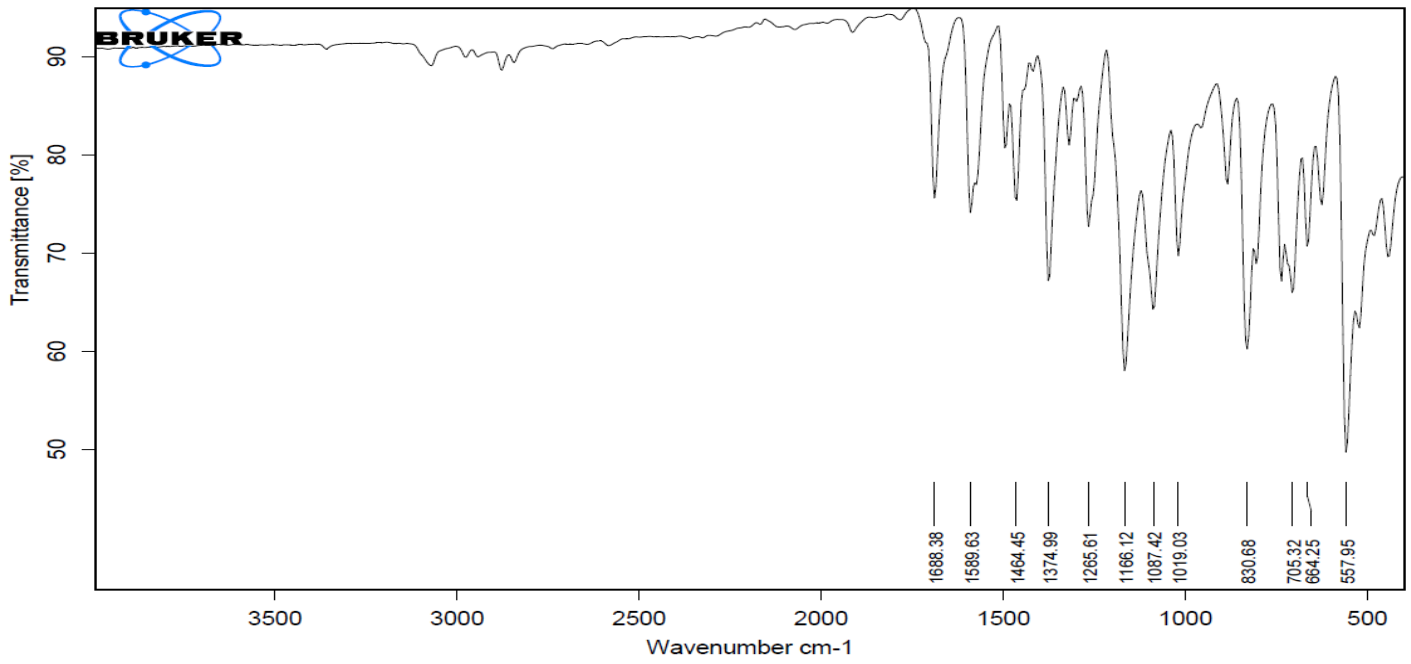

Figure 48: FTIR of **76m**

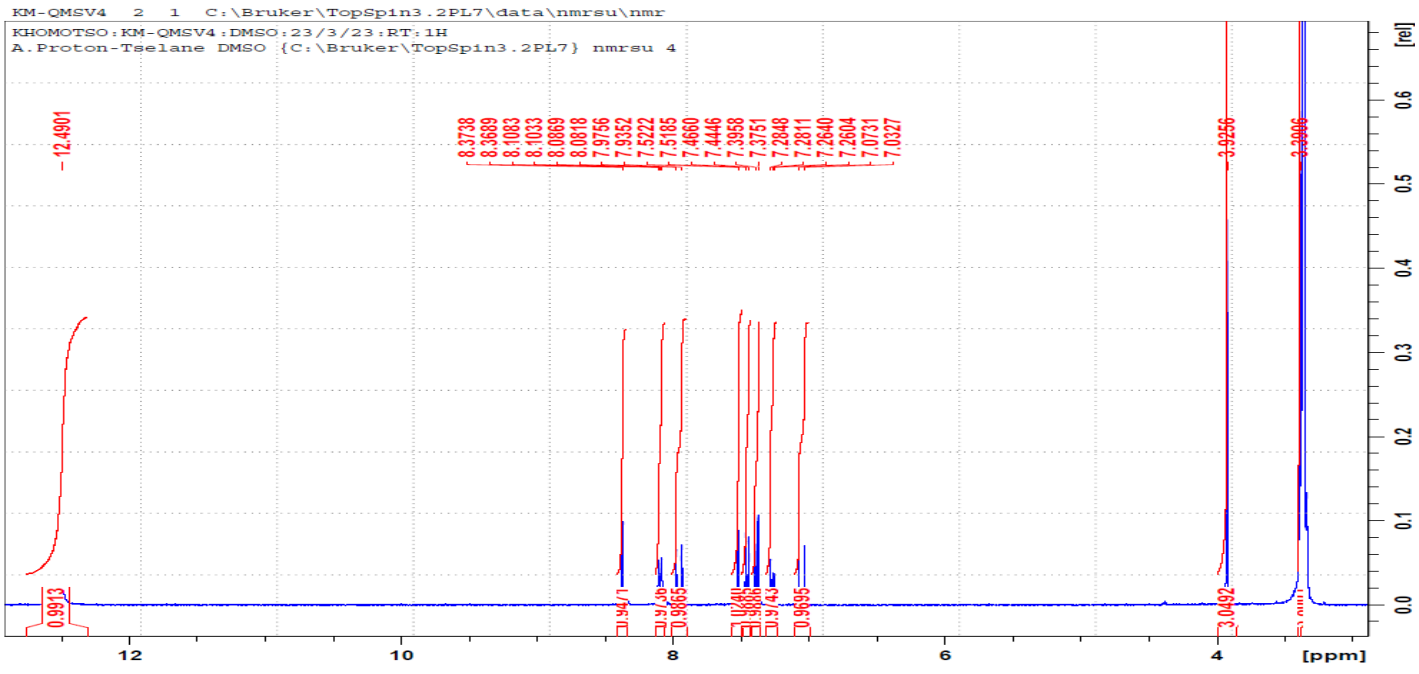

Figure 49: ^{1}H NMR of **77a**

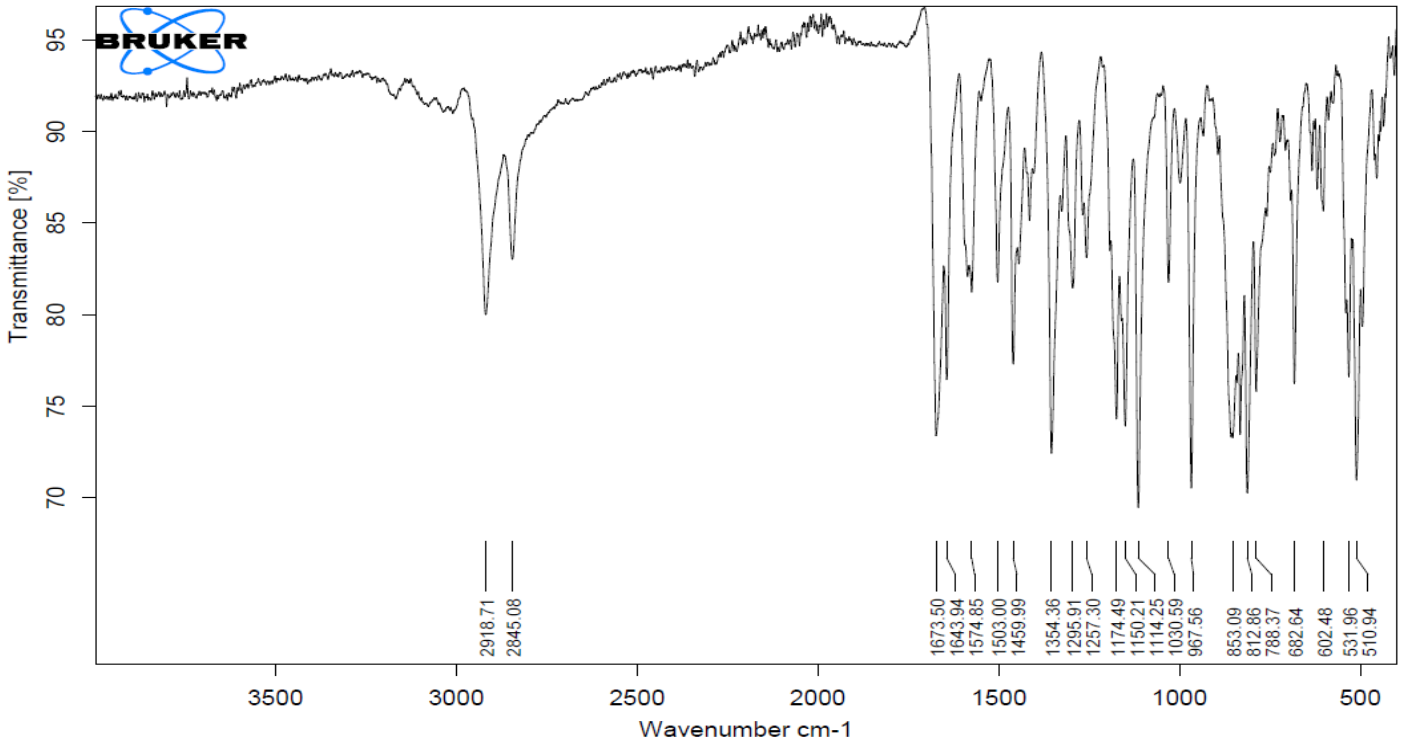

Figure 50: FTIR of **77a**

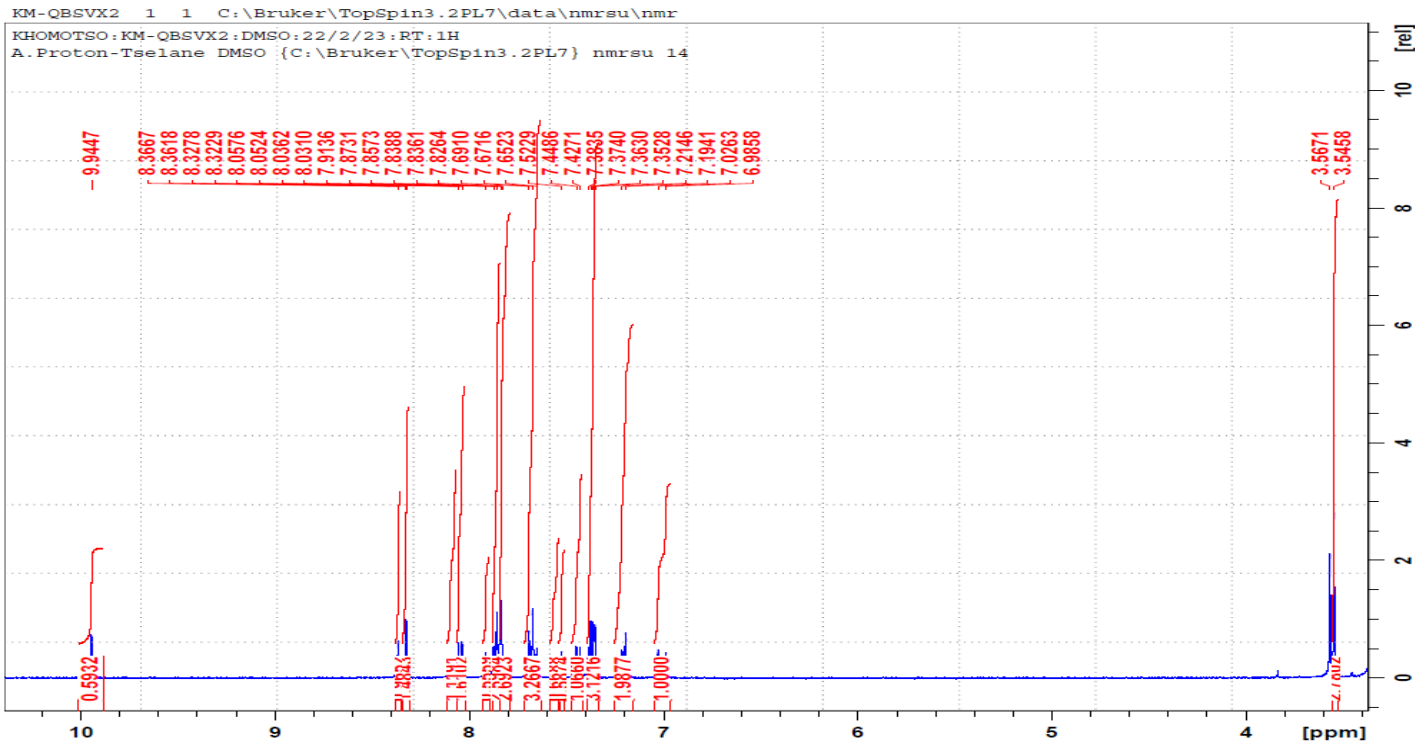

Figure 51: ^{1}H NMR of **77b**

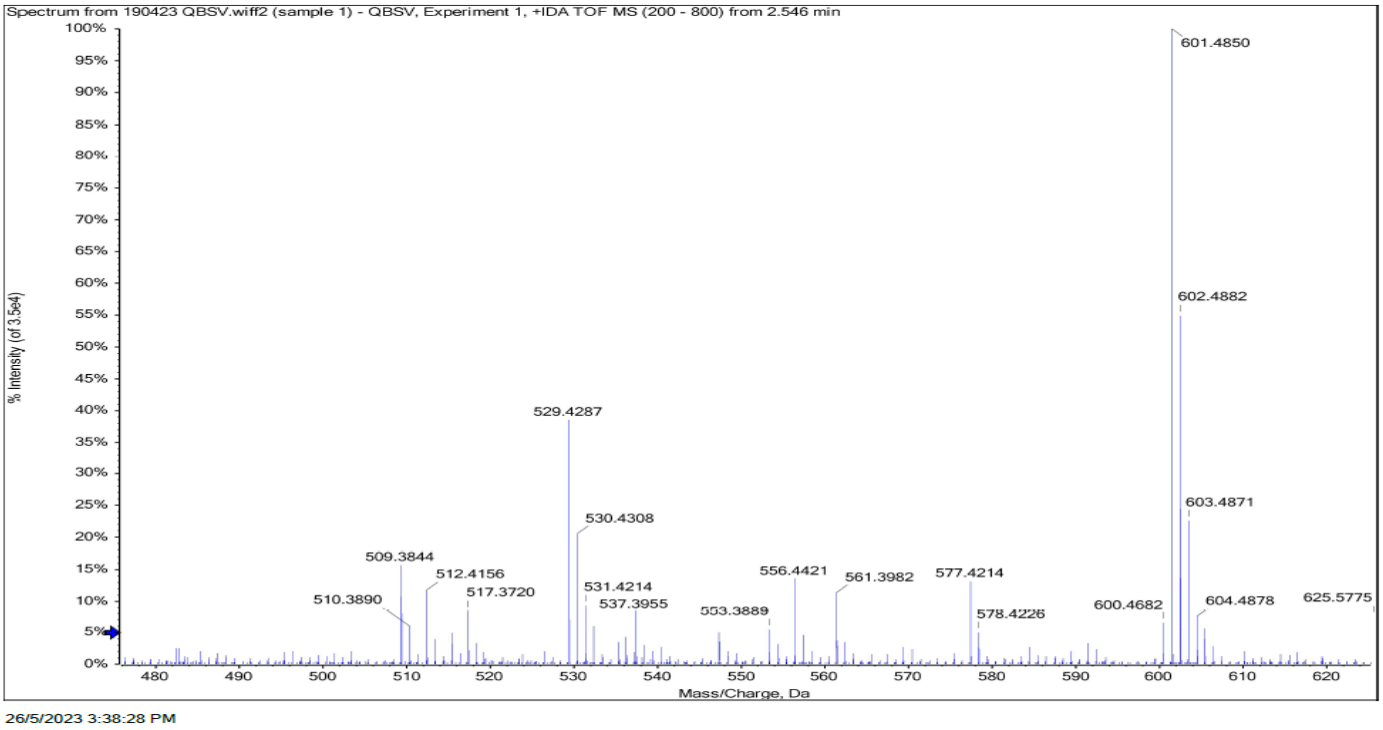

Figure 52: MS of **77b**

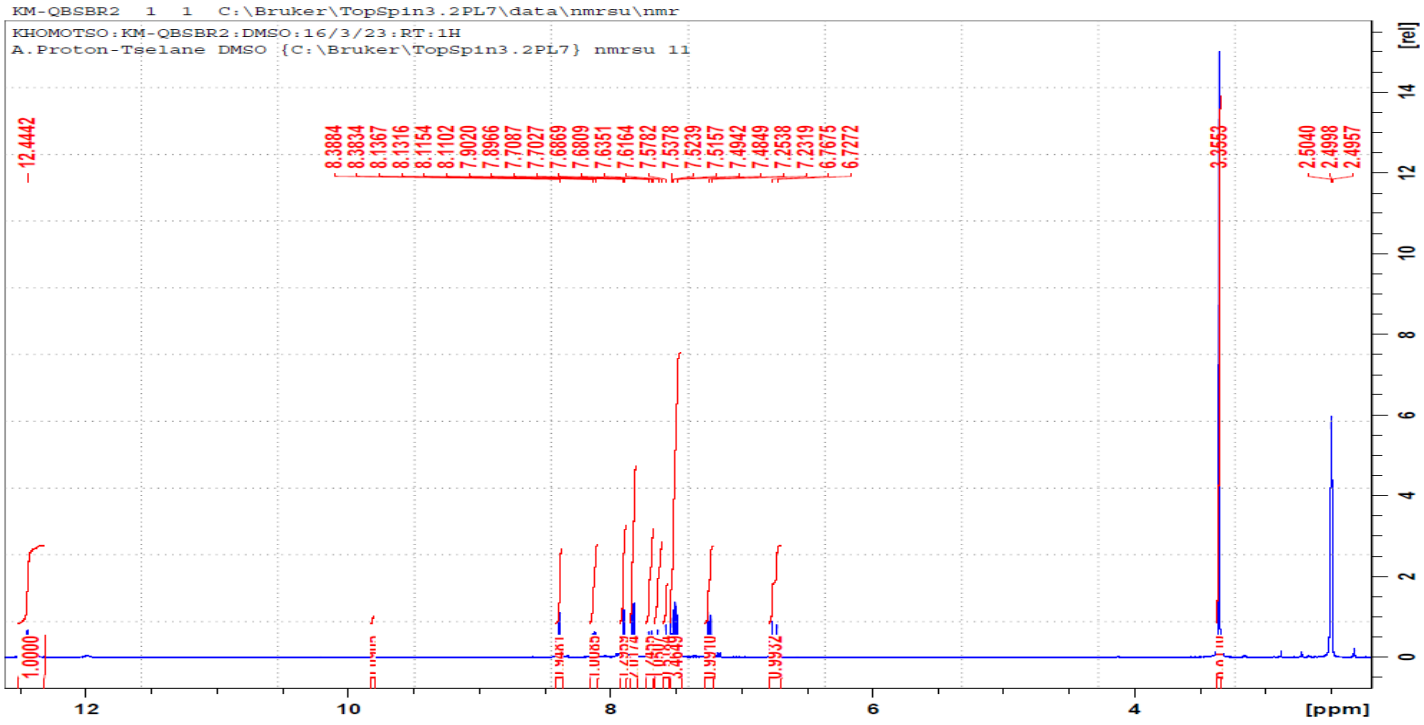

Figure 53: ^{1}H NMR of **77c**

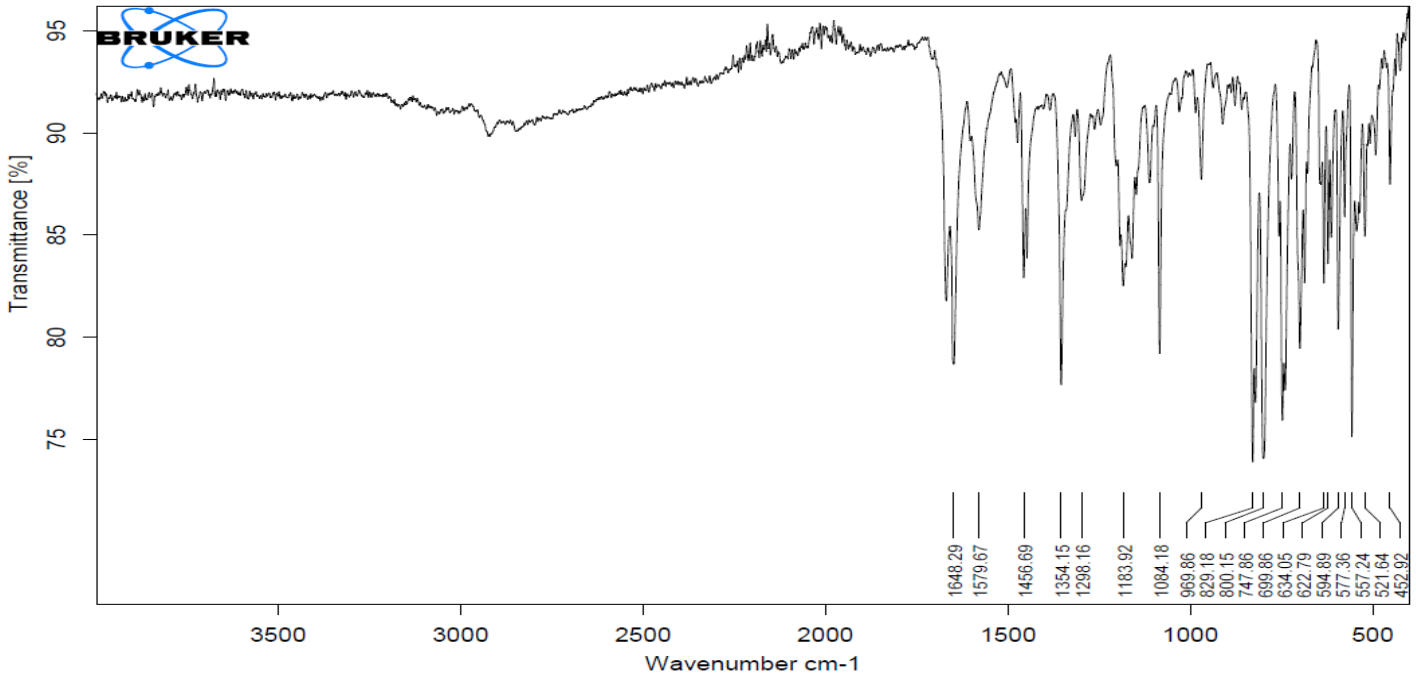

Figure 54: FTIR of **77c**

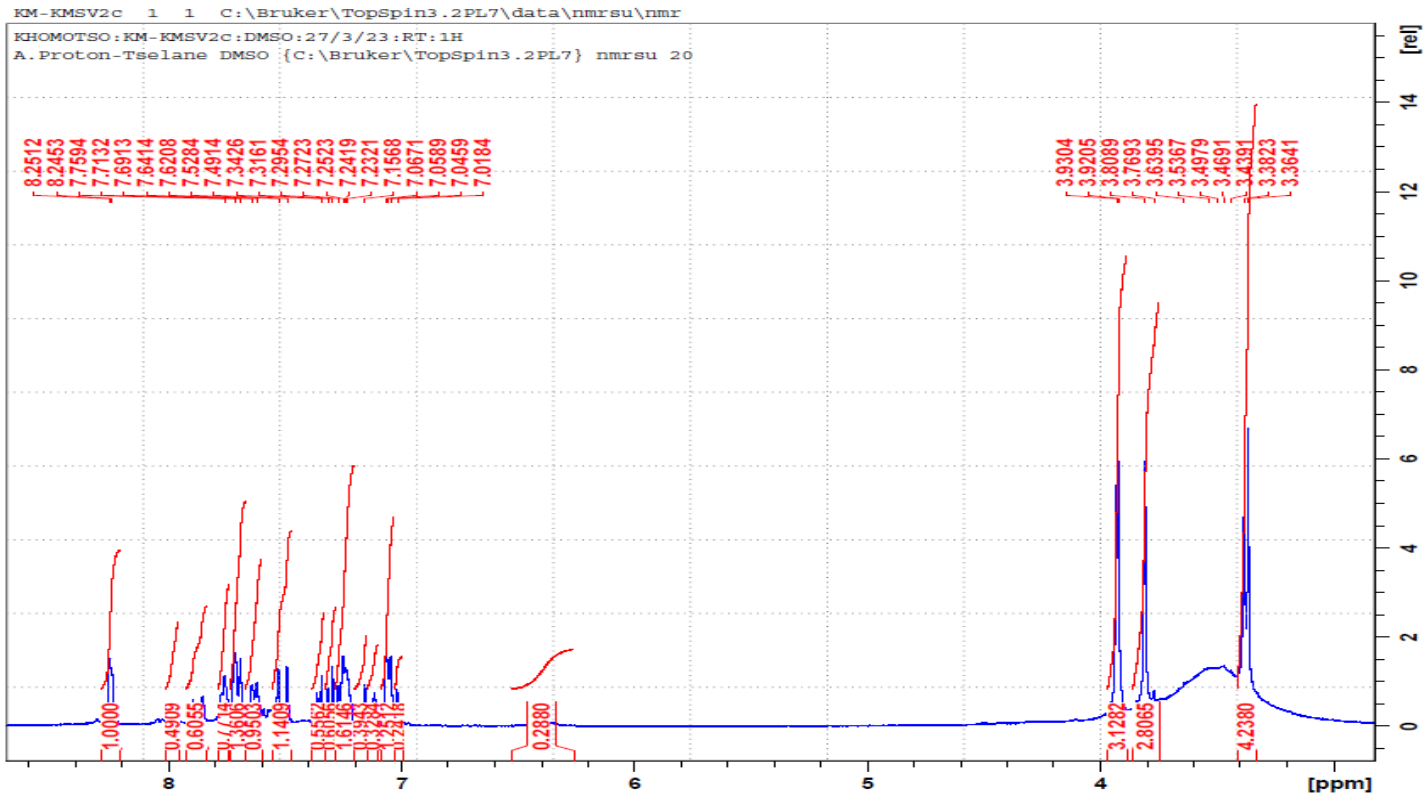

Figure 55: ^{1}H NMR of **77c**

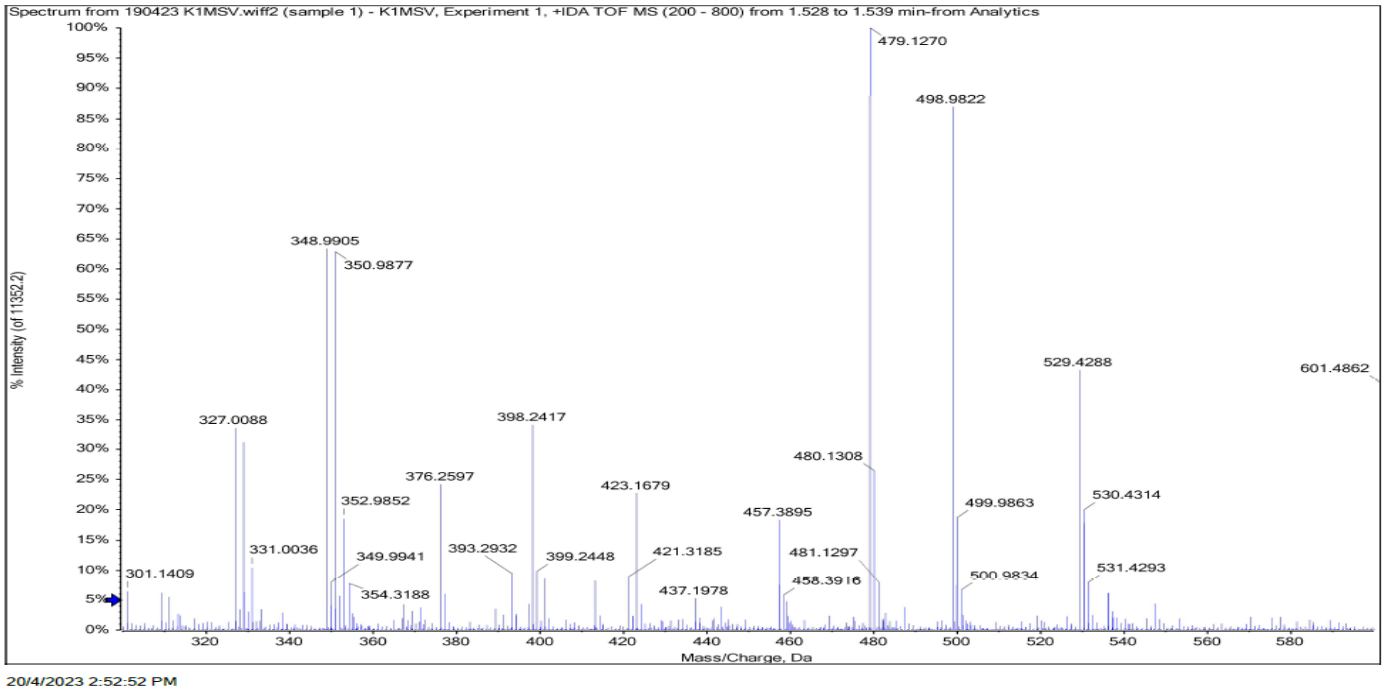

Figure 56: MS of **77c**

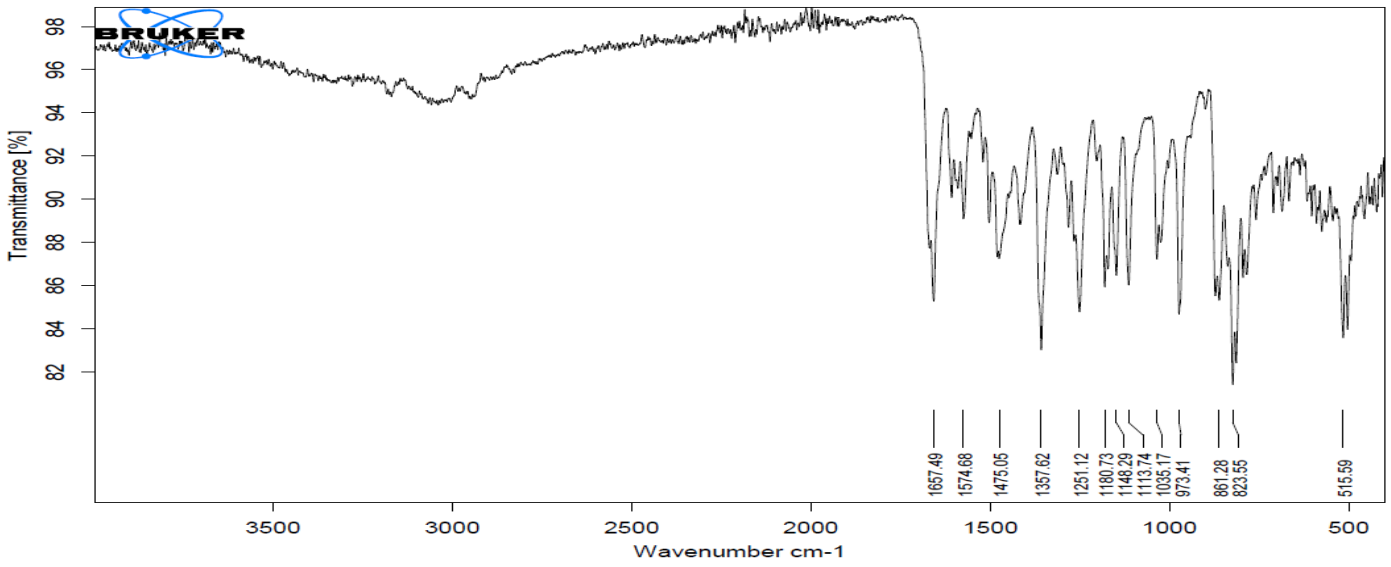

Figure 57: FTIR of **77c**

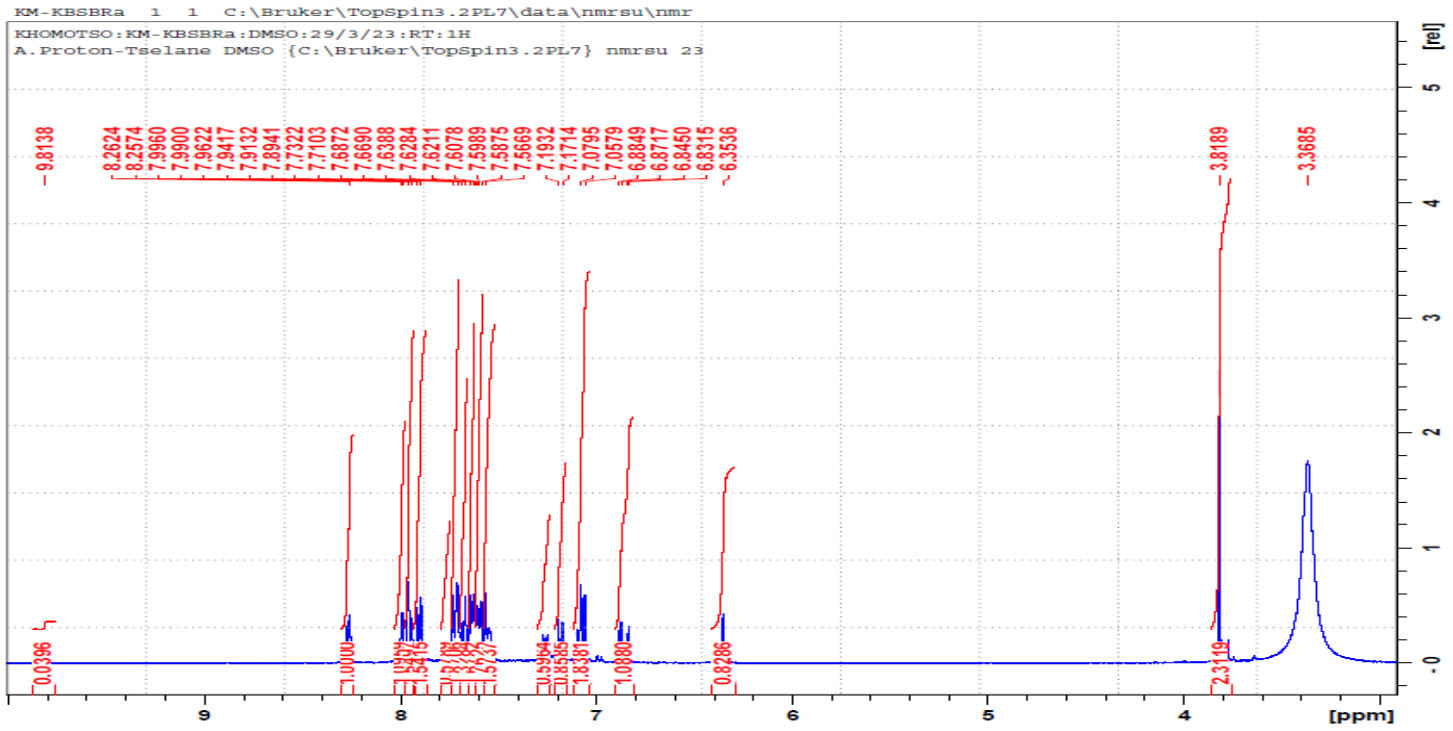

Figure 58: ^{1}H NMR of **77d**

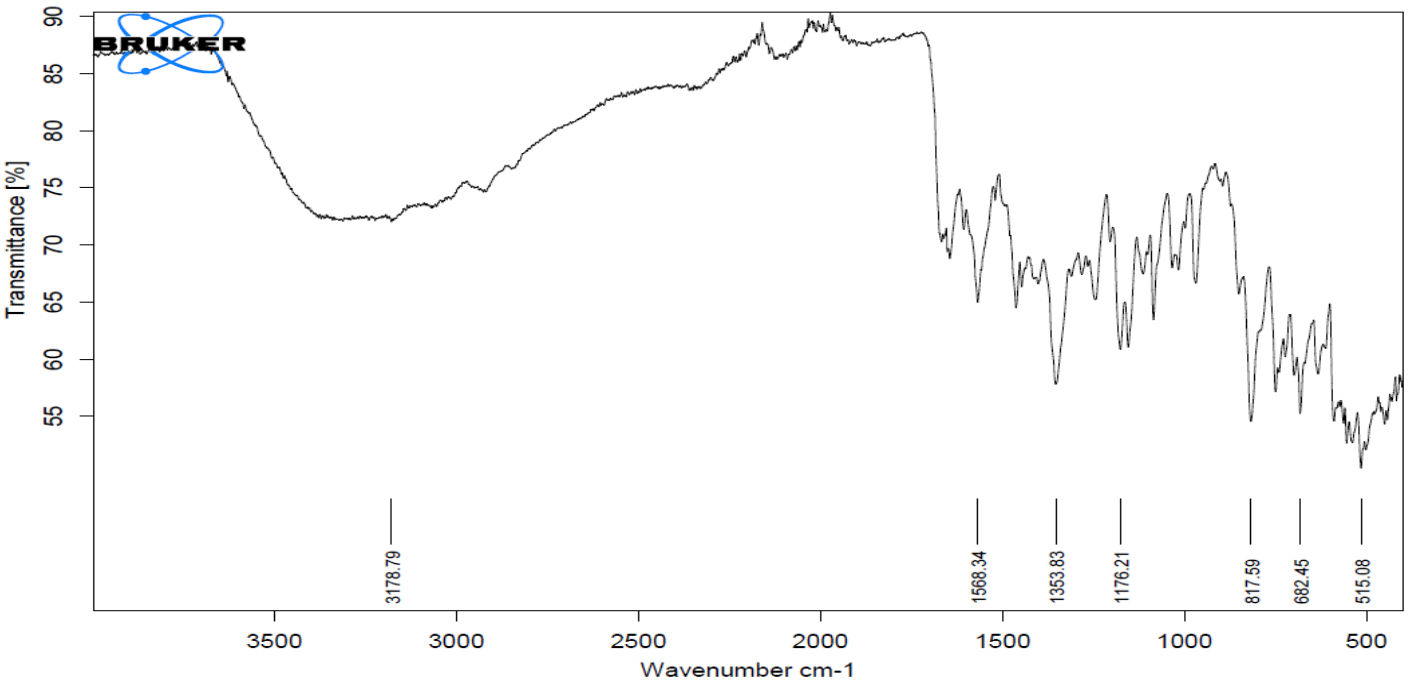

Figure 59: FTIR of **77d**

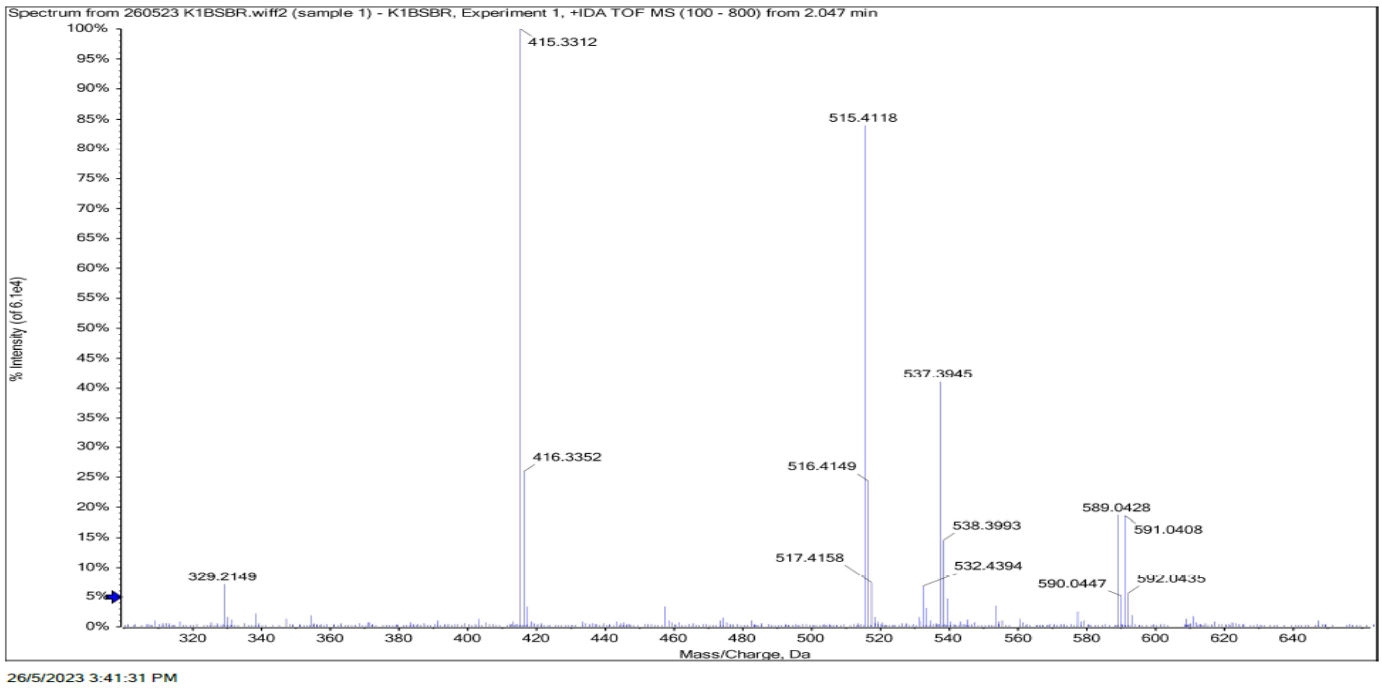

Figure 60: MS of **77d**

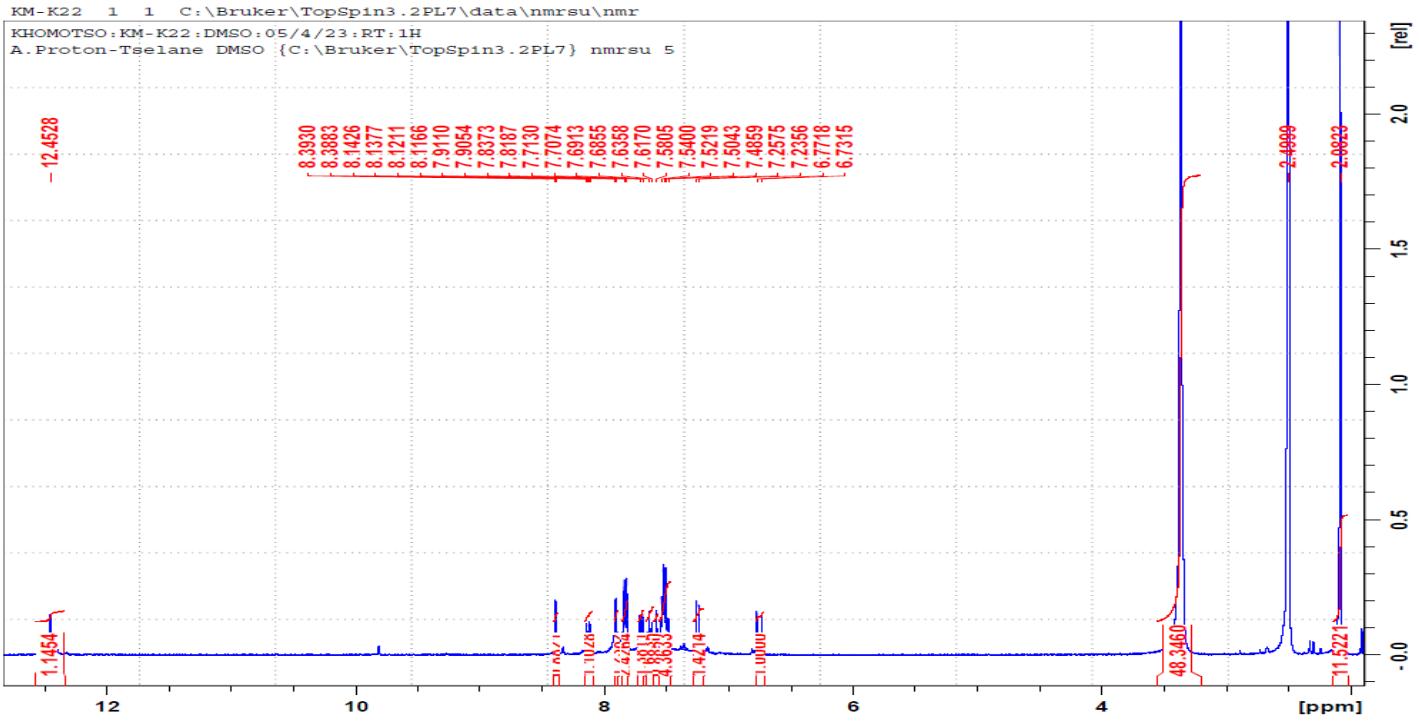

Figure 61: ^{1}H NMR of **77e**

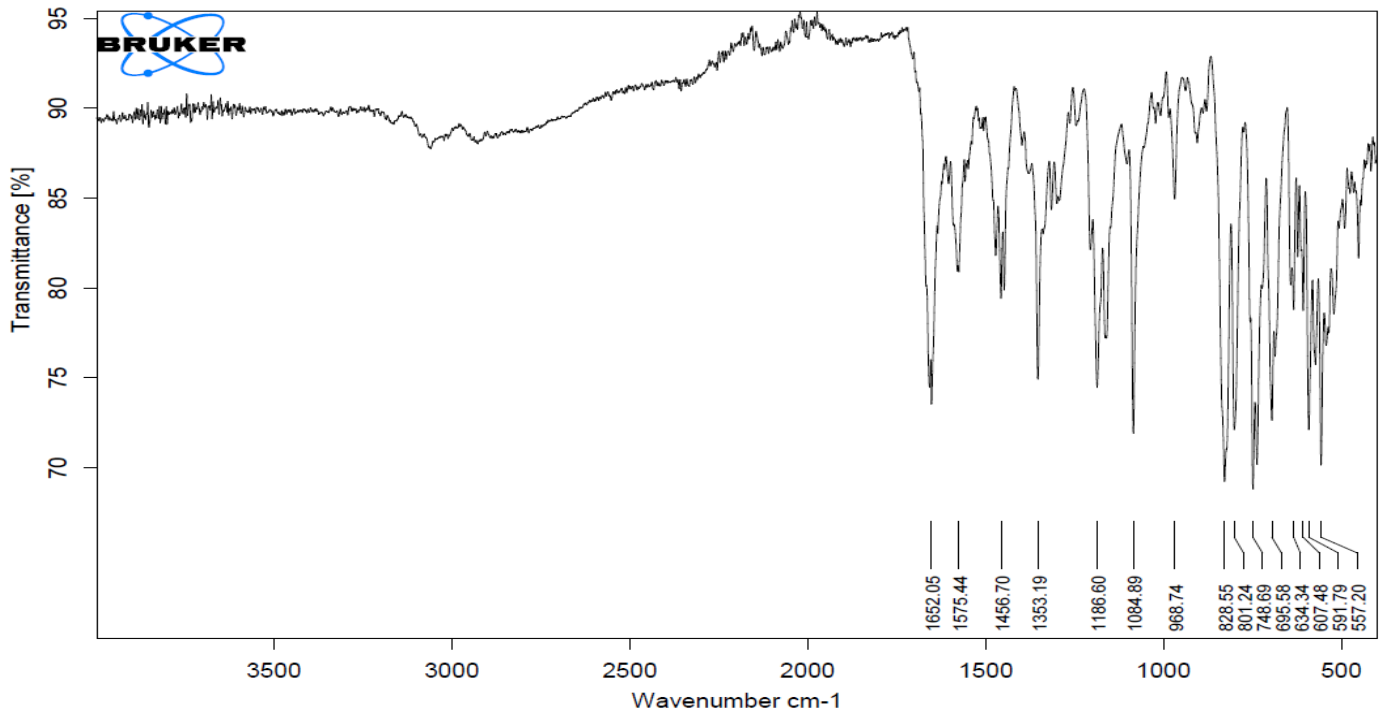

Figure 62: FTIR of **77e**

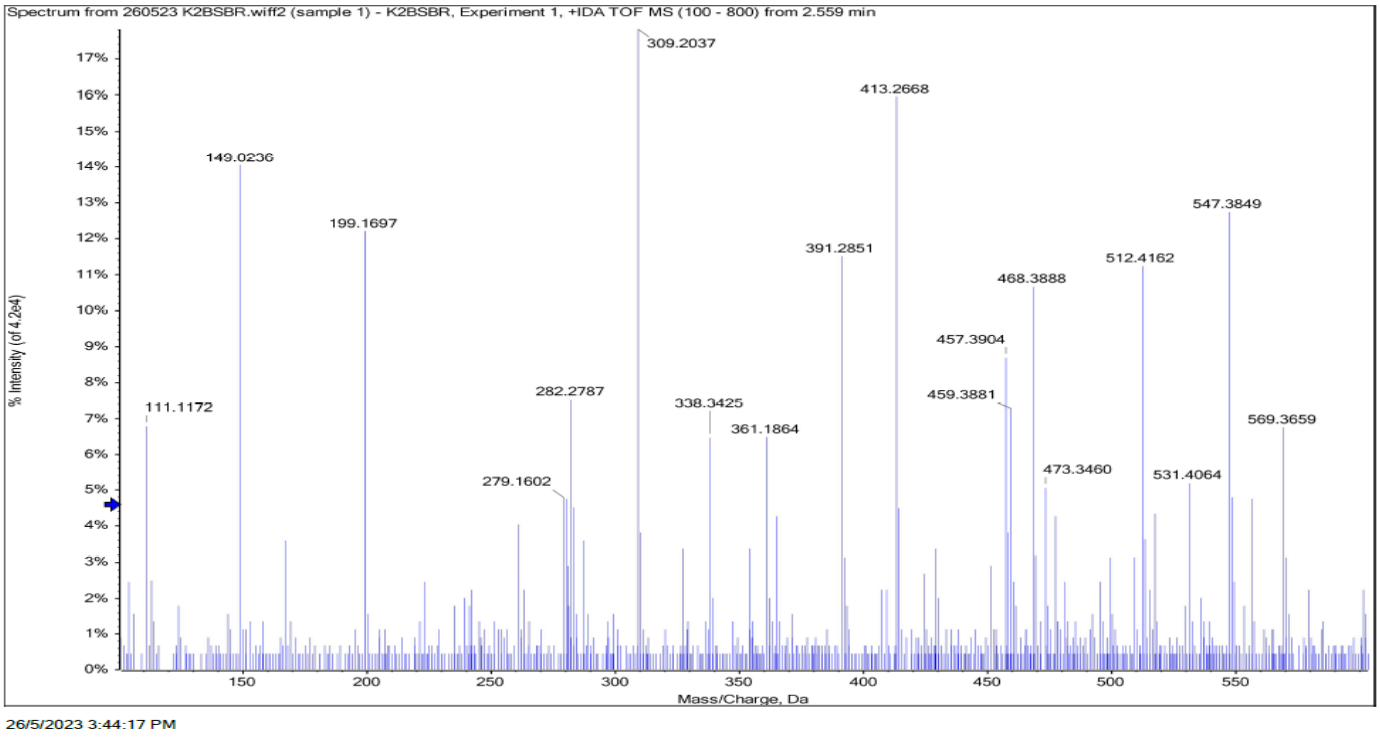

Figure 63: MS of **77e**

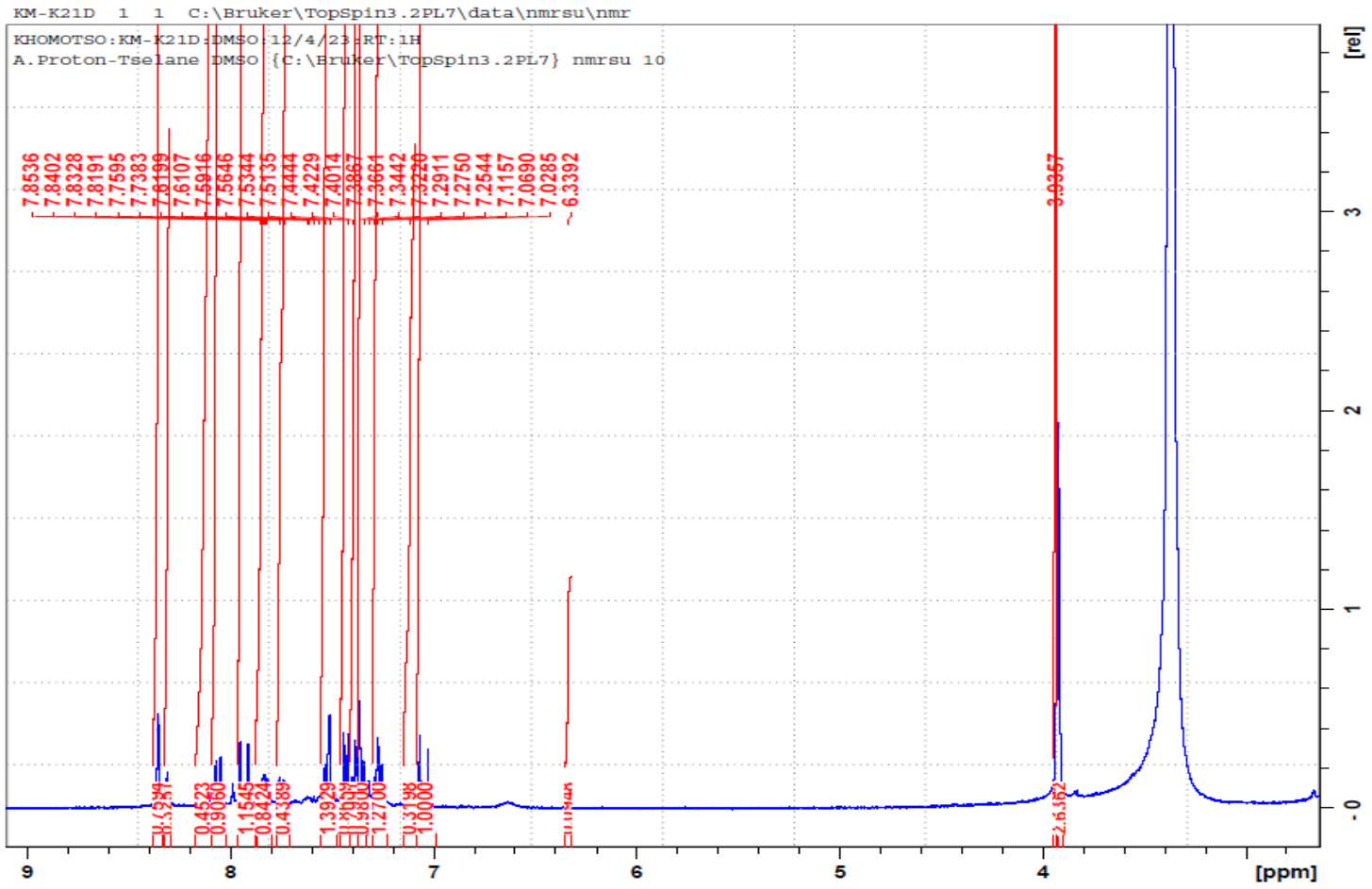

Figure 64: ^{1}H NMR of **77e**

Supplementary data x-ray data

Table 1. Atomic coordinates (x 10^4) and equivalent isotropic displacement parameters (Å^{2}x 10^3) for **76a** U(eq) is defined as one third of the trace of the orthogonalized U^{ij} tensor.

	x	y	z	U(eq)
C(1)	6888(2)	6846(3)	4102(2)	22(1)
C(2)	6465(2)	6423(3)	5173(2)	21(1)
C(3)	5289(2)	6997(3)	5491(2)	22(1)
C(4)	4568(2)	7948(3)	4747(2)	23(1)
C(5)	5011(2)	8373(3)	3687(2)	26(1)
C(6)	6184(2)	7807(3)	3363(2)	26(1)
C(7)	3306(2)	8487(3)	5102(2)	30(1)
C(8)	6922(2)	5238(3)	6960(2)	28(1)
C(9)	9564(2)	7682(3)	5214(2)	28(1)
O(1)	2576(2)	9260(2)	4519(2)	38(1)
O(2)	7239(1)	5441(2)	5803(1)	27(1)
O(3)	8046(1)	6160(2)	3769(1)	24(1)
O(4)	8986(2)	8941(2)	3263(2)	33(1)
O(5)	10191(2)	6260(2)	3323(2)	35(1)
S(1)	9263(1)	7349(1)	3792(1)	24(1)

Table 2. Bond lengths [Å] and angles [°] for **76a**

C(1)-C(6)	1.379(3)
C(1)-C(2)	1.398(3)
C(1)-O(3)	1.409(2)
C(2)-O(2)	1.355(2)
C(2)-C(3)	1.392(3)
C(3)-C(4)	1.390(3)
C(3)-H(3)	0.9500
C(4)-C(5)	1.393(3)
C(4)-C(7)	1.479(3)
C(5)-C(6)	1.388(3)
C(5)-H(5)	0.9500
C(6)-H(6)	0.9500
C(7)-O(1)	1.206(3)
C(7)-H(7)	0.9500
C(8)-O(2)	1.433(3)
C(8)-H(8A)	0.9800
C(8)-H(8B)	0.9800
C(8)-H(8C)	0.9800
C(9)-S(1)	1.747(2)
C(9)-H(9A)	0.9800
C(9)-H(9B)	0.9800
C(9)-H(9C)	0.9800

O(3)-S(1)	1.6002(16)
O(4)-S(1)	1.4247(17)
O(5)-S(1)	1.4236(16)
C(6)-C(1)-C(2)	122.4(2)
C(6)-C(1)-O(3)	120.3(2)
C(2)-C(1)-O(3)	117.15(19)
O(2)-C(2)-C(3)	125.6(2)
O(2)-C(2)-C(1)	116.31(19)
C(3)-C(2)-C(1)	118.1(2)
C(4)-C(3)-C(2)	119.9(2)
C(4)-C(3)-H(3)	120.1
C(2)-C(3)-H(3)	120.1
C(3)-C(4)-C(5)	121.2(2)
C(3)-C(4)-C(7)	118.3(2)
C(5)-C(4)-C(7)	120.5(2)
C(6)-C(5)-C(4)	119.3(2)
C(6)-C(5)-H(5)	120.4
C(4)-C(5)-H(5)	120.4
C(1)-C(6)-C(5)	119.2(2)
C(1)-C(6)-H(6)	120.4
C(5)-C(6)-H(6)	120.4
O(1)-C(7)-C(4)	124.6(2)

O(1)-C(7)-H(7)	117.7
C(4)-C(7)-H(7)	117.7
O(2)-C(8)-H(8A)	109.5
O(2)-C(8)-H(8B)	109.5
H(8A)-C(8)-H(8B)	109.5
O(2)-C(8)-H(8C)	109.5
H(8A)-C(8)-H(8C)	109.5
H(8B)-C(8)-H(8C)	109.5
S(1)-C(9)-H(9A)	109.5
S(1)-C(9)-H(9B)	109.5
H(9A)-C(9)-H(9B)	109.5
S(1)-C(9)-H(9C)	109.5
H(9A)-C(9)-H(9C)	109.5
H(9B)-C(9)-H(9C)	109.5
C(2)-O(2)-C(8)	116.89(18)
C(1)-O(3)-S(1)	119.51(13)
O(5)-S(1)-O(4)	119.39(11)
O(5)-S(1)-O(3)	102.55(10)
O(4)-S(1)-O(3)	109.28(10)
O(5)-S(1)-C(9)	110.14(12)
O(4)-S(1)-C(9)	109.80(11)
O(3)-S(1)-C(9)	104.46(10)

Table 3.Anisotropic displacement parameters (Å2x 103) for **76a**. The anisotropicdisplacement factor exponent takes the form: -2□2[h2a*2U11 + ... 12]h k a* b* U12]

	U^{11}	U^{22}	U^{33}	U^{23}	U^{13}	U^{12}
C(1)	18(1)	23(1)	25(1)	-4(1)	2(1)	0(1)
C(2)	19(1)	20(1)	25(1)	0(1)	-1(1)	-1(1)
C(3)	21(1)	24(1)	22(1)	-1(1)	2(1)	-1(1)
C(4)	20(1)	23(1)	27(1)	-4(1)	-1(1)	-1(1)
C(5)	24(1)	28(1)	26(1)	1(1)	-4(1)	1(1)
C(6)	25(1)	31(1)	22(1)	1(1)	1(1)	-2(1)
C(7)	24(1)	36(1)	30(1)	-3(1)	1(1)	5(1)
C(8)	28(1)	32(1)	24(1)	4(1)	0(1)	1(1)
C(9)	26(1)	28(1)	29(1)	-1(1)	-2(1)	0(1)
O(1)	28(1)	47(1)	37(1)	-5(1)	-3(1)	14(1)
O(2)	23(1)	32(1)	27(1)	7(1)	3(1)	5(1)
O(3)	20(1)	25(1)	29(1)	-5(1)	4(1)	1(1)
O(4)	31(1)	32(1)	37(1)	11(1)	4(1)	-1(1)
O(5)	24(1)	39(1)	41(1)	-6(1)	12(1)	5(1)

S(1)	20(1)	26(1)	25(1)	1(1)	6(1)	1(1)

Table 4. Hydrogen coordinates (x 10^4) and isotropic displacement parameters ($Å^2$x 10^3) for **76a.**

	x	y	z	U(eq)
H(3)	4978	6738	6216	27
H(5)	4515	9043	3191	31
H(6)	6499	8078	2641	31
H(7)	3053	8206	5841	36
H(8A)	6134	4605	7020	42
H(8B)	6829	6368	7308	42
H(8C)	7585	4600	7345	42
H(9A)	8892	8372	5538	42
H(9B)	10361	8285	5302	42
H(9C)	9608	6574	5599	42

Table 5. Torsion angles [°] for **76a**

C(6)-C(1)-C(2)-O(2)	178.6(2)
O(3)-C(1)-C(2)-O(2)	2.4(3)
C(6)-C(1)-C(2)-C(3)	0.3(3)

O(3)-C(1)-C(2)-C(3)	-175.98(17)
O(2)-C(2)-C(3)-C(4)	-177.6(2)
C(1)-C(2)-C(3)-C(4)	0.5(3)
C(2)-C(3)-C(4)-C(5)	-1.3(3)
C(2)-C(3)-C(4)-C(7)	178.07(19)
C(3)-C(4)-C(5)-C(6)	1.2(3)
C(7)-C(4)-C(5)-C(6)	-178.1(2)
C(2)-C(1)-C(6)-C(5)	-0.3(3)
O(3)-C(1)-C(6)-C(5)	175.82(19)
C(4)-C(5)-C(6)-C(1)	-0.4(3)
C(3)-C(4)-C(7)-O(1)	-177.1(2)
C(5)-C(4)-C(7)-O(1)	2.2(4)
C(3)-C(2)-O(2)-C(8)	-12.0(3)
C(1)-C(2)-O(2)-C(8)	169.77(18)
C(6)-C(1)-O(3)-S(1)	81.5(2)
C(2)-C(1)-O(3)-S(1)	-102.2(2)
C(1)-O(3)-S(1)-O(5)	-175.48(16)
C(1)-O(3)-S(1)-O(4)	-47.86(18)
C(1)-O(3)-S(1)-C(9)	69.58(18)

Table 6. Atomic coordinates (x 10^4) and equivalent isotropic displacement parameters ($Å^2$x 10^3) for **76b** U(eq) is defined as one third of the trace of the orthogonalized U^{ij} tensor.

	x	y	z	U(eq)
C(1)	4140(6)	11109(4)	5871(3)	33(1)
C(2)	5728(5)	10768(4)	6159(3)	32(1)
C(3)	6064(6)	9737(4)	6658(3)	34(1)
C(4)	4780(6)	9081(4)	6879(3)	30(1)
C(5)	3214(5)	9419(4)	6602(3)	33(1)
C(6)	2888(6)	10449(5)	6090(3)	37(1)
C(7)	3779(6)	12189(5)	5311(4)	40(1)
C(8)	3352(5)	8049(4)	8721(3)	26(1)
C(9)	2865(6)	9080(4)	9101(3)	35(1)
C(10)	1321(6)	9138(4)	9237(4)	40(1)
C(11)	274(6)	8161(5)	9013(4)	43(1)
C(12)	793(6)	7131(5)	8653(4)	40(1)
C(13)	2340(6)	7070(4)	8495(3)	32(1)
C(14)	8865(6)	9995(6)	6815(5)	55(2)
O(1)	4768(5)	12868(3)	5108(3)	49(1)
O(2)	5099(4)	8008(3)	7343(2)	33(1)
O(3)	5950(4)	6857(3)	8749(3)	43(1)
O(4)	6197(4)	9020(3)	8940(2)	38(1)
O(5)	7522(4)	9297(3)	6964(3)	46(1)

S(1)	5326(1)	7986(1)	8528(1)	30(1)
C(15)	1357(5)	6211(4)	5807(3)	32(1)
C(16)	-25(6)	5878(4)	6118(3)	33(1)
C(17)	-70(5)	4860(4)	6632(3)	34(1)
C(18)	1308(6)	4191(4)	6840(3)	33(1)
C(19)	2699(6)	4532(4)	6540(3)	36(1)
C(20)	2727(6)	5544(5)	6025(3)	37(1)
C(21)	1392(6)	7267(5)	5216(4)	43(1)
C(22)	3932(6)	3065(4)	8639(3)	30(1)
C(23)	4815(6)	4082(4)	8940(3)	35(1)
C(24)	6465(6)	4059(4)	9057(4)	38(1)
C(25)	7198(6)	3021(5)	8869(3)	39(1)
C(26)	6265(7)	2013(4)	8572(3)	40(1)
C(27)	4660(7)	2019(4)	8449(3)	39(1)
C(28)	-2768(6)	5107(6)	6771(5)	56(2)
O(6)	282(4)	7938(3)	5013(3)	48(1)
O(7)	1234(4)	3119(3)	7302(2)	39(1)
O(8)	1219(5)	1980(3)	8714(3)	50(1)
O(9)	1377(4)	4145(3)	8903(3)	41(1)
O(10)	-1368(4)	4426(4)	6951(3)	50(1)
S(2)	1829(1)	3090(1)	8483(1)	35(1)

Table 7. Bond lengths [Å] and angles [°] for **76b**

C(1)-C(6)	1.379(7)
C(1)-C(2)	1.398(6)
C(1)-C(7)	1.476(7)
C(2)-C(3)	1.384(7)
C(2)-H(2)	0.9500
C(3)-O(5)	1.341(6)
C(3)-C(4)	1.401(6)
C(4)-C(5)	1.378(7)
C(4)-O(2)	1.401(5)
C(5)-C(6)	1.391(7)
C(5)-H(5)	0.9500
C(6)-H(6)	0.9500
C(7)-O(1)	1.211(6)
C(7)-H(7)	0.9500
C(8)-C(9)	1.380(6)
C(8)-C(13)	1.383(6)
C(8)-S(1)	1.759(4)
C(9)-C(10)	1.370(7)
C(9)-H(9)	0.9500
C(10)-C(11)	1.398(8)
C(10)-H(10)	0.9500
C(11)-C(12)	1.378(8)

C(11)-H(11)	0.9500
C(12)-C(13)	1.383(7)
C(12)-H(12)	0.9500
C(13)-H(13)	0.9500
C(14)-O(5)	1.431(6)
C(14)-H(14A)	0.9800
C(14)-H(14B)	0.9800
C(14)-H(14C)	0.9800
O(2)-S(1)	1.612(3)
O(3)-S(1)	1.420(3)
O(4)-S(1)	1.420(3)
C(15)-C(16)	1.382(6)
C(15)-C(20)	1.393(7)
C(15)-C(21)	1.476(7)
C(16)-C(17)	1.380(7)
C(16)-H(16)	0.9500
C(17)-O(10)	1.359(6)
C(17)-C(18)	1.399(7)
C(18)-C(19)	1.384(7)
C(18)-O(7)	1.399(6)
C(19)-C(20)	1.374(7)
C(19)-H(19)	0.9500
C(20)-H(20)	0.9500

C(21)-O(6)	1.222(6)
C(21)-H(21)	0.9500
C(22)-C(23)	1.374(6)
C(22)-C(27)	1.398(7)
C(22)-S(2)	1.763(5)
C(23)-C(24)	1.384(7)
C(23)-H(23)	0.9500
C(24)-C(25)	1.392(7)
C(24)-H(24)	0.9500
C(25)-C(26)	1.386(7)
C(25)-H(25)	0.9500
C(26)-C(27)	1.343(8)
C(26)-H(26)	0.9500
C(27)-H(27)	0.9500
C(28)-O(10)	1.421(7)
C(28)-H(28A)	0.9800
C(28)-H(28B)	0.9800
C(28)-H(28C)	0.9800
O(7)-S(2)	1.611(3)
O(8)-S(2)	1.425(4)
O(9)-S(2)	1.415(4)
C(6)-C(1)-C(2)	121.3(4)
C(6)-C(1)-C(7)	118.8(4)

C(2)-C(1)-C(7)	119.9(4)
C(3)-C(2)-C(1)	119.9(4)
C(3)-C(2)-H(2)	120.0
C(1)-C(2)-H(2)	120.0
O(5)-C(3)-C(2)	126.2(4)
O(5)-C(3)-C(4)	115.8(4)
C(2)-C(3)-C(4)	118.0(4)
C(5)-C(4)-O(2)	119.2(4)
C(5)-C(4)-C(3)	122.2(4)
O(2)-C(4)-C(3)	118.4(4)
C(4)-C(5)-C(6)	119.3(4)
C(4)-C(5)-H(5)	120.4
C(6)-C(5)-H(5)	120.4
C(1)-C(6)-C(5)	119.3(4)
C(1)-C(6)-H(6)	120.4
C(5)-C(6)-H(6)	120.4
O(1)-C(7)-C(1)	125.2(5)
O(1)-C(7)-H(7)	117.4
C(1)-C(7)-H(7)	117.4
C(9)-C(8)-C(13)	122.0(4)
C(9)-C(8)-S(1)	118.5(3)
C(13)-C(8)-S(1)	119.5(3)
C(10)-C(9)-C(8)	118.7(5)

C(10)-C(9)-H(9)	120.7
C(8)-C(9)-H(9)	120.7
C(9)-C(10)-C(11)	120.4(5)
C(9)-C(10)-H(10)	119.8
C(11)-C(10)-H(10)	119.8
C(12)-C(11)-C(10)	120.1(5)
C(12)-C(11)-H(11)	119.9
C(10)-C(11)-H(11)	119.9
C(11)-C(12)-C(13)	120.0(5)
C(11)-C(12)-H(12)	120.0
C(13)-C(12)-H(12)	120.0
C(8)-C(13)-C(12)	118.8(4)
C(8)-C(13)-H(13)	120.6
C(12)-C(13)-H(13)	120.6
O(5)-C(14)-H(14A)	109.5
O(5)-C(14)-H(14B)	109.5
H(14A)-C(14)-H(14B)	109.5
O(5)-C(14)-H(14C)	109.5
H(14A)-C(14)-H(14C)	109.5
H(14B)-C(14)-H(14C)	109.5
C(4)-O(2)-S(1)	118.5(3)
C(3)-O(5)-C(14)	116.9(4)
O(3)-S(1)-O(4)	120.9(2)

O(3)-S(1)-O(2)	102.9(2)
O(4)-S(1)-O(2)	108.48(19)
O(3)-S(1)-C(8)	110.4(2)
O(4)-S(1)-C(8)	109.3(2)
O(2)-S(1)-C(8)	103.35(19)
C(16)-C(15)-C(20)	120.8(4)
C(16)-C(15)-C(21)	120.4(4)
C(20)-C(15)-C(21)	118.8(4)
C(17)-C(16)-C(15)	120.0(4)
C(17)-C(16)-H(16)	120.0
C(15)-C(16)-H(16)	120.0
O(10)-C(17)-C(16)	125.4(4)
O(10)-C(17)-C(18)	115.8(4)
C(16)-C(17)-C(18)	118.7(4)
C(19)-C(18)-C(17)	121.3(4)
C(19)-C(18)-O(7)	119.7(4)
C(17)-C(18)-O(7)	118.8(4)
C(20)-C(19)-C(18)	119.4(4)
C(20)-C(19)-H(19)	120.3
C(18)-C(19)-H(19)	120.3
C(19)-C(20)-C(15)	119.7(4)
C(19)-C(20)-H(20)	120.1
C(15)-C(20)-H(20)	120.1

O(6)-C(21)-C(15)	124.3(5)
O(6)-C(21)-H(21)	117.9
C(15)-C(21)-H(21)	117.9
C(23)-C(22)-C(27)	121.7(5)
C(23)-C(22)-S(2)	118.9(4)
C(27)-C(22)-S(2)	119.4(4)
C(22)-C(23)-C(24)	118.6(5)
C(22)-C(23)-H(23)	120.7
C(24)-C(23)-H(23)	120.7
C(23)-C(24)-C(25)	120.0(5)
C(23)-C(24)-H(24)	120.0
C(25)-C(24)-H(24)	120.0
C(26)-C(25)-C(24)	119.6(5)
C(26)-C(25)-H(25)	120.2
C(24)-C(25)-H(25)	120.2
C(27)-C(26)-C(25)	121.3(5)
C(27)-C(26)-H(26)	119.3
C(25)-C(26)-H(26)	119.3
C(26)-C(27)-C(22)	118.8(5)
C(26)-C(27)-H(27)	120.6
C(22)-C(27)-H(27)	120.6
O(10)-C(28)-H(28A)	109.5
O(10)-C(28)-H(28B)	109.5

H(28A)-C(28)-H(28B)	109.5
O(10)-C(28)-H(28C)	109.5
H(28A)-C(28)-H(28C)	109.5
H(28B)-C(28)-H(28C)	109.5
C(18)-O(7)-S(2)	118.5(3)
C(17)-O(10)-C(28)	116.8(4)
O(9)-S(2)-O(8)	120.9(2)
O(9)-S(2)-O(7)	108.3(2)
O(8)-S(2)-O(7)	102.8(2)
O(9)-S(2)-C(22)	109.8(2)
O(8)-S(2)-C(22)	110.1(2)
O(7)-S(2)-C(22)	103.2(2)

Table 8 Atomic coordinates (x 10^4) and equivalent isotropic displacement parameters ($Å^2$x 10^3) for **76k**. U(eq) is defined as one third of the trace of the orthogonalized U^{ij} tensor.

	x	y	z	U(eq)
C(1)	1064(3)	6587(2)	6830(2)	24(1)
C(2)	2397(3)	6419(2)	6329(2)	24(1)
C(3)	4051(4)	6573(3)	6718(2)	28(1)
C(4)	4364(4)	6875(3)	7645(2)	30(1)
C(5)	3033(4)	7025(3)	8152(2)	27(1)

C(6)	1397(4)	6905(3)	7757(2)	26(1)
C(7)	-713(4)	6417(3)	6409(2)	31(1)
C(8)	4629(3)	7376(3)	4590(2)	26(1)
C(9)	5757(4)	8482(3)	5026(2)	33(1)
C(10)	7519(4)	8741(3)	4902(2)	41(1)
C(11)	8094(4)	7900(3)	4357(3)	41(1)
C(12)	6942(4)	6787(3)	3929(2)	40(1)
C(13)	5185(4)	6512(3)	4044(2)	33(1)
O(1)	-1894(3)	6533(3)	6841(2)	46(1)
O(2)	2041(3)	6022(2)	5398(1)	28(1)
O(3)	1405(3)	6378(2)	3918(1)	36(1)
O(4)	2071(3)	8141(2)	5159(2)	34(1)
S(1)	2402(1)	7050(1)	4725(1)	26(1)
Br(1)	3420(1)	7373(1)	9418(1)	41(1)
C(14)	1575(4)	6327(3)	1722(2)	27(1)
C(15)	3325(4)	6962(3)	1985(2)	28(1)
C(16)	4646(4)	6492(3)	1718(2)	31(1)
C(17)	4225(4)	5344(3)	1176(2)	31(1)
C(18)	2498(4)	4703(3)	907(2)	29(1)
C(19)	1172(4)	5186(3)	1163(2)	30(1)
C(20)	146(4)	6792(3)	2060(2)	36(1)
C(21)	6362(4)	9724(3)	2029(2)	32(1)

C(22)	6809(5)	9709(3)	1151(3)	45(1)
C(23)	8552(6)	10002(4)	1008(4)	70(1)
C(24)	9787(6)	10272(4)	1720(5)	74(2)
C(25)	9334(6)	10275(4)	2586(4)	71(2)
C(26)	7582(5)	10010(3)	2763(3)	50(1)
O(5)	-1367(3)	6190(3)	1911(2)	47(1)
O(6)	3732(3)	8076(2)	2596(1)	33(1)
O(7)	3928(4)	10212(2)	2946(2)	51(1)
O(8)	3152(3)	9200(2)	1374(2)	40(1)
S(2)	4156(1)	9381(1)	2210(1)	32(1)
Br(2)	1904(1)	3107(1)	205(1)	43(1)

Table 9. Bond lengths [Å] and angles [°] for **76k**

C(1)-C(2)	1.386(4)
C(1)-C(6)	1.391(4)
C(1)-C(7)	1.489(4)
C(2)-C(3)	1.386(4)
C(2)-O(2)	1.408(3)
C(3)-C(4)	1.388(4)
C(3)-H(3)	0.9500
C(4)-C(5)	1.385(4)

C(4)-H(4)	0.9500
C(5)-C(6)	1.385(4)
C(5)-Br(1)	1.890(3)
C(6)-H(6)	0.9500
C(7)-O(1)	1.207(4)
C(7)-H(7)	0.9500
C(8)-C(9)	1.377(4)
C(8)-C(13)	1.388(4)
C(8)-S(1)	1.752(3)
C(9)-C(10)	1.392(5)
C(9)-H(9)	0.9500
C(10)-C(11)	1.377(5)
C(10)-H(10)	0.9500
C(11)-C(12)	1.385(5)
C(11)-H(11)	0.9500
C(12)-C(13)	1.383(5)
C(12)-H(12)	0.9500
C(13)-H(13)	0.9500
O(2)-S(1)	1.605(2)
O(3)-S(1)	1.423(2)
O(4)-S(1)	1.425(2)
C(14)-C(19)	1.392(4)
C(14)-C(15)	1.395(4)

C(14)-C(20)	1.487(4)
C(15)-C(16)	1.379(4)
C(15)-O(6)	1.409(3)
C(16)-C(17)	1.385(4)
C(16)-H(16)	0.9500
C(17)-C(18)	1.383(4)
C(17)-H(17)	0.9500
C(18)-C(19)	1.386(4)
C(18)-Br(2)	1.891(3)
C(19)-H(19)	0.9500
C(20)-O(5)	1.205(4)
C(20)-H(20)	0.9500
C(21)-C(22)	1.385(5)
C(21)-C(26)	1.386(5)
C(21)-S(2)	1.749(3)
C(22)-C(23)	1.380(6)
C(22)-H(22)	0.9500
C(23)-C(24)	1.370(8)
C(23)-H(23)	0.9500
C(24)-C(25)	1.370(8)
C(24)-H(24)	0.9500
C(25)-C(26)	1.402(7)
C(25)-H(25)	0.9500

C(26)-H(26)	0.9500
O(6)-S(2)	1.600(2)
O(7)-S(2)	1.417(2)
O(8)-S(2)	1.424(2)
C(2)-C(1)-C(6)	118.6(2)
C(2)-C(1)-C(7)	122.2(3)
C(6)-C(1)-C(7)	119.2(2)
C(1)-C(2)-C(3)	122.4(3)
C(1)-C(2)-O(2)	118.9(2)
C(3)-C(2)-O(2)	118.6(2)
C(2)-C(3)-C(4)	118.6(3)
C(2)-C(3)-H(3)	120.7
C(4)-C(3)-H(3)	120.7
C(5)-C(4)-C(3)	119.5(3)
C(5)-C(4)-H(4)	120.3
C(3)-C(4)-H(4)	120.3
C(6)-C(5)-C(4)	121.6(3)
C(6)-C(5)-Br(1)	118.5(2)
C(4)-C(5)-Br(1)	119.8(2)
C(5)-C(6)-C(1)	119.3(3)
C(5)-C(6)-H(6)	120.3
C(1)-C(6)-H(6)	120.3
O(1)-C(7)-C(1)	122.8(3)

O(1)-C(7)-H(7)	118.6
C(1)-C(7)-H(7)	118.6
C(9)-C(8)-C(13)	122.6(3)
C(9)-C(8)-S(1)	118.7(2)
C(13)-C(8)-S(1)	118.7(2)
C(8)-C(9)-C(10)	118.2(3)
C(8)-C(9)-H(9)	120.9
C(10)-C(9)-H(9)	120.9
C(11)-C(10)-C(9)	120.0(3)
C(11)-C(10)-H(10)	120.0
C(9)-C(10)-H(10)	120.0
C(10)-C(11)-C(12)	121.0(3)
C(10)-C(11)-H(11)	119.5
C(12)-C(11)-H(11)	119.5
C(13)-C(12)-C(11)	119.9(3)
C(13)-C(12)-H(12)	120.1
C(11)-C(12)-H(12)	120.1
C(12)-C(13)-C(8)	118.3(3)
C(12)-C(13)-H(13)	120.9
C(8)-C(13)-H(13)	120.9
C(2)-O(2)-S(1)	119.11(17)
O(3)-S(1)-O(4)	120.46(14)
O(3)-S(1)-O(2)	102.95(12)

O(4)-S(1)-O(2)	108.29(12)
O(3)-S(1)-C(8)	110.21(13)
O(4)-S(1)-C(8)	109.64(14)
O(2)-S(1)-C(8)	103.82(12)
C(19)-C(14)-C(15)	118.1(3)
C(19)-C(14)-C(20)	119.6(3)
C(15)-C(14)-C(20)	122.3(3)
C(16)-C(15)-C(14)	122.4(3)
C(16)-C(15)-O(6)	119.3(3)
C(14)-C(15)-O(6)	118.2(3)
C(15)-C(16)-C(17)	119.0(3)
C(15)-C(16)-H(16)	120.5
C(17)-C(16)-H(16)	120.5
C(18)-C(17)-C(16)	119.5(3)
C(18)-C(17)-H(17)	120.3
C(16)-C(17)-H(17)	120.3
C(17)-C(18)-C(19)	121.5(3)
C(17)-C(18)-Br(2)	119.8(2)
C(19)-C(18)-Br(2)	118.7(2)
C(18)-C(19)-C(14)	119.6(3)
C(18)-C(19)-H(19)	120.2
C(14)-C(19)-H(19)	120.2
O(5)-C(20)-C(14)	122.7(3)

O(5)-C(20)-H(20)	118.7
C(14)-C(20)-H(20)	118.7
C(22)-C(21)-C(26)	122.9(3)
C(22)-C(21)-S(2)	118.1(3)
C(26)-C(21)-S(2)	119.0(3)
C(23)-C(22)-C(21)	118.1(4)
C(23)-C(22)-H(22)	120.9
C(21)-C(22)-H(22)	120.9
C(24)-C(23)-C(22)	120.3(5)
C(24)-C(23)-H(23)	119.9
C(22)-C(23)-H(23)	119.9
C(23)-C(24)-C(25)	121.3(4)
C(23)-C(24)-H(24)	119.4
C(25)-C(24)-H(24)	119.4
C(24)-C(25)-C(26)	120.3(4)
C(24)-C(25)-H(25)	119.8
C(26)-C(25)-H(25)	119.8
C(21)-C(26)-C(25)	117.0(4)
C(21)-C(26)-H(26)	121.5
C(25)-C(26)-H(26)	121.5
C(15)-O(6)-S(2)	118.71(18)
O(7)-S(2)-O(8)	120.41(17)
O(7)-S(2)-O(6)	102.89(15)

O(8)-S(2)-O(6)	108.82(13)
O(7)-S(2)-C(21)	110.13(16)
O(8)-S(2)-C(21)	109.57(15)
O(6)-S(2)-C(21)	103.52(13)

Table 10. Anisotropic displacement parameters ($Å^2 x\ 10^3$) for **76k**. The anisotropic displacement factor exponent takes the form: $-2p^2[\ h^2 a^{*2} U^{11} + ... + 2\ h\ k\ a^*\ b^*\ U^{12}]$

	U^{11}	U^{22}	U^{33}	U^{23}	U^{13}	U^{12}
C(1)	23(1)	22(1)	27(1)	4(1)	1(1)	5(1)
C(2)	24(1)	23(1)	24(1)	2(1)	1(1)	5(1)
C(3)	23(1)	32(1)	31(1)	9(1)	6(1)	10(1)
C(4)	23(1)	33(1)	33(2)	9(1)	-3(1)	5(1)
C(5)	30(1)	23(1)	25(1)	4(1)	-1(1)	4(1)
C(6)	26(1)	24(1)	26(1)	6(1)	5(1)	7(1)
C(7)	22(1)	36(2)	32(1)	3(1)	0(1)	8(1)
C(8)	24(1)	31(1)	22(1)	6(1)	2(1)	8(1)
C(9)	32(2)	33(2)	33(2)	1(1)	0(1)	8(1)
C(10)	29(2)	41(2)	47(2)	5(1)	-8(1)	3(1)
C(11)	25(1)	48(2)	55(2)	21(2)	6(1)	14(1)
C(12)	37(2)	42(2)	50(2)	11(2)	14(1)	20(1)
C(13)	31(2)	32(2)	35(2)	2(1)	6(1)	10(1)
O(1)	25(1)	65(2)	47(1)	2(1)	3(1)	16(1)

O(2)	29(1)	28(1)	24(1)	1(1)	3(1)	6(1)
O(3)	29(1)	48(1)	26(1)	1(1)	-4(1)	7(1)
O(4)	34(1)	38(1)	35(1)	5(1)	5(1)	19(1)
S(1)	24(1)	32(1)	23(1)	3(1)	1(1)	10(1)
Br(1)	45(1)	46(1)	24(1)	3(1)	-5(1)	6(1)
C(14)	27(1)	32(1)	26(1)	10(1)	7(1)	10(1)
C(15)	31(1)	27(1)	25(1)	6(1)	4(1)	7(1)
C(16)	24(1)	35(2)	33(2)	10(1)	4(1)	7(1)
C(17)	30(1)	34(2)	33(2)	9(1)	8(1)	12(1)
C(18)	32(1)	28(1)	26(1)	6(1)	5(1)	7(1)
C(19)	26(1)	33(1)	29(1)	11(1)	3(1)	5(1)
C(20)	34(2)	44(2)	33(2)	9(1)	8(1)	16(1)
C(21)	31(1)	23(1)	40(2)	1(1)	3(1)	7(1)
C(22)	46(2)	36(2)	48(2)	-5(1)	14(2)	5(1)
C(23)	53(3)	54(2)	98(4)	-2(2)	37(3)	12(2)
C(24)	38(2)	45(2)	148(6)	23(3)	29(3)	19(2)
C(25)	44(2)	46(2)	122(5)	28(3)	-20(3)	11(2)
C(26)	45(2)	39(2)	62(2)	14(2)	-13(2)	6(2)
O(5)	27(1)	64(2)	52(2)	10(1)	10(1)	17(1)
O(6)	37(1)	33(1)	26(1)	3(1)	6(1)	6(1)
O(7)	59(2)	44(1)	49(2)	-11(1)	16(1)	19(1)
O(8)	37(1)	41(1)	42(1)	6(1)	-4(1)	13(1)
S(2)	33(1)	29(1)	32(1)	0(1)	5(1)	10(1)

Br(2)	48(1)	33(1)	43(1)	-2(1)	7(1)	9(1)

Table 11. Hydrogen coordinates (x 10^4) and isotropic displacement parameters (Å^{2}x 10^3) for **76k**

	x	y	z	U(eq)
H(3)	4950	6474	6358	33
H(4)	5483	6978	7929	36
H(6)	512	7037	8115	31
H(7)	-925	6210	5775	37
H(9)	5343	9053	5401	40
H(10)	8326	9498	5194	49
H(11)	9298	8087	4273	49
H(12)	7358	6213	3558	49
H(13)	4380	5751	3757	39
H(16)	5827	6948	1903	37
H(17)	5115	4999	991	38
H(19)	-4	4740	959	36
H(20)	438	7597	2408	43
H(22)	5942	9504	661	55
H(23)	8897	10017	413	84
H(24)	10980	10460	1611	89
H(25)	10212	10457	3069	85
H(26)	7245	10027	3360	60

Table 12. Torsion angles [°] for **76k**

C(6)-C(1)-C(2)-C(3)	-0.9(4)
C(7)-C(1)-C(2)-C(3)	-179.8(3)
C(6)-C(1)-C(2)-O(2)	176.1(2)
C(7)-C(1)-C(2)-O(2)	-2.9(4)
C(1)-C(2)-C(3)-C(4)	1.6(4)
O(2)-C(2)-C(3)-C(4)	-175.3(2)
C(2)-C(3)-C(4)-C(5)	-0.6(4)
C(3)-C(4)-C(5)-C(6)	-1.3(4)
C(3)-C(4)-C(5)-Br(1)	177.6(2)
C(4)-C(5)-C(6)-C(1)	2.0(4)
Br(1)-C(5)-C(6)-C(1)	-176.8(2)
C(2)-C(1)-C(6)-C(5)	-1.0(4)
C(7)-C(1)-C(6)-C(5)	178.0(3)
C(2)-C(1)-C(7)-O(1)	178.2(3)
C(6)-C(1)-C(7)-O(1)	-0.7(4)
C(13)-C(8)-C(9)-C(10)	0.7(5)
S(1)-C(8)-C(9)-C(10)	-179.0(2)
C(8)-C(9)-C(10)-C(11)	-0.1(5)
C(9)-C(10)-C(11)-C(12)	-0.4(5)
C(10)-C(11)-C(12)-C(13)	0.4(5)
C(11)-C(12)-C(13)-C(8)	0.2(5)
C(9)-C(8)-C(13)-C(12)	-0.7(5)

S(1)-C(8)-C(13)-C(12)	178.9(2)
C(1)-C(2)-O(2)-S(1)	94.2(3)
C(3)-C(2)-O(2)-S(1)	-88.7(3)
C(2)-O(2)-S(1)-O(3)	-161.9(2)
C(2)-O(2)-S(1)-O(4)	-33.3(2)
C(2)-O(2)-S(1)-C(8)	83.2(2)
C(9)-C(8)-S(1)-O(3)	145.7(2)
C(13)-C(8)-S(1)-O(3)	-34.0(3)
C(9)-C(8)-S(1)-O(4)	10.9(3)
C(13)-C(8)-S(1)-O(4)	-168.8(2)
C(9)-C(8)-S(1)-O(2)	-104.7(2)
C(13)-C(8)-S(1)-O(2)	75.7(2)
C(19)-C(14)-C(15)-C(16)	-0.6(4)
C(20)-C(14)-C(15)-C(16)	175.7(3)
C(19)-C(14)-C(15)-O(6)	-176.0(2)
C(20)-C(14)-C(15)-O(6)	0.3(4)
C(14)-C(15)-C(16)-C(17)	-0.6(4)
O(6)-C(15)-C(16)-C(17)	174.7(3)
C(15)-C(16)-C(17)-C(18)	0.7(4)
C(16)-C(17)-C(18)-C(19)	0.3(4)
C(16)-C(17)-C(18)-Br(2)	-177.6(2)
C(17)-C(18)-C(19)-C(14)	-1.6(4)
Br(2)-C(18)-C(19)-C(14)	176.4(2)

C(15)-C(14)-C(19)-C(18)	1.7(4)
C(20)-C(14)-C(19)-C(18)	-174.7(3)
C(19)-C(14)-C(20)-O(5)	4.1(5)
C(15)-C(14)-C(20)-O(5)	-172.2(3)
C(26)-C(21)-C(22)-C(23)	-0.4(5)
S(2)-C(21)-C(22)-C(23)	178.8(3)
C(21)-C(22)-C(23)-C(24)	1.3(6)
C(22)-C(23)-C(24)-C(25)	-0.9(7)
C(23)-C(24)-C(25)-C(26)	-0.6(7)
C(22)-C(21)-C(26)-C(25)	-1.0(5)
S(2)-C(21)-C(26)-C(25)	179.8(3)
C(24)-C(25)-C(26)-C(21)	1.5(6)
C(16)-C(15)-O(6)-S(2)	90.2(3)
C(14)-C(15)-O(6)-S(2)	-94.3(3)
C(15)-O(6)-S(2)-O(7)	161.5(2)
C(15)-O(6)-S(2)-O(8)	32.7(2)
C(15)-O(6)-S(2)-C(21)	-83.8(2)
C(22)-C(21)-S(2)-O(7)	-137.8(3)
C(26)-C(21)-S(2)-O(7)	41.4(3)
C(22)-C(21)-S(2)-O(8)	-3.2(3)
C(26)-C(21)-S(2)-O(8)	176.1(3)
C(22)-C(21)-S(2)-O(6)	112.8(3)
C(26)-C(21)-S(2)-O(6)	-68.0(3)